Order Number 9017184

Transient electromagnetics for permafrost

Walker, Gerald Grant, Ph.D.

University of Alaska Fairbanks, 1988

U·M·I
300 N. Zeeb Rd.
Ann Arbor, MI 48106

TRANSIENT ELECTROMAGNETICS FOR PERMAFROST

A

THESIS

Presented to the Faculty of the University of Alaska

in Partial Fulfillment of the Requirements

for the degree of

DOCTOR OF PHILOSOPHY

By

Gerald Grant Walker, B.S., M.S.

Fairbanks, Alaska

December 1988

TRANSIENT ELECTROMAGNETICS FOR PERMAFROST

RECOMMENDED:

Chairman Advisory Committee

Department Head

APPROVED:

Dean, College of Natural Sciences

Director of Graduate Programs

12/28/88

Date

TRANSIENT ELECTROMAGNETICS FOR PERMAFROST

Gerald Grant Walker

University of Alaska, Fairbanks, 1988

Abstract

Transient electromagnetic (TEM) soundings were carried out with a Geonics EM-37 instrument at more than forty sites in Alaska, primarily along a line from Reindeer Island to Glennallen, to investigate its application to the study of permafrost. Procedures were developed for correcting TEM sounding data for the effects of transmitter turnoff time. Best fit geoelectric models of horizontally layered earth were derived by computer inverse modeling, using program NLSTCI (Anderson, 1982), and used to interpret the soundings in terms of the thickness of permafrost at each site. The interpretations indicate permafrost thicknesses vary substantially between sounding sites on land, although the general trend of thicker permafrost at more northern latitudes is evident. Under favorable circumstances, the depth to the base of ice-bearing permafrost may be resolved within ±10%. Soundings taken over sea ice indicate that the thickness of the thawed sediments overlying ice-bearing permafrost can be determined, the subsea permafrost is multilayered beyond about 3 km offshore, but that the TEM system used may not resolve the base of ice-bearing subsea permafrost in this warm, high-salinity, and multilayered environment. An anomalous, double-sign reversal was obtained at a site in the Kuparuk region which was successfully modeled using a complex resistivity of the Cole-Cole type. The model parameters indicate that this unusual signature may be related to the known deposits of gas hydrates beneath the site suggesting that deep deposits of gas hydrates may be detectable form the ground

surface using the TEM method. Finally, it is noted that TEM soundings for permafrost are most productively performed in a line or grid tied to sites with known subsurface lithology so that modeling parameters may be constrained to physically reasonable values.

TABLE OF CONTENTS

Page

List of Figures ix

List of Tables xiv

Acknowledgements xv

Chapter 1: INTRODUCTION 1

1.1 Background 1

1.2 Thesis Outline 6

1.3 A Brief History of Permafrost Investigation 10

1.4 Electrical Conduction in Solids 15

1.5 Temperature Dependence of Resistivity 17

1.6 Bulk Resistivity and Archie's Law 21

1.7 Description of the TEM Method 22

Chapter 2: TEM THEORY 33

2.1 Introduction 33

2.2 Theory 35

2.3 Asymptotic Forms and Apparent Resistivity 42

2.4 Turnoff Correction 45

2.5 Summary 49

Chapter 3: AN ANALYSIS OF TEM SOUNDINGS 50

3.1 Introduction 50

3.2 West Dock Site 52

3.3 Deadhorse 61

3.4 Reindeer Island 69

3.5 Discussion and Conclusions 83

Chapter 4: TEM DETECTION OF SUBSEA PERMAFROST 89

4.1 Introduction 89

4.2 Experimental Details 91

4.3 Inverse Model Results 97

4.4 Discussion 112

Homogeneous Half-space Results 112

Two Layer Results 114

Three Layer Results 114

Six Layer Results 119

4.5 Summary 122

Chapter 5: TEM SIGN REVERSALS AND INDUCED POLARIZATION . 124

5.1 Introduction 124

5.2 Experimental Data 124

5.3 Theory 125

5.4 Modeling 132

5.5 Summary and Discussion 140

Chapter 6: SUMMARY, CONCLUSIONS AND RECOMMENDATIONS . 145

6.1 Summary and Conclusions 145

6.2 Recommendations 153

REFERENCES CITED 157

APPENDIX A: A TEM SOUNDING TRANSECT OF ALASKA 169

A.1 Introduction 169

A.2 Data Site Locations 170

A.3 Experimental Procedure 173
A.4 Interpretation 175
A.4.1 Barter Island 177
A.4.2 Prudhoe Bay 180
A.4.3 Deadhorse 182
A.4.4 Franklin Bluffs 183
A.4.5 Happy Valley 186
A.4.6 Galbraith Lake 186
A.4.7 Chandalar Camp 190
A.4.8 Slate Creek 190
A.4.9 Coldfoot 192
A.4.10 Bonanza Creek 195
A.4.11 Oldman Camp 195
A.4.12 Finger Mountain 197
A.4.13 Site at Dalton Mile 78.1 200
A.4.14 Yukon River 202
A.4.15 Site at Dalton Mile 34.4 204
A.4.16 Hess Creek 204
A.4.17 Livengood 207
A.4.18 Site at Elliott Mile 54.7 207
A.4.19 Washington Creek 210
A.4.20 Virgin Spruce 1 210
A.4.21 Virgin Spruce 2 214
A.4.22 Farm 216
A.4.23 Peat 218
A.4.24 Farmers Loop 220

A.4.25 Eielson 220
A.4.26 Quartz Lake 223
A.4.27 Sawmill Creek 223
A.4.28 Greely 225
A.4.29 Fielding Lake 228
A.4.30 Summit Lake 228
A.4.31 Sourdough 231
A.4.32 Glennallen 233
A.5 Summary 233

APPENDIX B: PROGRAMS 236
B.1 Introduction 236
B.2 Program RHOA 237
B.3 Program RESPONS 243
B.4 Program IPVAX 249

APPENDIX C: TRANSIENT SOUNDING DATA 255

LIST OF FIGURES

Figure		Page
1.1:	Transient electromagnetic site locations for soundings taken in 1983.	7
1.2:	Subsea transient electromagnetic sites for soundings taken in 1984.	8
1.3:	Resistivity of Soils as a function of temperature.	20
1.4:	Geonics EM-37 transmitter current waveform.	23
1.5:	Plan view of a TEM layout.	24
1.6:	Geonics EM-37 receiver gate locations for 3 and 30 Hertz.	25
1.7:	Four snapshots of the diffusion of the eddy current maximum from a TEM system.	27
2.1:	TEM cylindrical coordinate system and geoelectric, horizontally-layered earth.	34
3.1:	Dual induction later-log for ARCO Prudhoe Bay State # 1 discovery well.	53
3.2:	TEM sounding data and base model for West Dock.	54
3.3:	TEM curves showing the results of varying the first layer resistivity.	56
3.4:	TEM curves showing the results of varying the second layer resistivity.	57
3.5:	TEM curves showing the results of varying the third layer resistivity.	58
3.6:	TEM curves showing the results of varying the first layer thickness.	59
3.7:	TEM curves showing the results of varying the second layer thickness.	60
3.8:	Dual induction later-log from ARCO D.S. 12-3.	62
3.9:	TEM data and base model for the Deadhorse site.	64
3.10:	TEM curves showing the results of varying the first layer resistivity for Deadhorse site.	66

Figure Page

3.11: TEM curves showing the results of varying the second layer resistivity for Deadhorse site. 67

3.12: TEM curves showing the results of varying the first layer thickness for Deadhorse site. 68

3.13: Dual induction later-log for the Reindeer Island site. 70

3.14: TEM data and well log models for Reindeer Island site. 72

3.15: TEM curves showing the results of varying the first layer resistivity for Reindeer Island site. 73

3.16: TEM curves showing the results of varying the second layer resistivity for Reindeer Island site. 75

3.17: TEM curves showing the results of varying the third layer resistivity for Reindeer Island site. 76

3.18: TEM curves showing the results of varying the fourth layer resistivity for Reindeer Island site. 77

3.19: TEM curves showing the results of varying the fifth layer resistivity for Reindeer Island site. 78

3.20: TEM curves showing the results of varying the sixth layer resistivity for Reindeer Island site. 79

3.21: TEM curves showing the results of varying the first layer thickness for Reindeer Island site. 80

3.22: TEM curves showing the results of varying the second layer thickness for Reindeer Island site. 81

3.23: TEM curves showing the results of varying the third layer thickness for Reindeer Island site. 82

Figure Page

3.24: TEM curves showing the results of varying the fourth layer thickness for Reindeer Island site. 84

3.25: TEM curves showing the results of varying the fifth layer thickness for Reindeer Island site. 85

4.1: TEM sounding data, visually-matched model, and the 3 layer inverse model for the site 3 kilometers offshore. 93

4.2: TEM sounding data and inverse match for 750 meters offshore. . . 101

4.3: TEM sounding data and inverse match for 1 kilometer offshore. . 103

4.4: TEM sounding data and inverse match for 3 kilometers offshore. . 104

4.5: TEM sounding data and inverse match for 5 kilometers offshore. . 106

4.6: TEM sounding data and inverse match for 7 kilometers offshore. . 107

4.7: TEM sounding data and inverse match for 9 kilometers offshore. . 109

4.8: TEM sounding data and inverse match for 11 kilometers offshore. . 110

4.9: TEM sounding data and inverse match for the site on Reindeer Island (13 kilometers offshore). 111

4.10: TEM sounding data and inverse match for 14 kilometers offshore. . 113

4.11: Subsea permafrost profile inferred from the TEM soundings and inverse modeling. 117

4.12: Subsea permafrost profile from Ehrenbard et al. (1983). 118

5.1: TEM sounding field strength data showing two sign changes for the site in the Kuparuk Oil Feild, NWEILEEN. 126

5.2: Schematic representation of mineralized rock. 130

5.3: TEM response due to a polarizable half-space. 133

Figure Page

5.4: Family of TEM responses for two layers of simple resistivity with varying thickness. 135

5.5: Family of TEM IP responses for two layers, the top layer polarizable with varying thickness. 137

5.6: Family of TEM IP responses for two layers, the time constant varies from 10^{-5} to 10^{-1} seconds. 138

5.7: Family of TEM IP responses for two layers, the chargeability varies from 0 to 1.0. 139

5.8: Family of TEM IP responses for two layers, the frequency parameter varies from 0 to 0.96. 141

A.1: TEM sounding data and inverse match for Barter Island. 179

A.2: TEM sounding data and inverse match for West Dock, Prudhoe Bay. 181

A.3: TEM sounding data and inverse match for Deadhorse. 184

A.4: TEM sounding data and inverse match for Franklin Bluffs. 185

A.5: TEM sounding data and inverse match for Happy Valley. 187

A.6: TEM sounding data and inverse match for Galbraith Lake. . . . 189

A.7: TEM sounding data and inverse match for Chandalar Camp. . . . 191

A.8: TEM sounding data and inverse match for Slate Creek. 193

A.9: TEM sounding data and inverse match for Coldfoot. 194

A.10: TEM sounding data and inverse match for Bonanza Creek. . . . 196

A.11: TEM sounding data and inverse match for Oldman. 198

A.12: TEM sounding data and inverse match for Finger Mountain. . . . 199

A.13: Averaged raw TEM sounding data for the site at Dalton Mile 78.1 showing a single sign change. 201

Figure		Page
A.14:	TEM sounding data and inverse match for Yukon River.	203
A.15:	TEM sounding data and inverse match for Dalton Mile 34.4.	205
A.16:	TEM sounding data and inverse match for Hess Creek.	206
A.17:	TEM sounding data and inverse match for Livengood.	208
A.18:	Averaged raw TEM sounding data for the site at Elliott Mile 54.7.	209
A.19:	TEM sounding data and inverse match for Washington Creek.	211
A.20:	TEM sounding data and inverse match for Virgin Spruce 1.	213
A.21:	TEM sounding data and inverse match for Virgin Spruce 2.	215
A.22:	TEM sounding data and inverse match for the Farm site.	217
A.23:	TEM sounding data and inverse match for the Peat site.	219
A.24:	TEM sounding data and inverse match for Farmers Loop.	221
A.25:	TEM sounding data and inverse match for Eielson.	222
A.26:	TEM sounding data and inverse match for Quartz Lake.	224
A.27:	TEM sounding data and inverse match for Sawmill Creek.	226
A.28:	TEM sounding data and inverse match for Greely.	227
A.29:	TEM sounding data and inverse match for Fielding Lake.	229
A.30:	TEM sounding data and inverse match for Summit Lake.	230
A.31:	TEM sounding data and inverse match for Sourdough.	232
A.32:	TEM sounding data and inverse match for Glennallen.	234
B.1:	Program RHOA listing.	238
B.2:	Program RESPONS listing.	244
B.3:	Program IPVAX listing.	250

LIST OF TABLES

Table		Page
4.1:	Models used for inversion	94
4.2:	Curve matching geoelectric models for the 500 m loop size for the NPBS # 1 through Reindeer Island Line	95
4.3:	Computer inverse geoelectric models for 500 m loop size for the NPBS # 1 through Reindeer Island Line	95
A.1:	Sounding site locations	171

ACKNOWLEDGEMENTS

This thesis is dedicated to my wife, Bett Schaffhauser, for her loving support, proofreading, financial support and understanding. Love did not write this thesis, but it certainly helped.

The patience, exactness and scientific insight provided by Dr. Koji Kawasaki, the thesis committee chairman, are sources of inspiration which will endure. Another committee member, Dr. Thomas E. Osterkamp, was particularly helpful with borehole information at many of the sites and contributed in many other ways, including the proofreading of this thesis. In addition, the contributions provided by all the other committee members, Drs. Syun-Ichi Akasofu, Juergen Kienle, Kenneth J. Kokjer, John V. Olson, and Eugene Wescott, are greatly appreciated. The invaluable advice and proofreading provided by Dr. Joan Gosink are indeed over and beyond the call of duty.

The author gratefully acknowledges funding received from the United States Department of Energy, United States Geological Survey, National Science Foundation, Continental Oil Company, and the State of Alaska to support this research. Additionally, the efforts of John Petersen, Tim Matava and Victor Gruol greatly facilitated the TEM soundings. Geo-Physi-Con (now Earth Technology) often gave helpful instructions on the TEM method through Mark Blohm and Pieter Hoekstra. Conversations with David Fitterman and Walter Anderson of the United States Geological Survey greatly aided the process of computerized inverse modeling with program NLSTCI. Dr. James R. Wait provided theoretical and inspirational comments which have influenced the writing of this thesis.

Computer time provided by the University of Alaska and the Geophysical Institute enabled the processing of the TEM data and the typesetting for this thesis and is greatly appreciated.

Finally, the large motivation to provide for my twin sons (born August 19, 1988) goes beyond all previous motivations.

CHAPTER 1. INTRODUCTION

1.1 BACKGROUND

Permafrost is a permanently frozen layer of soil or other deposit sometimes including the bedrock and occurring at variable depth below the earth's surface primarily in arctic or subarctic regions. A working definition of permafrost has been given by Brown and Kupsch (1974) and Johnston (1981) as ground with a temperature below zero degrees Celsius for longer than one year (at least two consecutive winters and the intervening summer). As much as 75% of Alaskan land may have permafrost beneath the surface according to Ferrians (1965). Permafrost is continuous and very thick (up to 640 m near Prudhoe Bay) on the North Slope of Alaska. The Interior of Alaska has thinner, discontinuous permafrost and the southern part of Alaska has sporadic permafrost.

Permafrost is in quasistatic equilibrium with its natural environment. However, if some man-made construction disturbs the thermal regime of the ground, the permafrost may begin to degrade. Some permafrost is ice-rich, meaning that upon melting there is an excess of water, more than can be held within the pore spaces of the soil. These soils will collapse upon thawing. Therefore any structure built on or in such a soil will suffer stress when the permafrost melts. Man-made structures which have failed due to permafrost degradation include bridges, homes, airports, warehouses, roads, telephone poles, fences, wells and pipelines. Since permafrost can have such destructive effects upon man-made structures, knowledge of the presence and extent of permafrost is extremely important where construction is contemplated.

Permafrost is also of interest in hydrology because regions of ice-bearing soil hinder groundwater flow. Permafrost also influences the large and small scale patterns of surface drainage. Man-made structures, if they hinder surface and subsurface water flow, may create problems associated with water accumulation. The altered drainage patterns and exposure of soil surfaces may lead to topographic features such as palsas.

Permafrost near the surface will interact with vegetation in a complex way. Some vegetative types may insulate the ground during summer months leading to very cold ground temperatures and therefore thicker permafrost. The presence of near-surface permafrost limits the vegetative growth to only those types capable of growing in cold soils.

Permafrost can introduce problems for the geophysical exploration of mineral and petroleum resources. The presence of permafrost may dramatically alter seismic records. Erroneous interpretations of seismic reflection data resulted in costly drilling mistakes in the search of petroleum reserves in the permafrost areas of the Arctic, most notably in Prudhoe Bay, Alaska as noted by Specht et al. (1986). In addition, electrical grounding problems are often encountered in permafrost regions; these problems may alter signal strengths for geophysical exploration and for radio communication. Therefore, permafrost may confuse, confound and mislead a variety of mankind's endeavors. As Suslov is quoted by Lloyd (1962): "The geographer, climatologist, hydrologist, soil scientist, geomorphologist, botanist, entomologist, zoologist, agriculturalist, geologist, biochemist, engineer, architect, geophysicist, palaeontologist, archaeologist – all may find much to study and ponder in the regions where permafrost is found."

Information on whether or not permafrost occurs at a site may be obtained by drilling or excavating. These methods disturb the natural thermal regime of

the ground, are very expensive, and give no information on nearby undisturbed materials. Detection of lateral changes in material types or in permafrost occurrence requires the drilling of adjacent holes. Experienced drillers are often able to infer the presence of permafrost by examining drill samples and carefully recording the drilling rate which can be substantially lower in permafrost soils. However, some ice-bearing permafrost may not be sufficiently well-bonded at the transition zones near the table (top) and the base (bottom) of the ice-bearing permafrost to be detected by the driller.

The most direct method of determining the vertical extent of permafrost is by measuring the temperatures in a borehole. However, Lachenbruch et al. (1982) made a series of temperature measurements in a deep borehole on the North Slope of Alaska and showed that a period of time (up to several decades) is required after drilling for the temperature-depth profile to return to near normal (predrilling) conditions. Nevertheless, their results indicate that an estimate of the base of the permafrost ($\sim$ 600 m) accurate to within 5%, is possible within a few days to a few months after drilling.

Noninvasive, nondestructive, surface geophysical exploration techniques applied to the determination of permafrost occurrence, distribution, and thickness offer advantages of greater speed and lower cost over the use of drilling alone. Normally, however, without 'ground truth' from nearby boreholes, the vertical extent of permafrost cannot be assessed as accurately using these techniques as it can from in situ methods. The surface techniques are best used in the reconnaissance mode, that is, as an indicator of changes between boreholes and as a guide for determining the location of additional boreholes.

Surface geophysical exploration techniques which can be used for the investigation of the presence and extent of permafrost include seismic techniques and three

electrical techniques: direct current (DC) resistivity, frequency domain electromagnetics (EM), and transient electromagnetics (TEM). Seismic refraction techniques are valuable for the detection of the table of ice-bonded permafrost because seismic velocities in ice-bonded permafrost are generally higher than in unfrozen materials. Conversely, seismic refraction as well as reflection methods are generally not useful for the detection of the permafrost base where there is a change from high to low velocity. The three electrical techniques give information on the resistivity of the earth. Since the resistivity of permafrost can be orders of magnitude higher than the same material in the unfrozen state, a resistivity profile obtained at a given site can be used to infer the boundaries of the permafrost.

Although there is some debate about the relative merits of the three electrical techniques, the TEM method offers some advantages over the other two for soundings over deep permafrost. First of all, appropriate transmitter-receiver distances in the TEM method are usually smaller than the expected permafrost depth, a feature which is not true for the other two methods. This saves time in deployment of the system and makes the TEM method less sensitive to lateral resistivity variations as indicated in a recent paper by Sinha and Stephens (1983). Also, Ehrenbard et al. (1983) argue that the TEM method provides better resolution of the depth to the base of the permafrost than other electrical methods, because the estimate is relatively insensitive to the resistivity of the basement. Finally, because the soundings are easier to take and the experimental layout is less extensive, the overall productivity of the TEM method should be better over thick permafrost than the other electrical methods.

There are some disadvantages of the TEM method. These are mainly due to the relative newness of the technique vis á vis the more mature states of the DC

and EM methods and include the lack of computer software to invert TEM data to useful 2 and 3-dimensional resistivity models.

While the recent papers by Ehrenbard et al. (1983) and Sinha and Stephens (1983) (see Section 1.3 for a review of these papers) give general support to the use of the TEM technique for permafrost detection, many questions remain unanswered, in particular with respect to data correction procedures, uniqueness of interpretation, applicability to permafrost in a variety of settings, and other problems. Initially an investigation of the applicability of the TEM technique to permafrost was central to the aims of the present thesis; however, it is in the context of the questions on data correction procedures, parameter variations, and the existence of anomalous TEM data that the present work has evolved.

The following specific topics have been investigated in this thesis (the numbers in square brackets give the chapter numbers where discussion of the points appear – a more detailed description of each chapter follows in Section 1.2).

(1) Observation and modeling of an anomalous double sign reversal in TEM data from the Kuparuk area of the North Slope [5]. This type of anomalous TEM response has never before been reported in the literature.

(2) Correction for finite time of current turnoff (ramp time correction) in the TEM method [2,3,4,5]. The new and original correction procedures used for the data of this thesis predate a recent paper by Fitterman and Anderson (1987) wherein the effects of the turnoff time are explored in some detail.

(3) Estimation of instrumental error, parameter variation studies of output models and discussion of uniqueness in TEM geoelectric models [1,3]. These have not appeared in the literature on permafrost TEM data previously.

(4) Use of an existing computer program to invert TEM data in permafrost terrain [3,4,Appendix A]. The inverse modeling also allows an objective comparison of the match between the data and the geoelectric model. This is the first application of inverse modeling to permafrost TEM data.

(5) Detailed study of subsea permafrost [4]. A line of TEM soundings was taken over sea ice to determine the extent of permafrost. This study is similar to the one of Ehrenbard et al. (1983), but the analysis is more extensive and the results seem to compare more favorably with some of the known subsea permafrost parameters. Comparisons of 3 to 6 layer models are made showing

that interpretations of deeper subsea permafrost structures in a multi-layered medium suffer from rapid decrease of signal level due to the highly conductive environment and nonuniqueness in the solution space.

(6) TEM studies of many land sites with less than adequate ground truth [Appendix A]. This is a reconnaissance study of permafrost mainly along the Trans-Alaska Pipeline System (TAPS) corridor which indicates there are locations where permafrost may be thinner than might be expected from surface temperature data.

1.2 THESIS OUTLINE

For the general purpose of permafrost investigation, 32 TEM sounding sites, roughly along the Trans-Alaska Pipeline, were sounded during the summer (August and September) of 1983. The locations of the sounding sites are displayed in Figure 1.1. These sounding sites are described more fully in Appendix A and the interpretations of the soundings at two of these sites (West Dock and Deadhorse), where a reasonable amount of subsurface information is available, are discussed in Chapter 3. In 1984, some of the sites of 1983 were sounded again and an offshore line of sounding sites was established. This offshore line extended two kilometers inland along a line from the wellhead of the exploratory North Prudhoe Bay State #1 well through Reindeer Island and one kilometer past as shown in Figure 1.2. This line of sounding sites is discussed more fully in Chapter 4. The West Dock site and the Reindeer Island sites are further discussed in Chapter 3.

Section 1.3 of this thesis gives relevant historical information on permafrost. The fundamental principles underlying electrical conduction in solid earth materials are discussed in Sections 1.4. Section 1.5 places emphasis on the temperature dependence and the importance of freezing-point-depression for the resistivity of soils. Section 1.6 includes remarks on Archie's law, an empirical relation for the

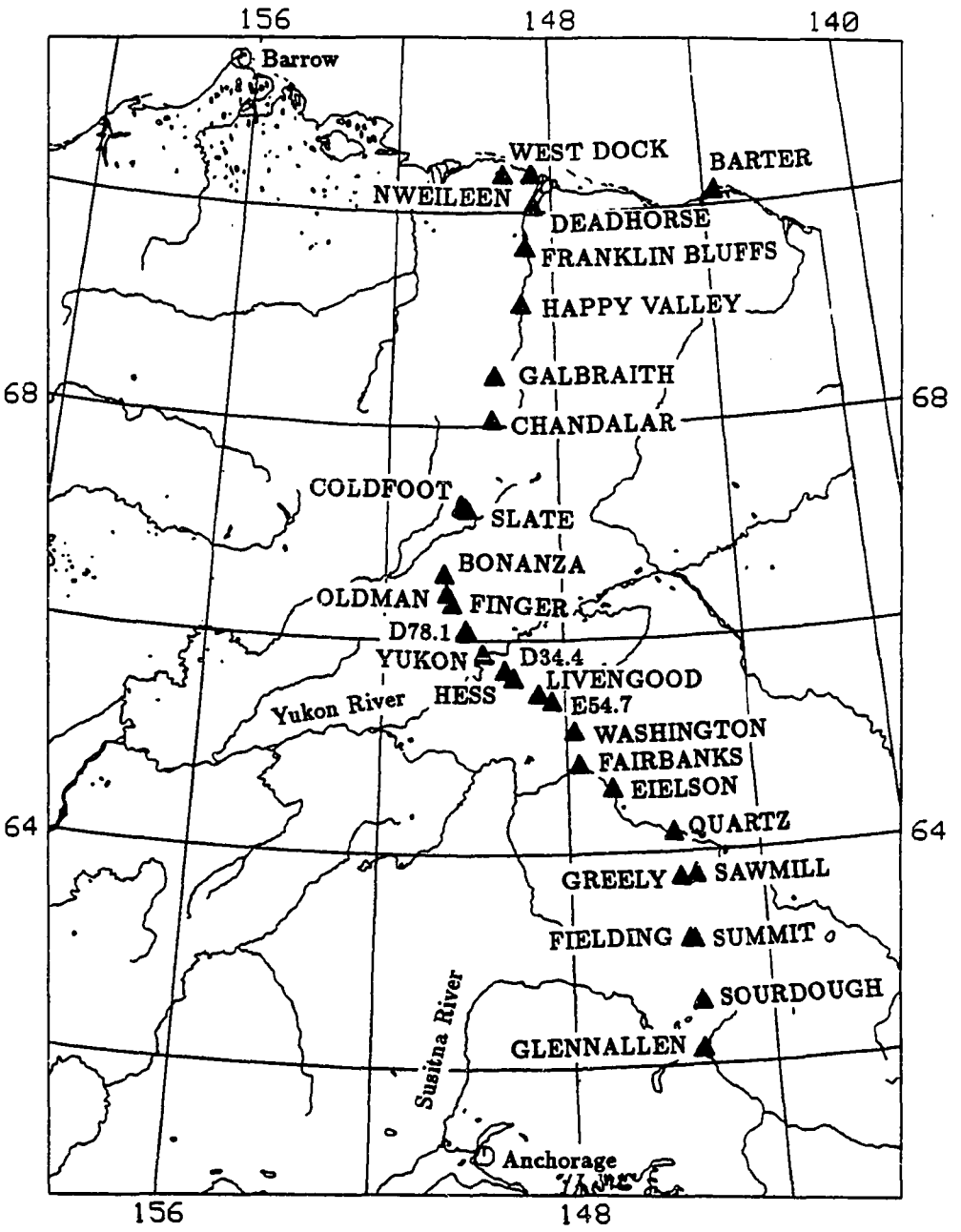

Figure 1.1 Transient electromagnetic sounding sites occupied during August and September of 1983. The sounding sites are denoted by triangles and capital letters. The Fairbanks site represents five separate sounding sites: Virgin Spruce #1, Virgin Spruce #2, Farm, Farmers Loop, and Peat sites.

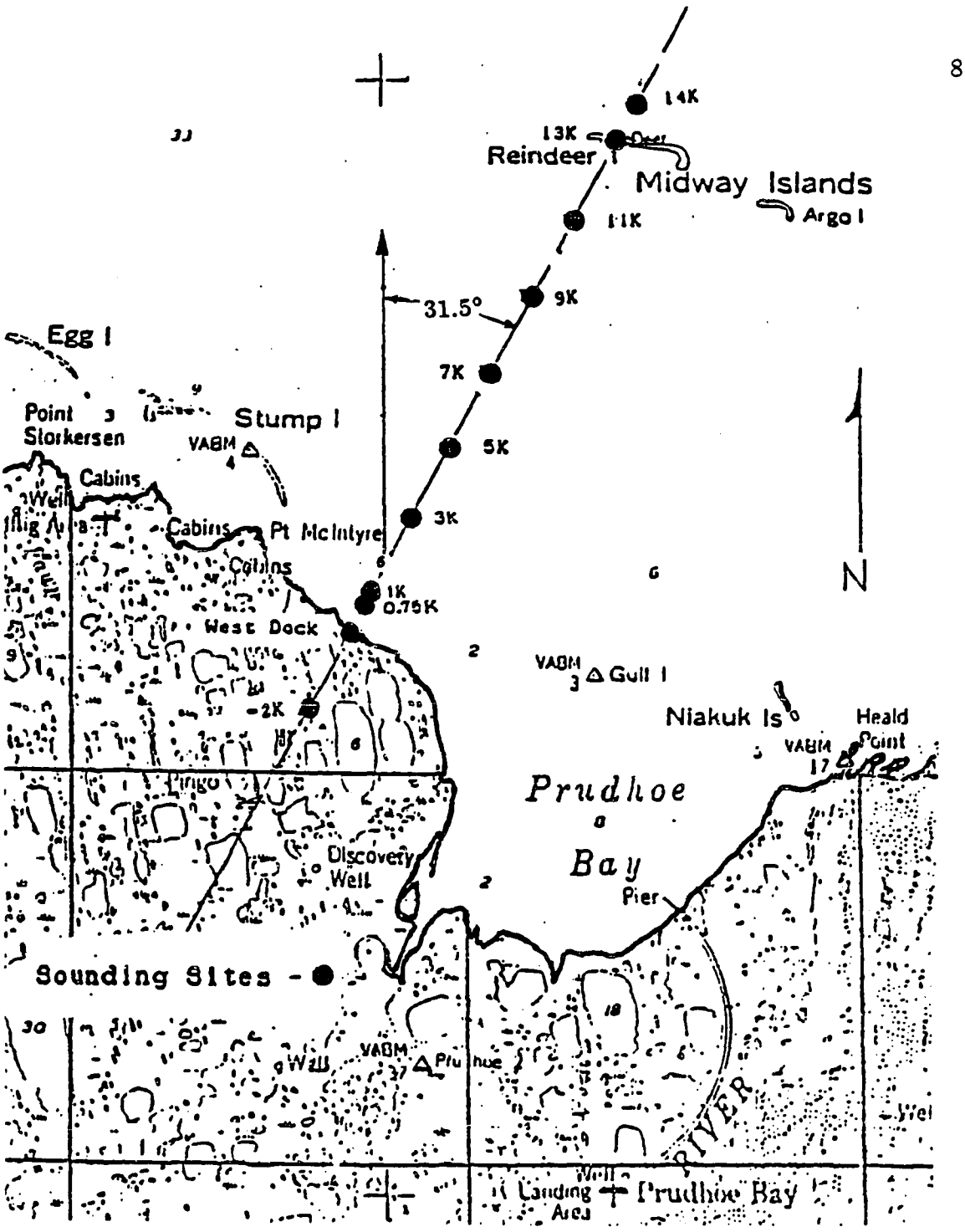

Figure 1.2 Subsea and associated transient electromagnetic sounding sites occupied during May of 1984. The site designations refer to the distance from the wellhead of North Prudhoe Bay State #1 exploratory well along a line through Reindeer Island.

resistivity of porous media. Section 1.7 describes the features of the TEM system used for this study and the experimental configuration.

For completeness, the theory of transient electromagnetic induction using the EM-37 is reviewed in Chapter 2. The general theory of the method is given in Section 2.2 and covers the analytic solutions for layered and homogeneous half-space earths. A method for determining the solution for an arbitrary number of layers is outlined. Asymptotic solutions for early and late times and their relationship to apparent resistivity are given in Section 2.3. The procedures used for correcting data for the drive current ramp turnoff time are also discussed.

Chapter 3 gives a detailed analysis of the TEM data from three sites for which a reasonable amount of well-log information from nearby locations is available to provide 'ground truth' on subsurface materials. The three sites are located on the North Slope of Alaska, one near the West Dock of Prudhoe Bay, a second on Reindeer Island in Prudhoe Bay, and a third a little south of Deadhorse Airport.

Chapter 4 gives the locations, experimental procedure, data and interpretations for the sites surveyed over sea-ice and on Reindeer Island. These sites are over very conductive materials and therefore require a different procedure for turnoff correction than is used at the sites described in the previous chapter and Appendix A. The correction procedure is discussed in this chapter. The conductive materials also lead to ambiguous inverse models due to rapid reduction of signals in the later gates.

Chapter 5 is a detailed discussion of an anomalous TEM response observed at a site in the Kuparuk region of the Alaskan North Slope. This response may be due to an Induced Polarization (IP) effect. The effect is modeled using complex resistivity in a layered earth. This approach may allow an understanding of anomalous TEM signatures which display sign changes. It is also possible that these sign changes

may indicate the presence of gas hydrate structures and thus that the TEM method could prove to be a valuable exploration tool for such energy resources.

The summary and conclusions are presented in Chapter 6. Appendix A gives the locations, experimental procedure, background data and interpretations for the majority of the TEM sites. These sites form a North-South transect of Alaska roughly along the trans-Alaska pipeline from Prudhoe Bay to Glennallen. Appendix B contains the programs used for ramp time correction, computation of apparent resistivity, plotting, introduction of induced polarization effects, and convolution-deconvolution. Appendix C contains all the TEM data as recorded in the field.

1.3 A BRIEF HISTORY OF PERMAFROST INVESTIGATION

The term "permafrost" was first used by Muller (1945). There were, however, numerous references to the occurrence of frozen ground existing below the level of the seasonal freeze-thaw zone well before this date. The earliest of these is believed to be given in the military reports of Glebov and Golovin around 1642 in Siberia as reported by Tsytovich (1963) and Washburn (1980). Legget (1963) cites the writing of Joseph Robson published in 1752 and James Isham in 1743 as very early observations of permafrost in the Canadian Northwest. More scientific investigations of permafrost did not take place until the 1800's when Middendorff (1853) reported temperature measurements taken in permafrost in Siberia.

Tamura (1905) gives a review of the mathematical theory of ice formation crediting the work of Joseph Fourier for the basic formulation of the mathematical theory of heat conduction. Stefan (1891) and Franz Neumann were the first to develop mathematical models describing the penetration of frost into the ground.

Their analyses laid the groundwork for the subsequent investigation of permafrost aggradation and degradation. The more general analysis of Neumann in 1862 is given in Reimann-Weber (1912) and Neumann's solutions are given in Carslaw and Jaeger (1959). The importance of the contributions of Neumann and Stefan is apparent in modern texts where their solutions are still presented. For example, Johnston (1981) and Lunardini (1981) use these solutions to provide the framework for modern analysis. It is not possible to achieve analytic solutions for any but the simplest transient heat conduction problems involving phase change (see Kawasaki et al., 1982). In modern analyses of the problem of freezing and thawing of ground, finite difference or finite element schemes are used in computer simulations of coupled heat and moisture transport to provide solutions for two and three-dimensional geometries.

It is well known that the frost penetrates from the surface downward due to cold temperatures at the surface of the earth. Therefore, climate is the most important element in determining the extent of permafrost. Another important element is the natural geothermal heat flow from within the earth; this heat flow tends to melt permafrost at its base. The thermal properties of the earth materials are also important. At a given site, permafrost thickness will be controlled by long-term temperatures at the surface. The thickness of permafrost, $\Delta X = K\Delta T/J$, depends upon the thermal conductivity K, the geothermal heat flux J, and the mean annual surface temperature (MAST) ΔT.

It is widely believed that much of the very thick permafrost is relict from past ice-ages when the global temperatures were colder. Hopkins (1967) maintains that geomorphological evidence of historical sea-level elevation fluctuations are an indicator of past global temperature fluctuations. Higher sea-level is associated with warm temperatures and lower sea-level is associated with cold temperatures. In this

scenario, the northern shores bordering the Arctic Ocean experienced local temperature changes of large magnitude as the water level rose and fell. The temperatures at the surface were coldest during exposure of the land and warmest when the land was covered with water. Historical cycles of submergence by water and subsequent emergence led to the present complex subsea permafrost environments as related by Vigdorchik (1980) and discussed in Chapter 4.

Much of the early knowledge of the extent of permafrost was discovered as a byproduct of the northward advance of civilization. Wells drilled for ground water, mining operations, construction of buildings, roads and railroads, and land clearing for crop cultivation uncovered information about the location of permafrost. Early maps of permafrost distribution were produced by pioneer permafrost investigators such as Péwé (1948) and Ferrians (1965) for the United States and Brown (1960) for Canada and the U.S.S.R.. Péwé (1982) has compiled pioneer encounters with permafrost in *Geologic Hazards of the Fairbanks Area, Alaska.*

The earliest electrical geophysical prospecting for minerals was done by Conrad Schlumberger in 1912 (see Alluad, 1977) using the direct current (DC) resistivity method. In the same year, Wenner (1912) reported the first use of the four-electrode array. Akimov and colleagues investigated seismic velocity and DC resistivity for the delineation of frozen ground in the 1930's (see Akimov et al., 1979). By the late 1930's, Joesting (1941) was using DC resistivity for mineral exploration in Alaska. Concurrently, DC resistivity was being used in the Soviet Union by Dostovalov (1947) for the same purpose.

The earliest work with DC resistivity showed the feasibility of determining the extent of permafrost. In 1939, Joesting reported to the Commissioner of Mines for the Territory of Alaska, "Resistivity work has been done on problems that are of indirect importance to prospecting ...[including the]... delineation of frozen and

thawed areas." Since these early studies were often undertaken to find the depth to bedrock, Joesting was dismayed when at Mammoth Creek the "main break ...[of the resistivity curve]... appears to be at the base of the frozen ground rather than at the top of bedrock." Joesting considered permafrost a complication of his problem of finding the depth to bedrock.

DC resistivity remains an important tool for the electrical investigation of permafrost even though the determination of thick permafrost requires array spacings that are as much as three times the expected permafrost thickness. Long wire lengths mean a great amount of time and labor in the field. Also, since the DC method energizes a half space proportional to the array dimension, the method suffers from a lack of horizontal resolution. DC resistivity is of great value for the determination of thin permafrost because the interpretation process is well known, the equipment is relatively portable, and array dimensions are more manageable than in its application for thick permafrost.

The development of electromagnetic tools for the exploration of subsurface properties (see Heiland, 1940) led to the use of these tools for the exploration of permafrost and is reviewed by Scott et al. (1978) and Scott and Brown (1980). Much background information for the application of frequency domain EM methods to permafrost is covered in Hoekstra and McNeill (1973). The theoretical and practical advantages of EM methods were recognized very early. Daniels et al. (1976) obtained the first known EM measurements made over thick permafrost. The earliest publications on the TEM method for permafrost investigation are by Ehrenbard et al. (1983) and Sinha and Stephens (1983).

Sinha and Stephens (1983) discuss deep electromagnetic soundings over permafrost in the Canadian Mackenzie Delta using both TEM and multi-frequency EM techniques. They claim that the transient system in the central induction mode is

is less susceptible to lateral inhomogenieties than the multi-frequency method. The difficulty with the multi-frequency method is primarily due to the very large transmitter to receiver distances required by this method in order to obtain exploration depths approximating the permafrost thickness. Using the TEM technique, Sinha and Stephens (1983) developed models which agreed with permafrost thickness to within 5% of that resulting from temperature logging, but they noted the possibility of equivalence (the nonuniqueness problem discussed elsewhere in this thesis) of different models. Sinha and Stephens (1983) obtained their results by matching forward modeled curves with the TEM data and did not take advantage of the finer tuning (resulting in a lower rms error between the data and the model) that is possible with computerized inverse modeling. Also, the interpreted TEM models predicted resistivities that are generally higher in magnitude than those obtained by uncorrected, in situ, borehole resistivity logs. The problem of correcting resistivity logs in permafrost is discussed in Chapter 3 of this thesis.

Ehrenbard et al. (1983) used TEM soundings along a line over sea ice in the Prudhoe Bay area of the North Slope of Alaska to construct a cross-section of subsea permafrost extending about 9 km offshore. Although the exact location of this line is proprietary information, it appears from the given location of Gull Island that the line extends across the mouth of Prudhoe Bay or is partly within Prudhoe Bay. Even though this profile line appears to extend over an area that may have a different paleohistory of submergence than that discussed in Chapter 4 of this thesis, the two subsea permafrost profiles are somewhat similar. Also, as in the paper of Sinha and Stephens (1983), models for the TEM data were selected by matching forward modeled curves. Ehrenbard et al. (1983) claim a sensitivity 3 times higher for the TEM technique than can be obtained by any other electrical technique for the determination of the depth to a conductor (permafrost base).

In summarizing the prior papers (Sinha and Stephens, 1983; Ehrenbard et al., 1983) on TEM soundings of permafrost, the following points should be noted.

(1) Both papers used the traditional, forward-modeling, curve-matching scheme to fit layered earth models. This scheme does not take advantage of the greater flexibility for varying the parameters of the models and the unbiased evaluation of the match between TEM data and the interpreted model which is afforded by the computerized inverse modeling technique.

(2) Neither paper assesses the effects of varying any particular parameter in the TEM models presented.

(3) Neither paper discusses the repeatability of the TEM data nor potential sources of errors in the TEM data.

(4) Corrections for the finite turnoff time of the transient transmitter (ramp time turnoff correction), which are important in the final output model, are apparently ignored in both studies.

(5) The differences between in situ borehole resistivity measurements and the models derived from the surface EM measurements are not discussed.

(6) Neither paper addresses the problem of nonuniqueness in the TEM models.

As indicated in Section 1.1, all of the above problems are considered in the present investigation.

1.4 ELECTRICAL CONDUCTION IN SOLIDS

The concept of resistivity, ρ, and its inverse, the conductivity, σ, comes from the property of any material, in reaction to an external electric field $\vec{E}$, to produce a current flow. The constitutive relation known as Ohm's Law, $\vec{J} = \sigma\vec{E}$, gives the current density, $\vec{J}$, as related to the material property σ. The property of resistivity of a material such as a soil depends in a complicated way on the physical configuration of the individual grains, their shape, their individual electrical properties, the temperature and pressure of their surroundings, the continuity and amount of void spaces within the material, and the proportion of the voids filled with liquids and the electrical properties of the liquid.

There are three distinctive types of electrical conduction in solids: 1) metallic, 2) semi-conductor, and 3) ionic. Metallic conduction involves electrons freely moving under the application of a small electric field. Semi-conductors require sufficient electric field strength to overcome the potential barrier between the normal state (charge not free to move) and the conductive state. Ionic conduction involves the transport of ions within the material, normally along paths within the pore spaces which contain a liquid electrolyte. An example of a liquid electrolyte is saline water. Most pore waters found in nature have sufficient dissolved ions to be classified as ionic conductors.

In metallic conduction, electrons in the conduction bands are weakly bound to their host molecule or atom and therefore are free to move upon the application of an external electric field. The force felt by the electrons is $\vec{F} = q\vec{E}$, where $\vec{F}$ is the force on the electron, q is the charge of the electron and $\vec{E}$ is the applied electric field. The electrons in metallic conductors are so weakly bound they may be analytically treated as a free "Fermi gas," see Kittel (1976). However, in a semi-conductor, there is an energy gap between the highest energy valence and the lowest energy conduction bands. Thermal excitation may raise the energy level of a valence electron into the conduction band, hence the name semi-conductor.

The energy gap is larger in some materials than in others. Most materials at normal temperatures that are not metallic conductors are semi-conductors. However, the energy gap is so large in some materials that little conduction is observed even at high temperatures. Electrolytic conductors may be classed as solid or liquid. Solid electrolytes are ionic bonded materials whereas liquid electrolytes are often composed of dissociated ions in a water solution. $NaCl$ becomes Na^+ and Cl^- in a water solution and these ions are free to move under an applied electric

field. Solid electrolytes are limited in movement since the molecules are still bonded together. Both electrolytic conduction types may give rise to polarization effects.

1.5 TEMPERATURE DEPENDENCE OF RESISTIVITY

As early as 1833, Faraday investigated the temperature dependence of resistivity upon phase change (freezing). Recent investigations (Hoekstra and McNeill, 1973; Olhoeft, 1975; and Pandit and King, 1979) clearly show that the resistivity of earthen materials dramatically increases upon freezing. This increase in resistivity upon freezing can be used to investigate the thermal state of the solid earth. It is clear from nuclear magnetic resonance (NMR) studies such as Tice et al. (1978) that unfrozen water exists within natural materials even at very cold temperatures. The dramatic change in resistivity, therefore, arises from a blockage of conduction paths when only a portion of the water content has changed to the ice phase (ice-bearing).

A decrease or lowering of the freezing point known as the freezing-point-depression may occur due to solutes, pressure, and soil particle effects. Soil particle effects may be broken into two classes, 1) those due to geometrical effects (interface curvature) and 2) those due to surface effects of an electrical or chemical nature.

Interface curvature effects are most dramatic in clays where the particle sizes are less than 0.004 mm in size. With decreasing particle size and hence increasing curvature, the freezing-point-depression due to interface curvature, ΔT_c, follows the relationship

$$\Delta T_c = \frac{4.44 \times 10^{-9}}{r}, \tag{1.1}$$

where the radius of curvature, r, of the soil grains is in meters and ΔT_c is in degrees

Celsius. This effect accounts for a part of the larger freezing-point-depression of clays over silts and of silts compared to sands.

Other soil particle effects are due to the nature of the particle surface. An empirical relation was used by Anderson et al. (1973) to predict the freezing-point-depression (ΔT_{sp}) due to all soil particle effects using the fractional unfrozen water content (W). Two constants (A, B) are empirically determined to match the data using the relation

$$\Delta T_{sp} = (W/A)^B. \tag{1.2}$$

Increasing salinity causes an increasing freezing-point-depression. The freezing-point-depression due to solutes (ΔT_s) for dilute solutions with ionic concentration ratios similar to sea water is

$$\Delta T_s = 0.0137 + 0.051990S + 0.00007225S^2, \tag{1.3}$$

where S is the concentration of salts in parts per thousand and ΔT_s is in degrees Celsius (Doherty and Kester, 1974).

Increasing depth in saturated soils produces higher hydrostatic pressure and increases the freezing-point-depression. The freezing-point-depression due to pressure, ΔT_p, may be related to the depth as

$$\Delta T_p = 7.53 \times 10^{-4}\ Z, \tag{1.4}$$

where Z is the depth in meters from the freshwater table (Doherty and Kester, 1974).

Since the freezing-point-depression and resistivity depend upon so many variables whose values are usually not well known, predicting the resistivity of permafrost as a function of temperature is not generally possible. While it is not possible to predict the electrical resistivity of permafrost, it has been well documented

that the resistivity of materials with electrolytic pore water increases dramatically upon phase change from liquid to solid state. The experimental results of several research studies as reviewed and summarized in Hoekstra and McNeill (1973) are shown in Figure 1.3. This figure shows that there is considerable change in the resistivity of common materials upon freezing, including for example, solid rocks with very little water content.

The temperature dependence of conductivity for temperatures above freezing for rocks saturated with electrolyte is

$$\sigma = \sigma_0[1 + \beta(T - 18)]. \tag{1.5}$$

This equation, from Heiland (1940), with temperature T, in degrees Celsius and proportionality constant β (β is about 0.025 per degree Celsius for most electrolytes), clearly shows an increase of conductivity with an increase in temperature. The conductivity of electrolytic conductors increases with temperature, whereas the conductivity of metallic conductors decreases with increasing temperature in the absence of phase change.

In this study, the primary conduction mechanism will be considered to be electrolytic because this mode of conduction is dominant in rocks and soils with dissolved ions in their pore waters. However, the bulk conductivity of a material depends upon the porosity, percentage of voids filled with pore water, temperature, and the conductivity of the pore water. The next two Sections discuss these relationships.

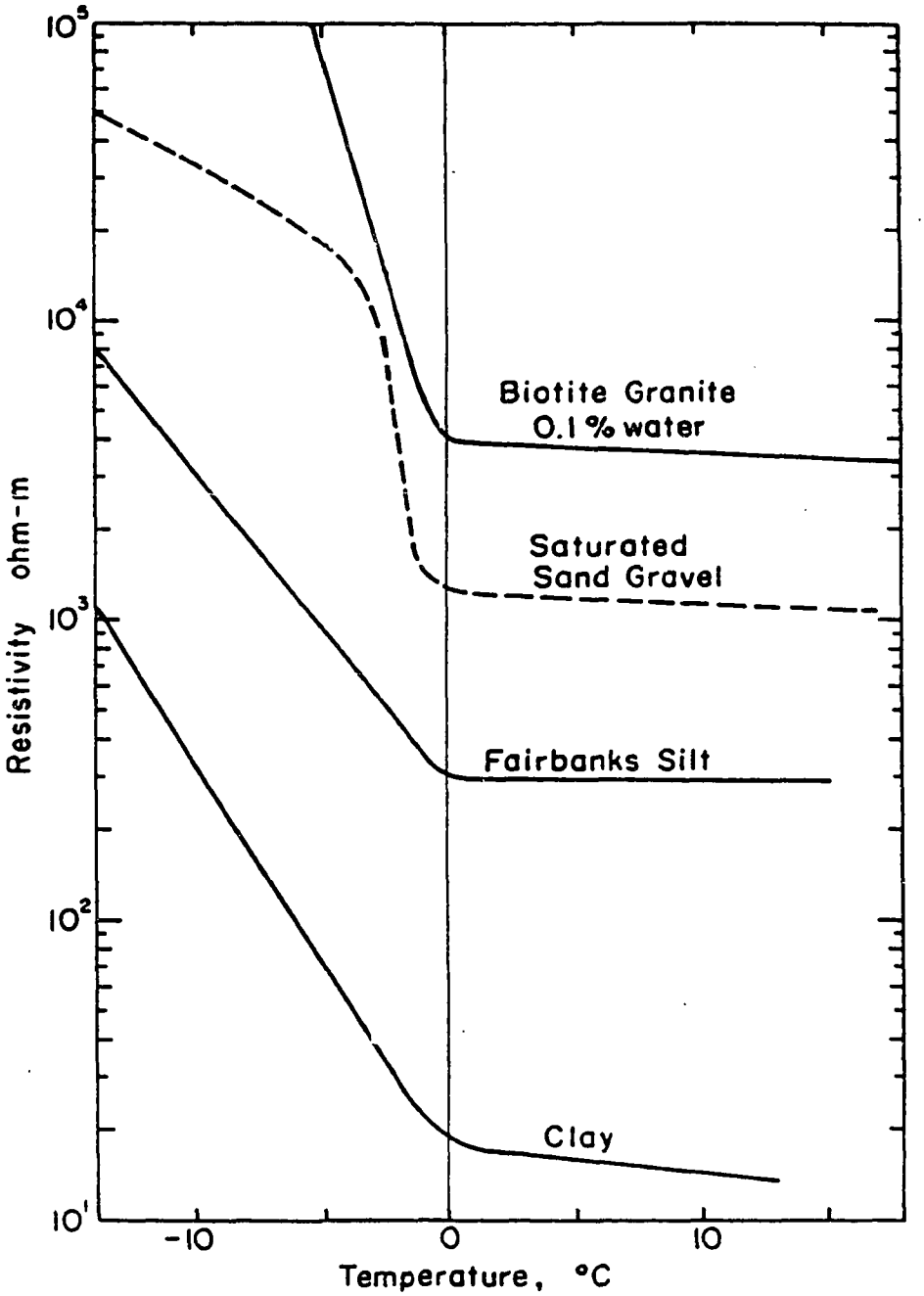

Figure 1.3 The resistivity of various soils and one rock type as a function of temperature adapted from Hoekstra and McNeill (1973).

1.6 BULK RESISTIVITY AND ARCHIE'S LAW

Archie's law (Archie, 1942), for thawed rock,

$$\rho = a\rho_w\theta^{-m}s^n, \tag{1.6}$$

gives the bulk resistivity (ρ) of a rock in terms of the resistivity of the pore water (ρ_w), the porosity (θ) of the rock, and the fraction (s) of pore spaces containing pore water. The constants a, m and n are determined by fitting experimental data for a material type to Equation 1.6. The conspicuous lack of an explicit term for the resistivity of the host rock which contains the electrolyte is primarily due to the very high resistivity of most dry rocks. Notable exceptions are metallic ores and graphite deposits. For many rocks a is about 1 and n and m are about 2.

Following the studies by Sen et al., (1981) on the electrical properties of fused glass beads saturated with an electrolytic solution, the conductivity, σ, is given by

$$\sigma = \sigma_w\theta^{1/(1-L)}, \tag{1.7}$$

where σ_w is the conductivity of the pore water, and the shape of the individual grains in the material matrix, relative to the applied field direction, determines the value of the constant L. Equation 1.7 exhibits a strong dependence on shape which defines the anisotropic electrical characteristics of a bedded material such as shale. For electrical fields perpendicular to the layering of a material having bedding planes, L approaches 1 and the conductivity approaches zero, whereas for electrical fields parallel to the layering, L approaches zero and the conductivity

approaches the conductivity of the pore water. If the matrix consists of spheres, $L = \frac{1}{3}$, Equation 1.7 then becomes

$$\sigma = \sigma_w \theta^{3/2}. \tag{1.8}$$

Equation 1.8 was verified for fused glass beads by Sen et al., (1981). In general, since soil particles are not spheroidal in shape, the exponent of the porosity term varies. Sandstone fits the model fairly well (spheroidal shaped particles) and the experimental evidence shows that the exponent of θ, $1/(1-L)$, varies between 1.2 to 4 for empirical fits to Archie's law.

1.7 DESCRIPTION OF THE TEM METHOD

The transient electromagnetic (TEM) method used for this study is the central induction method (receiver in the center of the transmitter loop) for measuring the vertical magnetic field (receiver loop is coplanar with the transmitter loop) which varies with time. The instrument used for all soundings was a EM-37 made by Geonics Limited of Canada. The method involves passing current through a transmitter loop lying flat on the surface of the earth. As schematically illustrated in Figure 1.4, the current is bipolar with twenty-five percent duty cycle on the positive current pulse and twenty-five percent on the negative current pulse. Note also that the current pulses have an exponential rise and a linear fall or turnoff. Time begins at the end of the ramp turnoff.

The transmitter loop, a single copper wire (# 10) with plastic shielding, is formed by connecting four separate wires at the corners of a square. As illustrated

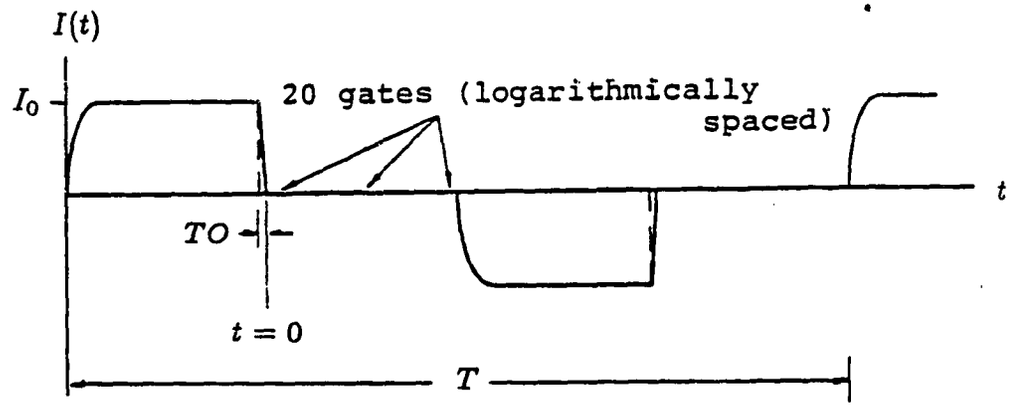

Figure 1.4 The Geonics EM-37 transmitter current waveform with a repetition period of T, a maximum current of I_0, and a ramp turnoff time of TO adapted from McNeill (1982).

in Figure 1.5, the plan view of a field site, a receiver coil is located coplanar with and at the center of the transmitter loop.

A three kilowatt generator runs a four hundred Hertz, three-phase, one hundred twenty volt alternator to provide power for the transmitter console. The transmitter console controls the pulse repetition rate and measures the resistance of the transmitter loop, the output current and the turnoff time. The transmitter console provides the current described in Figure 1.4 to the transmitter loop. The receiver console is battery powered and the transmitter derives its power from the alternator.

Both transmitter and receiver consoles are crystal-controlled for timing. The crystals are very stable, temperature-controlled oscillators. Initially the transmitter and receiver are connected together and the crystal oscillators are phase locked. The phase locking is necessary since the receiver console will be removed to the center of the transmitter for sounding measurements and precise timing is essential. While the transmitter runs at one corner of the transmitter loop, the receiver is connected to the receiver coil and measures the induced voltage during the off time of the

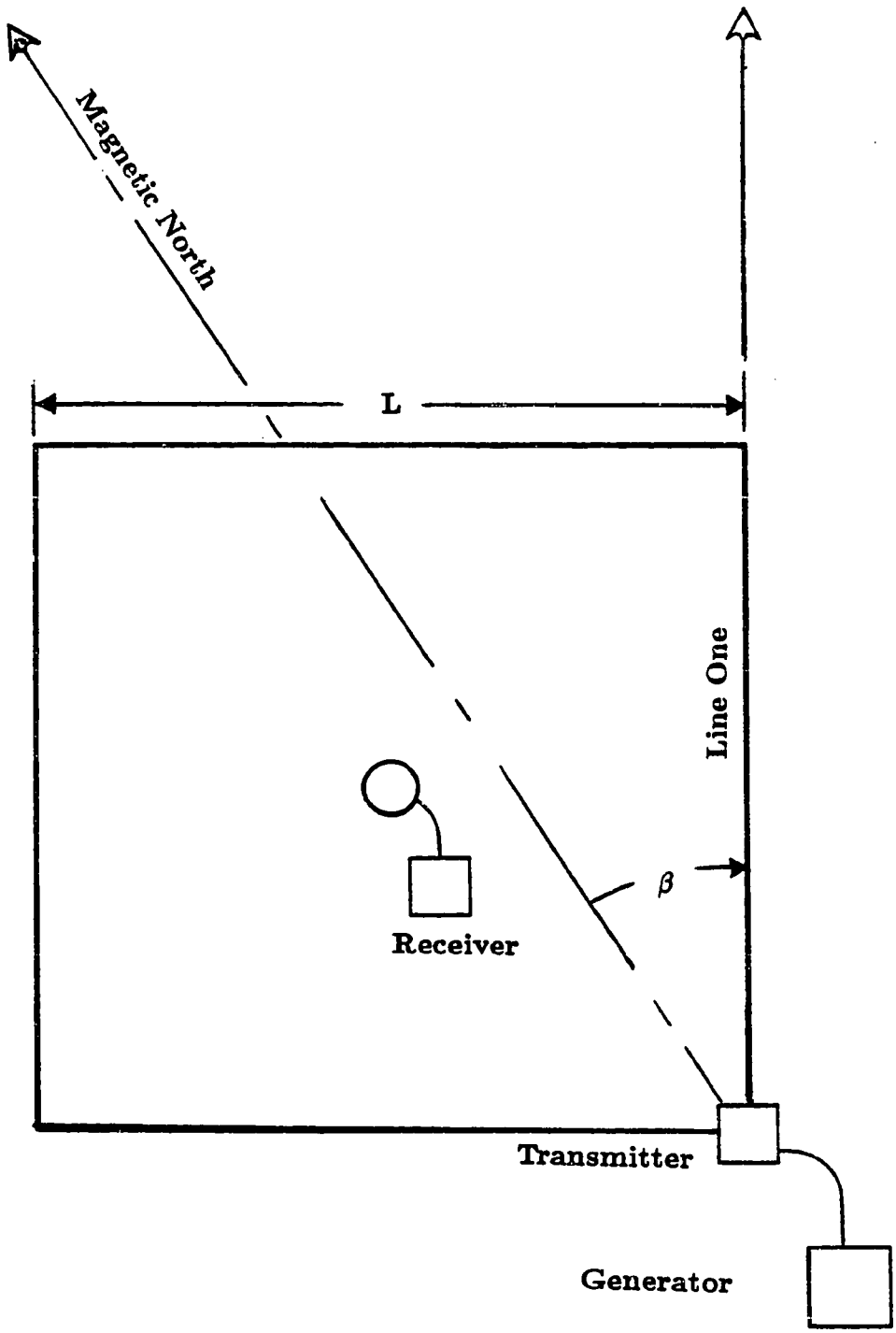

Figure 1.5 The plan view of a TEM field site showing the small receiver coil at the center of the large, square transmitter loop having sides of length L. The bearing of Line 1 is measured clockwise from Magnetic North.

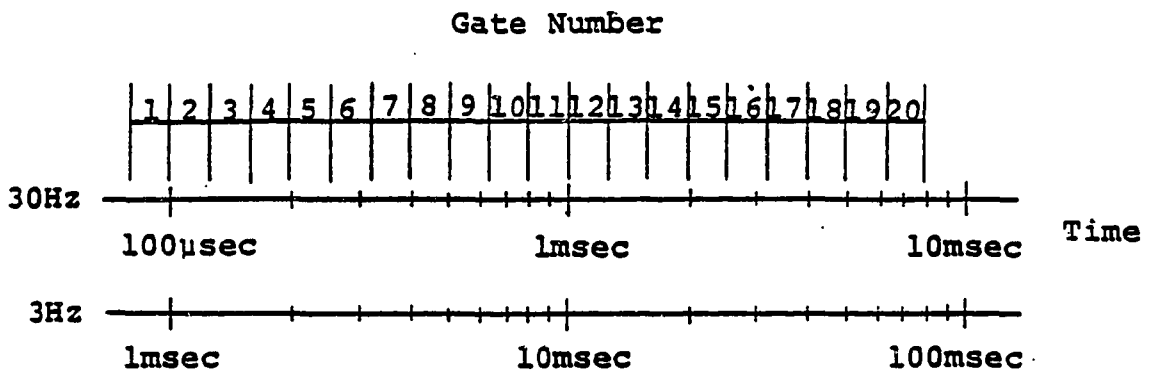

Figure 1.6 The Geonics EM-37 receiver gate locations for the repetition rates of 30 and 3 Hertz after McNeill (1982). Time starts at the end of the ramp turnoff. Note that the gate times and widths are evenly spaced in logarithmic time.

transmitter drive current. The off time begins at the end of the ramp turnoff time. The measured signal is taken at 20 discrete gates evenly spaced in logarithmic time as displayed in Figure 1.6. The times of the twenty gates (t_g) depend upon the repetition frequency of the transmitter current.

The receiver console controls the gain of the receiver electronics (2^n where n is the receiver gain setting), the stack setting (2^N pulses are averaged for a receiver display where N is the stack setting), and the polarity of the input connection to the receiver electronics. The receiver console requires the input of the transmitter turnoff time so that measurements are only taken after the ramp turnoff. Additionally, the receiver gives an indication of the outside noise.

The receiver console settings and gate voltages are recorded for each sounding. A single sounding set consists of two soundings recorded using different receiver polarity settings while all other receiver and transmitter settings are the same. A number of sounding sets are taken at each site with different gain and stack settings to check the operation of the TEM system and to give an indication of the repeatability of the data. If the data varies directly as the gain, then the medium

is displaying linear response. If the data taken with longer stacking times (higher stacking number) displays about the same variation as the data taken with a shorter stacking time, then longer stacking times were not necessary and each data set could be used in the production of apparent resistivity data. The data collected in the field are corrected for ramp time and converted to apparent resistivity. The ramp time correction procedure and definitions of apparent resistivity are explained in Chapter 2.

It is possible to gain an insight into the operating principles of the TEM method using the work of Nabighian (1979). In Figure 1.7 a sequence of plots is displayed which show the change in time of the current maximum induced in the ground following the abrupt termination of a magnetic dipole on the surface. At early times the current is close to the surface, but as time passes the current maximum diffuses downward and outward from the source. Because the signal received back at the receiver coil depends upon the strength of these currents, a major part of the received signal will come from the region of the current maximum. As the induced eddy current maximum diffuses downward with time, the received signal will be related to the resistivity of the ground at deeper depths. In addition, the eddy current maximum broadens in space as it diffuses downward, which means the received signal represents a larger volume as time goes on. The work of Raiche and Gallagher (1985) definitively shows that the diffusion velocity of this eddy current maximum is not a constant and depends strongly on loop size. Raiche and Gallagher (1985) claim that conversion to pseudodepth sections did not produce reasonable correlations to geoelectric structure.

The apparent resistivity of the ground may be related to the voltage induced in the receiver coil, the dimensions of the transmitter loop and receiver coil, the current in the transmitter coil and time (see Chapter 2 for the asymptotic forms

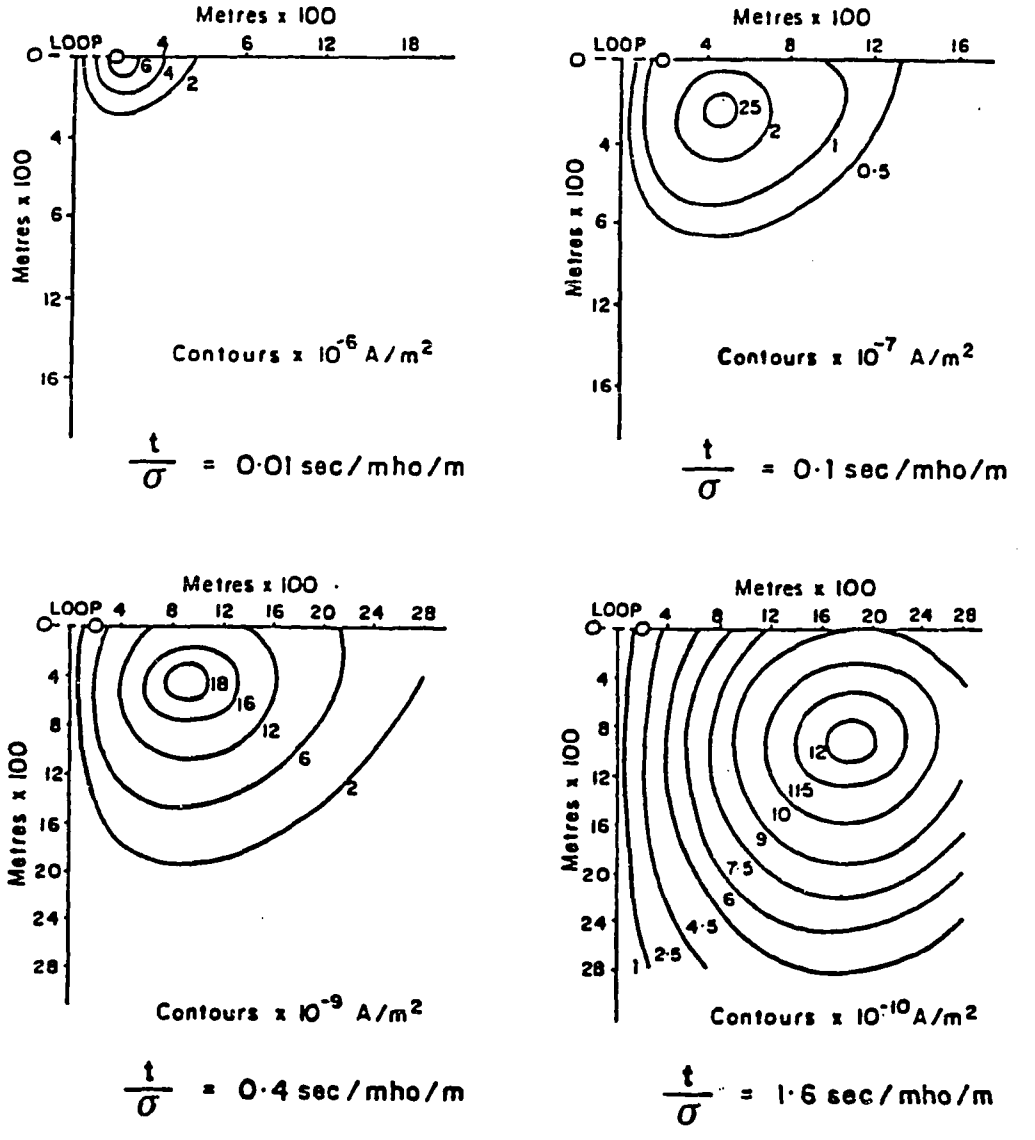

Figure 1.7 Four 'snapshots' of the diffusion of the eddy current maximum from a TEM system. (a) shows the eddy current maximum is near the surface in early time, in (b) the maximum has moved downward and outward, continuing to move in (c) and (d) downward and outward from the loop center as time goes on. The eddy currents flow perpendicular to the paper. (after Nabighian, 1979)

for the early and late time approximations for the apparent resistivity; Ehrenbard et al. (1983) also give a useful discussion of these asymptotic forms). Once the apparent resistivity data are calculated, computer programs are run with varying geoelectric models in an attempt to match a model to the data. Factors possibly complicating the interpretation of the TEM data include: 1) the nonuniqueness of the model solutions, 2) the medium in question may not fit the layered earth scenario, 3) the medium in question may not display simple resistivity response, e.g., induced polarization effects are present, 4) equipment and external sources may produce noise in the data, 5) a square loop is used whereas the theory is developed assuming a circular loop, and 6) a general lack of 'ground truth' (even dual induction resistivity later-logs (DIL) from wells offer ambiguities in interpretation).

From a modeling point-of-view, the nonuniqueness problem is the most disturbing. In simple terms, the problem is that it is possible to produce very similar apparent resistivity versus time curves using two different geoelectric models. The two curves may match the same TEM sounding data equally well. Often it is possible to trade off the thickness of a layer with its resistivity to obtain similar apparent resistivity curves. Parameter investigations do not address this important problem. The possibility for nonunique solutions increases as the number of layers in the geoelectric model increases. There is no solution to this problem, it can only be recognized as a possible cause of misinterpreting the TEM data.

It is not possible to address the effects of two- and three-dimensional resistivity variations upon the TEM sounding data of the present large scale study. Although some researchers have addressed this problem at great expense in computer time and software development, their programs are not available. Futhermore, the application of two- and three- dimensional computer programs is appropriate only for intensive small-scale studies of sites with good supplementary lithological data.

The works of Anderson and Newman (1985) and Newman et al. (1986) address the effects of two- and three-dimensional variations. The amount of variation present in the apparent resistivity curves depends strongly on the physical size and location of lateral resistivity variations in relation to the location of the TEM system. However, the selection of study sites for this investigation was limited to locations for which very little lateral variation in resistivity was expected. It is not certain at this time that lateral variations in resistivity can cause sign changes in the received signal. A recent paper by Smith and West (1988) argues that sign changes for the TEM system must be attributed to an induced polarization effect.

Induced polarization (IP) effects can occur in earth material that has dielectric properties or complex conductivity; this is discussed in Chapter 5 where it is shown that the induced polarization effect of a complex conductivity may produce multiple sign changes in the TEM system in the central induction mode. These effects may be present in varying degrees at many sites causing an erroneous interpretation of the TEM data.

Equipment limitations are produced when the equipment noise is larger than the actual signal. Since the received voltage signal inherently decreases dramatically with time, it eventually reaches the noise level which is fairly constant with time. In addition there are limitations based on frequency considerations. The bandwidth of the receiver antenna in the TEM system is 40 kilohertz and therefore provides an upper limit on the frequencies of use to the TEM system. The lower limit is the fundamental frequency of the transmitter repetition rate with a highest rate of 30 hertz. These frequency limitations correlate to approximate depths of investigation via the skin depth criterion, wherein the skin depth δ is the depth at which the electromagnetic field is reduced by a factor of $1/e$ of the incident amplitude. The skin depth (in meters) is related to the resistivity ρ (Ω-m) of the linear, isotropic,

and homogeneous medium and the frequency of the electromagnetic wave f (Hz) via

$$\delta = 500\sqrt{\rho/f}. \tag{1.9}$$

The frequency limitations mentioned above together with resistivity of about 50 Ω-m gives a skin depth of 645 meters at 30 Hz and 18 meters at 40 kHz. If the resistivity is 5 Ω-m then the skin depths become 204 meters and 5.6 meters, respectively. For the resistivity of 1000 Ω-m, the skin depths become 2886 meters and 79 meters, respectively. These numbers show that the transient system should be able to discern the depth to the base of a resistive layer such as permafrost in a variety of environments.

The possible error due to the field use of a square transmitter loop relative to a circular loop having the same area has been determined by Raiche (1987) to be less than 1 percent for the central induction TEM system. Thus, the formulation of the TEM method and inversion routines which are based on circular loops can be safely applied to the square loop without serious error.

Measurement errors in the current amplitude and the turnoff time are likely to have the greatest effect on the TEM data. An error in the reading of the analog meter used for both the current and turnoff time measurements may produce considerable variation in the apparent resistivity curves. It is not unusual to expect errors of ± 2 to 5 percent in the reading of an analog meter due to parallax and other sources of human error. Not only does the apparent resistivity depend upon the amplitude of the current, but the ramp turnoff time correction routine (to be discussed in Chapter 2) will have an additional effect on the net error. For the present study, an investigation of the result of such an error has been conducted. Assuming an error of ± 10 percent in the current, there will be a uniform error

of 6.7 percent in apparent resistivity neglecting the effects of the ramp turnoff correction procedure. With the effect of the correction procedure, an error which overestimates the current leads to an overestimate of apparent resistivity of 6.6 percent and if the current is underestimated, it will produce an underestimate in apparent resistivity of 6.8 percent in the first gate at 30 Hz. In other words, the effect of the ramp correction procedure is an additional 0.1 percent change. The error in the current will have a decreasing influence on successive gates as influenced by the the correction routine and would approach the 6.7 percent value.

The effect of an error in the turnoff time is somewhat more complicated to determine as this error reduces the certainty of our knowledge of absolute time for the receiver. Since the turnoff time is dialed into the receiver unit to coordinate timing, an error in this time will lead to errors in the actual gate times relative to the end of the ramp and they will be off by the error in the reading. This error in time overrides any other timing error (since the phase locked crystal oscillators are unlikely to vary more than one clock period, about one microsecond). Since a typical measurement of turnoff time is around 300 microseconds, an estimate of the maximum error in this reading is approximately $\pm$ 30 microseconds. This means that the actual receiver gate locations are off by 30 microseconds, throughout. This error will have the effect of slightly shrinking or stretching the apparent resistivity data curve, especially at early times. The possible instrumentation error in the timing of individual gates is unlikely to be more than one clock period and therefore is unlikely to produce appreciable errors in the TEM data.

In addition, the error in turnoff time will also affect the calculation of apparent resistivity. An overestimate in turnoff time causes an underestimate of apparent resistivity by 5.40 percent in the first gate, 5.20, 4.94, 4.65, 4.34, 3.96, 3.57, 3.2, 2.8, 2.41, 2.09, 1.79, 1.49, 1.23, 1.03, 0.83, 0.67, 0.55, 0.44, and 0.35 percent for

the succeeding gates through gate 20 because of the logarithmic time scale of the gates. If the turnoff time is underestimated then the apparent resistivity will be overestimated by 6.22 percent in the first gate, 5.96, 5.61, 5.23, 4.84, 4.38, 3.91, 3.46, 3.00, 2.56, 2.20, 1.87, 1.54, 1.26, 1.05, 0.84, 0.69, 0.56, 0.44, and 0.35 percent for the succeeding gates through gate 20.

The possible errors from the measurement of current and turnoff time are dominant over other sources of errors in the early gates. Such systematic errors are thought not to exceed $\pm$ 10%. In the data taken at 3 Hz and 0.3 Hz for the sea-ice sites discussed in Chapter 4, data from many of the later time gates were not used in the inverse modeling since the signal level was comparable to the equipment noise.

CHAPTER 2. TRANSIENT ELECTROMAGNETIC THEORY

2.1 INTRODUCTION

This chapter gives an approach to solving the transient electromagnetic (TEM) problem for a circular transmitter loop on the surface of the earth and a coplanar receiver loop at the center of the transmitter loop. This configuration is known as the central induction TEM sounding for the vertical magnetic field. The approach was presented by Morrison et al. (1969) and Ryu et al. (1970) and is reviewed here for completeness to clarify the physics of the technique.

The coordinate system and system geometry used are shown in Figure 2.1. This figure also shows a geoelectric layered-earth model with an arbitrary layer i having thickness h_i, conductivity σ_i, dielectric permittivity ϵ_i and magnetic permeability μ_i. Details of the operational configuration of the particular TEM system used and a figure showing the plan view of a sounding layout were given in Section 1.6.

The current driven through a large circular loop produces a transmitter magnetic dipole moment, $M_t = I_0 A$, where I_0 is the magnitude of the current in the single turn transmitter loop and $A = \pi R^2$ is the area of a transmitter loop of radius R. The problem is to solve for the voltage induced in the receiver coil as a function of time after abruptly terminating the drive current in the transmitter loop. To accomplish this task, the mathematical formalism leading to the integral equation solutions for the electromagnetic fields from a transient magnetic dipole over a layered medium is developed in Section 2.2. In Section 2.3 asymptotic forms for the solutions, especially as applied in the use of apparent resistivity are discussed. Section 2.4 discusses the application of turnoff corrections.

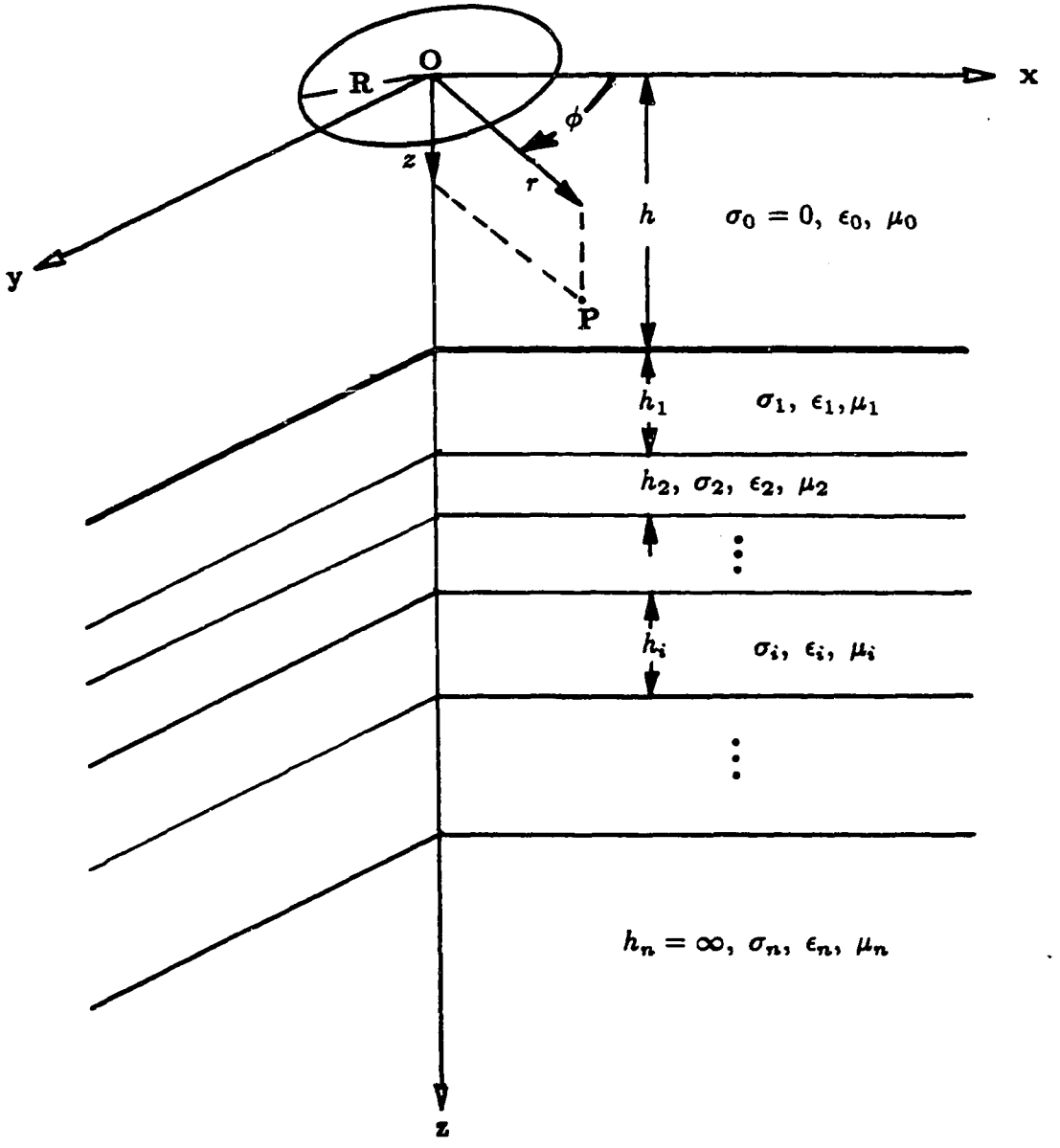

Figure 2.1 The TEM system configuration, cylindrical coordinate system (r, ϕ, and z) and the horizontally-layered earth used for the TEM theoretical development. Any layer i has conductivity σ_i, dielectric permittivity ϵ_i, magnetic permeability μ_i, and thickness h_i.

2.2 THEORY

This Section demonstrates that the TEM solutions for the voltage induced in a small receiver coil concentric to the center of a large circular transmitter loop over a one-dimensional, layered-earth may be expressed as a double integral. One integral is over frequency (inverse Fourier transform domain) and the other is over Hankel-transformed space involving a Bessel function.

The set of equations known as Maxwell's equations, in mks units, are given here as Equations 2.1 through 2.4:

$$\nabla \cdot \vec{D} = \varrho, \tag{2.1}$$

$$\nabla \cdot \vec{B} = 0, \tag{2.2}$$

$$\nabla \times \vec{E} = -\frac{\partial \vec{B}}{\partial t}, \tag{2.3}$$

and

$$\nabla \times \vec{H} = \vec{J} + \frac{\partial \vec{D}}{\partial t}. \tag{2.4}$$

In Equations 2.1 through 2.4, $\vec{E}$ is the electric field intensity in volts per meter, $\vec{H}$ is the magnetic field intensity in amperes per meter, $\vec{D}$ is the electric flux density (or displacement vector) in coulombs per square meter, $\vec{B}$ is the magnetic flux density in teslas and $\vec{J}$ is the current density in amperes per square meter. $\vec{E}, \vec{H}, \vec{B}$, and $\vec{D}$ are collectively known as the electromagnetic field. ∇ is the familiar del operator for three dimensional space derivatives. The symbol $\cdot$ refers to vector dot product and the symbol $\times$ refers to the vector cross product operations. The symbol ϱ represents free charge density in coulombs per cubic meter.

James Maxwell (1873) originally compiled these equations in a brilliant treatise which summarized all the existing knowledge of the macroscopic interactions

of electric and magnetic fields. For a more extensive historical development see Paris and Hurd (1969) and Jackson (1975) wherein the contributions of the many researchers leading to Maxwell's synthesis are extolled.

The simplest possible constitutive relations,

$$\vec{J} = \sigma \vec{E}, \tag{2.5}$$

$$\vec{B} = \mu \vec{H}, \tag{2.6}$$

and

$$\vec{D} = \epsilon \vec{E}, \tag{2.7}$$

(see Stratton, 1941, and Holt, 1963, for more information), are used which relate the electromagnetic properties of a material to the electromagnetic fields present. The units of conductivity σ are siemens per meter (recall that a siemen is an inverse ohm and that the reciprocal of conductivity is resistivity, $\sigma = 1/\rho$, so that the units of resistivity are ohm-meters). The units of dielectric permittivity ϵ are farads per meter and the units of magnetic permeability μ are henries per meter. Thus the medium in question is taken to be linear, isotropic, and homogeneous.

Using Equations 2.5 through 2.7 and assuming time harmonic solutions of the form $e^{(i\omega t)}$, where the term i is the square root of -1, allows Maxwell's equations to be produced in forms which are only functions of $\vec{E}$ and $\vec{H}$ as shown in Equations

2.8 through 2.11.

$$\nabla \cdot \epsilon \vec{E} = 0, \tag{2.8}$$

$$\nabla \cdot \mu \vec{H} = 0, \tag{2.9}$$

$$\nabla \times \vec{E} = -\imath\omega\mu\vec{H}, \tag{2.10}$$

and

$$\nabla \times \vec{H} = (\imath\omega\epsilon + \sigma)\vec{E}. \tag{2.11}$$

In Equation 2.8, the right hand side is zero upon the assumption that no free charge is available in the ground. A layered earth or a half-space medium is assumed, following the early works of researchers such as Wait (1951, 1960) and Bhattacharyya (1957, 1959, 1963, 1964) for transient vertical dipole sources. By taking advantage of the cylindrical symmetry of the system configuration and the dipole source, one notes that only E_ϕ, H_z and H_r components are present as outlined in Morrison et al. (1969) and Ryu et al. (1970).

The ∇ operations may then be expanded and rewritten as

$$\imath\omega\mu H_r = \frac{\partial E_\phi}{\partial z}, \tag{2.12}$$

$$\imath\omega\mu H_z = -\frac{1}{r}\frac{\partial (rE_\phi)}{\partial r}, \tag{2.13}$$

and

$$\frac{\partial H_r}{\partial z} - \frac{\partial H_z}{\partial r} = (\imath\omega\epsilon + \sigma)E_\phi + J_s. \tag{2.14}$$

J_s is the source current density and the material properties are those of any particular layer or of the half-space.

It is now possible to eliminate H_z and H_r from the equations by substitution and arrive at equation 2.15, which can be solved for E_ϕ and from which all other fields may be derived.

$$\left[\frac{\partial^2}{\partial z^2}+\frac{\partial^2}{\partial r^2}+\frac{1}{r}\frac{\partial}{\partial r}-\frac{1}{r^2}+k^2\right]E_\phi = \imath\omega\mu_0\frac{I(\omega)\,R}{r}\delta(r-R)\delta(z). \qquad (2.15)$$

In this equation, R is the radius of the transmitter loop, I is the magnitude of current flowing in the transmitter loop, the Dirac delta functions, δ, specify the physical location of the current source, and the subscript zero denotes free space. k is the complex wave number where

$$k_i^2 = \omega^2\mu_i\epsilon_i - \imath\omega\mu_i\sigma_i. \qquad (2.16)$$

The subscript i denotes the ith layer. Equation 2.15 is a scalar differential equation for the angular component of the electric field intensity in a medium subjected to a step change in current.

The form of equation 2.15 is amenable to solution by application of the Hankel transform pair

$$F(\lambda) = H_1(F(r)) = \int_0^\infty F(r)J_1(\lambda r)rdr \qquad (2.17)$$

and

$$H_1^{-1}(F(\lambda)) = F(r) = \int_0^\infty F(\lambda)J_1(\lambda r)\lambda d\lambda. \qquad (2.18)$$

$J_1(\lambda r)$ is the first order Bessel function. For more information on Hankel (Fourier-Bessel) transforms see Mathews and Walker (1970). Upon Hankel transformation, the following is obtained

$$\left[\frac{\partial^2}{\partial z^2} + k_0^2 - \lambda^2\right] E_s(\lambda, z, \omega) = \imath\omega\mu_0 RI(\omega) J_1(\lambda R)\delta(z). \tag{2.19}$$

Since the electric field is always only in the ϕ direction, the subscript ϕ is dropped in favor of the subscript s to indicate that the field is in the region containing the source. Upon use of the Fourier transform on z, a linear equation results. Upon application of the inverse Fourier transform back to z, the following is obtained

$$E_s(\lambda, z, \omega) = -\frac{\imath}{2}\omega\mu_0 RI(\omega) J_1(\lambda R)\frac{exp(-u_0 z)}{u_0}, \quad (z > 0), \tag{2.20}$$

where u_0 is in free space and in general

$$u_i = \sqrt{\lambda^2 - k_i^2}. \tag{2.21}$$

In free space, u_0^{-1} is an e-folding length scale, which is a measure of the attenuation of the field strength. Similarly, u_i^{-1} is an e-folding length scale for any particular layer.

For all regions not containing the source current, Equation 2.19 becomes a homogeneous equation because the right hand side is zero in the absence of a source. The solutions will consist of fields with an $exp(\pm u_i z)$ dependence. Applying the boundary conditions of continuity of the tangential E and H field components at the interfaces between layers provides a solution using the recursion method, in a direct analogy to the plane wave problem of the audio-magnetotelluric method (see Cagniard, 1953, and Telford et al., 1976).

The input impedance at the surface of any layer i is

$$Z^i(\lambda,\omega) = \frac{E_\phi}{H_r}. \tag{2.22}$$

The intrinsic impedance of any layer i is

$$Z_i(\lambda,\omega) = -\frac{\imath\omega\mu_i}{u_i}. \tag{2.23}$$

Wait (1962) derives the following expression for the input impedance of a n-layered earth from the interfacial boundary conditions

$$Z^i = Z_i \frac{Z^{(i+1)} + Z_i tanh(u_i h_i)}{Z_i + Z^{(i+1)} tanh(u_i h_i)}. \tag{2.24}$$

Solving Equation 2.24 n times beginning from the surface of the last layer where

$$Z^n = Z_n \tag{2.25}$$

gives the input impedance of the sequence of n layers. Equation 2.25 simply states that the input impedance of a uniform medium (the last layer or a half-space) is equal to the intrinsic impedance of that medium, and can be derived by noting that $h_n = \infty$.

The solution to the total E field, which includes both the source (or incident) field (Equation 2.20) and the secondary (or reflected field) for a loop of current at an elevation h above the ground is

$$E(r,h,\omega) = -\imath\omega\mu_0 RI(\omega) \int_0^\infty \frac{exp(-u_0 h)}{u_0} \frac{Z^1}{Z^1 + Z_0} J_1(\lambda R) J_1(\lambda r) \lambda d\lambda. \tag{2.26}$$

Using the inverse Fourier transform (see Kreyszig, 1983) one obtains

$$E(r,h,t) = \frac{1}{2\pi} \int_{-\infty}^{+\infty} E(r,h,\omega) e^{\imath\omega t} d\omega. \tag{2.27}$$

Once the solution field is known, the expected voltage as a function of time in

a circular receiver coil coaxial with the transmitter loop is

$$v(t) = 2\pi n_0 r_0 E(r_0, h, t), \tag{2.28}$$

where n_0 is the number of turns of the receiver coil and r_0 is the receiver radius. Integral equation solutions of similar form for a layered earth have been derived by Wait (1982), Kaufman and Keller (1983) and others.

The expression used by Anderson (1981) for E is easily derived from Equations 2.26, 2.27, and 2.28 using a variable transformation, assuming a causal system for the earth, a step function drive current, and a transmitter loop on the ground ($h = 0$). Anderson (1974) showed that

$$v(t) = \frac{n_0\ r_0^2\ I_0}{\sigma_1\ R^3} \int_0^\infty Real\left[\frac{H_z(\sqrt{b})}{H_z(0)}\right] cos(b\ \Upsilon) db, \tag{2.29}$$

where

$$b = R^2\ \frac{\sigma_1\ \mu_0\ \omega}{2}, \quad \Upsilon = \frac{2\ t}{\sigma_1\ \mu_0\ R^2},$$

and

$$H_z(\omega) = RI_0 \int_0^\infty \left[\frac{exp(-u_0 z)}{u_0} \frac{Z^1}{Z_0 + Z^1}\lambda - \frac{exp(-\lambda z)}{2}\right] J_1(\lambda R)\ \lambda\ d\lambda + \frac{I_0}{2\ R}. \tag{2.30}$$

The complex frequency function $H_z(\omega)$ is derived from Equation 2.13 using Equation 2.26. $H_z(0)$ is the zero frequency (or DC) vertical magnetic field used to normalize Equation 2.29.

The additional term at the end of Equation 2.30 is the zero frequency term (for a loop placed on the ground, $H_z(0) = I_0/2R$) added and subtracted so that the integral is insured convergence. The subtracted term occurs within the kernel of the integral. Without this mathematical artifice, the function to be evaluated

oscillates wildly as the position of the loop approaches the ground ($h \rightarrow 0$), because of the two Bessel functions of Equation 2.26.

Anderson (1974) chooses this form for ease in numerically computing the TEM decay curve. This process involves the computation of the double integral via an approximation using a filter for the Bessel function convolved with a cubic splined frequency function H_z. Recall that the frequency function is derived by an iterative procedure which depends upon the resistivities and thicknesses of the layered earth. This procedure is extremely fast and, if the frequency function has sufficient points per decade in frequency, extremely accurate for most realistic resistivities and thicknesses. The procedure has been incorporated into the programs of Anderson (1981, 1982). These programs have greatly aided the present research. As a test of the forward program (Anderson, 1981) which computes the TEM decay, results of published papers from Sinha and Stephens (1983), Ehrenbard et al. (1983), and Kaufman and Keller (1983) were reproduced. The reproduction of the published results of others gives assurance that Anderson's programs are operating properly.

2.3 ASYMPTOTIC FORMS AND APPARENT RESISTIVITY

The complexity of the integral equation for the solution to the TEM decay led numerous researchers to look for simpler equations to use. Over limited periods of time, depending upon the resistivities and thicknesses of the layered earth and the transmitter parameters, formulas for late time and early time may be very useful tools for interpretation. An apparent resisitivity is defined, as is common in other types of electrical prospecting, to aid in interpretation. This definition involves approximation of a decay curve using early or late time approximations to

the full field equation. An equation for the full field for a homogeneous half space (HHS or one layer extending to infinite depth) at an arbitrary radius r, with step current drive and neglecting displacement currents (Kaufman and Keller, 1983), comparable to Equation 2.20, is

$$E_\phi = -\frac{3M_t\rho}{2\pi r^4}\left[\Theta(u) - \sqrt{\frac{2}{\pi}}(u + \frac{u^3}{3})exp(\frac{-u^2}{2})\right], \tag{2.31}$$

$$u = \frac{2\pi r}{\zeta}, \quad \zeta = 2\pi\sqrt{\frac{2t\rho}{\mu_0}}, \tag{2.32}$$

where E_ϕ is the electric field in the ϕ direction in the plane of the loop, ρ is the resistivity of the half-space, ζ has units of length and u is dimensionless, M_t is the transmitter dipole moment (current, I, times transmitter loop area, $A = \pi R^2$, times number of turns–one loop only for this study), and $\Theta(u)$ is the probability integral

$$\Theta(u) = \sqrt{\frac{2}{\pi}}\int_0^u exp(\frac{-x^2}{2})dx. \tag{2.33}$$

These equations describe the electric field strength with respect to both distance and time under simplifying assumptions. Since u is proportional to $r/\sqrt{t}$, the limiting forms of the solution provide information on early and late time trends in the field strength.

Using the voltage induced in a receiver coil from Equation 2.28 and the principle of reciprocity, a specific expression for the voltage displayed on the transient system EM-37 may be derived as

$$v = \frac{3\ M_r\ M_t\ \rho\ 2^n}{\pi\ R^5}\left[\Theta(u) - \sqrt{\frac{2}{\pi}}(u + \frac{u^3}{3})exp(\frac{-u^2}{2})\right], \tag{2.34}$$

where v is the measured voltage in volts, M_r is the receiver moment defined as the preamplifier gain (dimensionless) times the effective area (number of turns times

the receiver loop area) of the receiver loop and n is the receiver gain setting. By expanding the $\Theta(u)$ function as a power series in u, using one expansion as $u \rightarrow \infty$ and another as $u \rightarrow 0$, asymptotic forms for Equation 2.31 for early and late time may be derived. This procedure gives an expression for early time (defined as $\zeta/R < 2$ by Kaufman and Keller, 1983)

$$E_\phi \longrightarrow -\frac{3\ M_t\ \rho}{2\ \pi\ r^4}. \tag{2.35}$$

Note that Equation 2.35 does not depend upon time and that this tendency is clearly evident in the data of the sites over sea ice discussed in Chapter 4.

The asymptotic form for the solution field E_ϕ representing late times (defined as $\zeta/R \gg 1$) is

$$E_\phi \longrightarrow -\frac{\mu^{5/2}\ \sigma^{3/2}\ r\ M_t}{40\ \pi\ \sqrt{\pi}\ t^{5/2}}. \tag{2.36}$$

Equations 2.35 and 2.36 are used to define apparent resistivity to aid in interpreting the TEM data. Note that Equation 2.36 indicates the time dependence to be $t^{-5/2}$.

Recalling Equation 2.28, using the expression for E_ϕ for early time, and reversing the order of the equation gives a definition for the early time apparent resistivity

$$\rho_e = \frac{v\ \pi\ R^5}{3\ M_t\ 2^n\ M_r}. \tag{2.37}$$

Note that early time resistivity does not depend upon time.

In a similar manner, an expression for the late time apparent resistivity, ρ_a, is found to be

$$\rho_a = \frac{1}{\pi}\left[\frac{M_t\ 2^n\ M_r}{20\ v}\right]^{2/3}\left[\frac{\mu}{t}\right]^{5/3}. \tag{2.38}$$

Normally μ is taken to be the magnetic permeability of free space, $\mu_0 = 4\pi 10^{-7}$ henries per meter. It was determined that the forward program curves agreed very well with the Soviet theoretical curves (Rabinovich and Stepanova, 1972).

This late time approximation used to define ρ_a gives an indication of the change in resistivity with time. In turn, the ρ_a versus time decay curve may be inverted or curve-matched to derive a geoelectric model of ρ_a versus depth. One advantage to the use of the apparent resistivity concept is that the decay of the ρ_a versus time is less rapid than the original sounding data (v versus t), i.e., $t^{-5/3}$ rather than $t^{-5/2}$, thereby requiring a smaller dynamic range in the inversion program.

2.4 TURNOFF CORRECTION

As mentioned in the previous section, the analytic forms for the TEM decay obtained for a dipole source assumes a step current drive. While it is not physically realizable, the step current is nonetheless a useful starting point. The actual current drive shown in Figure 1.4 indicates a ramp turnoff time, not a step. Since the data are observed with a ramp drive input and the theory uses a step drive, one must be altered relative to the other to allow for proper matching with the theoretical curves of Rabinovich (1978) and Rabinovich and Stepanova (1972), for example. The forward modeling program TCILOOP from Anderson (1981) used by the author also assumes the drive current is turned off instantaneously. The procedure taken in these studies was to develop a computer program to correct the sounding data to that which would have been taken with a step drive; this procedure is called turnoff (TO) correction.

A recent paper by Fitterman and Anderson (1987) discusses the need for ramp time correction and a procedure for obtaining the theoretical ramp response from the theoretical step response which was combined with TCILOOP (Anderson, 1981) to produce the forward modeling program FWDTCI. As of the time of the writing

of this thesis, the ramp correction of Fitterman and Anderson (1987) has not been applied to the inverse program of Anderson (1982). The ramp correction procedures described in this thesis were developed prior to the publication of the paper of Fitterman and Anderson (1987) and did not require modification of the inverse program of Anderson (1982).

Corrections for a ramp time turnoff are based on the assumption that the earth is a linear transform system and, therefore, the response due to a drive current with a ramp turnoff time is related to the response due to a current turned off instantaneously (step response) by

$$m(t_g) = \frac{1}{TO} \int_{t_g}^{t_g+TO} s(t)dt, \tag{2.39}$$

where TO is ramp turn-off time, $m(t_g)$ is measured response, $s(t)$ is step response, and t_g is gate time (measured from the end of ramp turnoff).

The importance of the turnoff correction may be understood by considering the effects of various turnoff times over a homogeneous half-space. As a check of the correction routine, a 50 Ω–m half-space was forward modeled using the program FWDTCI for turnoff times of 350 and 700 μs. The resulting apparent resistivity versus time curves were then treated as raw data for input in the inverse program of Anderson (1982). First the data were input directly without correction for a ramp turnoff time and then with the correction developed in this thesis (see Appendix B for a listing of the correction program).

With the uncorrected apparent resistivity data used as input in the inverse program and an initial model consisting of a 50 Ω–m half-space, the resulting inversions gave half-space resistivities of 71 and 106 Ω–m respectively for the 350 and 700 μs ramp turnoff times. These results show that uncorrected data cannot be inverted to the right value (50 Ω–m) for the half space. Indeed, a better match

to the uncorrected data might have been obtained by models with more than a single layer!

To apply the correction procedure for the finite ramp turnoff time developed for this thesis (program RHOA, Appendix B) the apparent resistivities for the 50 Ω−m half space obtained from the FWDTCI program for the turnoff times of 350 and 700 μs were first converted into voltages using the late time definition of apparent resistivity (Equation 2.38). (These data sets may be regarded as "raw" field data that need to be corrected for a known ramp turnoff time.) These sets of voltage values were then corrected for the 350 and 700 μs ramp times by the program RHOA and the corrected values used as input for the inverse program NLSTCI. Both sets of data gave resistivities of just over 50 Ω−m (off by less than 3%) for the half space indicating the correction procedure works reasonably well. The small difference between the inverse model result and the true half-space resistivity is due to the fact that the correction routine assumes late time ($t^{-5/2}$) behavior in voltage whereas the relatively low resistivity of a 50 Ω−m half-space reaches late time behavior at about gate 7 (using 400 m square transmitter loop). The correction routine performs better as the resistivity of the earth increases.

The data discussed in the following chapters were corrected for ramp time turnoff. In Chapter 3, the TEM data from West Dock and Deadhorse displayed the characteristics of late time behavior and therefore Equation 2.38 could be used assuming a decay of $t^{-5/2}$ in voltage. Generally the data from the sites of Appendix A also were characteristic of late time behavior and used the same correction procedure.

As discussed in Chapter 4, an unusually conductive environment of saturated, saline, and unfrozen subsea sediments produces apparent resistivity curves which

are not representative of late time behavior. (Note that small ρ implies small values for ζ, invalidating the late time criterion.) Therefore, ramp time corrections based on the asymptotic form for a time decay of $t^{-5/2}$ could not be used. Instead, corrections were computed using the full field expression for the response of a homogeneous half space. The definition of apparent resistivity based on early time behavior is used to estimate a value for the first layer resistivity which was then used to correct for the ramp turnoff time. However, it turned out that the curves corrected for ramp time for the sites offshore differed only slightly from the uncorrected curves. Furthermore, the geoelectric model interpreted for the uncorrected curve was usually the best model for the corrected curve. Also, the first layer resistivity (ρ_1) found from the early time approximation was usually the best choice for the first layer of the model and tended to agree with the ρ_1 found by matching theoretical curves.

The following procedure was used to implement the correction. First, the value of resistivity for the top layer ρ_1, is found using the early time definition or by curve matching. Then the homogeneous half-space response ($s(t)$, the step response) for a uniform earth with a resistivity of ρ_1 is calculated using the full field expression of Equation 2.31. The expected measured response ($m(t)$) is then calculated using Equation 2.39 and the ratio of $s(t_g)/m(t_g)$ at each gate is taken to obtain the correction factor for each gate. Finally, the correction factor is multiplied by the experimental measured voltage at each gate to obtain the corrected voltages. Once the voltages are corrected, they are used in Equation 2.38 to produce apparent resistivity curves. Finally, the best fit geoelectric model is obtained by using the inverse modeling program of Anderson (1982).

The induced polarization effect in TEM soundings described in Chapter 5 requires yet another method for turnoff correction. Since the curves displayed by

the TEM IP sometimes change sign, the approximations of early and late time were of little use. In this case, the correction was done by a deconvolution-convolution process as discussed in Chapter 5.

2.5 SUMMARY

The theory of the TEM method using coplanar transmitter and receiver coils in the central induction configuration, was reviewed in Section 2.2. The solution to the TEM soundings over a layered earth may be expressed as a double integral over inverse Hankel and inverse Fourier domains. In Section 2.3, the asymptotic forms for early and late time approximations were given. Asymptotic forms for the apparent resistivity were then defined. The reasons for turnoff corrections were discussed in Section 2.4 and a method for implementing the corrections was developed. The data of each of the the following three chapters require different turnoff correction procedures.

CHAPTER 3. AN ANALYSIS OF TEM SOUNDINGS

3.1 INTRODUCTION

The purpose of this chapter is to examine the results obtained using the transient electromagnetic (TEM) method at three particular sites for which a reasonable, although not necessarily complete nor accurate amount of information was available in the form of subsurface resistivity and other data from well logs. All three sites were located in the North Slope region of Alaska. One site was located near the West Dock of Prudhoe Bay in the vicinity of the North Prudhoe Bay State Number 1 exploratory well. A second site was located on Reindeer Island which is approximately 13 kilometers offshore near Prudhoe Bay. (These two sites were along a line of TEM sites which extended over ice to investigate subsea permafrost. This work is presented in Chapter 4). The third site was located just south of Deadhorse Airport. Details of the location of the Deadhorse and West Dock sites as well as many other sites sounded along a transect of Alaska are presented in Appendix A.

The dual induction later-log (DIL) is a single-frequency, electromagnetic induction device which is lowered down a well hole to give a continuous record of the resistivity with depth. This type of well log is the best indicator of subsurface resistivity available and has been used in the interpretation of the base of ice-bearing permafrost by Osterkamp and Payne (1981) and Osterkamp et al. (1985). For each well log, the DIL record displays the results of three devices, two induction type instruments (ILM and ILD) and a focussing-electrode instrument (LL8). The ILM and ILD differ primarily in the separation between the transmitter and receiver

coils which governs the sounding depth into the sides of the borehole. The results of the deeper sounding device (ILD) are of greater interest as we are interested in the bulk features of the resistivity with depth.

Resistivity logs in permafrost present special problems, because they primarily reflect the resistivity of the thawed and thermally disturbed materials near the borehole associated with the drilling process. For example, it can be estimated from the Schlumberger Log Interpretation charts that the ILD DIL resistivities should be multiplied by a factor of at least 1.3, but more probably by a factor of 2 to 5 to obtain a better estimate of the formation resistivities. These logs, however, are useful in the delineation of the depths of the high resistivity zones and hence provide invaluable information on formation thicknesses for inverse modeling.

In the subsequent discussions, the ILD DIL well log for a well nearby each site is presented and a gross average of resistivity as a function of depth is inferred to produce a forward model of TEM data that can be compared with the data. Interpretations given for the Appendix A sites, including two of the three sites discussed here, are the results of extensive forward and inverse modeling using the NLSTCI program of Anderson (1982). The model which results from this process is the base model used in the parameter investigations for each of the three sites. Curves resulting from varying each parameter in the layered earth (thicknesses and resistivities) are displayed in multiple plots.

The results of these parameter investigations are discussed in terms of the potential resolution of individual parameters. A nearby DIL log is compared with the inverse model and an evaluation of the capability of the EM-37 to resolve the thickness of each layer under these circumstances is discussed.

3.2 WEST DOCK SITE

The DIL well log from PBS #1, which is located 3 miles south of the West Dock site, is duplicated here in Figure 3.1 with the ILD "inked-in" by hand for clarity. This well log was used because no DIL log was available from the exploratory well North Prudhoe Bay State #1 at the time of this investigation. Osterkamp and Payne (1981) show that the interpreted depth to the base of permafrost for North Prudhoe Bay State #1 from a temperature logging was 560 m while that for Prudhoe Bay State #1 was 561 m from the DIL log. In addition, other well logs near the shore and nearby the West Dock site show a similar DIL well log to that of Prudhoe Bay State #1. It is clear that the resistivity profile is extremely complex, but to a first approximation the profile is taken to consist of three distinct values corresponding to three different layers. The first layer is taken to have a resistivity of 80 Ω-m down to 289 meters (948 feet) depth. A second layer has a resistivity of 30 Ω-m for 274 meters (900 feet) and the basement layer is 3 Ω-m. The model is indicated by dotted lines in Figure 3.1.

This three layer model was then forward modeled for its TEM response and the results are displayed in Figure 3.2 together with the actual TEM sounding data. In this figure, the squares denote the TEM data and the circles which are connected by lines are the apparent resistivity values from the forward modeling of the three layer model from the DIL. Triangles represent the solution obtained with the inverse model. The base model is displayed as an insert in this figure and in all the figures for the parameter investigations for this site.

It is apparent that the two sets of data, calculated from the three layer model and observed, differ considerably. A part of the difference may arise from the

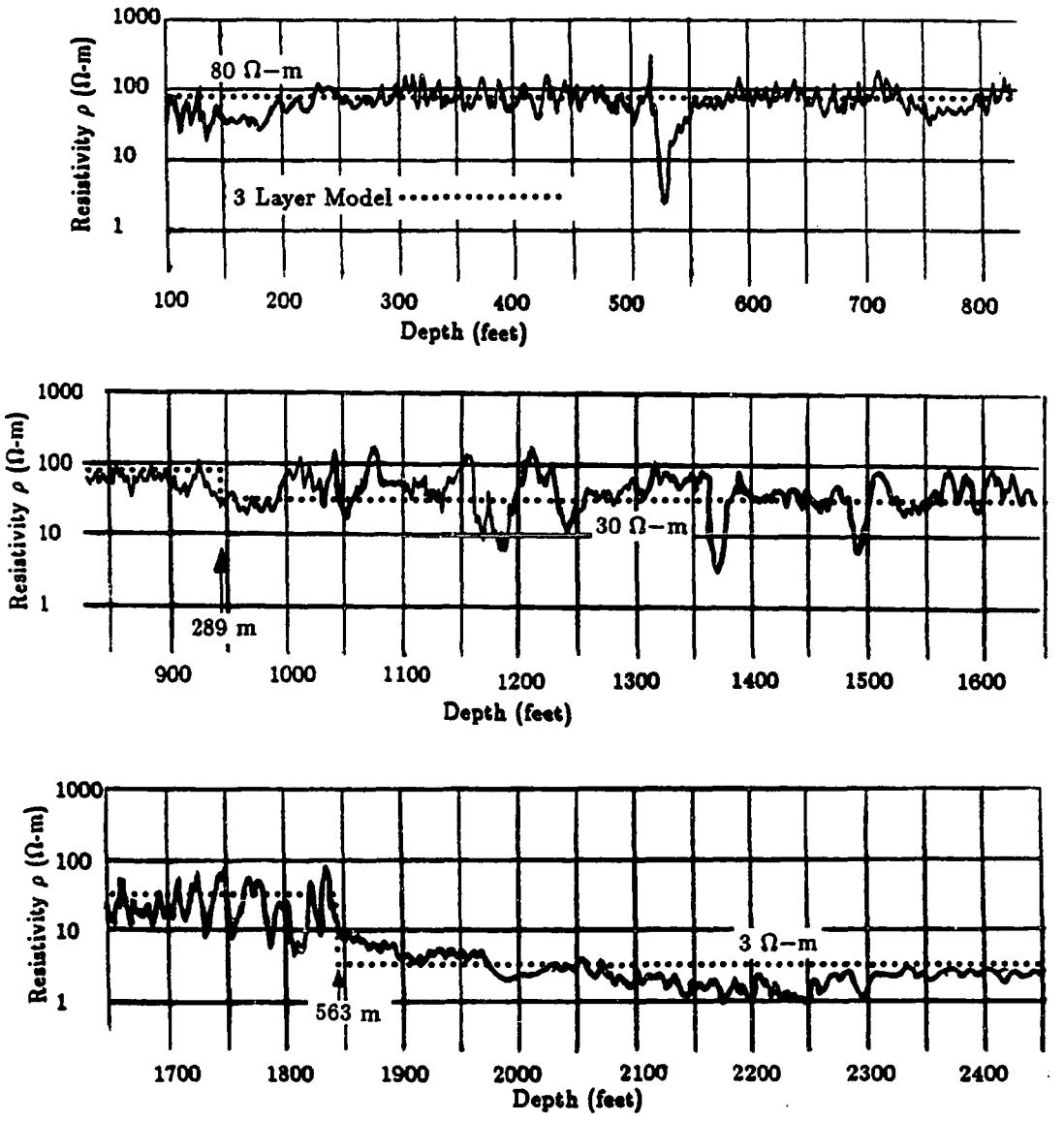

Figure 3.1 Dual induction later-log (DIL) from ARCO Prudhoe Bay State # 1 discovery well. The deep later-log has been enhanced by hand. Note the resistivity scale is logarithmic whereas the depth is linear.

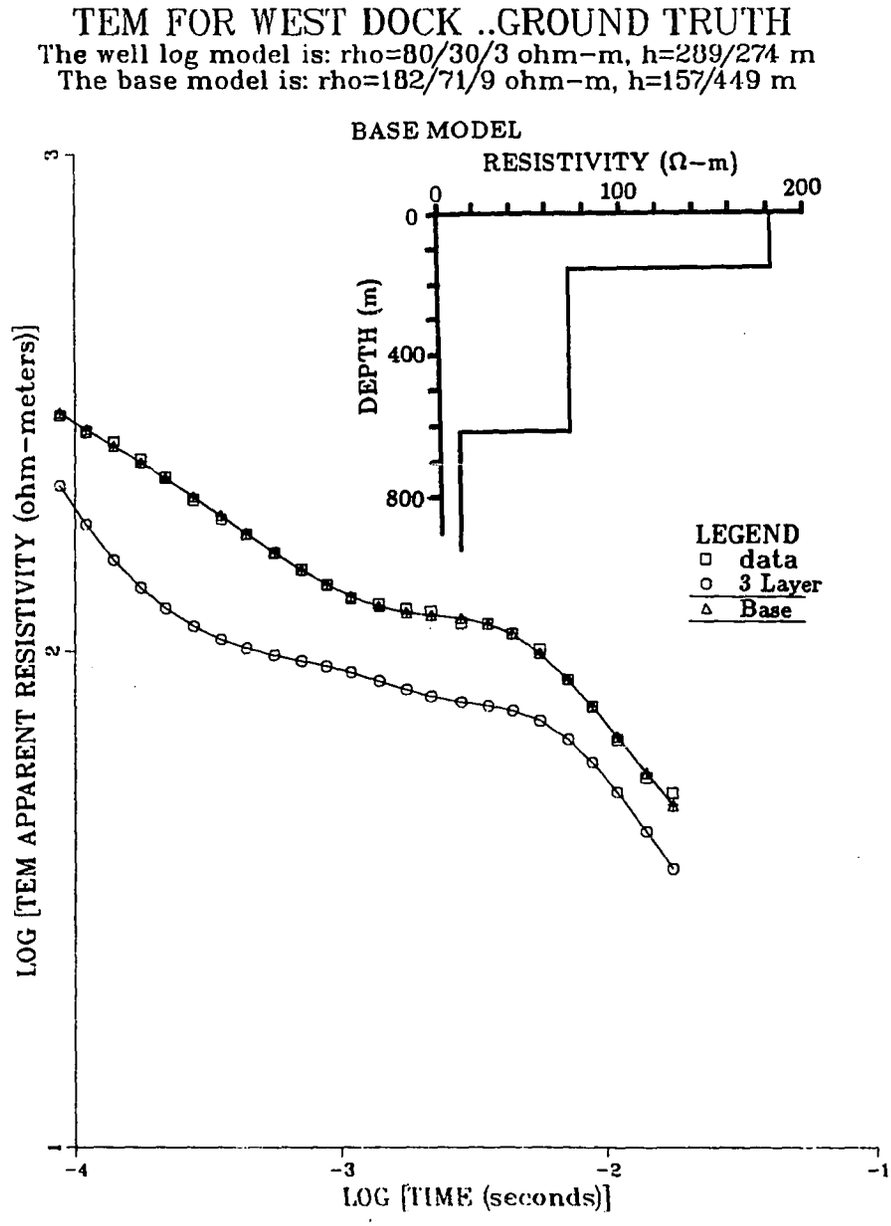

Figure 3.2 TEM sounding data plotted as apparent resistivity versus time compared to the well log model theoretical curve and the model resulting from computer inverse modeling (base model) for Prudhoe Bay West Dock site.

extremely simple geoelectric model used here when in fact there is considerable variation in the DIL as shown in Figure 3.1. Another difficulty is that drilling produces a thermal disturbance and the DIL soundings must penetrate through a warmer, less resistive zone to the permafrost or colder material. Thus the DIL resistivity values may not be accurate. Finally, the DIL also gives no information on the first 100 feet of material and this material has been been assigned the same resistivity as the material below 100 feet. It is actually remarkable that the forward modeling based on the DIL resistivity gives a profile as close to the shape of the TEM profile as it does.

Although the geoelectric model from the well log does not match the data very well at this site, the base model from inverse modeling (triangles) does give a fairly good match to the observed data. The geoelectric model from inverse modeling for three layers calls for a 182 Ω-m first layer that is 157 meters thick, a second layer of 71 Ω-m that is 449 meters thick, and a basement resistivity of 9 Ω-m.

Parameter investigations were undertaken using the resulting inverse model as the base model from which to vary the individual parameters of interest: the resistivities of the three layers and the thicknesses of the first and second layer. The results of these parameter investigations are shown in Figures 3.3, 3.4, 3.5, 3.6 and 3.7.

Figures 3.3, 3.4, and 3.5 show the result of varying the resistivity of the first, second and third layer, in turn, with the other parameters held fixed at the values of the base model. Figure 3.6 shows the variation of the apparent resistivity as the first layer thickness is varied. Figure 3.7 shows the variation when the second layer thickness is varied.

The effects on the apparent resistivity curves due to varying the first layer resistivity are most dramatically evident in the early time gates whereas varying

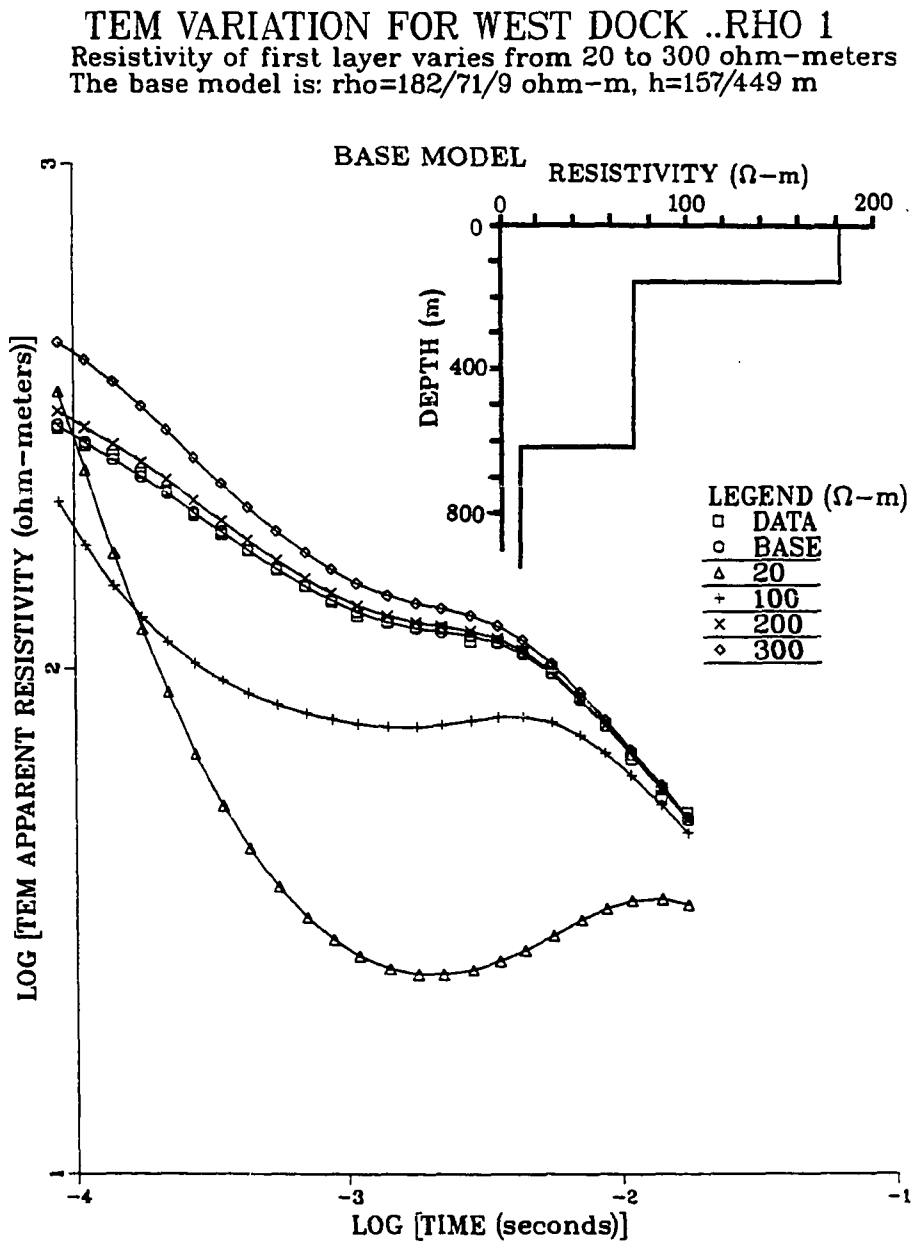

Figure 3.3 TEM apparent resistivity versus time showing the effect of varying the first layer resistivity between 20 and 300 Ω-m for the site near Prudhoe Bay West Dock.

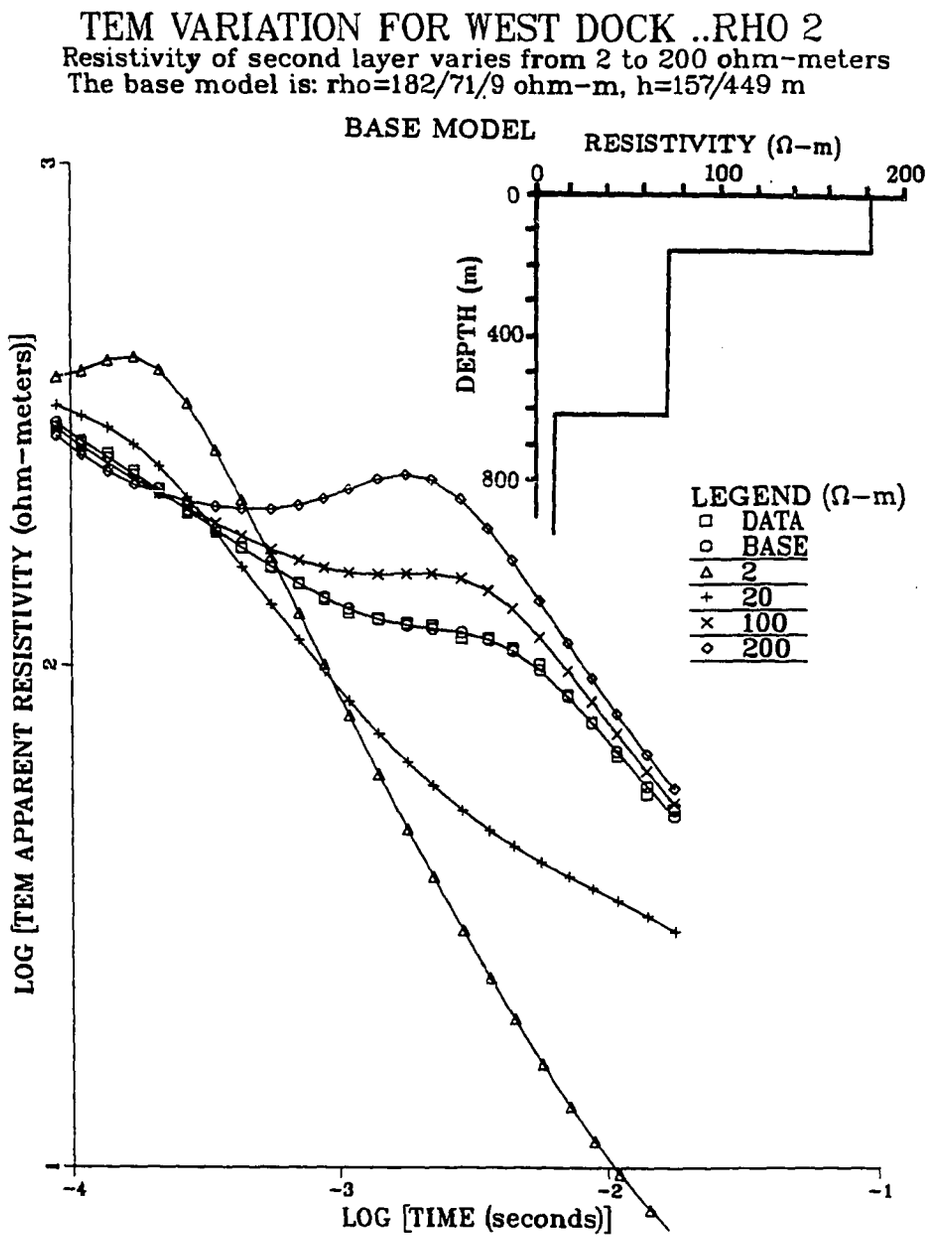

Figure 3.4 TEM apparent resistivity versus time showing the effect of varying the second layer resistivity between 2 and 200 Ω-m for the site near Prudhoe Bay West Dock.

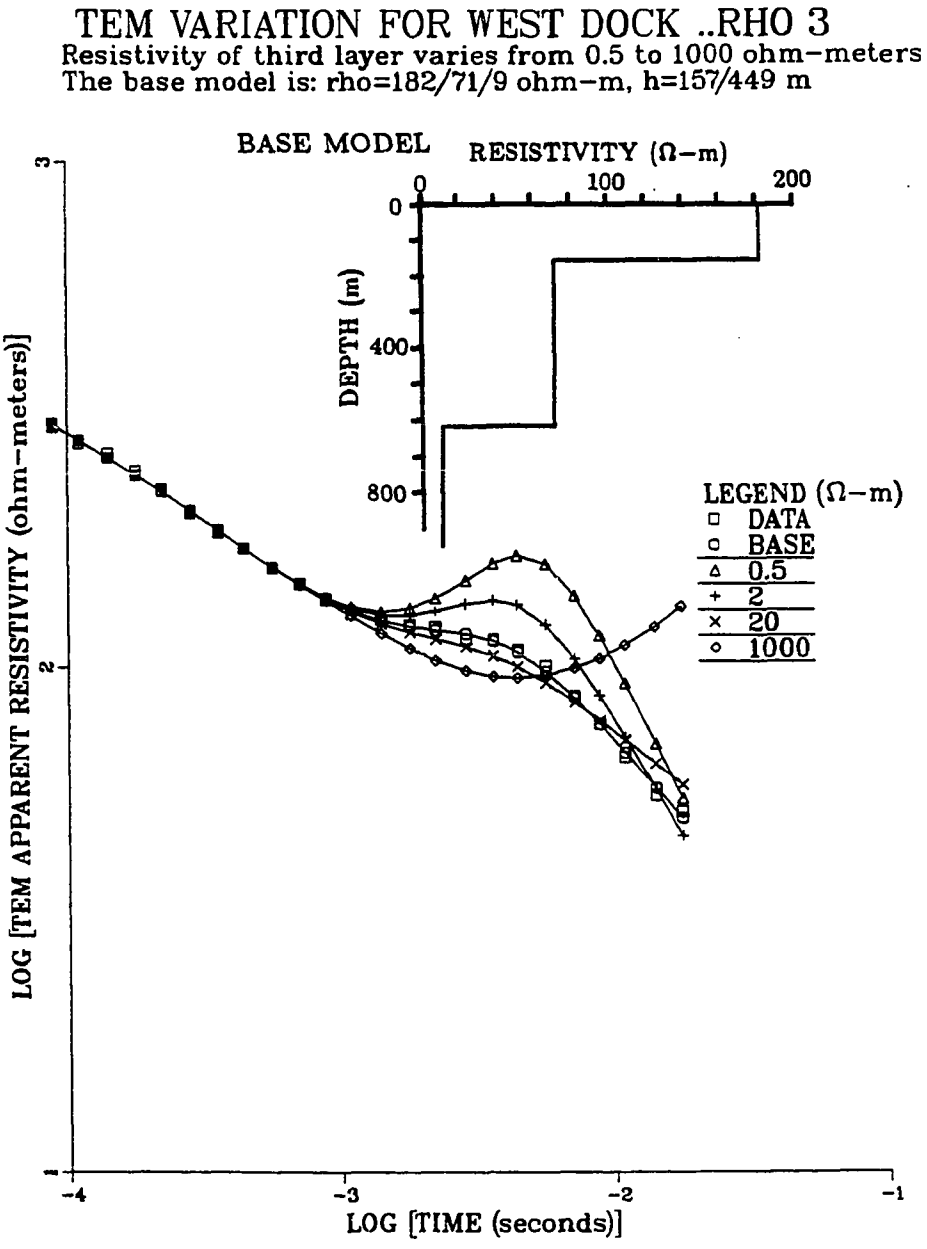

Figure 3.5 TEM apparent resistivity versus time showing the effect of varying the third layer resistivity between 0.5 and 1000 Ω-m for the site near Prudhoe Bay West Dock.

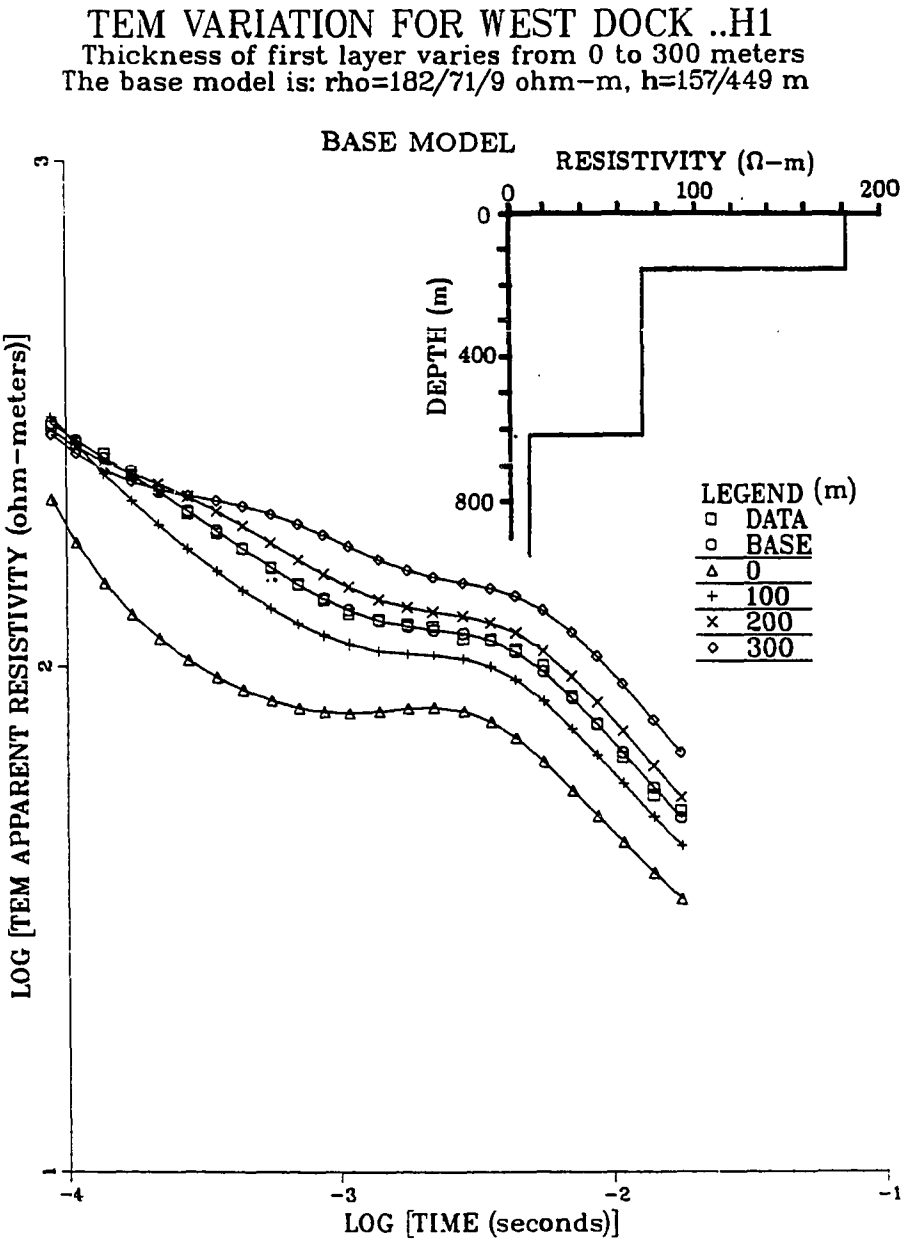

Figure 3.6 TEM apparent resistivity versus time showing the effect of varying the first layer thickness between 0 and 300 m for the site near Prudhoe Bay West Dock.

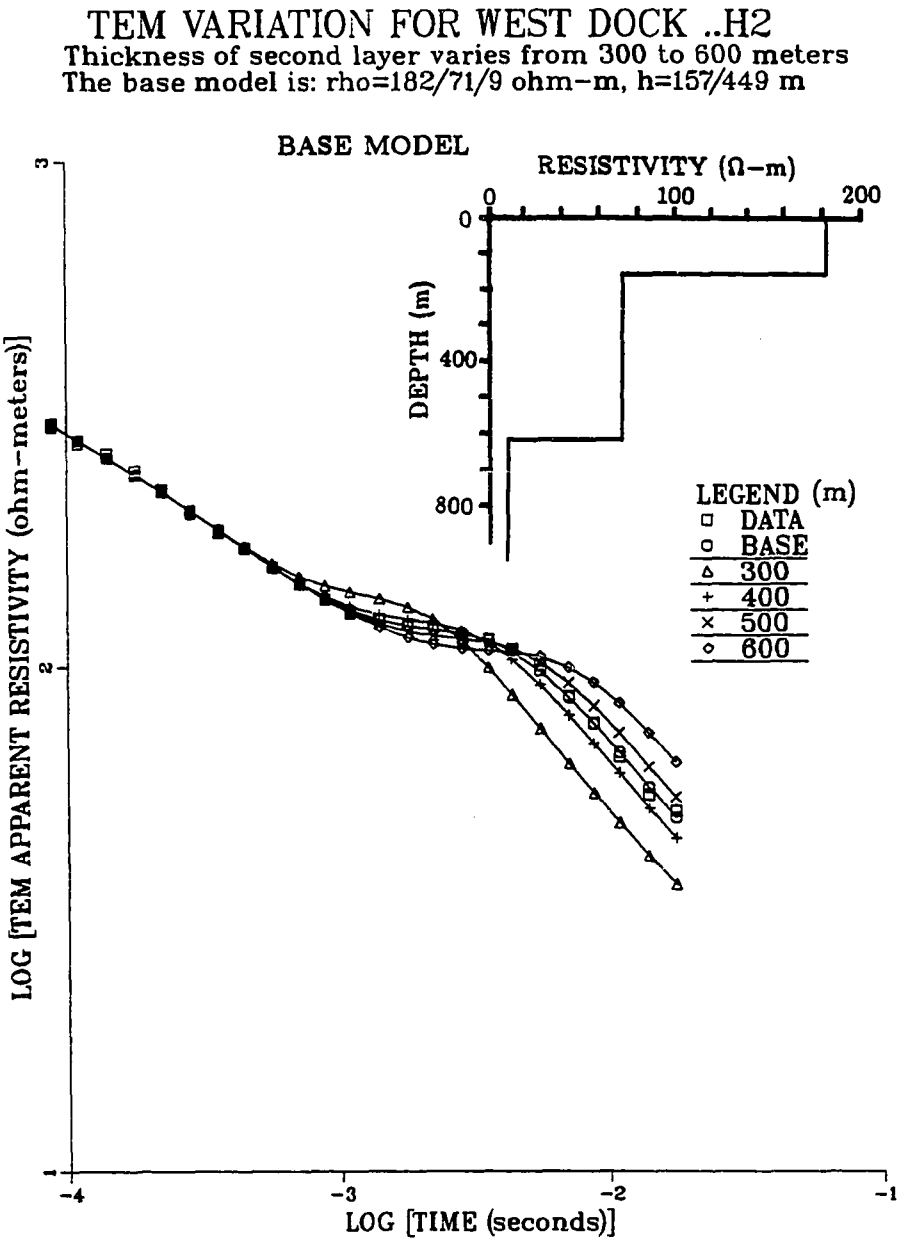

Figure 3.7 TEM apparent resistivity versus time showing the effect of varying the second layer thickness between 300 and 600 m for the site near Prudhoe Bay West Dock.

the third layer resistivity produces effects mostly evidenced in the later gates. It is evident that the curves do not match the data well when the first and second layer differ in resistivity by $\pm 10\Omega$-m or less from the base model and about $\pm 5\Omega$-m in the third layer. It is also evident that a difference of 25 meters between the base model and a chosen value for the thickness of the first layer would stand out and that a resolution of 5 meters may be possible without resorting to computer analysis. In addition, a difference of 10 meters between the base model and the chosen parameter value does not give a very good match to the actual data. These results, of course require that one fixes the other parameters, but if the other parameters were known values, then these parameter studies will allow us to establish some limits on the uncertainty of the values of the remaining parameters.

Osterkamp and Payne (1981) gives the depth to the base of ice-bearing permafrost as determined from the DIL to be 560 meters. The present study shows from the inverse model that the depth to the base is 606 meters, which gives a percentage difference of +8.2 % between the TEM data and the more direct indications of the base.

3.3 DEADHORSE

The Deadhorse site was sounded with a square transmitter loop 400 meters on a side with 20 amperes of current. Details on this site can be found in Appendix A. The DIL from a well located nearby (ARCO D.S. 12-3) is shown in Figure 3.8. Again, note the complex nature of the profile; if most of the major complexitities are ignored and only the mean value is estimated for layering, the profile may be considered to consist of 2 or 3 major layers. For the 2 layer model, the first layer

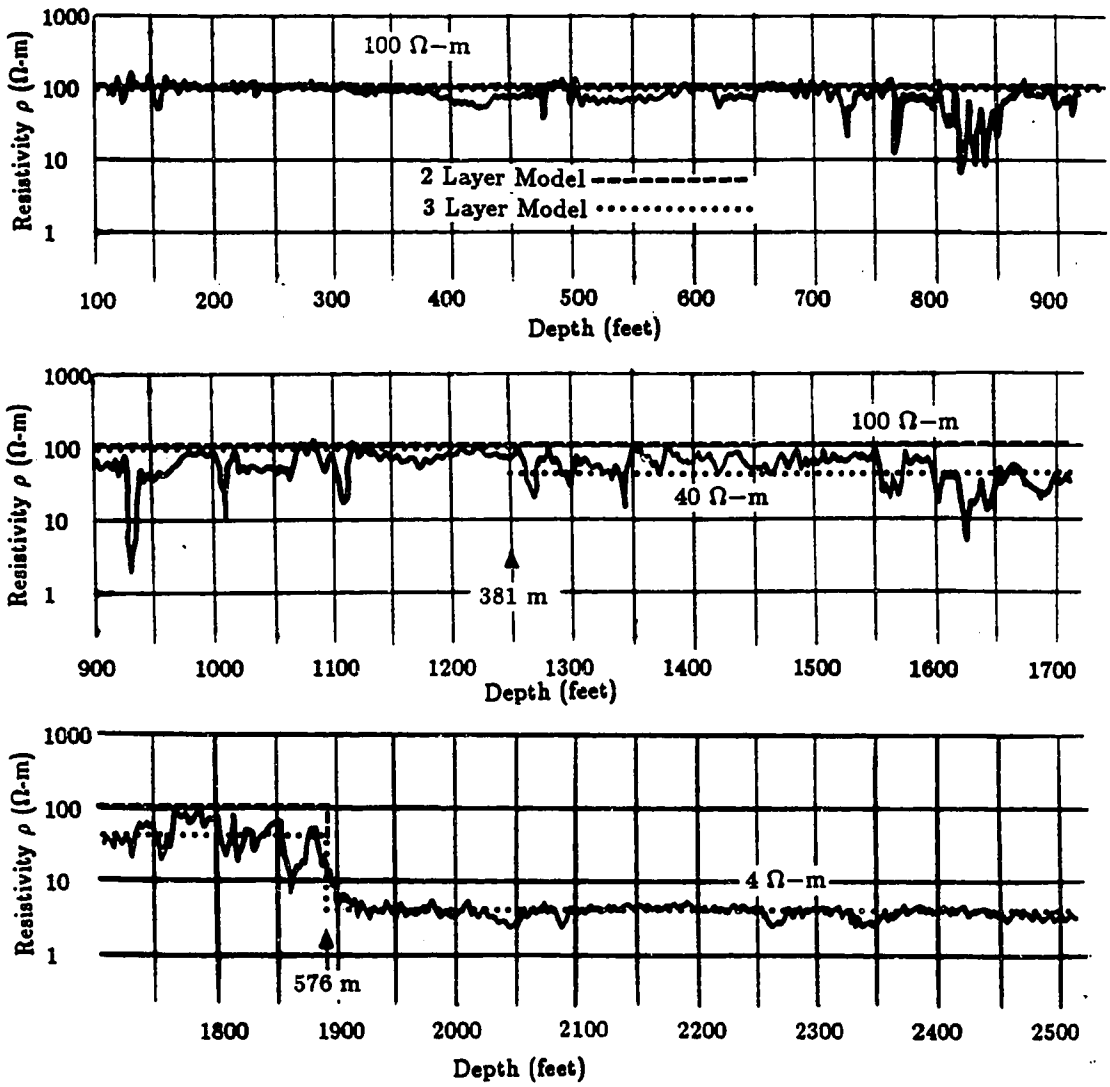

Figure 3.8 DIL record from ARCO D.S. 12-3 located near the Deadhorse TEM site.

layer resistivity is 100 Ω-m with a thickness of 576 meters and the basement has 4 Ω-m resistivity. In Figure 3.8 the 2 layer model is indicated by a dashed line. In the 3 layer model, the first layer is inferred to be 100 Ω-m and 381 meters thick, the second layer is 40 Ω-m and 195 meters thick, and the basement layer has 4 Ω-m resistivity. The three layer model is indicated as a dotted line in Figure 3.8.

The two and three layer models given above were used to produce the theoretical curves shown in Figure 3.9. Also displayed on this figure are the TEM data and the results of inverting the data using the NLSTCI program of Anderson (1982) with the simple two and three layer models from the DIL as starting points. Note that none of the models fit the observed data. The large absolute difference between the forward models from the DIL and the observed data may be due to a difference in absolute calibration between the two instruments but it is more likely to be due to the large thermally-disturbed zone around the well having increased conductivity. In addition, both inverse models were unsatisfactory. The fact that the inverse program often does not iterate to a satisfactory model is the result of 1) the form of the TEM data and 2) the sensitivity of the inverse process to the starting model. This sensitivity comes about because the program does not search the entire solution space available (within the limits set by the input parameter file) but examines the parameter space nearby the starting model (which is often very dissimilar to the solution space near another starting model). This aspect of the program is necessary to hold down run times.

The form of the data at this site is difficult to fit. The primary difficulty in finding a good match to the TEM data is the unusually sharp peak that occurs in the data. In an initial parameter investigation of the thickness and resistivities, it was apparent that no variation of these parameters could produce the sharply peaked waveform. In addition, the later time gates show a pronounced leveling

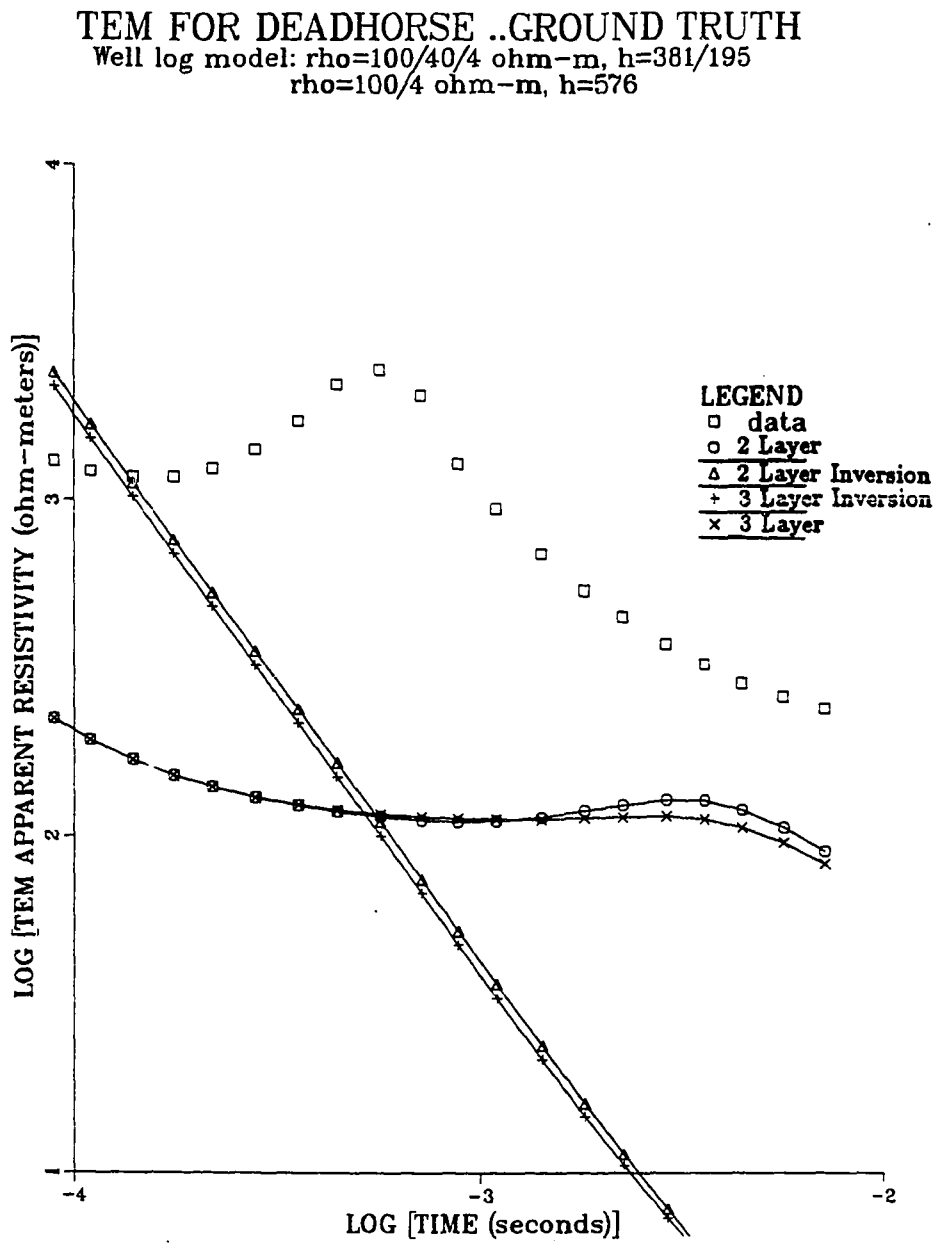

Figure 3.9 TEM data and the theoretical curves for two models from the DIL record plotted as apparent resistivity versus time.

out. It was not possible to produce a model with these characteristics using up to four layers with the parameters varied over a wide range of values. This site is an example for which the data could not be very well matched with any of the models devised. Possible reasons for this will be discussed at the end of this chapter.

Although none of the models gave results which matched the data very well, a two layer model matched as well as any in the sense that the rms error between the data and the inverse model was comparable with any model using more layers. This model is the base model (shown as circles in Figure 3.10) which consists of a first layer resistivity 1040 Ω-m and a thickness of 616 meters and a basement resistivity of 2.14 Ω-m.

Figures 3.10, 3.11, and 3.12 show the results of varying the resistivity of the first layer, the resistivity of the second layer, and the thickness of the first layer, respectively, with the base model described in the preceding paragraph. The base model is displayed as an insert in each of the figures.

Figure 3.12 suggests that if all the other parameters were well known, that a thickness change of 20 meters would easily be resolvable from the two layer model that best matched the data, namely the base model.

Even though the best match between the inverse model and the data is not very good in a visual sense, the error in the estimate of the depth to the base of ice-bearing permafrost, from the TEM 2 layer model relative to that estimated by Osterkamp (personal communication) directly from the DIL namely 576 meters, is only +6.9 %.

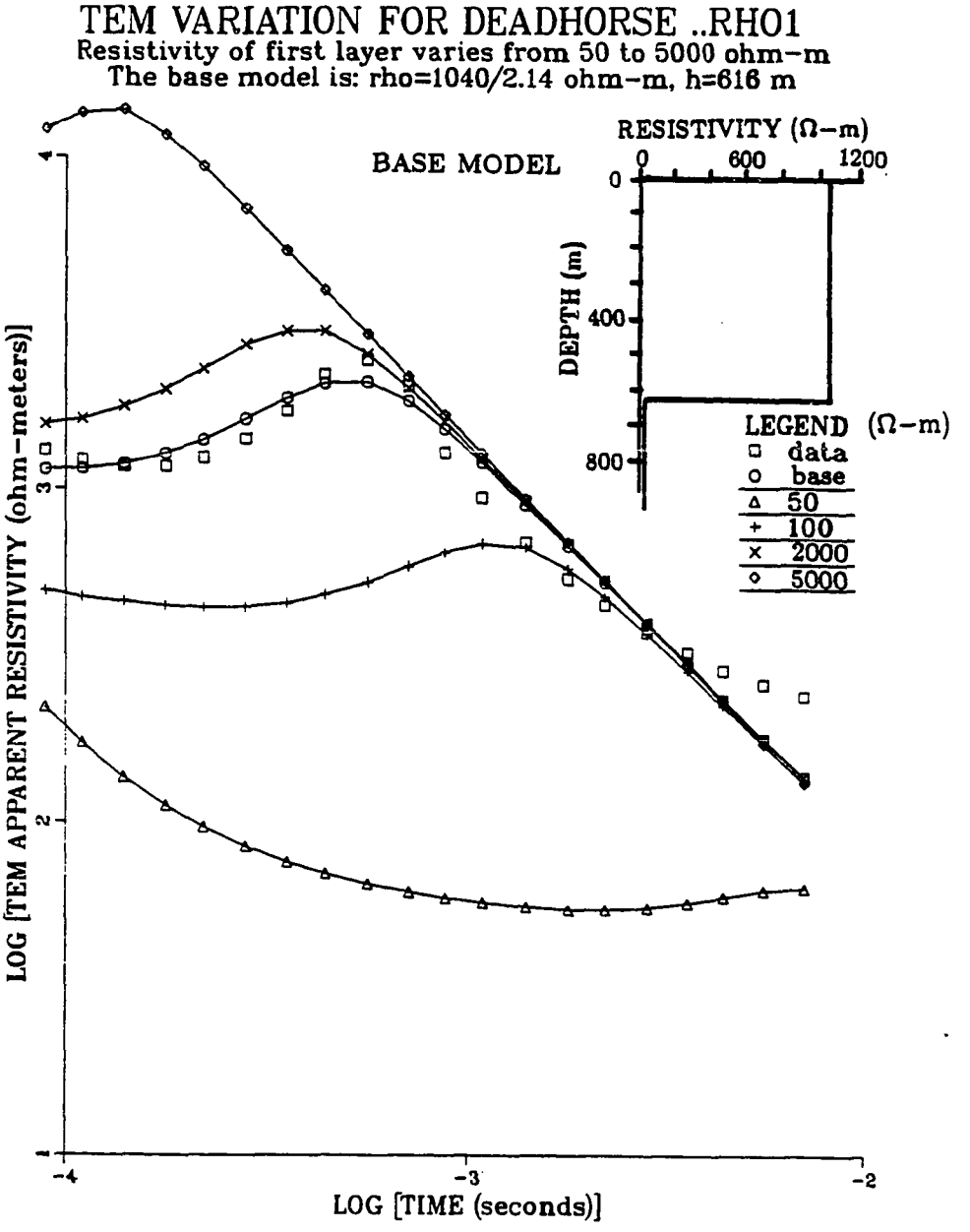

Figure 3.10 TEM apparent resistivity data versus time for Deadhorse site. The resistivity of the first layer is varied in this sequence of apparent resistivity curves for the inverse base model.

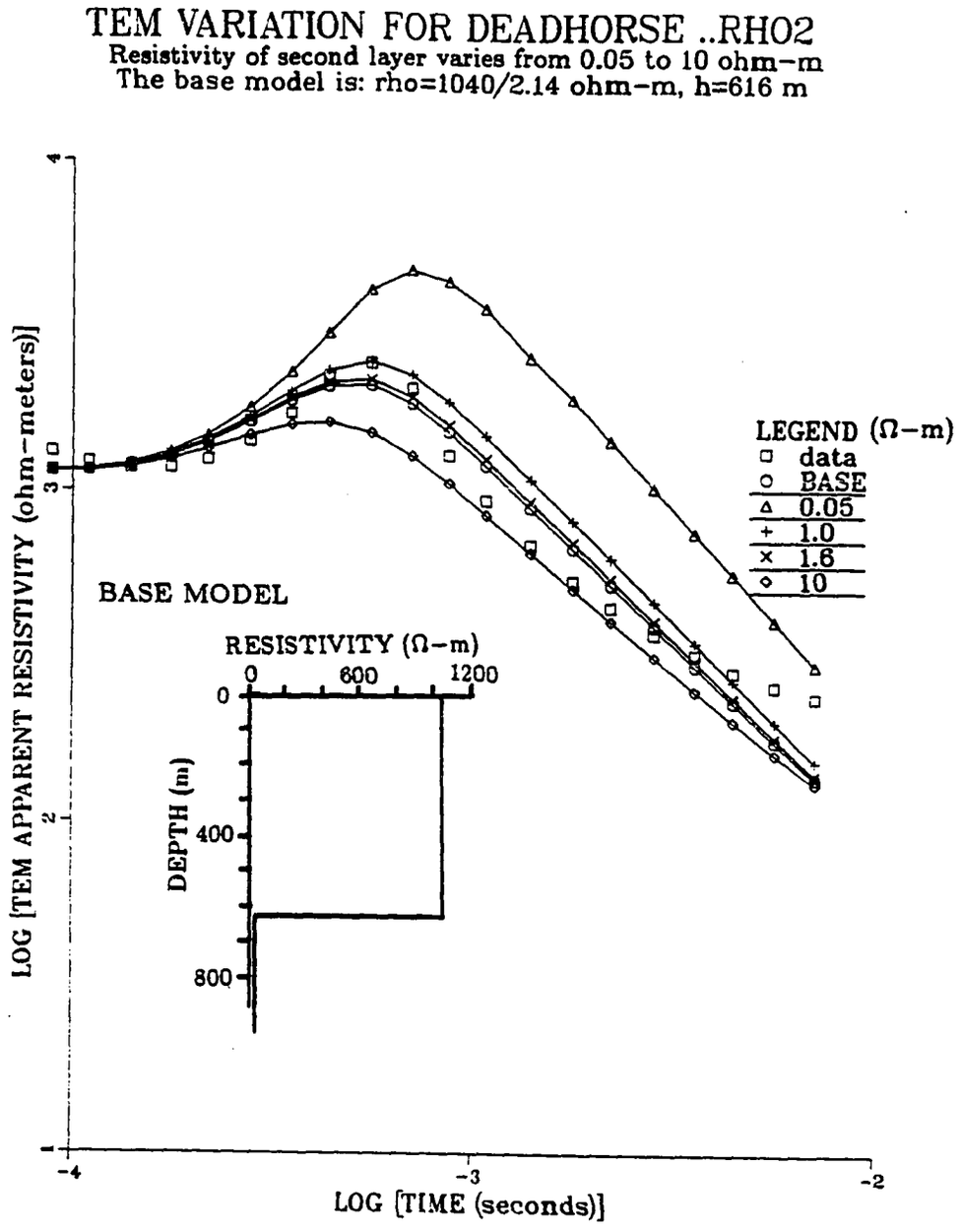

Figure 3.11 TEM apparent resistivity data versus time for Deadhorse site. The resistivity of the second layer is varied in this sequence of apparent resistivity curves for the inverse base model.

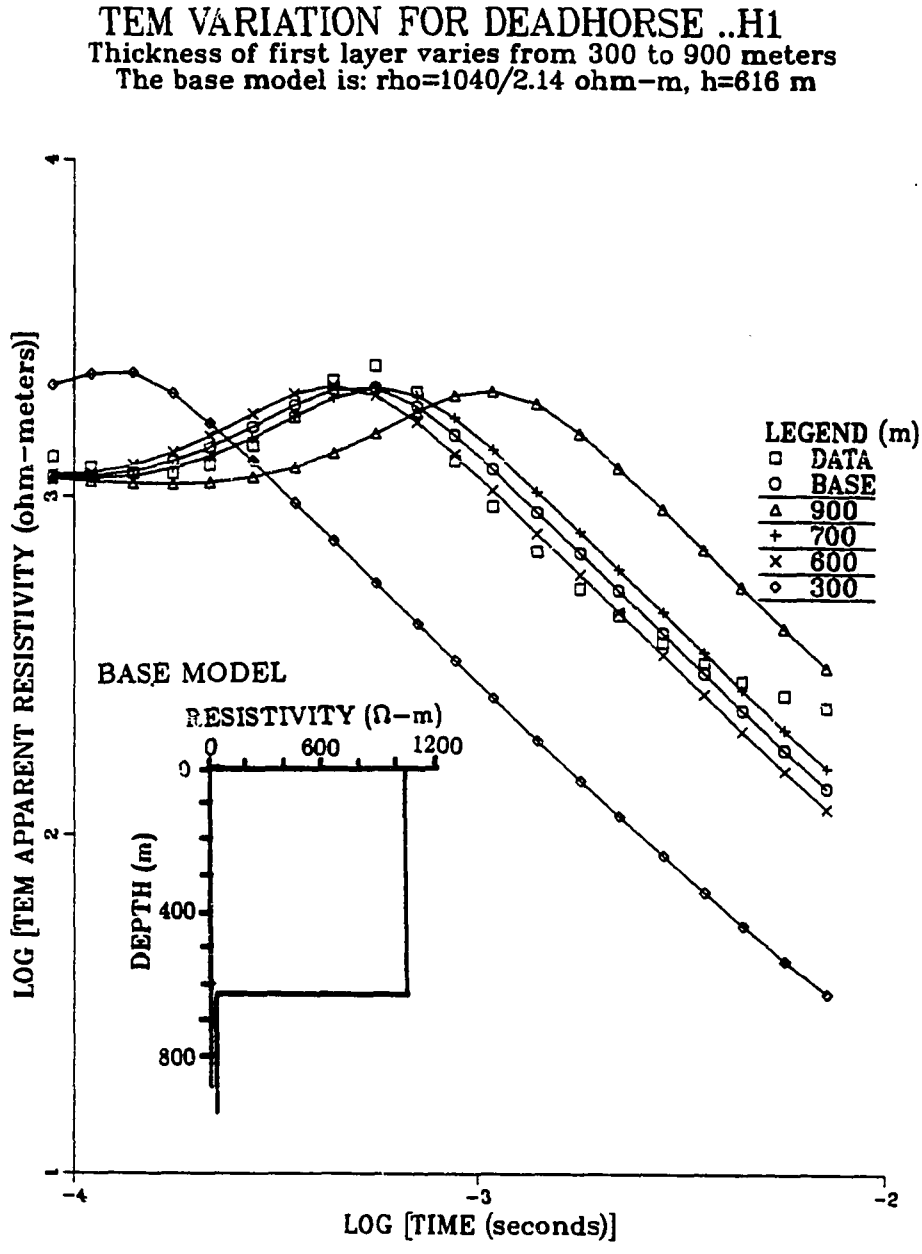

Figure 3.12 TEM apparent resistivity data versus time for Deadhorse site. The thickness of the first layer is varied in this sequence of apparent resistivity curves for the inverse base model.

3.4 REINDEER ISLAND

Figure 3.13 shows the DIL from the Sohio Reindeer Island stratigraphic test well. The driller's log for this well identifies the section from about 86 meters depth to about 156 meters depth as having relatively high clay content (up to 50 percent). The higher clay content may be associated with the trend of a higher resistivity in this same section of otherwise fairly uniform sands and gravels. The higher resistivity may be due to the material being frozen, as is suggested by the decreased drill rate. Another higher resistivity section starting at about 256 meters depth also appears to be associated with a high percentage of clays and a lower drill rate. Clay begins at about 246 meters depth, accounting for as much as 90 percent of the material. The higher resistivity section extends to about 336 meters which is interpreted as the depth to the base of ice-bearing permafrost at this site. Clay content is not uniformly high throughout this entire region of higher resistivity. Part of the difference in resistivity between the higher resistivity and lower resistivity zones may be due to a difference in pore water salinity between what appears to be frozen fine-grained sediments and unfrozen coarser-grained sediments. These effects are discussed in more detail in Chapter 4.

The DIL indicates a 4 or a 6 layer model would be a reasonable representation of the resistivity profile at this site. A 4 layer model is inferred to have a first layer of 10 Ω-m resistivity 19 m thick (inferred from drilling logs, not the DIL), a second layer 237 meters thick with a 2 Ω-m resistivity, a third layer of 20 Ω-m resistivity (perhaps ice-bonded) 80 m thick, and a basement layer with 2 Ω-m resistivity. This 4 layer model is indicated by a dotted line in Figure 3.13. A 6 layer model differs from the 4 layer model in that the 6 layer incorporates an 80 m thick layer of

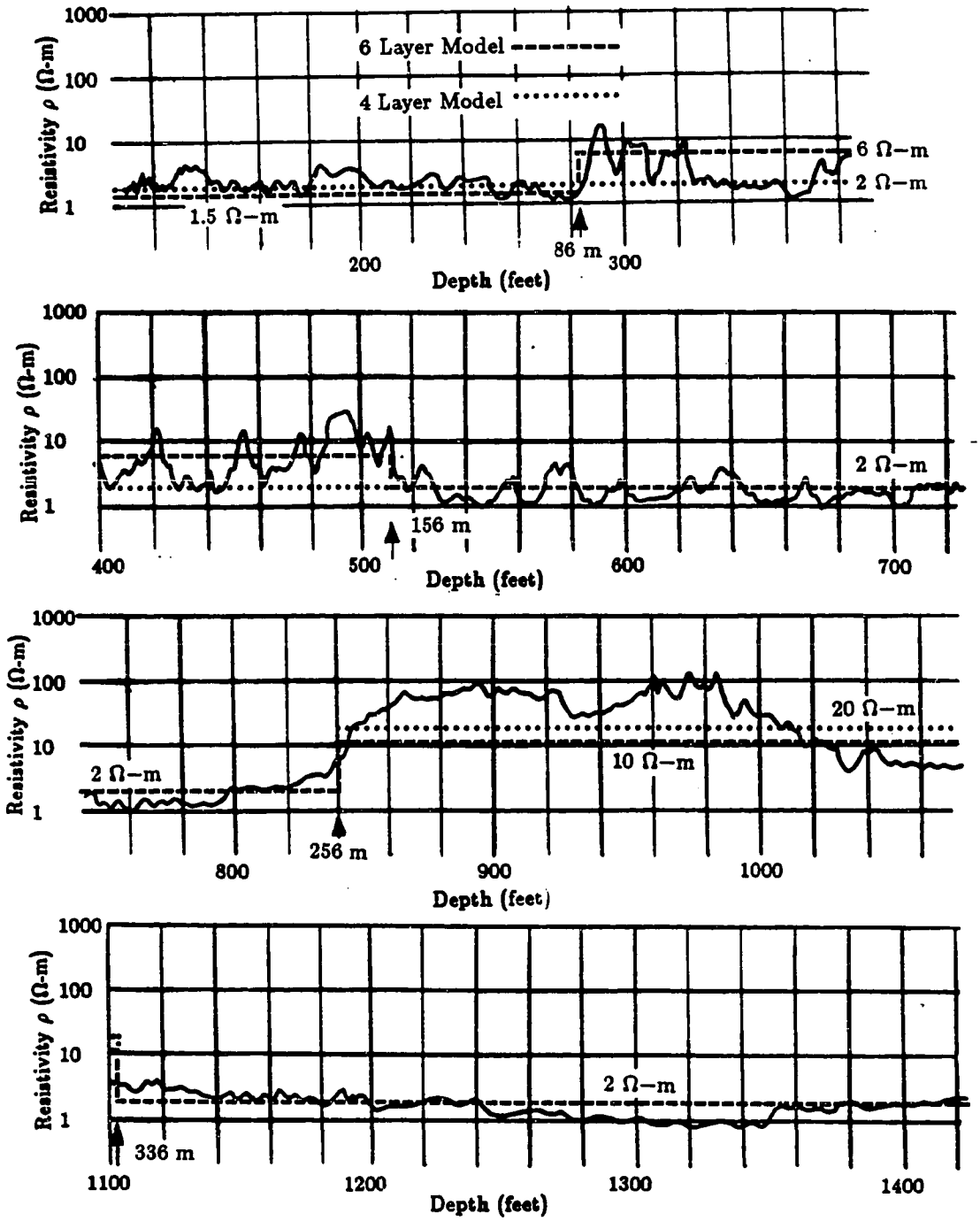

Figure 3.13 DIL record from Reindeer Island Stratigraphic test well displaying multilayered structure in resistivity.

slightly higher (6 Ω-m) resistivity within the 237 m of material. The 6 layer model parameters consists of a first layer 19 m thick with 10 Ω-m resistivity, a second layer 67 meters thick with 1.5 Ω-m resistivity, a third layer 70 meters thick with 6 Ω-m resistivity, a fourth layer 100 meters thick with 2 Ω-m resistivity, a fifth layer 80 meters thick of 10 Ω-m resistivity, and a sixth layer of 2 Ω-m resistivity. This 6 layer model is indicated in Figure 3.13 as a dashed line.

Parameter values used for the two geoelectric models and their theoretical apparent resistivity curves are shown together with the TEM data at this site in Figure 3.14. The later TEM gates are not reliable due to the equipment noise. Note that the resistivities of the data are relatively low reflecting the more saline environment. Again, the models inferred from the DIL record do not match the TEM data very well, although they clearly match better than those of the Deadhorse site discussed previously. Because there are so many parameters in these models, there is a serious problem with nonuniqueness in the models for this site.

As in the previous examples, a large number of inverse models were examined and a model showing the best match (that match which has the least rms error between the data and the inverse model) selected as the base model. The parameters of this base model are $\rho_1 = 5.5\Omega$-m, $\rho_2 = 2\Omega$-m, $\rho_3 = 5.5\Omega$-m, $\rho_4 = 2\Omega$-m, $\rho_5 = 70\Omega$-m, $\rho_6 = 3\Omega$-m, $h_1 = 18.5$ m, $h_2 = 60$ m, $h_3 = 60$ m, $h_4 = 79$ m, and $h_5 = 93$ m. Note that this model is not dramatically different from the 6 layer model inferred from the DIL in constrast to the previous sites studied.

A parameter investigation was then undertaken using the base model. Figure 3.15 demonstrates the effect of varying the first layer resistivity. In Figure 3.15 and the subsequent figures for the parameter investigations for this site is the base model displayed as an insert. An examination of Figure 3.15 reveals that the the apparent resistivity curves are not very sensitive to the resistivity of a thin (compared to

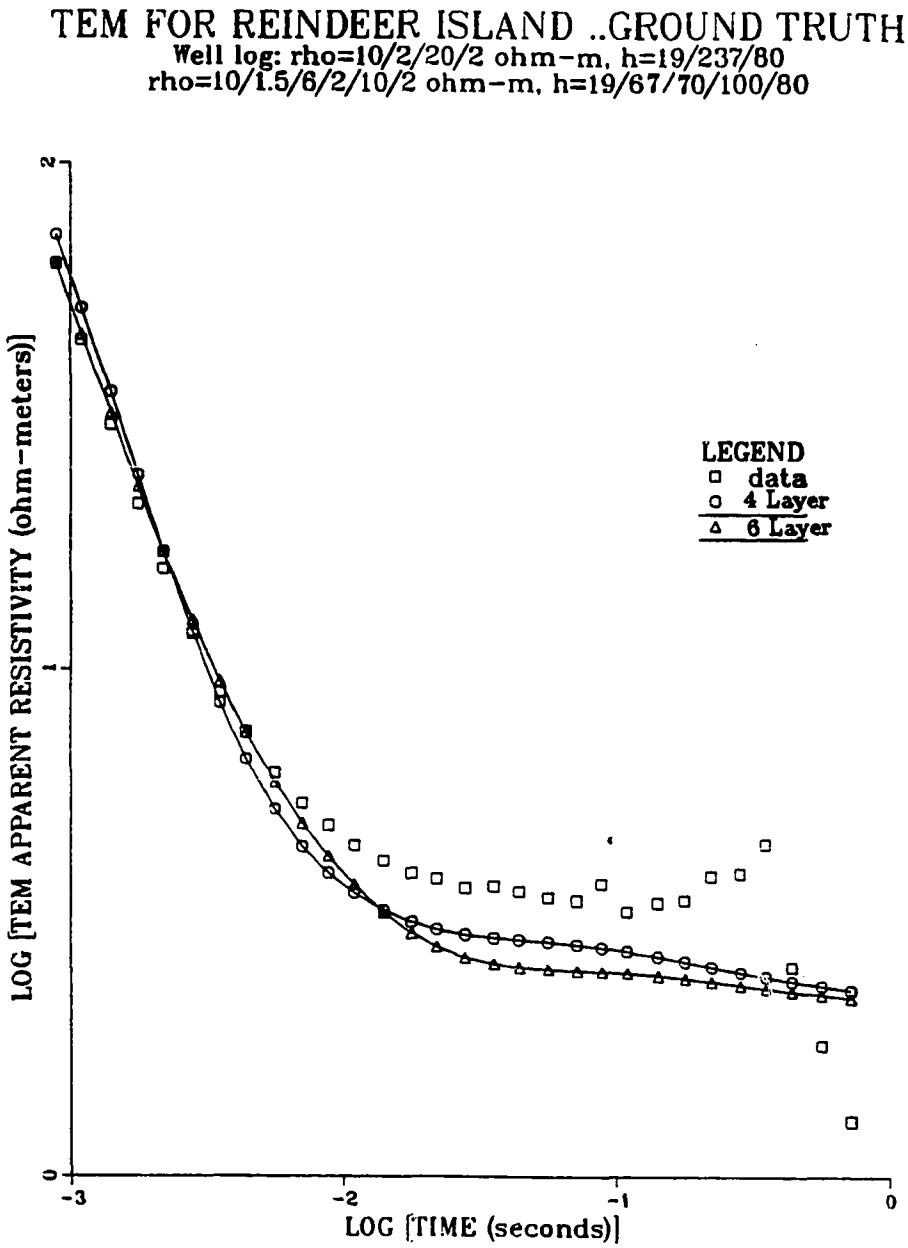

Figure 3.14 TEM theoretical curves of apparent resistivity versus time for the geoelectric models inferred from the DIL for Reindeer Island site. Shown are the curves for the 4 layer and 6 layer models and the actual TEM data taken.

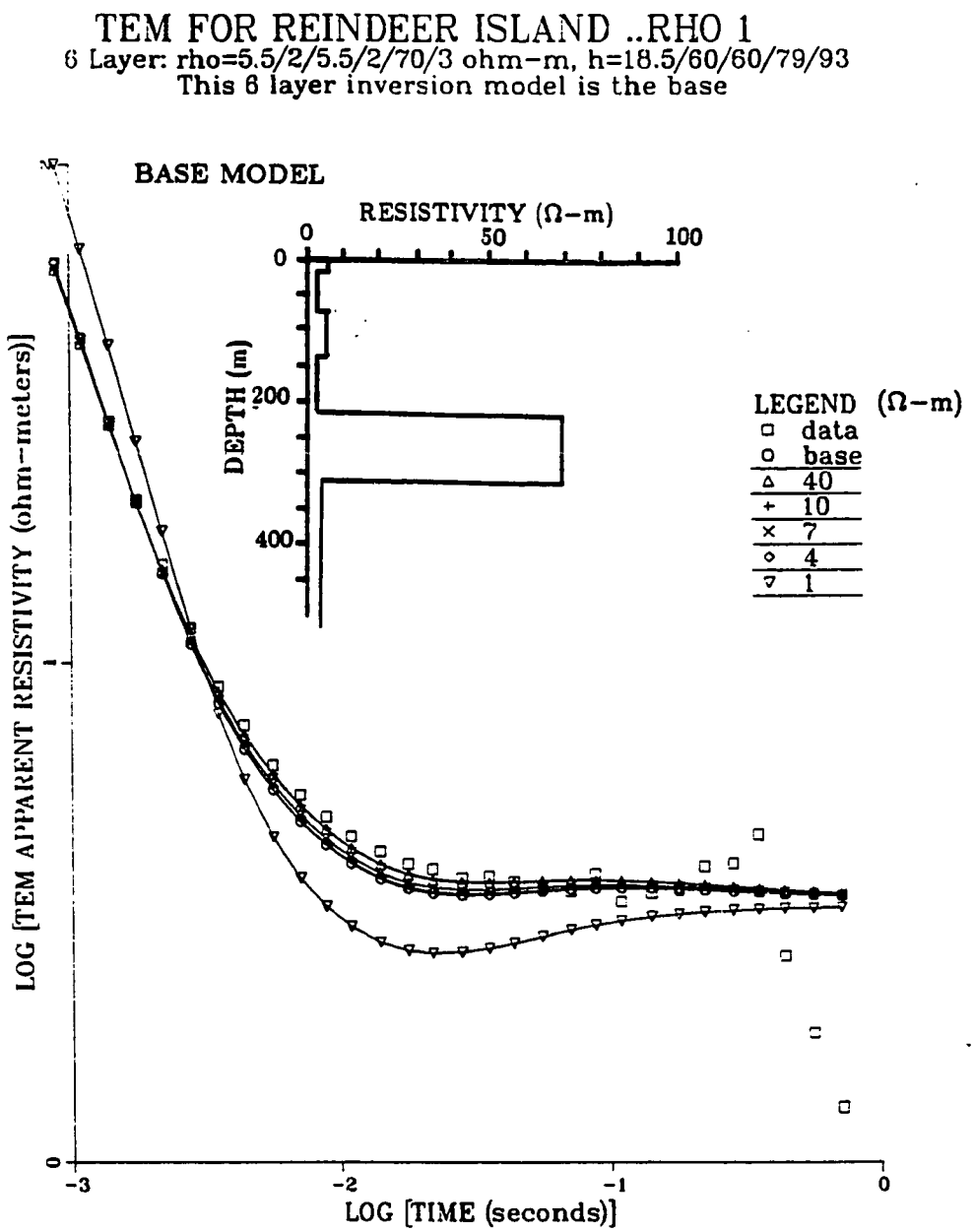

Figure 3.15 TEM curves of apparent resistivity versus time for Reindeer Island varying the first layer resistivity.

the transmitter loop dimensions) layer provided it has a relatively higher resistivity than the next layer down.

An examination of Figure 3.16, obtained by varying the second layer resistivity reveals that the curves are fairly sensitive to the resistivity of the second layer. A comparison of Figure 3.15 at the same time allows one to see how it is possible to vary the resistivity of the first layer and the resistivity of the second layer interactively to obtain nearly equivalent fits to the data. This illustrates the principle of nonuniqueness in the production of interpreted models for multi-layered media. In fact, there may exist many nearly equivalent models that fit the data equally well. Figures 3.17, 3.18, 3.19, and 3.20 show the results of varying the resistivities of the third, fourth, fifth and sixth layers. The effect of the resistivity of the basement layer (sixth) is one of the most dramatic, showing that the resistivity of the basement will have the greatest effect on the later time gates. Although the later gates are more unreliable, the trend of the data before the unreliable gates shows the basement resistivity must be near 2 to 3 Ω-m.

In Figure 3.21, the effect of varying the first layer thickness is shown. If all other parameters were known, it would be possible to discern the thickness of this layer to perhaps within ± 2 meters relative to the base model. Figure 3.22 shows the effect of varying the thickness of the second layer. Note the serious problem with nonuniqueness as is suggested by comparing Figures 3.21 and 3.22. This difficulty is even more serious than can be inferred from Figures 3.21 and 3.22 because the resistivities also enter into the nonuniqueness. However, if all the other parameters were known, the thickness of the second layer relative to the base model could easily be discerned to within ± 5 meters. Figure 3.23 shows the variation in thickness of the third layer. This is a relatively high resistivity layer and shows that the model is not very sensitive to this thickness. However, it may be possible to discern a change

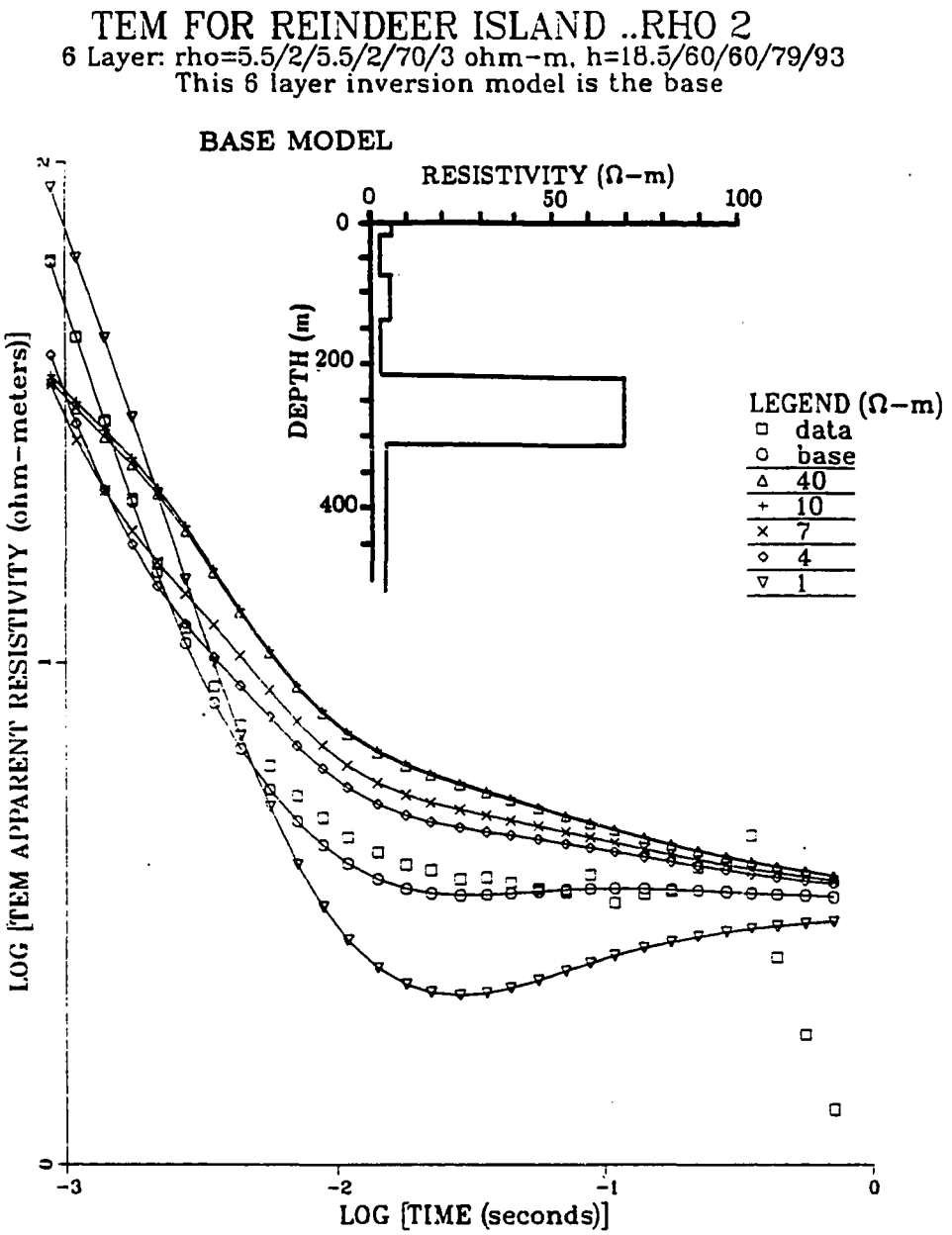

Figure 3.16 TEM curves of apparent resistivity versus time for Reindeer Island varying the second layer resistivity.

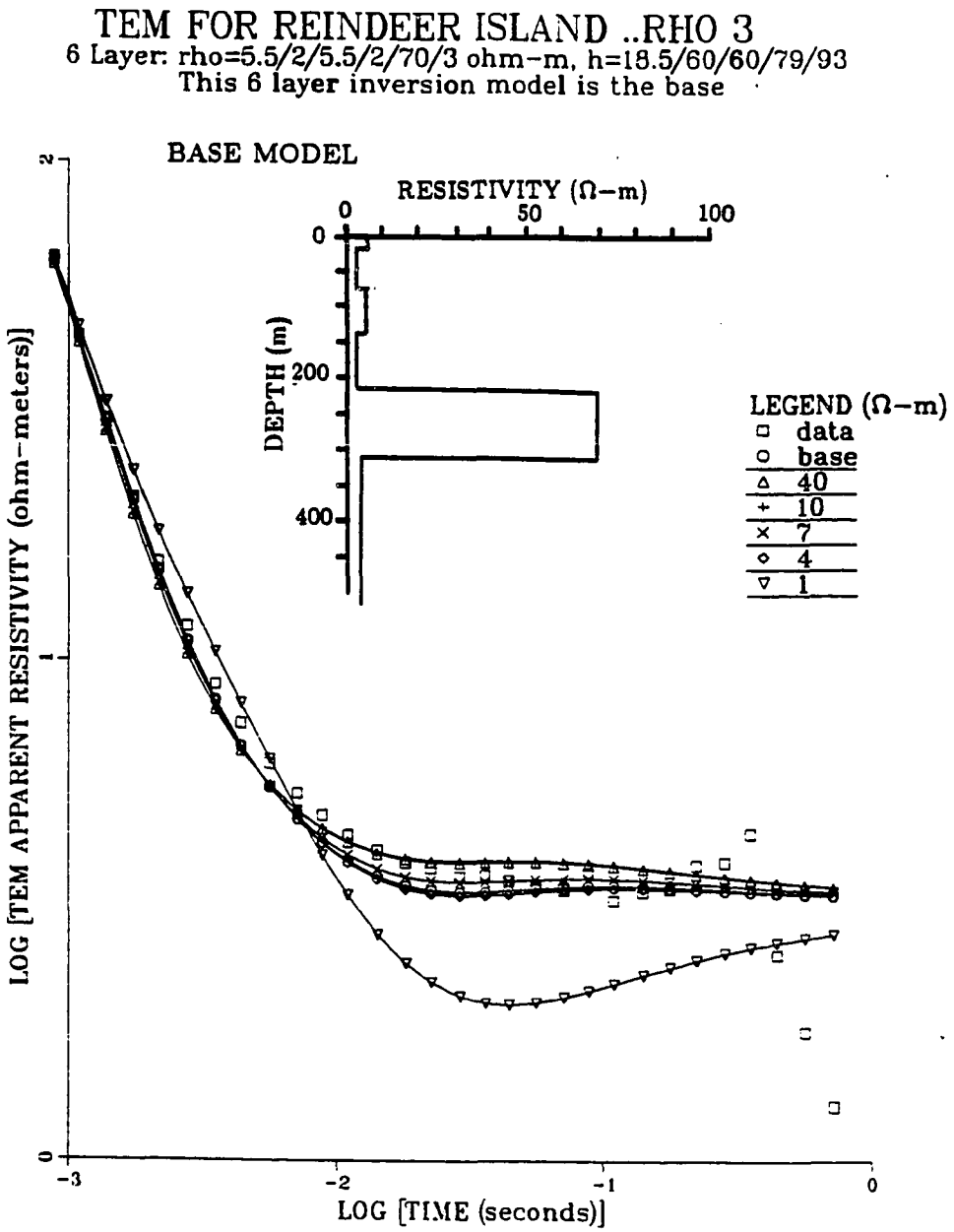

Figure 3.17 TEM curves of apparent resistivity versus time for Reindeer Island varying the third layer resistivity.

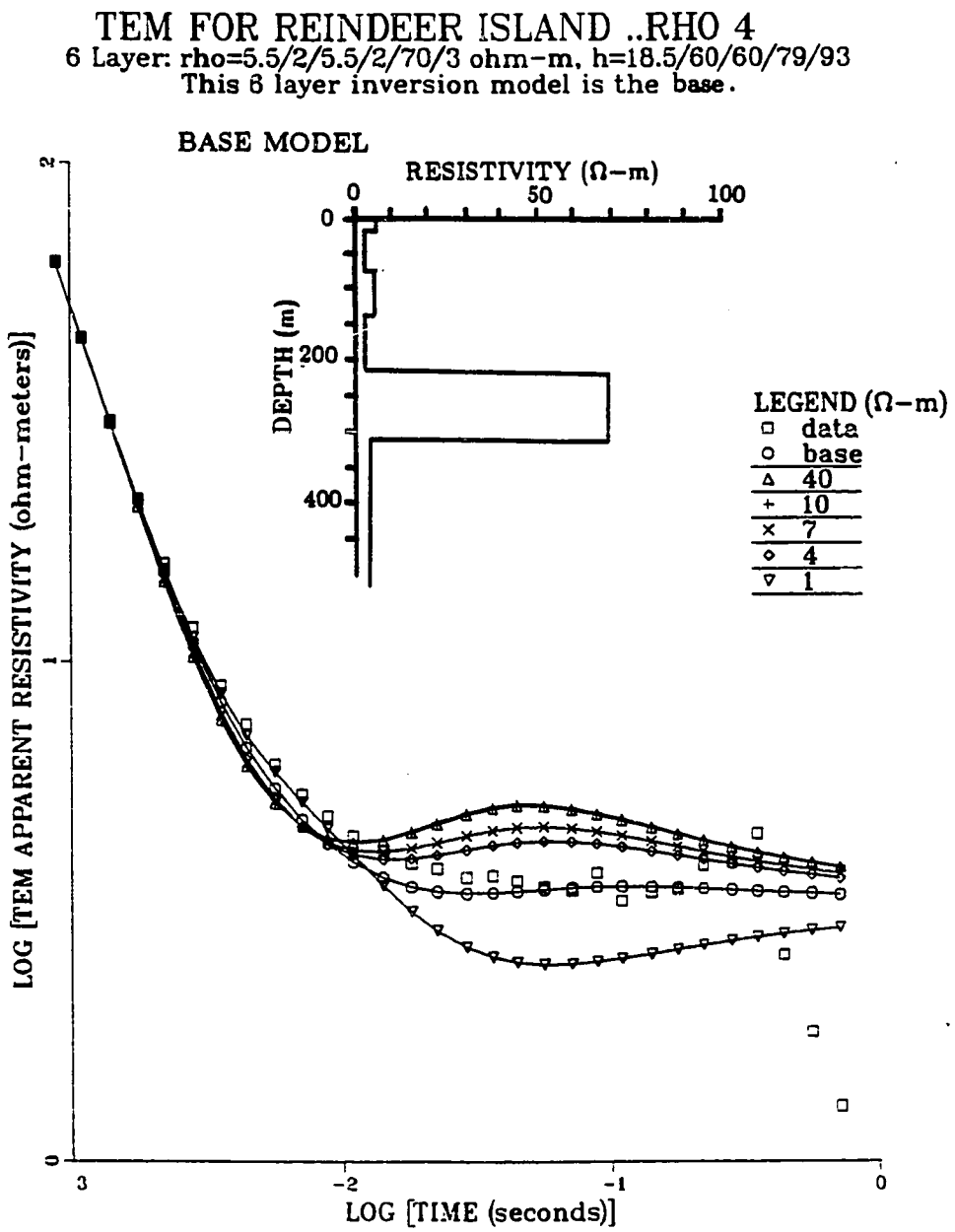

Figure 3.18 TEM curves of apparent resistivity versus time for Reindeer Island varying the fourth layer resistivity.

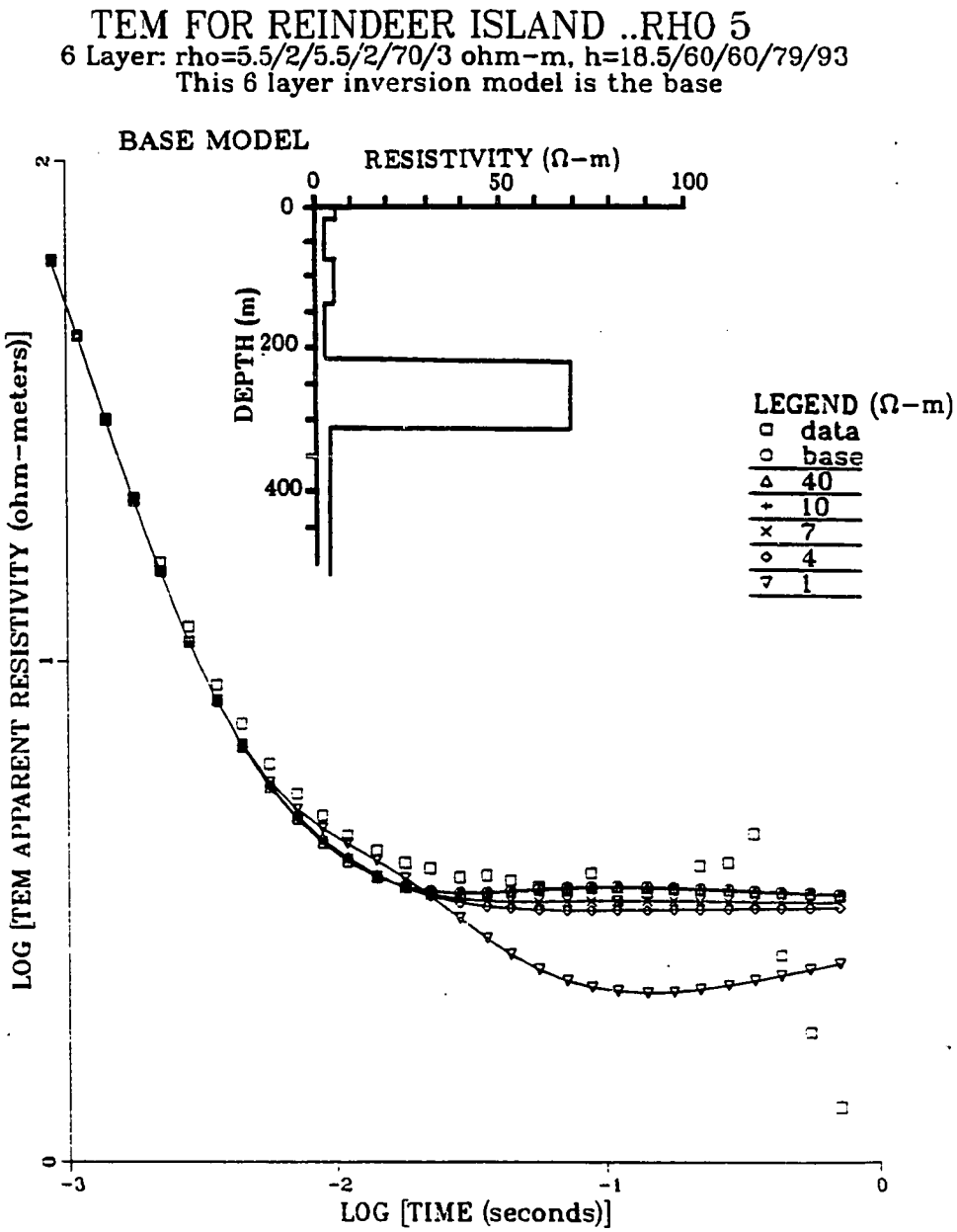

Figure 3.19 TEM curves of apparent resistivity versus time for Reindeer Island varying the fifth layer resistivity.

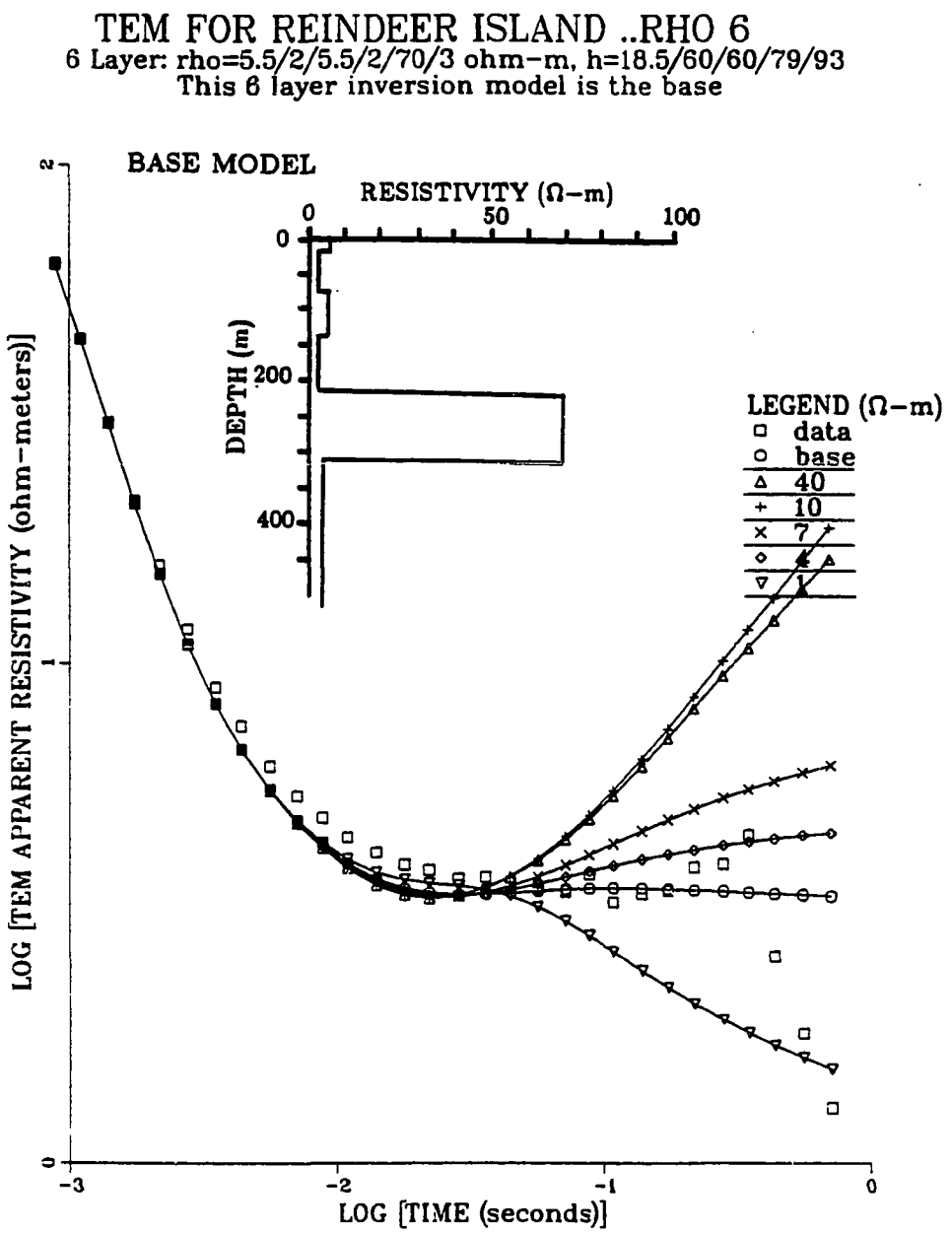

Figure 3.20 TEM curves of apparent resistivity versus time for Reindeer Island varying the sixth layer resistivity.

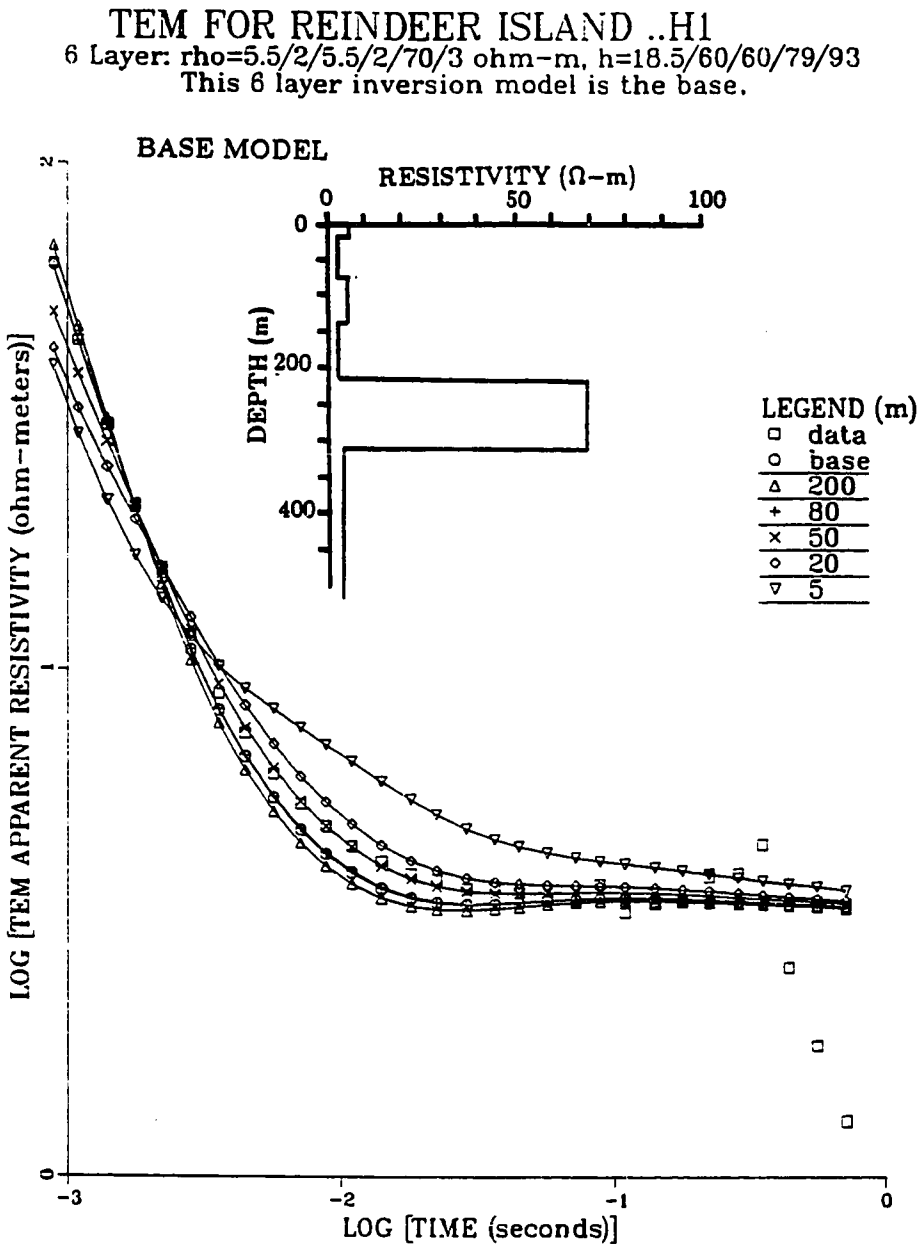

Figure 3.21 TEM curves of apparent resistivity versus time varying the thickness of the first layer for the Reindeer Island site.

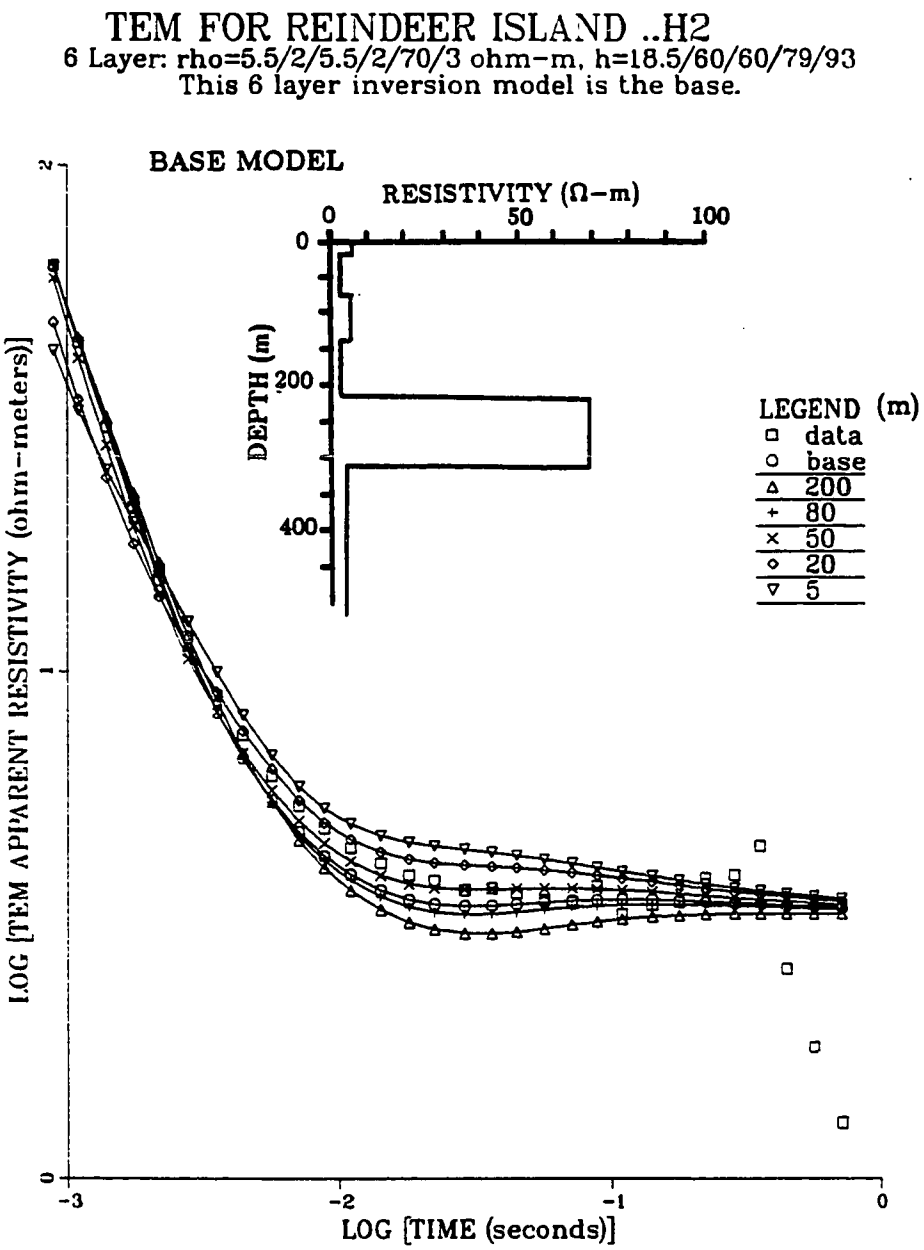

Figure 3.22 TEM curves of apparent resistivity versus time varying the thickness of the second layer for the Reindeer Island site.

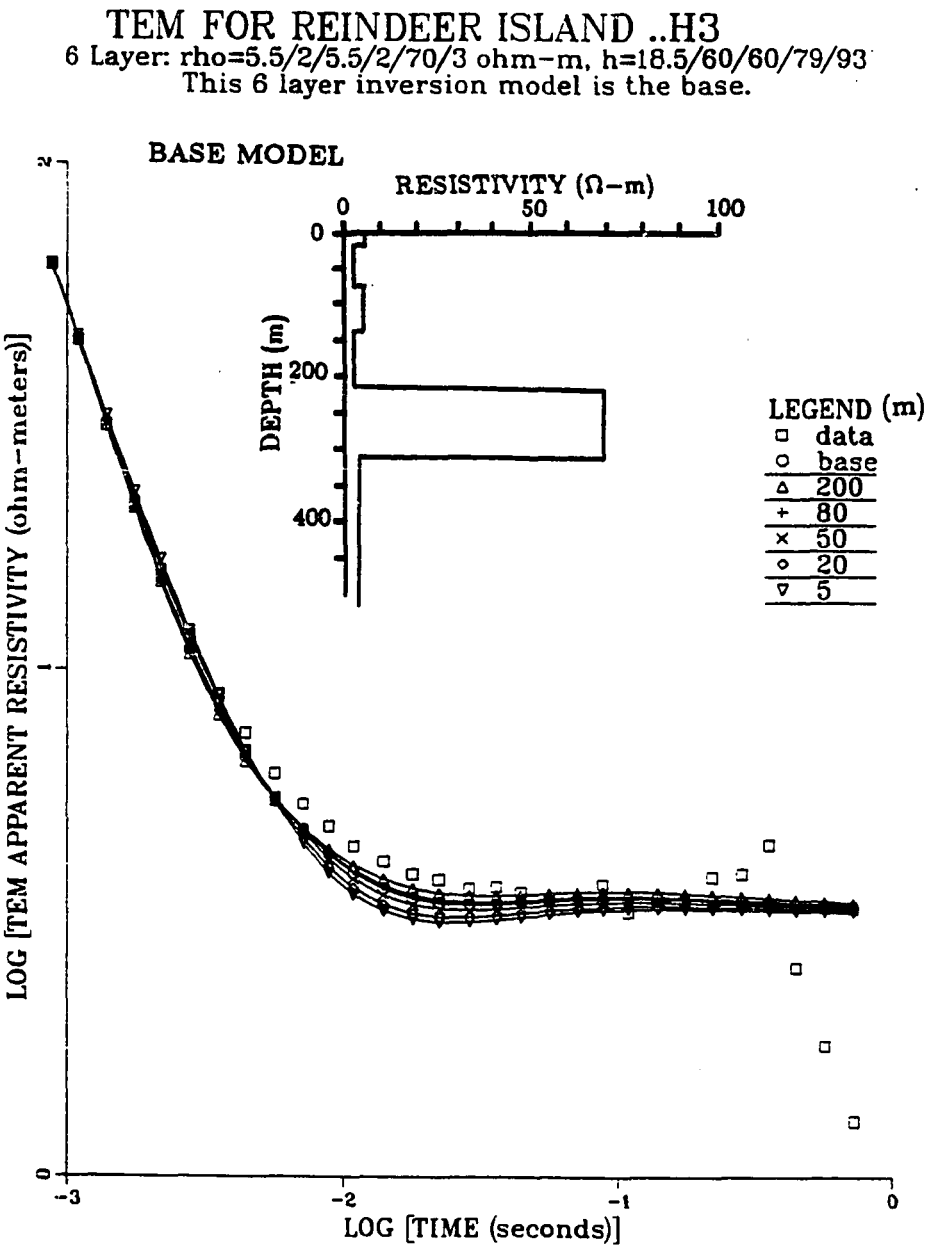

Figure 3.23 TEM curves of apparent resistivity versus time varying the thickness of the third layer for the Reindeer Island site.

in thickness of ±10 meters relative to the base model. Figure 3.24 shows how much more sensitive the model is to the thickness of the relatively less resistive fourth layer. It would be possible to discern a difference of ±5 meters without difficulty. Figure 3.25 shows the results of varying the thickness of the layer with the highest resistivity in the entire sequence, the fifth layer. Once again, the model is not very sensitive to thickness of this layer but it may be possible to discern a difference of ±10-20 meters relative to the base model.

To get a rough idea of the resolution of the TEM system in estimating the base of permafrost, a gross estimate of the resolution of each layer can be taken to be about ±10 percent of the thickness of the layer although the more resistive layers may be resolved with less certainty. Since the total depth resolution requires the addition of the uncertainities for each layer, this means that the total depth can only be resolved to about ±10 percent. If the base of the fifth layer is taken to be the base of ice-bearing permafrost, its total depth is 310 meters. Therefore, an estimate of the depth resolution is about ±31 m. The actual depth estimated from the DIL is about 336 m whereas the result of the inverse model gives a value which is smaller by -7.6 percent. It is very important to recognize that the determination of the actual resolution of the system for the depth to the base of ice-bearing permafrost is much more complicated, involving not only the nonuniqueness of the TEM models, but also the possibility of other complicating factors discussed below.

3.5 DISCUSSION AND CONCLUSIONS

Models based on computer inverse modeling of the data from three TEM sounding sites on the North Slope of Alaska have been examined and compared with the

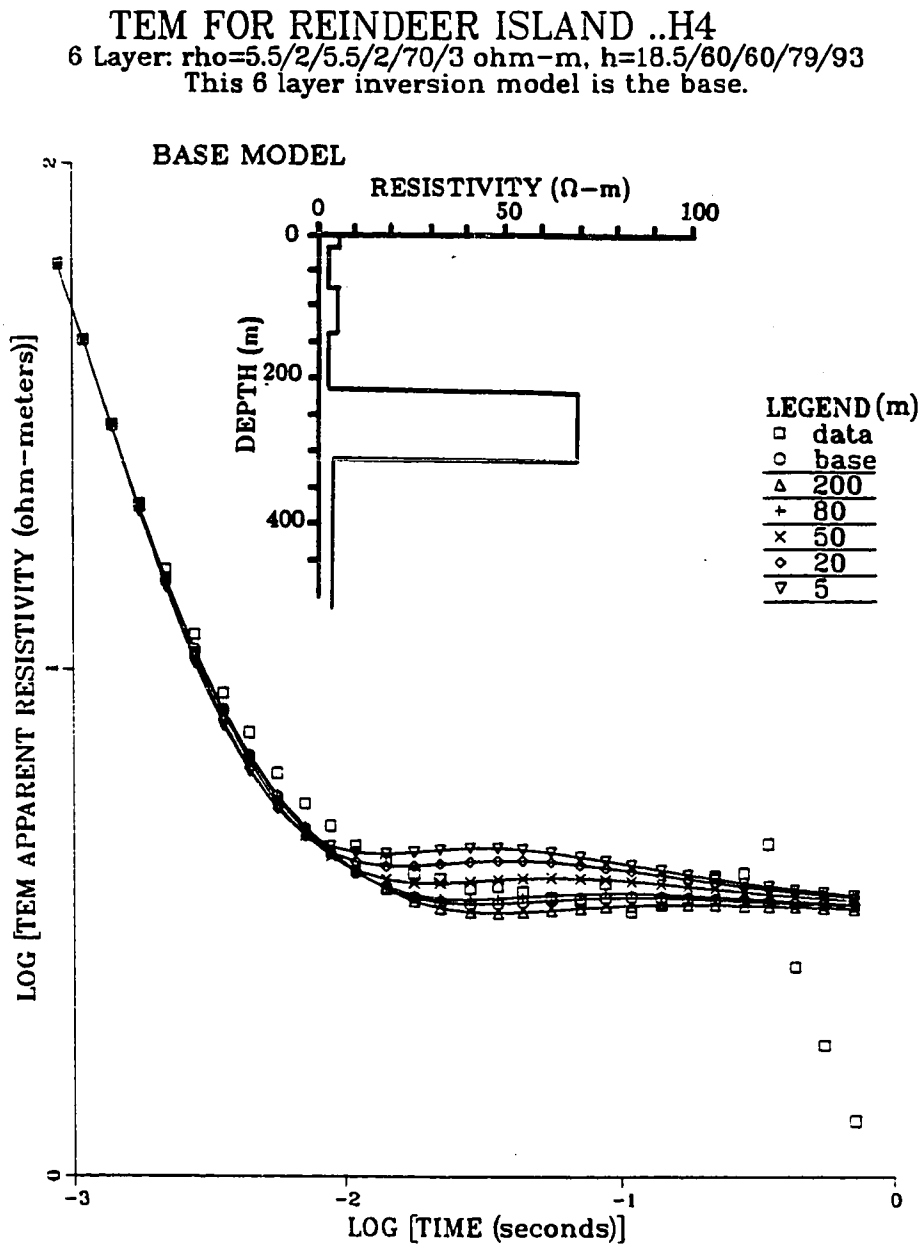

Figure 3.24 TEM curves of apparent resistivity versus time varying the thickness of the fourth layer for the Reindeer Island site.

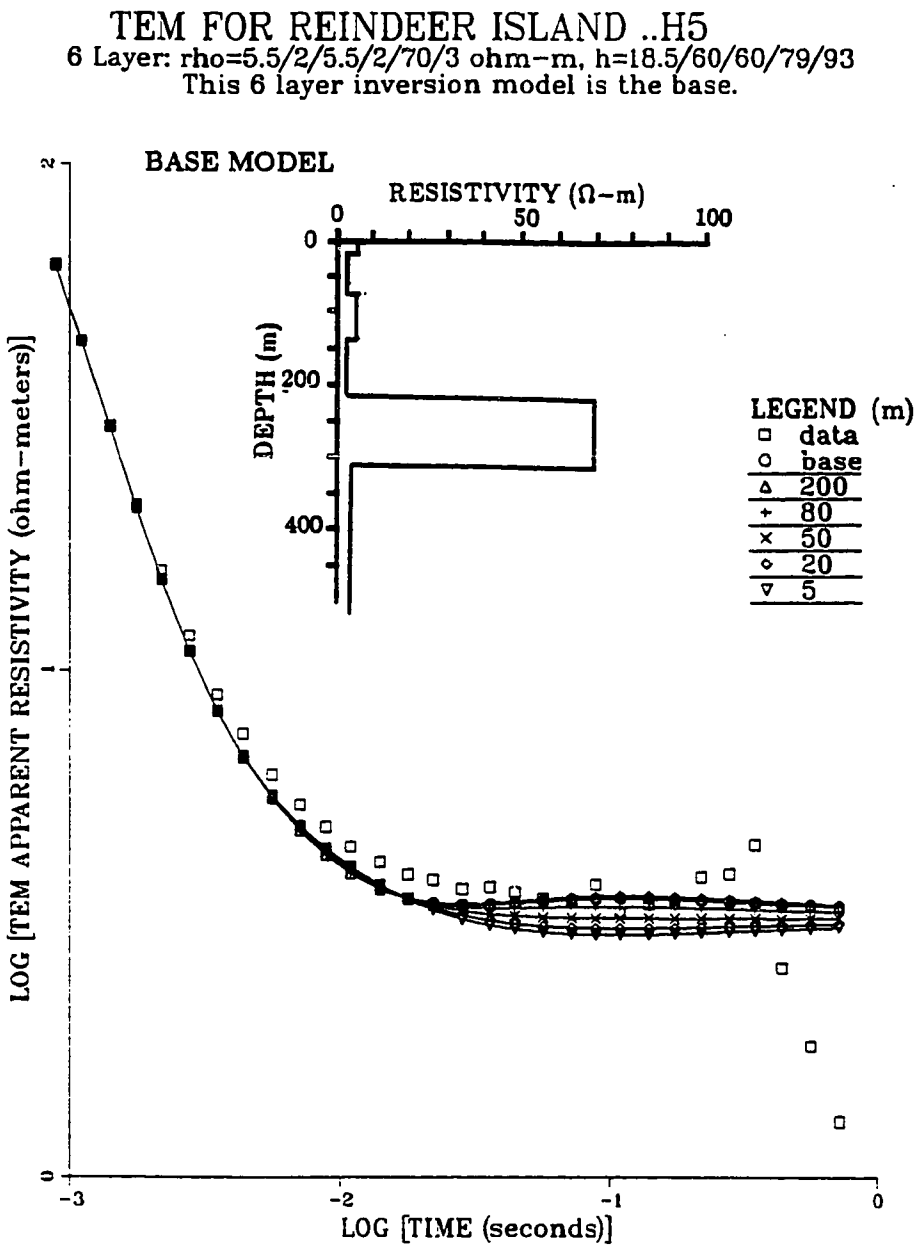

Figure 3.25 TEM curves of apparent resistivity versus time varying the thickness of the fifth layer for the Reindeer Island site.

DIL records from nearby drill sites. At each site, a parameter investigation was conducted using the result of the computerized inverse modeling as a base model for the parameter changes. These investigations all show that the value of a particular parameter may be determined to within ±10 percent as an upper limit, if all the other parameters are known and held fixed. In particular, these studies suggest that the depth to permafrost may be determined to within 10 percent of the actual value under certain circumstances.

It is not the intention of the author to claim that the resolution of the TEM method is in actuality better or worse than this estimate. To determine the actual resolution capability of the TEM method would require a much more extensive investigation of the parameter space in each particular instance with true known values for the parameters. Each site discussed displays considerably different apparent resistivity curves and different models based on the DIL, and therefore, a different parameter space. Since the parameter space for a particular model type is being used to model specific site data, the best approach to a description of the resolution of the TEM method would be to examine the error between the data and the curve predicted by the model. A complete map of the parameter possibilities must be examined, not just the variations around a local solution.

Finally, mention should be made of some complicating factors that may affect the conclusions based on the parameter study and comparison with the DIL data. The DIL data gives no information about lateral inhomogenieties in resistivity and further, the DIL devices are fixed frequency instruments that give no information on materials that may possess resistivity that is frequency dependent. The DIL resistivity data probably give reasonable estimates of the base of the ice-bearing permafrost and depths to other lithological features, but the magnitude of the resistivities are probably not representative of true formation resistivities in

the permafrost zone. DIL resitivities cannot be corrected to obtain true permafrost formation resistivities using the existing Schlumberger Interpretation charts, because borehole sizes at shallow depths and the high resistivities of permafrost fall well outside the range of applicability of these charts. Reliable corrections for the DIL data require a complete knowledge of the extents of the thawed and thermally disturbed annuluses around a borehole, the soil electrical characteristics and the response function of the resistivity instrument.

Another complication is the possible occurrence of three-dimensional resistivity structures beneath the site of the soundings. Modeling studies using simple resistivity contrasts between three-dimensional bodies and the host material by Anderson and Newman (1985) show that there is a definite increase in the steepness of the apparent resistivity curves obtained in the TEM central induction mode relative to the simple, layered or homogeneous earth case. This may explain the difficulty encountered in fitting the Deadhorse TEM data (Section 3.3) because this site displays a very steep apparent resistivity curve.

In Chapter 5, a case of an anomalous TEM response is discussed which is modeled by an induced polarization (IP) effect. The presence of materials exhibiting IP effects underlying the TEM sounding site may alter the response of the TEM system such that the existing inverse program used, which assumes simple resistivity for the earth, produces inverse models that cannot be made to exactly match the data.

Despite all the potential difficulties, the results of the inverse modelings appear to give reasonably good estimates for the depth to the base of ice-bearing permafrost when a reasonable starting model is available as for the three sites studied here. In Appendix A, a large number of TEM sites, where little or no ground truth in the usual sense is available, are studied. Where no in situ well logs are available,

the depth to ice-bearing permafrost can be estimated by thermal modeling if the local climate is known. That any of the final models for the permafrost depth differ greatly from the estimates based on thermal modeling would suggest other unexpected materials or processes occur at the site, e.g. mineralization with low resistivity and three-dimensionality or unfrozen conditions caused by hydrologic flow. In this sense, the TEM method can be a valuable aid in assessing the distribution, thickness and electrical characteristics of permafrost.

CHAPTER 4. TEM DETECTION OF SUBSEA PERMAFROST

4.1 INTRODUCTION

This chapter gives the geoelectric interpretations of a set of transient electromagnetic (TEM) sounding data taken along a line from the NPBS #1 well through Reindeer Island, approximately 13 kilometers offshore. Geophysical measurements have been made along this line (Osterkamp and Harrison, 1977; Sellmann and Chamberlain, 1980; Rogers and Morack, 1980) which provide an estimate of the depth to the ice-bonded subsea permafrost table. The TEM interpretations presented in this chapter are based on computer generated inverse models of a horizontally layered earth.

Subsea permafrost which underlies the Beaufort Sea offshore of Prudhoe Bay is thought to be remnant of permafrost formed when sea levels were lower and land surfaces that are presently inundated were exposed to cold air temperatures (Hume et al., 1972). Just onshore, the ice-bearing permafrost is thick (640m) (Osterkamp et al., 1985). Near the seabed, a thawed layer of subsea sediments exists which generally thickens with distance offshore. An ice-bearing zone exists below the thawed sediments. This ice-bearing zone shows evidence of layering and some of these layers may be thawed while others appear to be well-bonded (Osterkamp and Payne, 1981). In this area of the Beaufort Sea, geomorphological evidences of historical sea level fluctuations suggest that the North Slope close to the sea may have had sea-water invasions many times in the past (Hopkins, 1967). Recently the sea has been moving inland at about one meter per year (Hume et al., 1972). Because of the gradual rise in sea level, the ice-bearing subsea permafrost is thought

to thin with distance offshore as suggested by the thermal modeling of Lachenbruch et al. (1982), Osterkamp and Harrison (1982), and Osterkamp et al. (1985).

It is evident from the above discussion that the lithology of the permafrost zone offshore is complex. It can be inferred from this that the variation of resistivity versus depth is also complex and the DIL logs from offshore islands confirm this showing evidence for a number of unfrozen and ice-bearing layers. Because of the sea water, thawed saline seabed, and relatively warm permafrost, the resistivities encountered offshore in the permafrost zone should be very low relative to land sites for the same depths. Under these circumstances, the use of electromagnetic induction methods such as the TEM to delineate the complex structure and the base of subsea permafrost does not appear favorable, because the skin depth is relatively shallow, on the order of a few hundred meters (see Chapter 1.7 Equation 1.9). Nevertheless, Ehrenbard et al. (1983) used the TEM method in an earlier study to estimate the thickness of the unfrozen layer and the depth to the base of subsea permafrost along a line in the Prudhoe Bay area, near, but apparently not parallel with the line studied in this chapter. The rationale for the study in the present chapter is to verify that the TEM method can be used to characterize subsea permafrost using a more sophisticated, inverse program and a more complete geophysical data set than was apparently available to Ehrenbard et al. (1983) and thus to complement the existing data on offshore permafrost along the West Dock–Reindeer Island line.

4.2 EXPERIMENTAL DETAILS

Sounding sites were located on sea ice at 0.75, 1, 3, 5, 7, 9, 11, and 14 kilometers from shore along a line, bearing N 31.5° E, from NPBS # 1 well which extends through Reindeer Island where a site at 13 kilometers offshore was located. These sounding sites are denoted as black circles in Figure 1.2. The Reindeer Island site and a site just onshore (0 km, West Dock site) were discussed in Chapter 3. At the time of the soundings during the spring of 1984, there were approximately 1.5 to 2 m of sea ice over shallow ($\leq$ 7m) sea water. Sounding data taken at the sites at 0 and -2 kilometers onshore were very noisy due to man-made electromagnetic interference; there were also numerous pipelines in the immediate vicinity of the sites and thus the data from them are not interpreted here. The West Dock data reported in Chapter 3 was sounded in 1983.

TEM soundings were taken with a Geonics EM-37 at repetition rates of 30, 3 and 0.3 Hz with a square transmitter loop, 500 m on a side, and a small coplanar receiver coil located at the center of the transmitter loop, except for the 0.75 km (no large loop used) and the 14 km (400 meter loop) sites. All the sites were also sounded with a 250 meter transmitter loop, which aided in interpreting the data of the 500 meter loop.

Sounding data were reduced to field strength at the receiver coil and statistics (mean and standard deviation) for each time gate were computed. The data were corrected with algorithms written by the candidate using the full field expression (see Chapter 2, equation 2.34) rather than the simpler late stage approximation which was applicable for the sites discussed in Chapter 3. Once corrected for the ramp time turnoff, the data were converted to apparent resistivity and interpreted

using the results of visual matching and computerized inverse modeling for a layered earth.

Initial interpretations of the transient soundings were completed by visually matching a variety of forward modeled theoretical curves with the TEM sounding data. The forward model with the best apparent match to the data was used to infer the layered earth. These visual interpretations usually differ markedly from those arrived at by using the NLSTCI inverse program of Anderson (1982). Superior matches with the sounding data were obtained with the inverse process by allowing the program to iterate to the solution with the least root mean square (rms) error.

An example of a comparison between the models as determined by the matching technique and by inverse modeling is presented in Figure 4.1. The 500 meter transmitter soundings at three kilometers offshore, which may be considered typical, have been reduced to apparent resistivity and plotted versus the square root of time on log-log scales in Figure 4.1. The interpreted model from the inverse program (dashed curve) and the visual interpretation (solid curve) show that the inverse result is a superior match.

Table 4.1 lists all the models attempted using the inverse modeling technique. Many different models were conceived in an attempt to find the one which gave the best fit to the data. Table 4.2 and 4.3 compare the predictions obtained from curve matching and computerized inverse modeling respectively. The resistivities are given in units of Ω−m and the layer thicknesses in m.

Table 4.2 lists all the sea ice sounding sites and the visual (curve matching) model results for 2 or 3 layers. Table 4.3 gives the results of computer inverse modeling for all the sites using the 1, 2, 3, and 6 layer models. Presentation of the results to 0.1 m in thickness and 0.01 Ω-m in resistivity is not intended to indicate resolution, but to make more complete information available for future researchers.

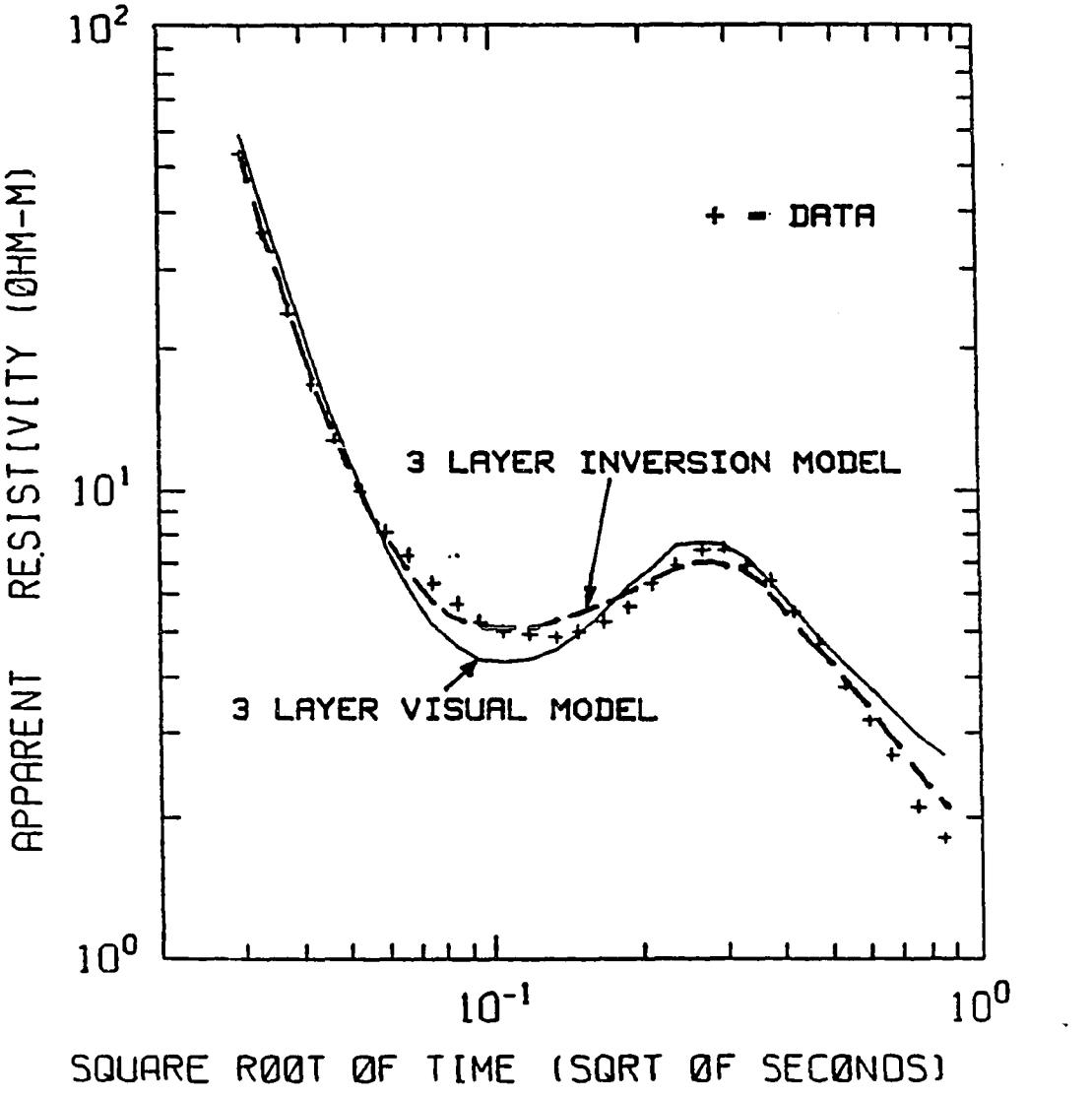

Figure 4.1 TEM apparent resistivity data plotted versus the square root of time compared to the visually-matched model and the computer inversion model for the 3 kilometer site.

TABLE 4.1 MODELS USED FOR INVERSION

1) Homogeneous Half-Space (HHS): matches data to a single resistivity (ρ).

2) Two layer:
   - ρ_1 : sea-water and thawed sediments.
   - ρ_2 : higher resistivity ice-bearing region.

3) Three layer:
   - ρ_1 : sea-water and thawed sediments.
   - ρ_2: ice-bearing permafrost.
   - ρ_3 : conductive basement.

4) Four layer:
   a) : ρ_1 : sea-water.
   - ρ_2 : thawed sediments.
   - ρ_3 : ice-bearing permafrost.
   - ρ_4 : conductive basement.

   b) : ρ_1 : sea-water and thawed sediments.
   - ρ_2 : partially thawed sediments.
   - ρ_3 : ice-bearing permafrost.
   - ρ_4 : conductive basement.

5) Five layer:
   a) : ρ_1 : sea-ice.
   - ρ_2 : sea-water.
   - ρ_3 : thawed sediments.
   - ρ_4 : ice-bearing permafrost.
   - ρ_5 : conductive basement.

   b) : ρ_1 : sea-ice.
   - ρ_2 : sea-water and thawed sediments.
   - ρ_3 : partially thawed sediments.
   - ρ_4 : ice-bearing permafrost.
   - ρ_5 : conductive basement.

   c) : ρ_1 : sea-water and thawed sediments.
   - ρ_2 : ice-bearing permafrost.
   - ρ_3 : thawed sediments.
   - ρ_4 : ice-bearing permafrost.
   - ρ_5 : conductive basement.

6) Six layer:
   a) : ρ_1 : sea-water.
   - ρ_2 : thawed sediments.
   - ρ_3 : ice-bearing permafrost.
   - ρ_4 : thawed sediments.
   - ρ_5 : ice-bearing permafrost.
   - ρ_6 : conductive basement.

   b) : ρ_1 : sea-water.
   - ρ_2 : thawed sediments.
   - ρ_3 : partially thawed sediments.
   - ρ_4 : slightly higher resistivity partially thawed sediments.
   - ρ_5 : ice-bearing permafrost.
   - ρ_6 : conductive basement.

TABLE 4.2 CURVE MATCHING GEOELECTRIC MODELS FOR THE 500 m LOOP SIZE FOR THE NPBS #1 THROUGH REINDEER ISLAND LINE
(except for 14 kilometer site which uses 400 m loop size)

Models		Sounding Site, kilometers offshore						
		1	3	5	7	9	11	14
	ρ_1	3.6	2.8	2.0	1.8	1.8	1.6	1.8
	ρ_2	200	200	200	200	200	10	10
	ρ_3	1.0	1.0	1.0	1.0			1.0
	h_1	60	130	175	175	150	120	100
	h_2	500	500	300	300			300
	RMS	24.2	1.9					

TABLE 4.3 COMPUTER INVERSE GEOELECTRIC MODELS FOR 500 m LOOP SIZE FOR THE NPBS #1 THROUGH REINDEER ISLAND LINE
(except for 14 kilometer site which uses 400 m loop size)

Models		Sounding Site, kilometers offshore						
		1	3	5	7	9	11	14
HHS	ρ_1	4.99	3.63	2.19	1.94	1.85	1.71	2.29
	ρ_1	3.31	3.22	2.11	1.75	1.66	1.52	1.76
2	ρ_2	8.80	4.69	2.64	2.81	2.96	3.30	3.02
Layer	h_1	26.7	53.6	89.9	52.4	51.8	51.2	30.1
	RMS	4.58	1.49	1.47	0.62	0.77	1.33	0.69
	ρ_1	3.38	3.17	1.88	1.84	1.89	1.74	2.06
	ρ_2	21.26	8.69	10.01	51.38	10.05	23.92	18.81
3	ρ_3	0.54	0.50	1.74	0.64	1.37	1.93	2.00
Layer	h_1	35.13	100.0	99.62	118.8	112.2	95.22	66.52
	h_2	535.6	583.7	222.5	100.1	75.9	69.67	59.00
	RMS	5.60	0.38	0.57	1.08	1.88	2.38	0.55
	ρ_1	0.27	0.40	0.45	0.42	0.39	0.30	0.67
	ρ_2	3.68	3.26	1.99	2.05	2.09	2.10	2.26
	ρ_3	6.95	6.01	2.55	9.80	7.06	5.04	3.74
6	ρ_4	8.97	1.83	1.92	1.03	1.79	1.52	0.51
	ρ_5	55.69	55.40	9.82	25.75	21.06	13.69	5.00
Layer	ρ_6	0.17	0.29	0.57	0.51	0.42	1.82	0.45
	h_1	0.14	0.13	0.69	1.76	2.08	2.01	2.00
(6a and	h_2	26.14	71.26	116.80	129.40	130.05	102.48	65.75
6b from	h_3	70.13	190.26	24.53	105.87	63.54	136.24	148.34
Table 4.1)	h_4	34.46	23.83	34.55	61.76	47.49	40.00	8.09
	h_5	418.58	397.97	349.99	240.39	231.12	236.70	220.78
	RMS	1.40	0.24	0.37	0.27	0.20	1.31	0.30

The soundings in both Table 4.2 and 4.3 are for the 500 meter transmitter loop data except for the 14 km site at which a 400 meter transmitter loop was used. Both Table 4.2 and 4.3 give the rms errors of the models compared to the sounding data. The thickness of the first layer is taken from the sea ice surface. Some of the visual results used a different number of data points and therefore the error is not listed.

Because it is known from theory and forward modeling that the thickness of the first layer is best resolved with a transmitter loop having a side dimension of similar size, the results of the 2 layer inverse modeling of the 250 meter transmitter loop data were used to estimate the thawed layer thickness. This estimate was then used as a first guess for the first layer thickness in the initial model for the larger transmitter loop data inverse modeling. The final models from the inverse modeling of the larger (400 and 500 m) loop sizes are shown in Table 4.3.

The purpose of the iterative process in the NLSTCI program is to reduce the residual vector, defined as the array of absolute differences between the geoelectric model prediction and the field data taken at each time gate, to its least possible value by altering the values of model parameters, resistivities and thicknesses. Due to the extreme conductivity of these materials, all offshore soundings displayed early time behavior for the first several gates, in marked contrast to the higher resistivity materials reported for most of the sites of Chapter 3 and Appendix A. Early time behavior is exhibited by a response which does not depend upon time (see Chapter 2 on asymptotic solutions). Therefore, the apparent resistivity decreases rapidly in these time gates and the early gates have a much larger apparent resistivity than later gates. For data having these characteristics, the convergence procedure of the NLSTCI program iterates to models that tend to fit the data at early times relatively better than at later times because it is based upon absolute residual errors.

Thus, it was decided to alter the definition of the residual vector for NLSTCI to one divided by the magnitude of the resistivity at that time gate. The change allowed the data from all time gates to be treated equally in the matching process. A change was necessary as the apparent resistivity decreased by several orders of magnitude during the sounding; therefore the early gates would be given decided preference in the matching process. Once altered, the NLSTCI program iterated to solutions which gave better results at late times. These solutions were often helpful in leading to newer models, but were not always the best fit overall.

4.3 INVERSE MODEL RESULTS

A comparison of the errors obtained with the visual matching process with the inverse modeling process shows the superiority of the fit obtained with the inverse modeling procedure. The inverse modeling procedure appears to predict a thinner layer of thawed sediments above the ice-bearing permafrost than does the visual matching method, and suggests there is only a relatively small resistivity contrast between the thawed and ice-bearing layers for these two methods. This thinner thawed layer compares more favorably with drilling and seismic data along the line (Osterkamp and Harrison, 1977; Sellmann and Chamberlain, 1980; Rogers and Morack, 1980).

Drilling and seismic data from the shallow offshore region bordering the Beaufort Sea in the Prudhoe Bay area suggests a somewhat crude but reasonably general geoelectric model of the subsurface structure consisting of three layers: 1) a low resistivity layer of sea water and thawed sediments, 2) a high resistivity layer of ice-bearing sediments and 3) a low resistivity basement. However, it is known

that resistivity varies dramatically with depth from well logs taken on Gull Island (ARCO Gull Island State #2), a few kilometers to the east of the TEM transect, on Reindeer Island (SOHIO Reindeer Island Stratigraphic Test Well), and on Niakuk Island on the east side of Prudhoe Bay (British Petroleum Niakuk #1). In fact, the Gull Island resistivity well log (see Osterkamp and Payne, 1981), shows several large variations in resistivity between 90 m depth and 250 m depth. These changes are on the order of a factor of ten and may represent as many as seven distinct layers. This complexity cannot be resolved by the transient system. Still, examination of the well logs available onshore as well as those offshore give some clues to possible lithologic control of the resistivity layering. There appears to be a consistent sequence of fine-grained material underlying the coarse-grained sands and gravels. This layer, which has been identified as having a high clay content from drilling logs, may act as a barrier to salt transport downwards as suggested by Osterkamp and Payne (1981). The presence of this sequence is indicated by an increase in the gamma ray log and an increase in the resistivity log. The fine-grained material appears at a depth of about 180 m near West Dock and dips with distance offshore to about 250 m in depth at Reindeer Island.

The resistivity of the strata within the fine-grained sequence is greater, presumably because it is frozen and probably has a lower soil solution salinity. If such a lithologic control on resistivity does exist, its effect will be to increase the minimum number of layers in our model. From the available information, it is evident that the variation of resistivity with depth is complex. However, it is desirable to have as simple a model as possible that still retains the essential features of the subsea strata identified as permafrost.

While a three layer model is desirable from the standpoint of being the simplest possible model from which the thickness of ice-bearing permafrost may be obtained,

the six layer model, albeit a very complex model (which may not be resolvable with the available data), is more realistic, physically, in that it incorporates more of the known structural details.

Models incorporating a sea-ice layer did not differ significantly from the models without sea-ice, because the TEM sounding method is not sensitive to a thin (layer thickness much less than the transmitter loop diameter) highly resistive layer on the surface of a very conductive half-space. However, there was considerable change in the apparent resistivity curves when a highly conductive sea-water layer was incorporated, even though this layer was less than 7 m thick. It is unclear whether or not the results of models incorporating a thin sea-water layer are superior to those models which combine the sea-water and unfrozen sediments into a single layer.

Models for all transmitter loop sizes were run in two modes in which: 1) the inverse program treated each data point equally and 2) the inverse program weighted the data points according to the standard deviation for that point. Standard deviations were calculated for each data point using a limited data set. Normally, at each sounding site at least six sets of readings were recorded. Alternate readings have reversed polarities such that natural and artificial sources of telluric fields are eliminated. This means three data points for each gate time were used to compute standard deviations. The system noise level claimed by McNeill (1980) was readily verified because, whenever signal strength dropped into the noise, the standard deviations became very large. Generally, the results of the models using weighting completely ignored data points occurring later in time because of their inherently greater noise. This feature aided the simpler, one and two layer matching process, but it was of questionable value with the more complicated multi-layered models.

Models were also run for which some elements of the model were constrained and the remaining elements were allowed to vary in the inverse process. Some of the initial modeling was done in this fashion with the resistivities held constant, but it was quickly discovered that no one set of resistivity values would give realistic models for all of the sounding sites. Initial modeling clearly indicates that the three layer model is so simple that one must vary the resistivities as well as thicknesses to obtain reasonable inverse models for the entire transect. It may be that the 6 layer models could be constrained in resistivities and still give reasonable results but a limitation of resources has prevented pursuing such computer modeling.

All models presented here were arrived at using the inverse program in a mode wherein the model elements were only allowed to vary within certain limits. As an example, the limits for ρ_1 at a particular site may be 1 to 5 ohm-meter and so the inverse program will take the initial estimate for ρ_1 and only vary this parameter within those limits. Therefore, these results will be biased not only by the initial models given, but also by the limits imposed, a point that is extremely important when considering the very complex 6 layer models. In the following figures (Figures 4.2 through 4.10), the sounding data taken with 250 meter (solid black circles) and 500 meter (plus signs) transmitter loops are presented for the offshore sites. The 500 meter soundings were typically taken with sounding frequencies of 3 and 0.3 Hertz (except for the 1 kilometer site) whereas the 250 meter soundings were taken at 30 and 3 Hertz. Whenever possible, the information from the smaller transmitter loop was used to aid the interpretation of the larger transmitter loop sounding.

Figure 4.2 displays the data and the decay curves for 2 and 3 layer models for the site 750 m offshore (within the figure for each site, an inset displays the geoelectric models used for that site). Only the smaller 250 meter transmitter loop was used at this site. Two models are shown which are the best fits from the inverse

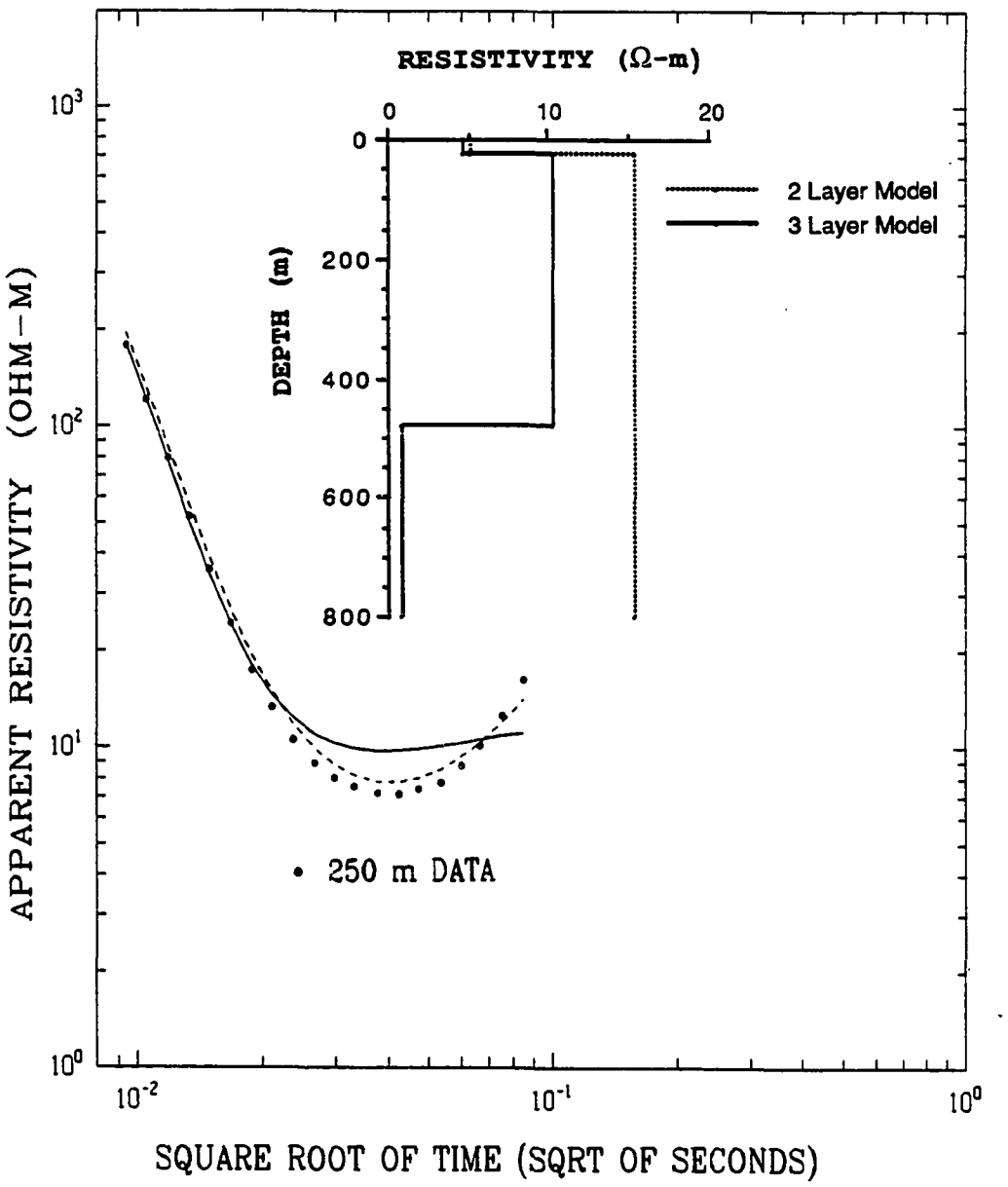

Figure 4.2 TEM data and models for the site 750 m offshore. The inverse models shown are for 3 layers (solid line) and 2 layers (dashed line) for the 250 meter data.

models. The thickness of the thawed layer from these models is approximately 26 m measured from the sea ice surface to the ice-bearing permafrost. Osterkamp and Harrison (1985) found a depth (measured from the seabed) of 25 m to the ice-bonded permafrost table at 700 m offshore by probing.

Figure 4.3 displays the data and models for the 1 kilometer site. The 250 meter transmitter loop data are shown as solid black circles and the 500 meter loop data are shown as plus signs. The curves shown for the 500 meter data are solid for 6 layers and dashed for 3 layers, both from the inverse models of Table 4.3. In all of the subsequent figures for the offshore line, except for on Reindeer Island, the curves for the 500 meter data are from the models of Table 4.3. The 250 meter curves are solid for 6 layers and dashed for 2 layers. Typical of all the subsequent figures, the dashed 250 meter curve represents the response of an inverse 2 layer model derived from the 250 meter data, whereas the solid 250 meter curve represents the response from a forward model synthesized for the 250 meter loop size from the 6 layer inverse model obtained from the data of the 500 meter loop.

The 2 layer model from the inverse modeling of the 250 meter data calls for approximately 30 m of material above the ice-bearing permafrost table. This material includes the sea ice, sea water, and thawed materials. Approximate depth to the ice-bonded permafrost table from the sea ice surface is 31 m from drilling and sampling data (Sellmann and Chamberlain, 1980).

Data and models shown in Figure 4.4 are for the 3 kilometer site. This is the last site where the distinctive rounded peak in later time is well above the noise level. The peak is characteristic of a strong resistivity change: higher resistivity to lower resistivity. At sites farther offshore, past 3 kilometers, the later time gates, where the peak is to be found, have signal strengths that approach or that are in the system noise level and, therefore, are unreliable for interpretations. Intelligent

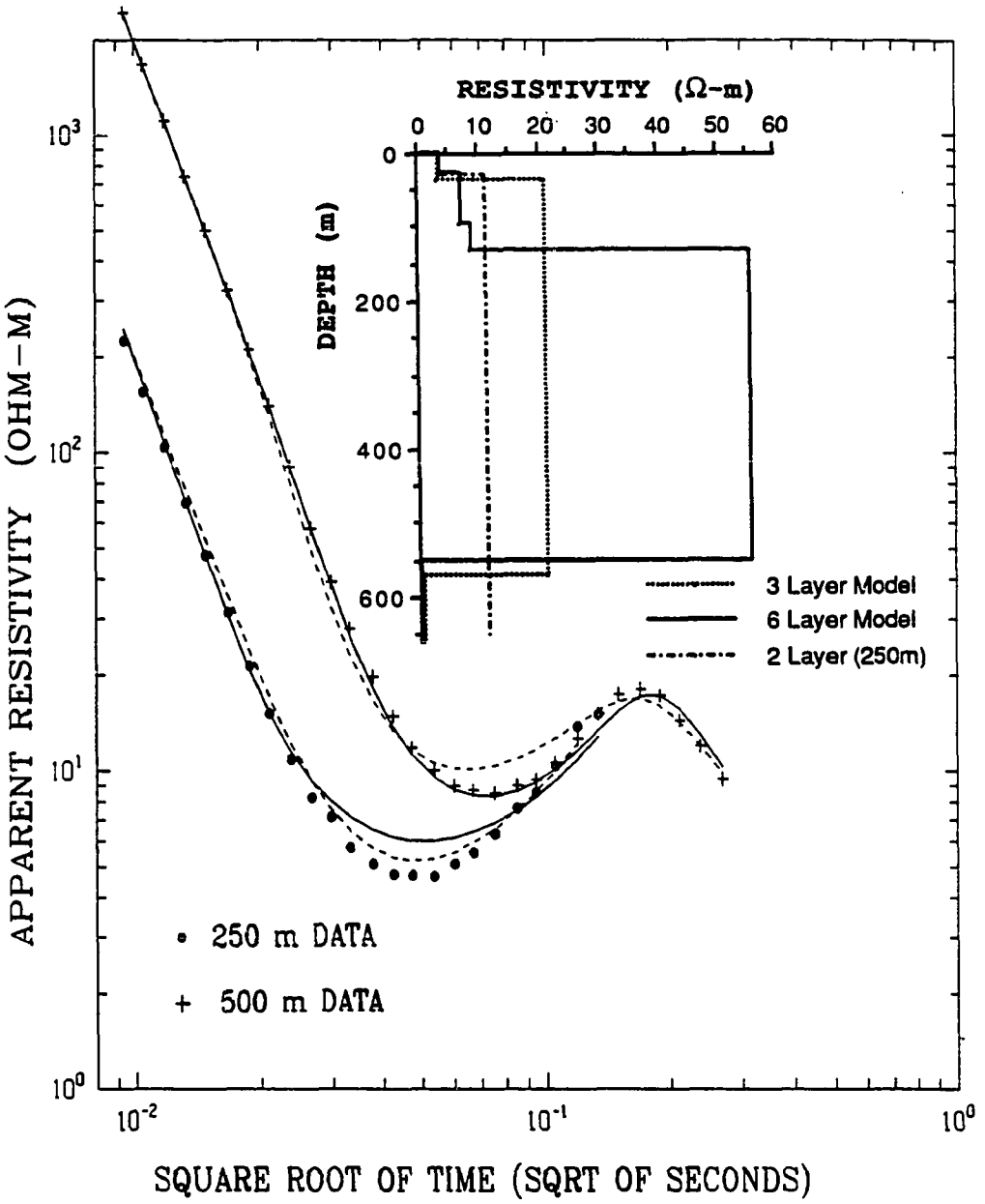

Figure 4.3 TEM data and models for the 1 kilometer site. The model curves are for 6 layers (solid line) and 3 layers (dashed line) for the 500 meter data and 3 layers (solid) and 2 layers (dashed) for the 250 meter data.

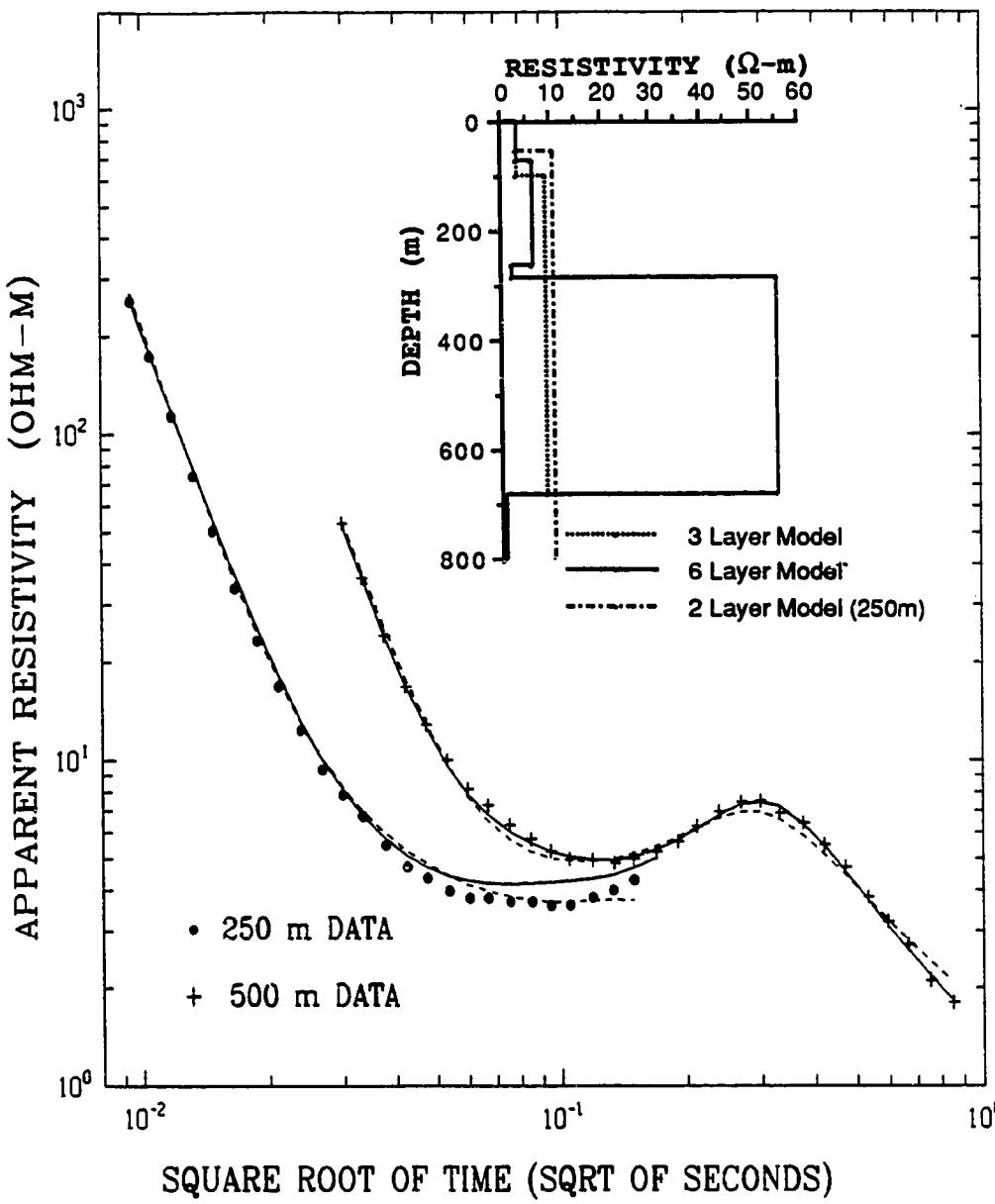

Figure 4.4 TEM data for the 3 kilometer site. The model curves shown are 6 layer (solid line) and 3 layer (dashed) for the 500 meter data and 6 layer (solid) and 2 layer (dashed) for the 250 meter data.

stacking (averaging a large number of received signals in a particular time gate and then eliminating signals which are not within, say, one standard deviation of the mean and reaveraging) has been demonstrated which is capable of reducing the noise in the later time gates (P. Hoekstra, personal communication). It is only through such reduction of noise, which allows resolution of the peak, that some of the questions can be answered regarding the continuous nature of an ice-bonded layer with increasing distance offshore. The TEM 2 layer inverse model for the 250 meter transmitter loop data calls for about 55 m of unfrozen material at this site. In contrast, the 6 layer inverse model for the 500 meter data predicts 71 m of thawed material. Sellmann and Chamberlain (1980) report a depth to ice-bonded permafrost from the seabed of about 65.1 m at 3.5 km along this line.

Data and models for the 5 kilometer site are shown in Figure 4.5. The 2 layer 250 meter inverse model suggests that there is about 90 m of unfrozen material. On the other hand, the 6 layer inverse model from the 500 meter data calls for about 117 m of unfrozen material. Ice-bonded permafrost is about 60 to 70 m below the sea ice surface (Sellmann and Chamberlain, 1980).

TEM data and models for the 7 kilometer site are shown in Figure 4.6. The 2 layer inverse modeling of the 250 meter transmitter loop data predicts the existence of about 115 m of unfrozen material at this site. The 6 layer inverse model from the 500 meter data calls for about 130 m of unfrozen material here. These results disagree with the depth measured by Sellmann and Chamberlain (1980) who detected the ice-bonded permafrost table at 44.1 m below the seabed by drilling at 6.8 km offshore along this line. This point is not shown in Figure 4.11, which displays primarily the results of the seismic data. It is possible that the drilling encountered an isolated pocket of frozen material but the difference between the

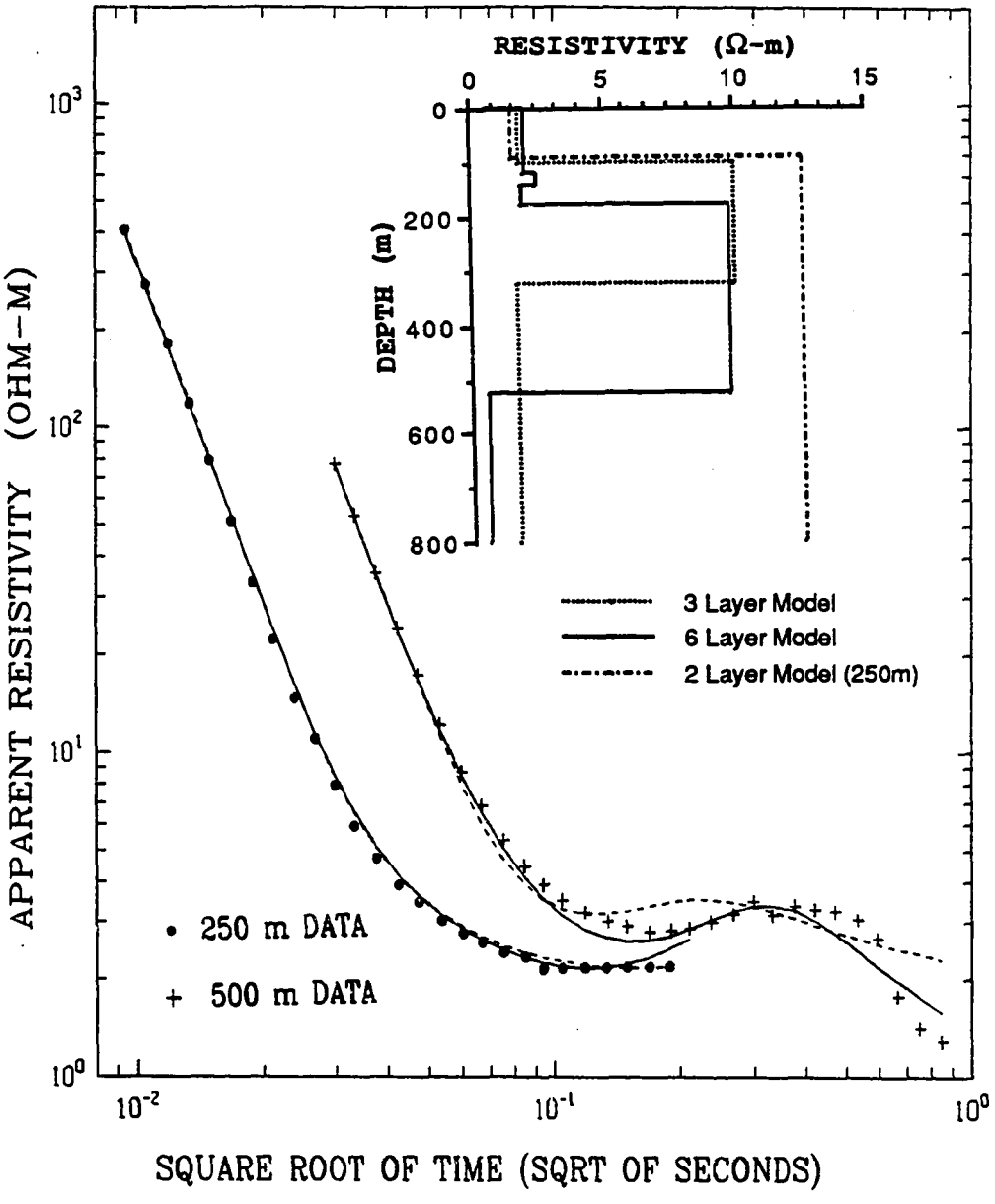

Figure 4.5 TEM data for the 5 kilometer site. The model curves shown are 6 layer (solid line) and 3 layer (dashed) for the 500 meter data and 6 layer (solid) and 2 layer (dashed) for the 250 meter data.

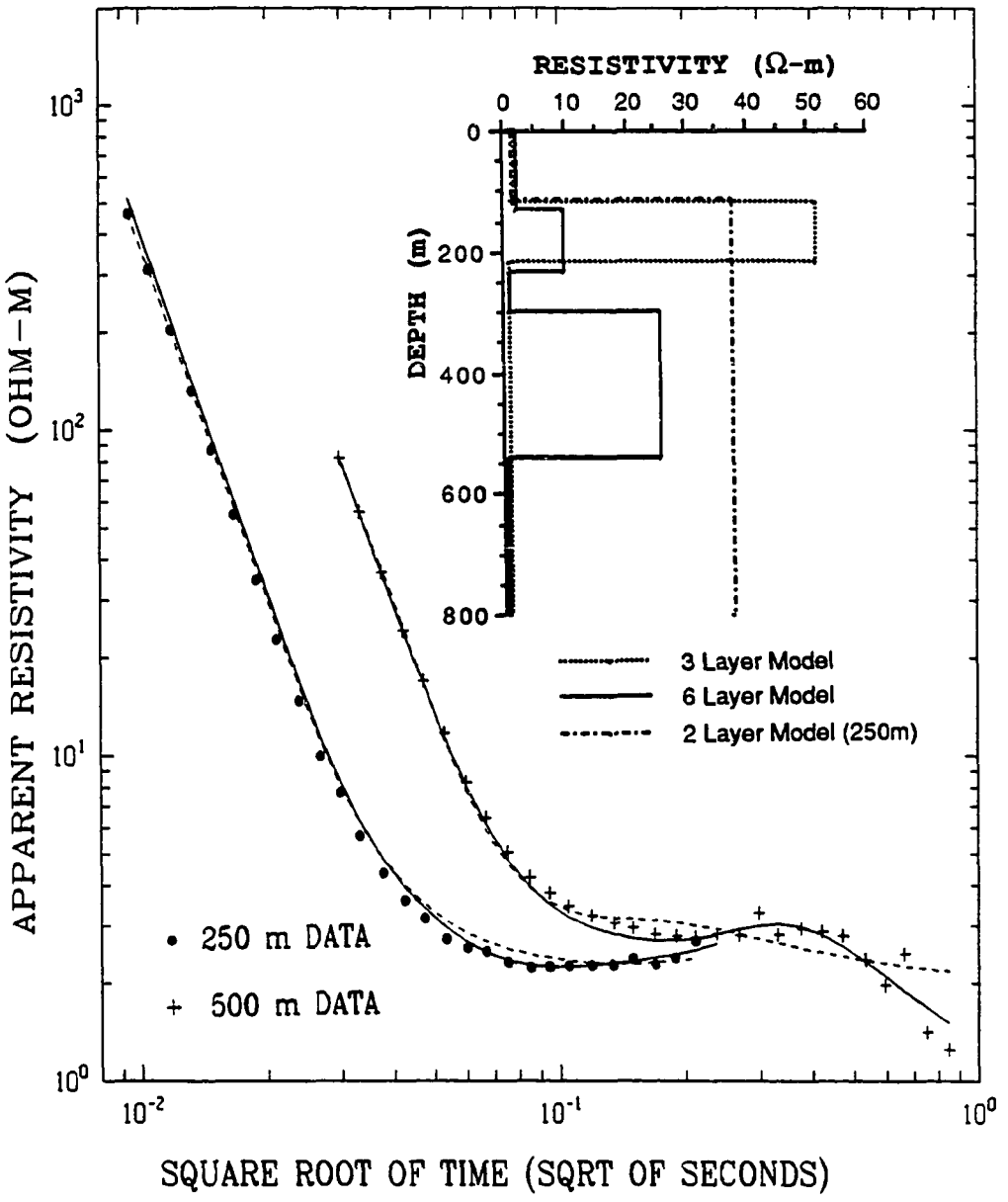

Figure 4.6 TEM data for the 7 kilometer site. The model curves shown are 6 layer (solid line) and 3 layer (dashed) for the 500 meter data and 6 layer (solid) and 2 layer (dashed) for the 250 meter data.

modeling results and the results reported by Sellmann and Chamberlain (1980) is alarmingly large.

TEM data from the 9 kilometer site and models are shown in Figure 4.7. The unfrozen layer thickness from the 250 meter transmitter loop data inverse model is about 110 m and the 500 meter data 6 layer inverse model gives about 130 m for this unfrozen zone thickness. Information presented in Sellmann and Chamberlain (1980) suggests a depth of 110 to 145 m from the sea ice surface to the ice-bonded permafrost table.

TEM data and models for the 11 kilometer site are shown in Figure 4.8. The unfrozen thickness at this site from the 250 meter transmitter loop data, 2 layer inverse model is about 95 m (1.32 Ω−m over 39 Ω−m), whereas the 500 meter data, 6 layer inverse model calls for a thickness of about 103 m. A summary of available data on depth to ice-bonded permafrost from Sellmann and Chamberlain (1980) provides an estimate of about 110 m from the sea ice surface.

Data for the site on Reindeer Island (13 kilometer) are shown in Figure 4.9 along with the 6 layer model derived from the well log (dashed line) and the 6 layer inverse model (solid line). The resulting model differs only slightly from the well log model derived from roughly average resistivities and thicknesses observed on the DIL resistivity log, which was found to be fairly well represented by 6 layers. Six layer resistivities from the well log beginning with the first layer are: 10.0, 1.5, 6.0, 2.0, 10.0, and 2.0 Ω-m and thicknesses of the first five layers are 19, 60, 80, 100, and 80 m, respectively. This well log model was the input model for the NLSTCI program to produce the forward sounding curve and inverse result shown in Figure 4.9.

The inverse model for the 13 kilometer site consists of the following resistivities beginning with the first layer: 5.46, 2.04, 5.46, 2.12, 70.42, 3.26 Ω-m and the

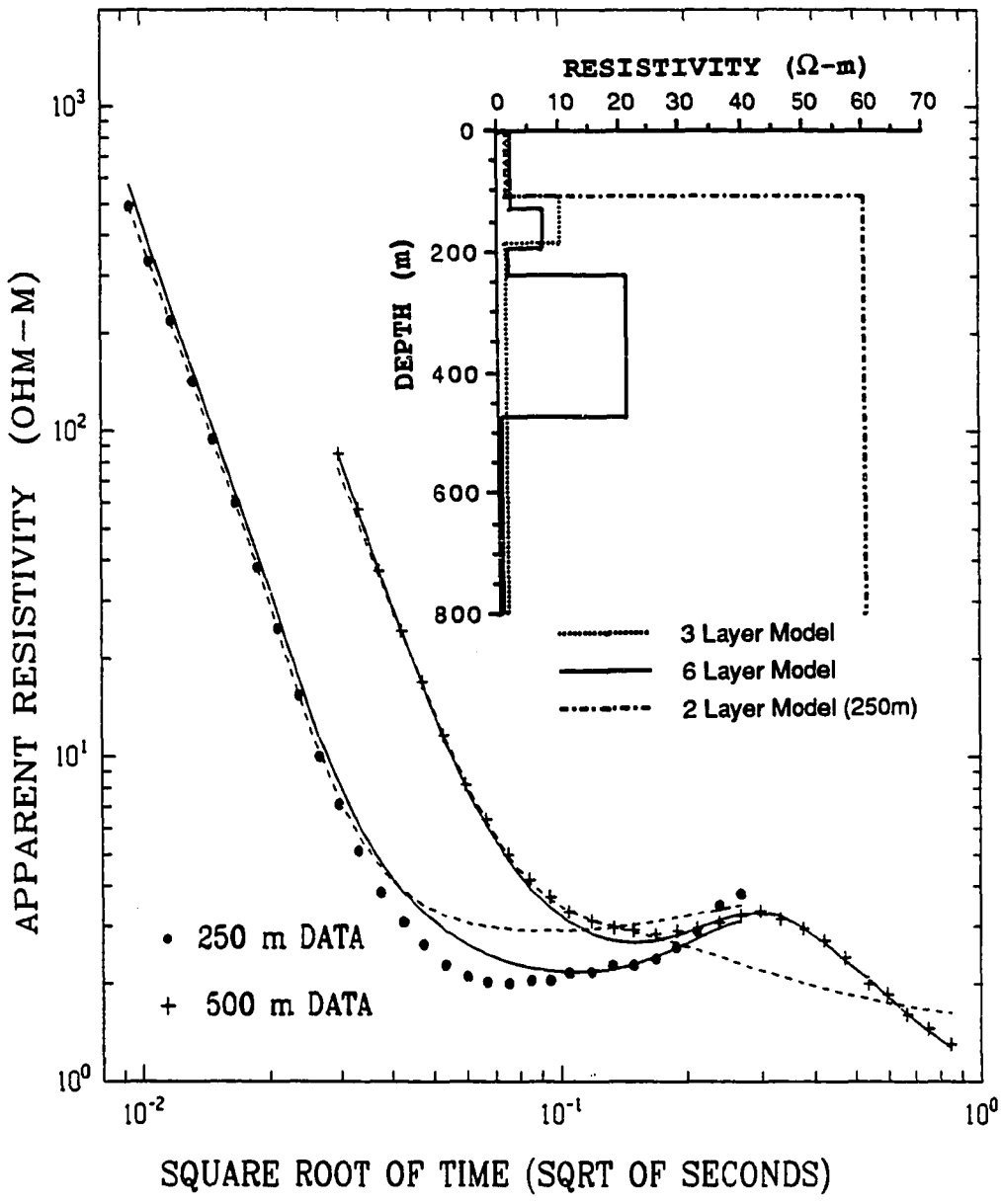

Figure 4.7 TEM data for the 9 kilometer site. The model curves shown are 6 layer (solid line) and 3 layer (dashed) for the 500 meter data and 6 layer (solid) and 2 layer (dashed) for the 250 meter data.

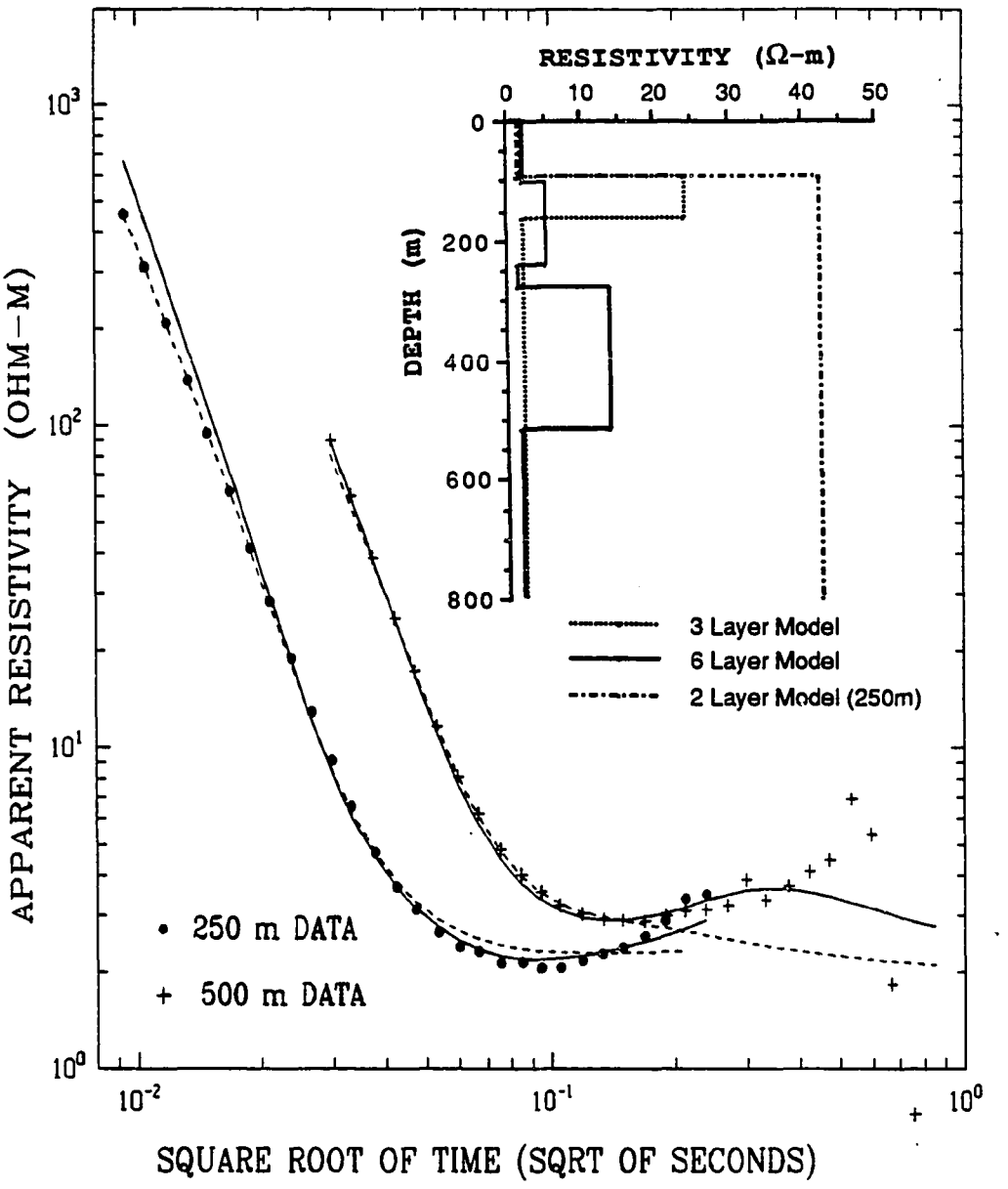

Figure 4.8 TEM data for the 11 kilometer site. The model curves shown are 6 layer (solid line) and 3 layer (dashed) for the 500 meter data and 6 layer (solid) and 2 layer (dashed) for the 250 meter data.

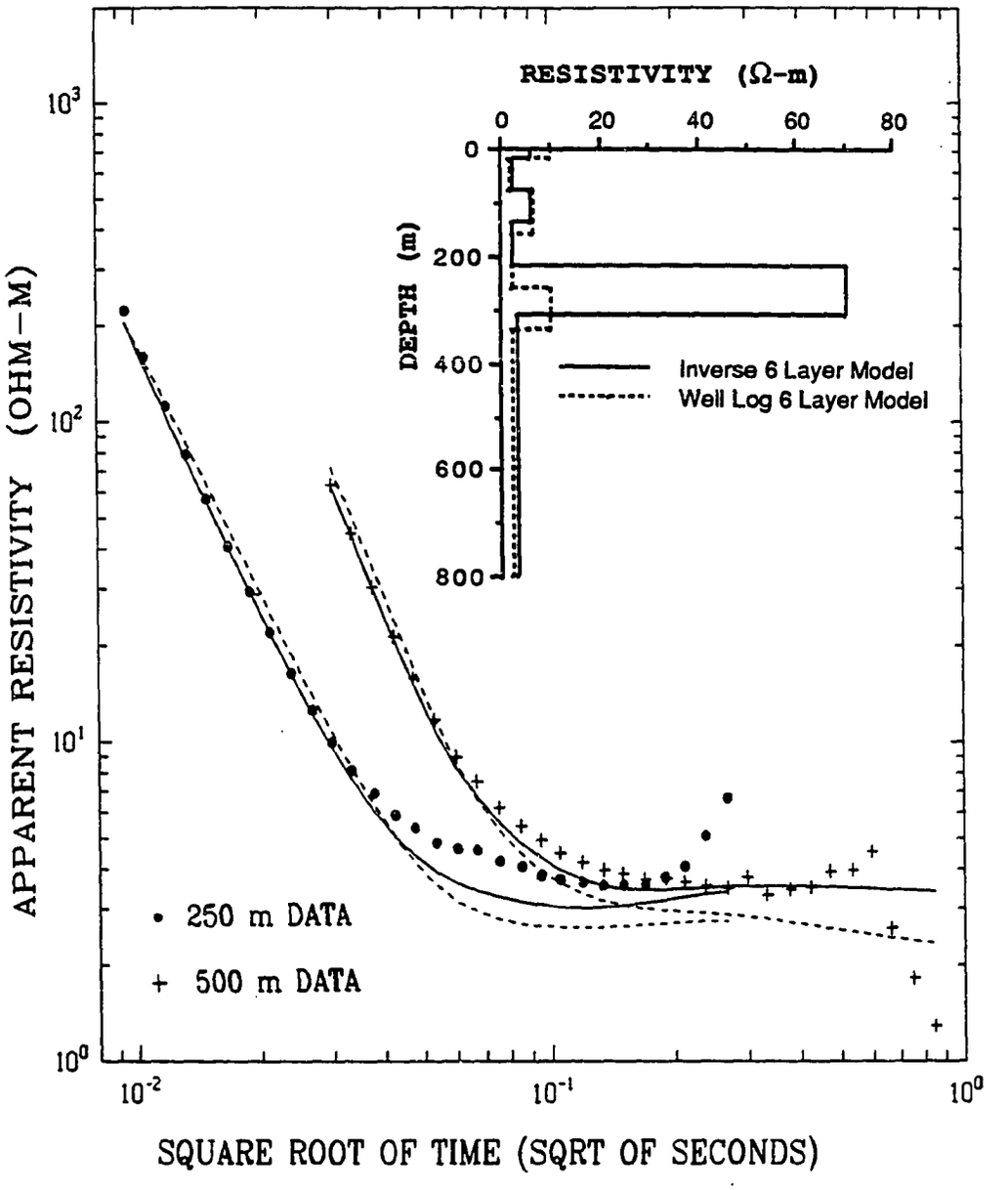

Figure 4.9 TEM data for the 13 kilometer site. The model curves shown are for 6 layers (dashed lines) derived from the well log and 6 layer (solid lines) inversions for the 400 meter data and the 250 meter data.

thicknesses of the first five layers are 18.51, 59.71, 60.49, 79.43, and 92.74 m, respectively. The curves for the 250 meter data are the same as for the 6 layer models obtained from the 500 meter data, but recomputed via forward modeling for the smaller transmitter loop.

Data for the site at 14 kilometers offshore (1 kilometer past Reindeer Island) are shown in Figure 4.10. A large ice ridge present north of the island at the time of the sounding precluded the use of a 500 meter transmitter loop and, therefore, a 400 meter loop was used at this site. First layer thickness from the 250 meter transmitter loop data, 2 layer inverse model is about 32 m whereas the 6 layer inverse model calls for about 66 m of material above the ice-bearing permafrost table. Data summarized by Sellmann and Chamberlain (1980) were extrapolated for an estimate of the depth from the sea ice surface to ice-bonded permafrost of only about 20 m. However, the data is skimpy beyond Reindeer Island.

4.4 DISCUSSION

Homogeneous Half-Space Results

Homogeneous half-space (HHS, Table 4.3) results clearly show that the bulk resistivity decreases with distance offshore except for the 14 kilometer site. The general decrease in resistivity with increasing distance offshore may be a result of increasing temperature, a change to finer-grained soils, silts and clays or increasing thickness of the thawed layer, or decreasing thickness of the ice-bearing permafrost. It is likely that the general trend in resistivity is a combination of all these factors.

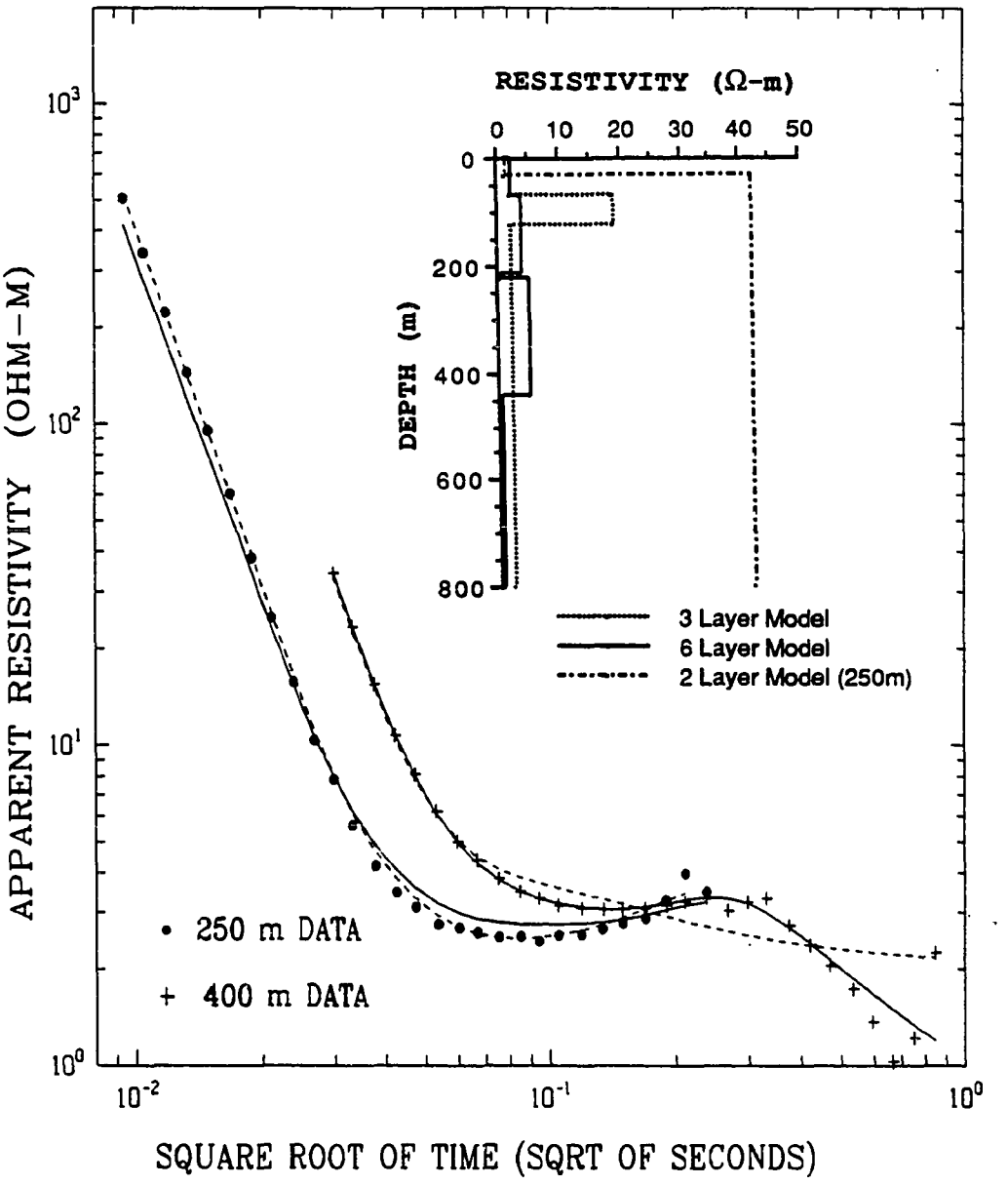

Figure 4.10 TEM data for the 14 kilometer site. The model curves shown are 6 layer (solid line) and 3 layer (dashed) for the 500 meter data and 6 layer (solid) and 2 layer (dashed) for the 250 meter data.

Note that the 2 layer results for the 500 meter loop size show less variation in the first layer resistivity.

Two Layer Results

Again, the general trend, namely, that the first layer resistivity decreases with distance offshore, is evident in these results shown in Table 4.3 for the 500 meter loop size. These models clearly show that the resistivity contrast between the 2 layers may be very small.

From these results, the thickness of the thawed layer is inferred to increase from 27 m at 1 km to to 90 m at 5 km. From 7 to 11 km the unfrozen layer is about 50 m thick and 30 m at 14 km. While the transient results are in good agreement with the seismic and drilling data for the 250 m sounding data, the results of the larger loop size inverse modeling seldom agree. This is expected since the smaller loop size should resolve the first layer better than the larger transmitter loop. However, they do agree in general trends and are in much better agreement with the seismic and drilling data than the results of Ehrenbard et al. (1983) for the same distances offshore. Some probable causes of the disagreement with the results of Ehrenbard et al. (1983) are discussed in the next section.

Three Layer Results

Three layers are the least possible number of layers for a physical model from which we may be able to estimate the thickness of the ice-bearing layer. The

ice-bearing thickness is one of 5 parameters (the three layer resistivities and the thickness of the first two layers). None of these parameters are known absolutely. In fact, each parameter will vary and cannot be assigned an initial constant value. It should be noted that the thickness of the second layer will primarily be evident in the late time (low frequencies will give late time behavior; low frequency electromagnetic waves penetrate to greater depths, while the higher frequencies are highly attenuated (Kaufman and Keller, 1983)). Since the later time gates have a much greater likelihood of being very noisy due to decreased signal strength, we can expect some difficulty in resolving the least known parameter: the thickness of the entire ice-bearing sequence in the subsea environment.

Table 4.3 which lists the resulting models for the 3 layer inverse modeling shows that: 1) the ratio between the first two layer resistivities is usually less than 10, 2) the model values for resistivities are bounded but the results show significant variation at the same depth from site to site, 3) the permafrost layer as deduced from the modeling tends to thin with distance offshore and 4) the thawed layer first thickens with distance offshore and then thins as Reindeer Island is approached. Because the signal strength at later times in the transient decay tends to be more greatly influenced by deeper, more conductive layers, the 3 layer TEM results probably give an indication of the base of the first ice-bearing layer, not the base of the permafrost which consists of a sequence of ice-bearing and unfrozen layers. This can be inferred from an examination of the response curves for Reindeer Island shown in Figure 3.25. Variation of the deepest relatively resistive layer thickness produces curves that are not dramatically altered in the first 14 gates. In other words, the primary response in a multi-layered system will be to the layers lying nearer the surface. Under some circumstances, then, one may expect

significant differences to occur in estimating the depth to the base of permafrost using models with different numbers of layers.

The resulting models for three layers have been used to construct the subsea permafrost profile shown in Figure 4.11; the permafrost table and base at NPBS #1 well are also shown (see Chapter 3 for details of the TEM West Dock and Reindeer Island sites). A sketch of the results of drilling and seismic data (Osterkamp and Harrison, 1977; Sellmann and Chamberlain, 1980; Rogers and Morack, 1980) along this same line, for the thickness of the thawed sediments, are shown for comparison. Osterkamp et al. (1985) estimate the base of ice-bearing permafrost from well logs as shown by the lower dashed line in Figure 4.11. The offshore data point at 4 km for the base of ice-bearing permafrost is based on the logs from Gull Island which is approximately 6 km southeast of the 4 km point on the NPBS #1 to Reindeer Island line and thus may not give a good estimate of the base of permafrost.

Ehrenbard et al. (1983) present a 3 layer subsea permafrost profile obtained with the TEM method, which, although not along the same line as in the present study, is in the same general area and may be compared to the profile presented here. Station B in Figure 6 (reproduced in this thesis as Figure 4.12) of the paper by Ehrenbard et al. is stated to be located near Gull Island. The distances shown in Figure 4.12 indicate that station B is about 3.2 km from shore. The USGS topographic map Beechey Point (B-3), Alaska revised in 1975 shows the closest proximity of Gull Island to shore is about 4 km and thus there is some doubt about the exact location of the sounding line shown in Figure 4.12. However, if the profile line is taken to be perpendicular to shore as stated in the text and it passes through or near Gull Island, the line would intersect shore at least 3 km south and east of West Dock and have a bearing which takes it across the mouth of Prudhoe Bay. The inferred location and bearing of the sounding line from Ehrenbard et al.

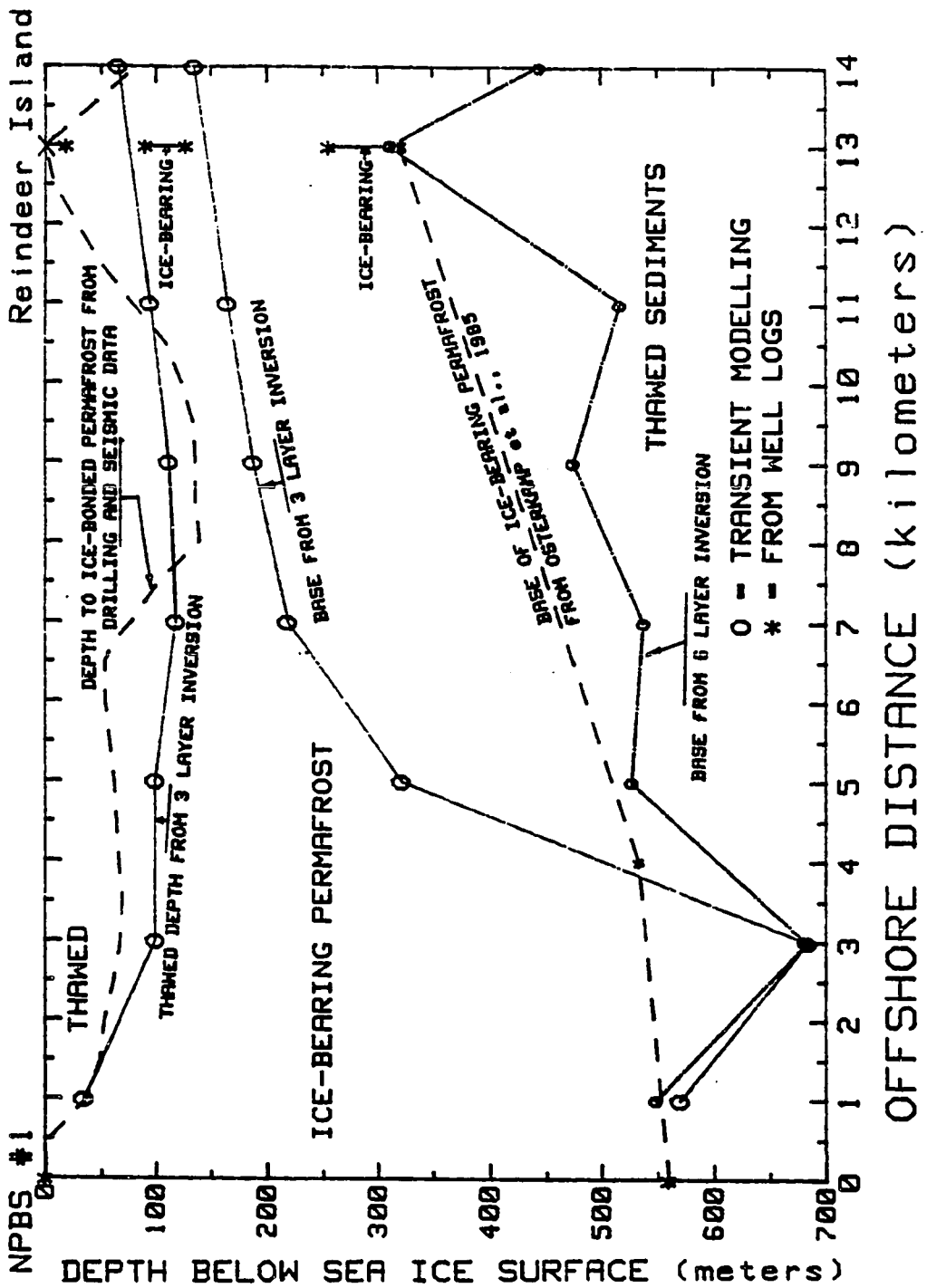

Figure 4.11 Subsea permafrost profile for sounding sites along a line from ARCO drillhole NPBS #1 through Reindeer Island.

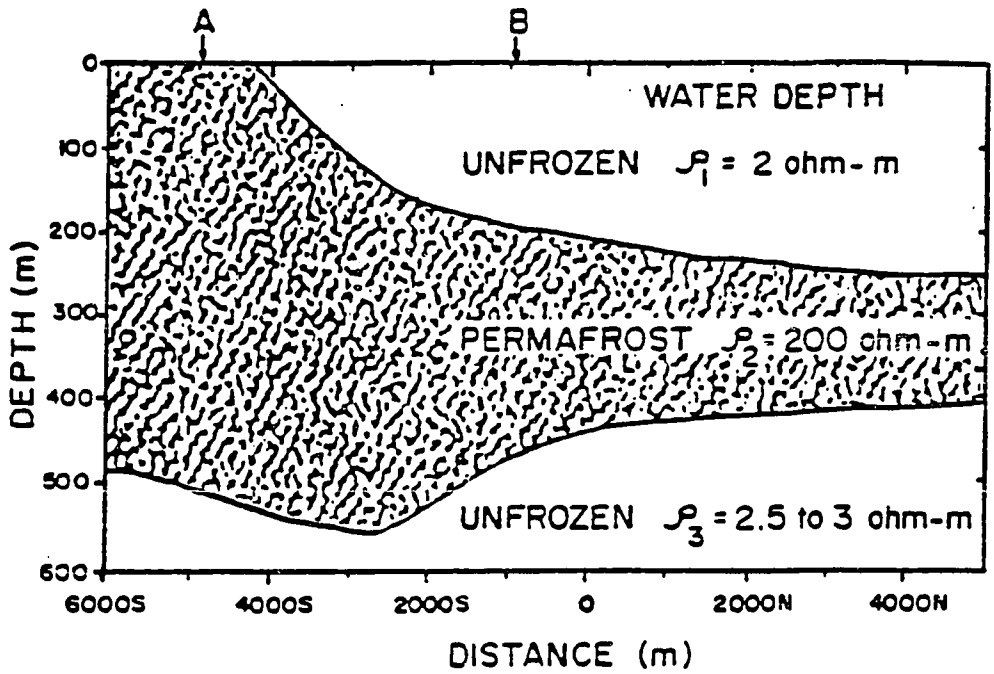

Figure 4.12 Subsea permafrost profile from Ehrenbard et al. (1983) along a line from shore to near Gull Island using the TEM method.

(1983) is considerably different from the one studied in this thesis and therefore the subsea permafrost beneath these lines may have undergone somewhat different evolutionary histories.

It is important to note that the paper by Ehrenbard et al. uses a simple 3 layer model to represent the layering at Gull Island, although the Gull Island DIL indicates there are 3 comparable higher resistivity zones in the section between the bottom of the well casing (100 feet, 30.5 m) and 550 feet (167.6 m). The higher resistivity sections may indicate the existence of several layers which should be taken into account in the interpretation process. In addition, the estimates for the permafrost table from Ehrenbard et al. are two to five times deeper than information from drilling and seismic data suggests. The results of the present study indicates that the simple three layer model is unlikely to represent the permafrost

section beyond about 3 km offshore. It should also be noted that the resistivity values from the TEM modeling by Ehrenbard et al. are larger than the resistivities from the Gull Island DIL. Higher TEM estimates of resistivity are also consistent with the results of this thesis and the work of Sinha and Stephens (1983).

The three layer model results of this thesis show that the thawed sediments increase in thickness offshore to a maximum of about 118 m at 7 kilometers offshore. They also predict that the ice-bearing permafrost thickness increases slightly from 560 m onshore to 584 m at 3 kilometers offshore, rapidly decreases to 100 m at 7 kilometers offshore and slowly decreases to 59 m at 14 kilometers offshore. It must be emphasized again that the predictions of subsea permafrost thickness in terms of a three layer model beyond three kilometers offshore are not likely to be accurate. This is due to the presence of a fairly thick, high conductivity seabed layer and the multi-layered ice-bearing region. The general trend of thinning with distance from shore predicted by the three layer model is, however, probably real.

Six Layer Results

While the data may be fit more closely by using an increased number of layers, the resolution of the thickness of the ice-bearing layer may not improve. As an example, consider the results of the 3 and 6 layer models for the 3 km site which are shown in Figure 4.4. Displayed in this way the 6 layer model clearly appears to be a superior fit. Also when a comparison of their rms error is made, as tabulated in Table 4.3, it can be concluded that in all cases the 6 layer models were superior fits.

However, it seems unlikely that the lower, more highly resistive (perhaps ice-bonded) layer in the 6 layer model extends so far offshore with only a nominal decrease in thickness, in disagreement with the well log at Gull Island. On the other hand, as indicated above, the three layer inverse models may only resolve the depth to the first higher conductivity layer and not discern the entire ice-bearing sequence of thawed and frozen layers. Only future exploration will determine which of the two, or perhaps some intermediate model, is the most correct. The large variations in ice-bearing thickness and a lack of a reasonable decrease in thickness of the ice bearing layers with increasing distance offshore for the six layer models display the difficulty associated with resolving the ice-bearing thickness using a greater number of layers.

Resistivities for the seawater and unfrozen layers obtained in this thesis are similar to those of Corwin (1983, 1985) using the DC resistivity method in the same general area. However, there seems to be too large a variation between sites in the resistivities obtained by both the DC and TEM methods for unfrozen near-surface layers. For the TEM method, this is at least partially due to the nonuniqueness of the parameters used in inverse modeling and the large bounds allowed.

The base of ice-bearing permafrost from the 6 layer results are shown in Figure 4.11. Depth to the base is 684 m at 3 km, decreases to 538 m at 7 km, and decreases to 445 m at 14 km. This prediction compares more favorably with the results of Osterkamp et al. (1985) beyond 3 km than does 3 layer modeling, but as indicated above, the predicted thickness falls off much too slowly. The permafrost table, taken as the top of layer 3 from the 6 layer modeling, agrees reasonably well with the 3 layer modeling. At Reindeer Island, the TEM interpretation for 6 layers calls for the base of ice-bearing permafrost at a depth of 311 m which is in good agreement

with Osterkamp et al. (1985). This fortuitous result comes from the tighter control possible with the DIL information shown in Chapter 3.

In concluding this section, some general remarks should be made concerning the models derived. Figure 4.11, which summarizes the results of some previous studies and the results presented here, clearly shows there is a large disagreement between the 3 and 6 layer results for the depth to the base of permafrost with each other and with the depths as inferred by Osterkamp et al. (1985) from the well logs of the widely separated drill holes. From the standpoint of the thermal regime (Osterkamp, personal communications), neither the shallow depths given by the 3 layer models nor the slowly decreasing deep permafrost base predicted by the 6 layer models appear realistic. On the other hand, the base estimated by Osterkamp et al. (1985) is founded upon three widely separated drill holes, one of which (Gull Island) is not on the line of the present study.

The results of the 3 and 6 layer modeling are clearly unsatisfactory in their agreement with the base of ice-bearing permafrost. From modeling, it is apparent that the major response of the TEM system will be to the first conductive layer beneath an ice-bearing layer. Since the 3 layer models cannot take into account a more complicated layering, the data are best matched with a relatively thin ice-bearing layer over a conductive basement. In contrast, the 6 layer models take into account a more complicated layering but suffer from a greater possibility for nonuniqueness. Both the 3 and 6 layer models suffer from a lack of control information that would allow limiting the possible range of resistivities and thicknesses to more realistic (but unknown) values. It is clear that the Reindeer Island 6 layer inverse model gives a reasonable estimate of the permafrost base. However, the disagreement between the 3 and 6 layer models and the extrapolated Osterkamp et al. (1985) base of permafrost, suggests that the TEM method (as in the EM-37

circa 1984) lacks the capability of detecting the base of subsea permafrost beyond 3 km offshore although it appears very useful for detecting the table of ice-bearing subsea permafrost and perhaps detecting trends in permafrost thickness.

4.5 SUMMARY

Transient electromagnetic soundings were taken along a line from the North Prudhoe Bay State (NPBS) No. 1 well through Reindeer Island in the Beaufort Sea during Spring, 1984. The primary goal of these soundings was to assess the use of the TEM method to delineate the depth to, and the thickness of, the ice-bearing subsea permafrost layer based on computer inverse modeling.

Offshore, there were about 1.5 to 2 m of sea ice over shallow ($\leq$ 7m) sea water underlain by saline sediments. A thawed layer of sediments near the seabed is underlain by ice-bearing permafrost.

A subsea permafrost profile along the line, showing the depths to, and thicknesses of ice-bearing permafrost was inferred from the interpretations. The 3 layer model results show that the thawed sediments increase in thickness offshore to a maximum of about 118 m at 7 kilometers offshore. They also predict that the ice-bearing permafrost thickness increases slightly from 560 m onshore to 583 m at 3 kilometers offshore, rapidly decreases to 100 m at 7 kilometers offshore and slowly decreases to 59 m at 14 kilometers offshore. The 6 layer model predicts that the base of ice-bearing permafrost is 527 m deep at 5 km offshore, 517 m deep at 11 km, and 445 m deep at 14 km. From this model, the depth to the base of the thawed layer has a maximum value of about 132 m at 9 km and a value of 131 m at 7 km in contrast to the 118 m depth obtained in the 3 layer model.

The depths to the base of the ice-bearing permafrost obtained by both the 3 and 6 layer models are in disagreement with each other. Between the 5 km site and Reindeer Island, the 6 layer inverse modeling results predict larger depths to the base of ice-bearing permafrost than expected while the 3 layer inverse modeling results predict depths that are too shallow. The 6 layer modeling suffers from noise in the later time gates and nonuniqueness in the solution space while the 3 layers models are dominated by the response from the first conductive layer beneath the first ice-bearing layer. In its present state of development (EM-37), the TEM method does not appear capable of resolving the base of a multi-layered sequence of ice-bearing subsea permafrost.

CHAPTER 5. TEM SIGN REVERSALS AND INDUCED POLARIZATION

5.1 INTRODUCTION

The purpose of this chapter is to present transient electromagnetic (TEM) central induction data for the vertical magnetic field which display two sign changes and to show that induced polarization is a plausible mechanism to produce such data. The data were taken in northern Alaska in a locality of known gas hydrate deposits near N.W. Eileen State #1 well. Induced polarization (IP) effects were modeled by allowing the conductivity of the earth to be complex using the Cole-Cole model. Section 5.2 discusses the data taken at the site. Section 5.3 discusses the theory of the Cole-Cole model and its selection to simulate IP effects. Section 5.4 gives the modeling results and discusses the correction for ramp time turnoff using the deconvolution-convolution process.

5.2 EXPERIMENTAL DATA

Transient soundings taken in August 1983 with a Geonics EM-37 instrument were repeated with a second EM-37 in May 1984 at a site in the Kuparuk Oil Field on the North Slope of Alaska. Each of the soundings was taken in the central induction mode (receiver in the center of the transmitter loop) for the vertical magnetic field using a square transmitter loop, 400 meters on a side. For both sets of soundings, the receiver loop had an effective area of 100 square meters

with a preamplifier gain of 52.1. The contribution from the gain of the receiver was removed from each data set and all data sets taken on a sounding date were averaged to produce the data plotted on Figure 5.1. The raw data are given under NWEI1 and NWEI2 in Appendix C.

For the 1983 measurements, the current in the transmitter was 20 amperes and had a ramp turnoff time (TO) of 320 microseconds, whereas for the 1984 measurements the current was 22 amperes with a TO of 760 microseconds. The longer TO of the 1984 sounding results in the last gate being partly in the turn on cycle of the next current pulse, thus producing the larger signal for this gate. Also shown in Figure 5.1 are the data from another site, near Galbraith Lake in northern Alaska, using the same transmitter and receiver configuration parameters with 20 amperes of current and a TO of 315 microseconds; these data are the more typical time signature for TEM soundings which show no sign changes and are included for comparison. In Figure 5.1 the noise level is approximately 1.0 microvolt at late times computed from the information in McNeil (1980). For each sounding, several sets of data were taken at different settings of gain, polarity, and stacking; every set of data displayed two sign changes.

5.3 THEORY

Direct current (DC) induced polarization (IP) is a well known geophysical prospecting method as outlined in Telford et al. (1976) and Wait (1982). The basic concept is that charge displacement takes place inside a medium due to an external field. Some original work on on this subject was done by Debye (1929). In this theory, the microscopic properties of simple polar molecules are used to

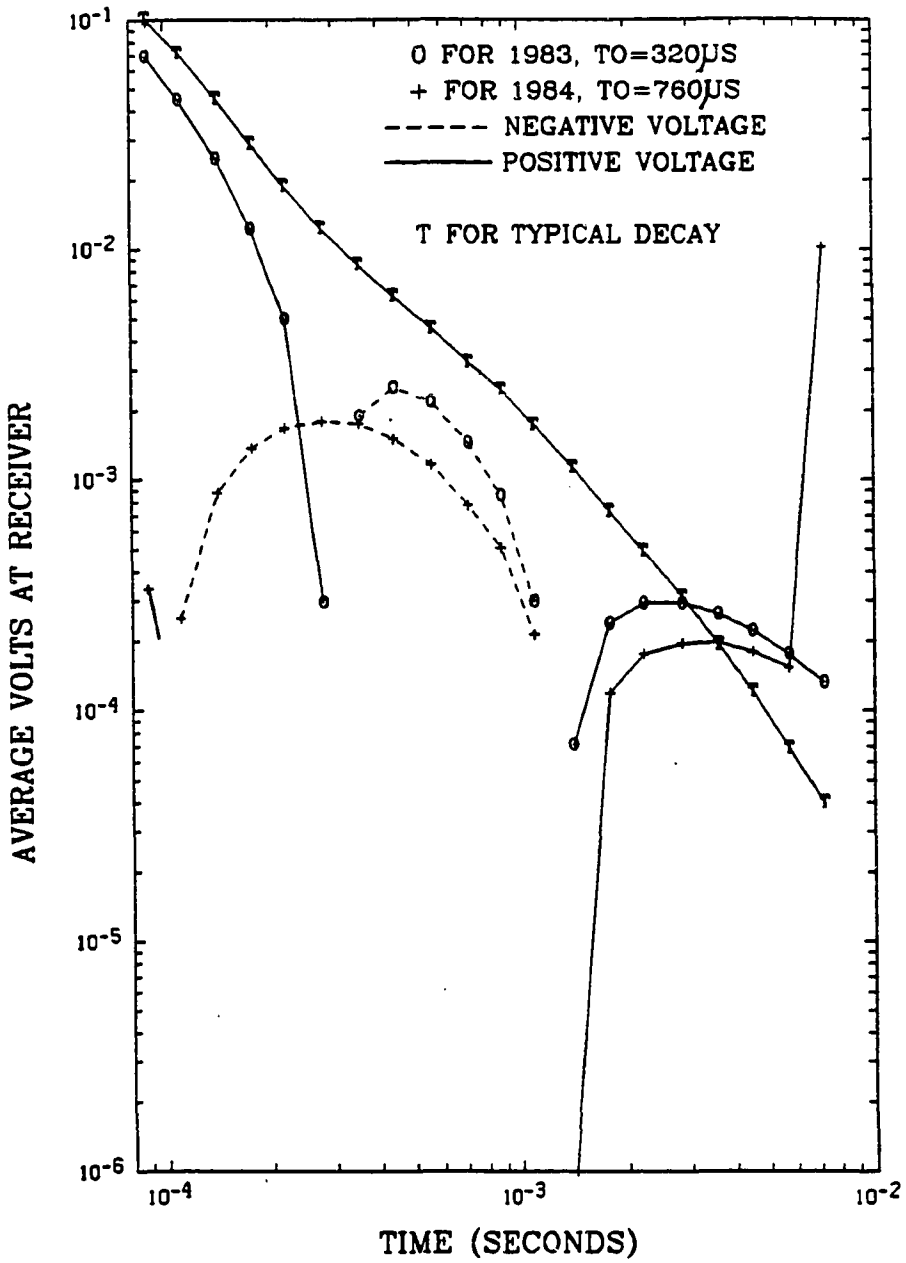

Figure 5.1 TEM data for the NW Eileen site taken at two different years and the data for Galbraith Lake (see Section A.4), a more typical sounding which displays no sign changes.

describe the macroscopic observations of dispersion. Dispersion simply means that an electromagnetic wave does not interact with the media in the same way for all frequencies. Some frequencies will have greater attenuation than other frequencies; in other words, the properties of the media are frequency dependent.

The observation of dispersion in the laboratory led Debye and other researchers to explanations based on the theoretical properties of the media. A common thread in these works is the assumption that the polar molecule will tend to oscillate with some resonant frequency ω_0. Upon the assumption of a single resonant frequency, the polarization vector $\vec{P}$ becomes complex and so also must the dielectric permittivity as discussed in Debye (1929), Jackson (1975), Stratton (1941), and Born and Wolf (1975). In the model developed by Debye, as related in the classic work *Polar Molecules*, published in 1929, the complex and real parts of the dielectric permittivity may be graphed as a semi-circle (the model is now referred to as the Debye model and the permittivity graphs as Debye diagrams; see Hill et al., 1969 for more details on Debye diagrams). Later work based on this idea have given rise to more elaborate and complicated descriptions of the physical nature of the real media given in terms of either or both a complex dielectric permittivity and a complex conductivity. These complications have been somewhat reduced by Wait (1982) who defines complex resistivity in terms of a simple resistivity and simple conductivity. Wait's statement that "It seems redundant and undesirable to allow σ and ϵ to be complex, as one finds in recent writings," demonstrates a frustration with the lack of commonality between the various descriptions used for dispersion.

In contrast, the conductivity and the permittivity may both be complex as stated in Keller and Frischnecht (1966). Keller and Frischnecht support their statement on physical arguments, that polarizability is due to: 1) the displacement of the electron cloud (which occurs in about 10^{-9} seconds), 2) reorientation of polar

molecules, 3) ionic bond displacement, and 4) mobile charges collected at boundaries (as in mineral polarization). Each contribution occurs at a different characteristic relaxation time and therefore produces dispersions at different characteristic frequencies. Keller and Frischknecht also state that hydrocarbons exhibit molecular polarization. The approach calling for a complex conductivity and a complex dielectric permittivity is followed by Olhoeft (1975) in his formulation for permafrost electrical properties. Recalling the expression for the complex wave number k as defined by Equation 2.16, and allowing the conductivity and the dielectric permittivity to be complex via:

$$\sigma = \sigma' + \imath\sigma'', \quad \epsilon = \epsilon' - \imath\epsilon'', \tag{5.1}$$

where the single prime is the real part and the double prime is the imaginary part for each complex quantity, leads to:

$$k^2 = \mu\,\omega\,(\omega\epsilon_e - \imath\sigma_e), \tag{5.2}$$

where $\epsilon_e = \epsilon' + \sigma''/\omega$ and $\sigma_e = \sigma' + \omega\epsilon''$ are the effective dielectric permittivity and effective conductivity, respectively.

The Debye formula, based on a theoretical analysis of a polar molecule with a single relaxation time and nonzero DC conductivity, gives the complex dielectric permittivity as:

$$\epsilon(\omega) = \epsilon' - \imath\epsilon'' = n^2 + \frac{\epsilon_s - n^2}{1 + \imath\omega\tau}, \tag{5.3}$$

where n is the index of refraction and ϵ_s is the static dielectric permittivity.

A number of researchers, in their endeavor to find a model which describes the observed dispersive properties of real materials more adequately have felt compelled

to use more complicated forms than the Debye formula. In these more complicated forms the relationship between the real and imaginary parts of the permittivity have been altered such that the Debye diagram is no longer a semi-circle centered on the real axis. However, the reformulations do match the data for natural materials much better. For example, the data displayed by Olhoeft (1975) on the electrical properties of permafrost were modeled with a Cole-Cole model (see Cole and Cole, 1941):

$$\epsilon(\omega) = \epsilon' - i\epsilon'' = n^2 + \frac{\epsilon_s - n^2}{1 + (i\omega\tau)^{(1-a)}}, \tag{5.4}$$

which reduces to the Debye model for $a = 0$.

It is beyond the scope of this thesis to deal with all dispersion models. It is of note, however, that the Cole-Cole model used in the present study is not directly related to the theoretical model of Debye. Rather, it is derived in a different manner using a simplified electrical network model (see Pelton et al., 1978) to represent mineralized rock. Figure 5.2 displays the mineralized rock model with a metallic grain partially blocking an ionic conduction path within the pores. Also shown is the extremely simple equivalent circuit for the mineralized rock where R_0 is the unblocked conduction path resistance and R_1 represents the partially blocked conduction path resistance. The metallic-ionic interface is simulated by the $(i\omega\chi)^{1/c}$ term in the figure. This oversimplified model displays a "Cole-Cole" relaxation. The Cole-Cole frequency parameter c is related to the distribution of relaxation times with $c = 1$ corresponding to single relaxation time. The parameter χ represents a capacitance when $c = 1$, and ω is the angular frequency.

These quantities can be related to the chargeability m and time constant τ by $m = 1/(1 + R_1/R_0)$ and $\tau = \chi(R_0/m)^{1/c}$.

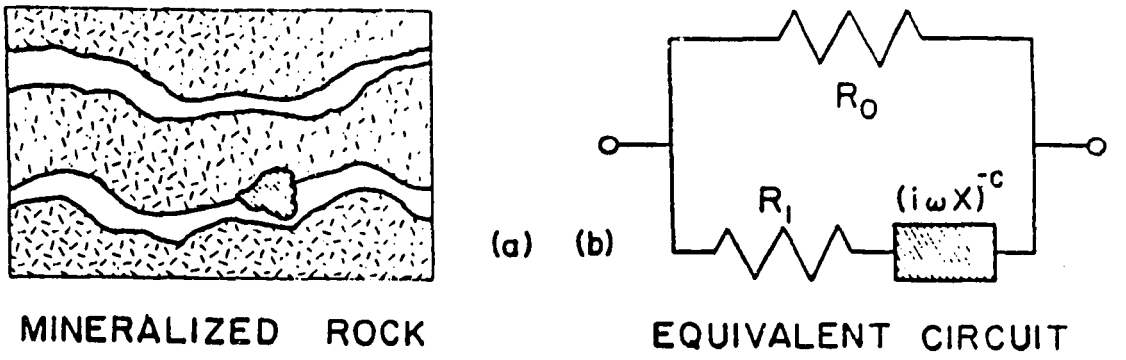

Figure 5.2 A mineralized rock with ionic conduction taking place in the pore spaces is shown in a) with a metallic grain partially blocking the conduction path in one conduction path. In b) is shown the simplified circuit used to simulate the rock. (after Pelton et al., 1978)

Lee (1981) gives a form of this model adapted to conductivity which is given here as Equation 5.5.

$$\sigma = \sigma_0 \left[\frac{1 + (\imath\omega\tau)^c}{1 + (1 - m)(\imath\omega\tau)^c} \right]. \tag{5.5}$$

In Equation 5.5, $\imath$ is $\sqrt{-1}$, ω is angular frequency in radians per second, τ is the model time constant in seconds, c is the Cole-Cole frequency constant, σ is conductivity in siemens per meter, σ_0 is the DC or zero frequency conductivity, and m is the model chargeability.

The so-called Cole-Cole model used in this work (Equation 5.5) is quite different from the complex dependence called for in the Cole-Cole model for permittivity (Equation 5.4). The dissimilarity between the formulations is understandable, because the model described by Equation 5.5 (Section 5.4) is an electrical analog for mineralized grains which block a conductive pore space in a host rock, that is somewhat oversimplified. This model does not reduce to the Debye model (based on dielectric dispersion) upon assumption of $c = 1$ regardless of the choice of m. The time constants and chargeabilities in the two models cannot be simply related

as the descriptions are for two different fundamental properties of matter (e.g. dielectric permittivity and conductivity). One way to compare the two descriptions is through the complex wave number as in Equation 5.2. When the descriptions are compared in this way, the complex wave number does not have the same form in the two descriptions.

The use of this model here is justified on the grounds that other researchers, for example, Raiche (1983) and Lee (1981), have used this model in their discussions of the sign changes in TEM soundings and thus this formulation is provided a direct comparison to check the program operation with previous work. Additional support for the use of an IP effect modeled with complex conductivity is given in a recent paper of Smith and West (1988) which argues against instrumental effects, 2 or 3-dimensional resistivity geometries, complex magnetic permeability, and displacement currents as possible sources of sign changes in TEM soundings. Smith and West (1988) claim that the earth must be polarizable to produce sign changes in TEM soundings and use the Cole-Cole form to model the dispersive nature of the medium. Futhermore, the modeling of Smith and West (1988) show that TEM sign changes are possible with a single relaxation frequency.

The observation that Olhoeft (1975) makes, namely that the frequency parameter $(1 - a)$ of permafrost is near 1, is very different to the findings of others on mineralized rock where the frequency parameter is between 0.1 and 0.6. It is difficult to compare the types of modeling with different forms of the $\imath\omega\tau$ dependence. The point is that both theory and empirical fits to the data require some form of an $\imath\omega\tau$ dependence to simulate the dispersive nature of all real materials. In this thesis, a relatively simple electrical network is used to model electromagnetic dispersion.

5.4 MODELING

Alterations were made in the NLSTCI program from Anderson (1982) to allow for a complex conductivity in each layer for a one-dimensional layered earth. The complex conductivity is that of the Cole-Cole model used by other researchers, namely, Pelton et al. (1978), Lee (1981), and Raiche (1983) and is shown in Equation 5.5. Sign reversals cannot occur in a layered earth of simple resistivity with TEM central induction soundings for the vertical magnetic field as shown by the definitive work of Gubatyenko and Tikshayev (1979). Lee (1981) and Raiche (1983) show that single sign reversals first reported in the literature by Spies (1980) may be produced with an IP effect and their work was used as a qualitative check for this work.

Figure 5.3 displays the response from a half space with complex conductivity. The two sign changes are prominent and the expected field strength is well above the noise level.

In addition to predicting the IP effects, a program called RESPONS.VAX (see Appendix B for a listing) has been developed here to predict the effects of a ramp turnoff time (TO) by a deconvolution-convolution process (McGillem and Cooper, 1974). The program begins by calculating the step response for a given model using the FWDTCIP.VAX program with four times the number of calculated points as the TEM Geonics EM-37 would produce in data. Since the calculated points are evenly spaced in logarithmic time and equal time divisions are required for a straight forward convolution process, the step response is fit with a cubic spline and resampled for evenly spaced divisions in time. Now the step response

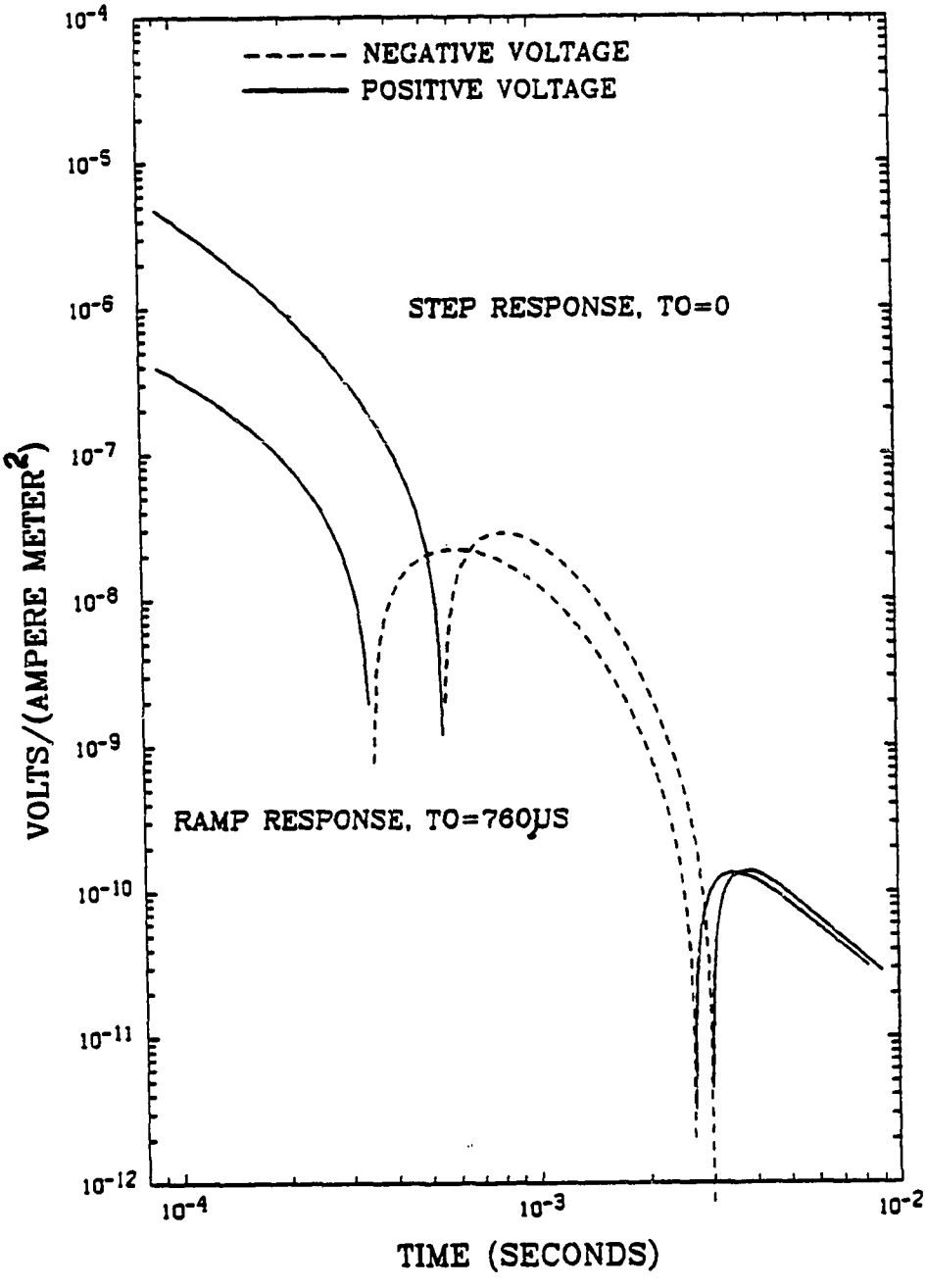

Figure 5.3 Predicted TEM response due to the induced polarization effect of a Cole-Cole complex conductivity. The model parameters are $\mathbf{c} = 1$, $\tau = 6.9 \times 10^{-4}$ seconds, $\rho = 1000$ Ω-m and $m = 0.5$.

is deconvolved using algebraic division to obtain the impulse response. The ramp response is obtained by convolving the ramp drive with the impulse response.

It is possible to demonstrate the occurrence of two sign changes and the effect of a non-zero TO as shown in Figure 5.3. Clearly, an increase in turnoff time causes an apparent shift in the TEM curve with sign changes occurring earlier in time. The change in TEM decay curves due to the longer turnoff time qualitatively explains the difference between the two sets of observed data at the Kuparuk site. As has been mentioned in Section 5.2, the instrument used in the 1984 sounding had a turnoff time of 760 microseconds, whereas the instrument used in 1983 had a turnoff time of 320 microseconds.

It is desirable to obtain a reasonable fit to the observed data by changing the parameters of the TEM IP mechanism. However, this problem is very difficult since so many parameters are required to characterize a single layer in the model. Resistivity and thickness are two parameters that are still required to characterize a layer, but when IP effects are considered, the Cole-Cole parameters of time constant (τ), chargeability (m), and frequency parameter (c) must also be specified....for each layer. Nonetheless, a parameter variation was conducted using the model given in Equation 5.5 with the TEM IP response of Figure 5.3 as a base for each parameter investigation. The model chosen for investigation consisted of two layers simplified by assuming the IP effect arises from the upper layer only (the lower layer has simple resistivity only).

Figure 5.4 displays a series of TEM IP decay curves presented as a three-dimensional figure. The display shows the log of the predicted field strength, in units of volts per ampere square meter, plotted as a function of log time. The first slice is the response for a layer 1000 meters thick of 1000 Ω-m material over 50 Ω-m material. Subsequent slices are for decreasing thickness of the first layer until the

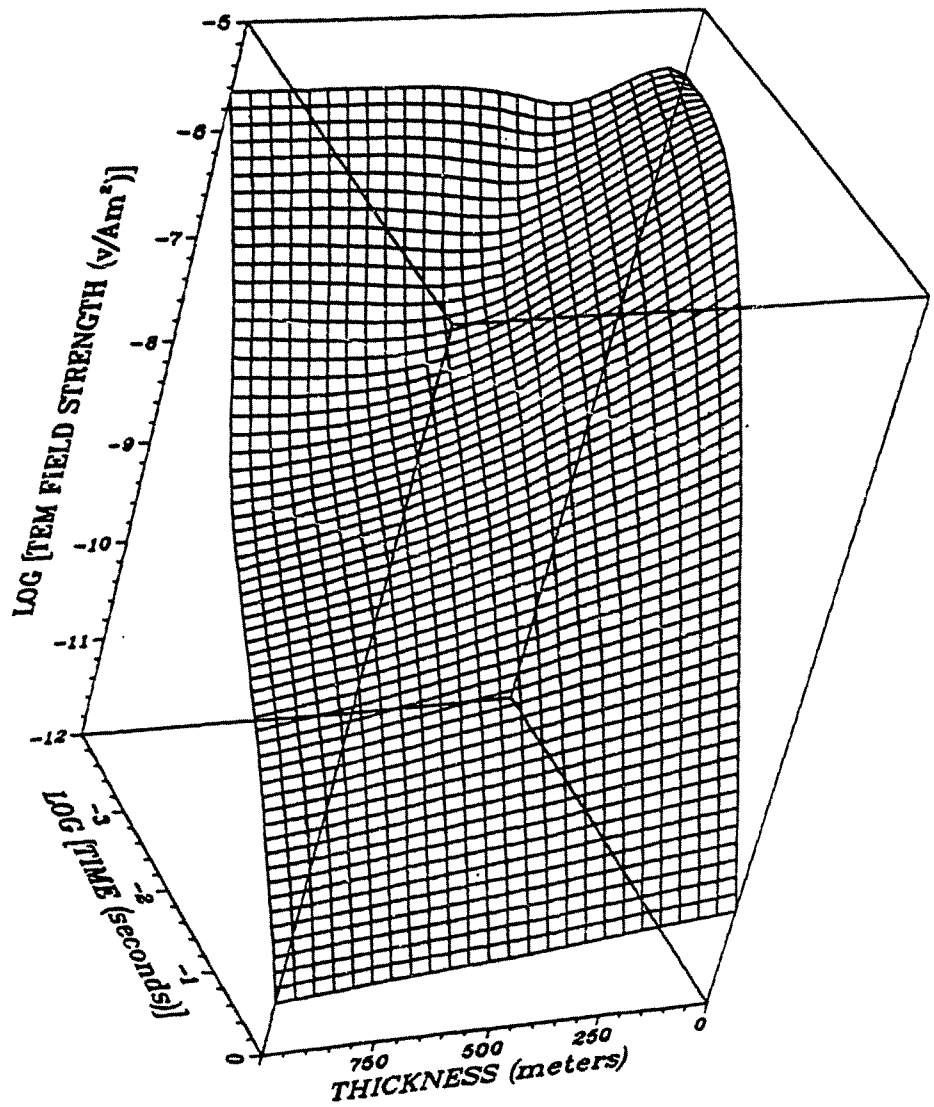

Figure 5.4 Family of predicted TEM responses presented as a three dimensional figure. This set of curves is for materials with no IP effect to show a typical sounding decay.

last slice which is the decay for a homogeneous half-space of 50 Ω-m. This figure shows the normal response for materials having no IP effects for a transmitter loop of 400 meters radius. Subsequent Figures (5.5, 5.6, 5.7, and 5.8) display the figures for parameter changes for: first layer thickness, time constant τ, chargeability m, and frequency parameter c, respectively.

Figure 5.5 displays the three dimensional figure which shows the variation of the TEM IP response when the first layer thickness is varied. The model used is for a 2 layer system with the same resistivities used in Figure 5.4 but, now the first layer produces an IP effect while the basement layer retains simple resistivity. The first layer has Cole-Cole parameters of $\rho_0(= 1/\sigma_0) = 1000\Omega$-m, $c = 1.0$, $\tau = 6.9 \times 10^{-4}$ seconds, and $m = 0.5$ As the thickness of the IP producing layer approaches zero, the sign reversal region (appears as a bump) disappears.

Figure 5.6 displays the three-dimensional figure which shows the variation in the TEM IP response when the time constant τ is varied from 1.0×10^{-5} to 1.0×10^{-1} seconds. Resistivities remain 1000 over 50 Ω-m and the other Cole-Cole parameters are $c = 1.0$ and $m = 0.5$. The sign reversal region appears as a bump near the center of the figure. This display shows that for the particular choice of parameters, there is a limited range in time constant which will produce an IP response. For this figure and the subsequent figures, the curve drawn on the extreme right (in this figure, $log\ \tau = -1$) corresponds to the homogeneous half-space of simple resistivity 50 Ω-m resistivity as was the case for the Figures 5.4 and 5.5. This curve is used as a reference curve.

Figure 5.7 displays the three-dimensional figure of the family of TEM IP curves resulting from varying the chargeability m from 0 to 0.96. The resistivities remain the same as previous figures while the other Cole-Cole parameters are $c = 1.0$ and $\tau = 6.9 \times 10^{-4}$ seconds.

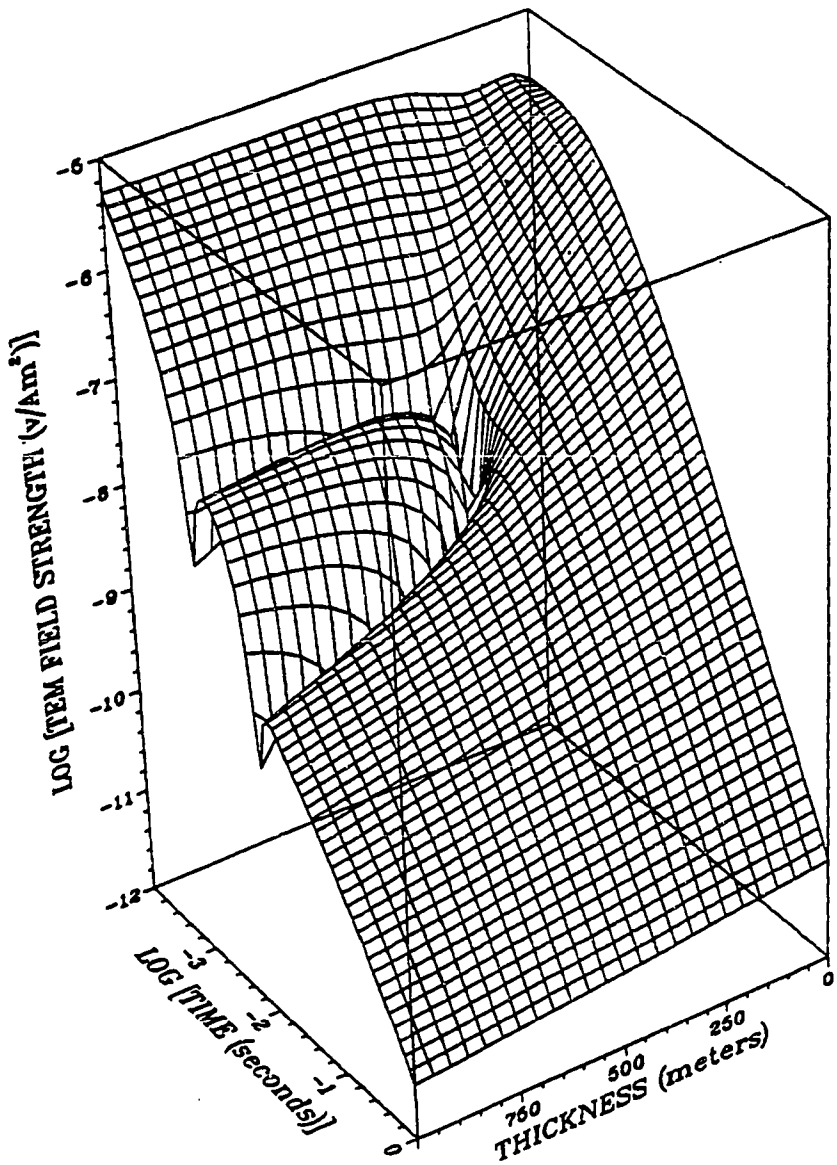

Figure 5.5 Family of predicted TEM IP responses showing the variation as the first layer (layer with IP effects) thickness is varied. The region with a pronounced bump near the center of the figure is the region of the sign change.

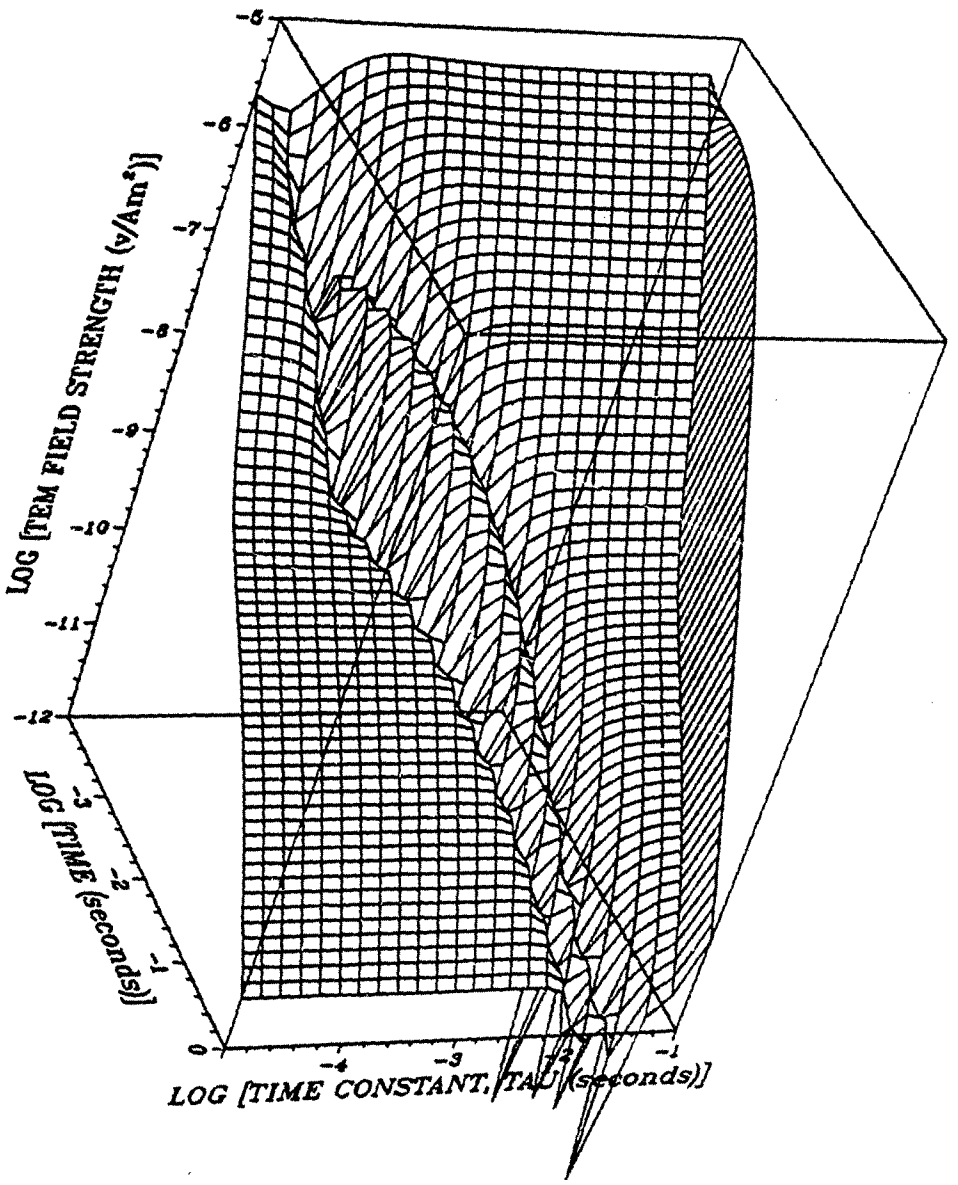

Figure 5.6 Family of predicted TEM IP responses showing the effect of changing the time constant, TAU$= \tau$, from 10^{-5} to 8×10^{-2} seconds.

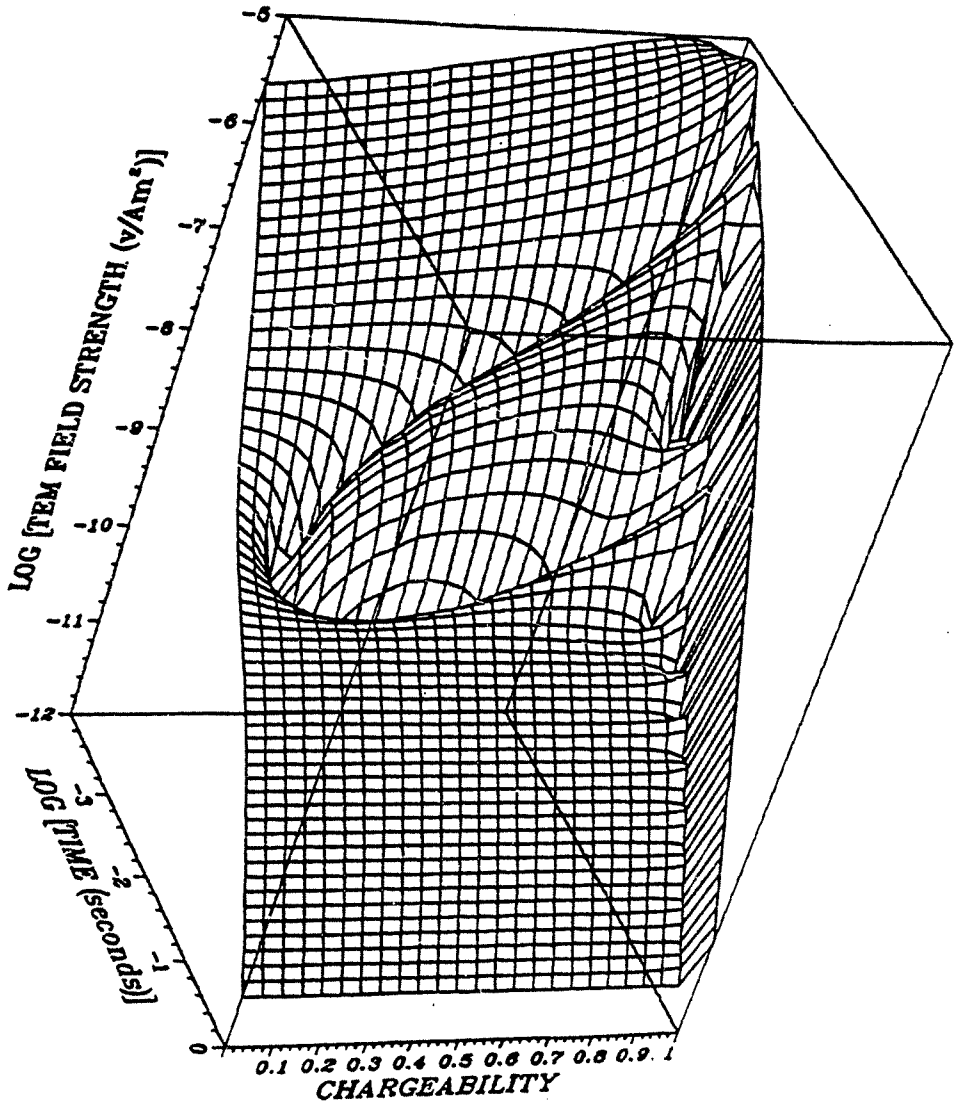

Figure 5.7 Family of predicted TEM IP responses showing the effect of varying the chargeability m from 0 to 0.96.

Figure 5.8 displays the three-dimensional figure of the family of TEM IP curves resulting from varying the Cole-Cole frequency parameter c from 0.0 to 0.96. The sign reversal is more pronounced as c approaches 1.0.

The three-dimensional figures shown here have been developed specifically in an attempt to model double sign changes. In a very similar way, single sign change figures may be developed with appropriate selections of the Cole-Cole model parameters, resistivities, and thickness.

5.5 SUMMARY AND DISCUSSION

The data of Figure 5.1 and the modeling of Figure 5.3 display very similar characteristics and demonstrates the potential viability of the IP model to produce anomalous TEM signatures. It is not, however, intended to claim that only IP effects may be responsible for such anomalous signatures. It may be possible that two or three-dimensional resistivity structures give rise to sign changes. There has been considerable effort expended to date by other researchers: Anderson and Newman (1985) and Newman et al. (1986) on the effects of three-dimensional resistivity structures. While this modeling is still being developed, Gerald W. Hohmann (private communications, 1986) reports that sign changes "normally do not occur with three-dimensional modeling" in the TEM method used to obtain data for this thesis. The curves published by Anderson and Newman (1985) are for three-dimensional structures with large conductivity contrasts; none of these curves display sign changes. In addition, the study of lithology by Collett (1983) and the studies by Daniels et al. (1976) and Osterkamp et al. (1985) on permafrost thickness support a layered earth scenario, at least on the scale of one or two kilometers, in

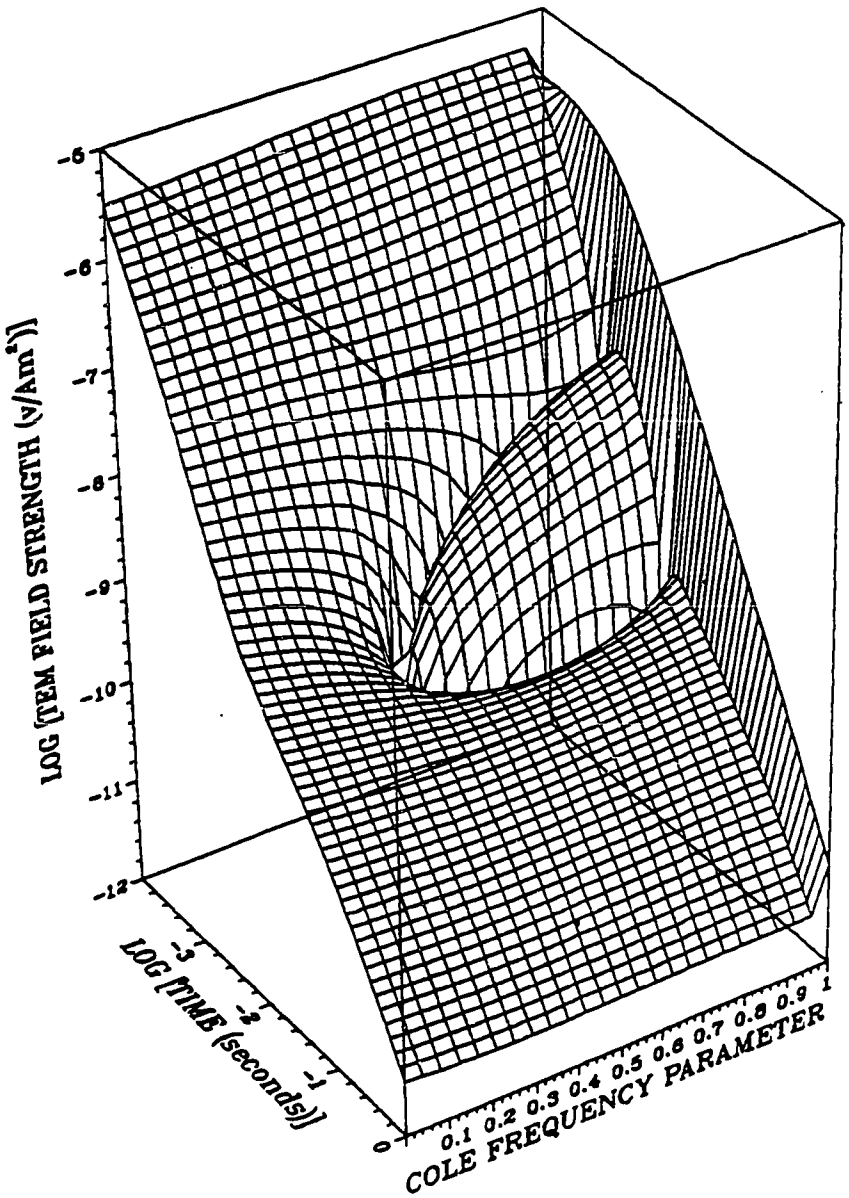

Figure 5.8 Family of predicted TEM IP responses showing the effect of varying the first layer Cole frequency parameter *c* from 0.0 to 0.96.

this area of North Slope. Smith and West (1988) argue that a medium must be polarizable for the TEM signature to change sign.

While other researchers have reported the occurrence of single sign reversals in TEM data (Spies, 1980), no previous reports of the double sign reversals shown by the data have occurred in the literature. Modeling, using a Cole-Cole model of complex conductivity with $c = 1$, $\tau = 6.9 \times 10^{-4}$ seconds, $\rho = 1000$ Ω-m and $m = 0.5$, has shown that the IP effect can produce double sign reversals. Some comments should be directed towards this choice of parameter values. The origin of the anomalous signal in Figure 5.1 is unknown, but because it has been modelled with an IP effect and the earth is taken to be strictly layered, all the electrical properties of the materials that are known to exist at permafrost depths beneath the Kuparuk site must be considered. As mentioned previously, the permafrost extends to a depth of about 500 meters (Osterkamp et al., 1985) in the immediate area and it is thought that no more than 10 or 20 meters could be unfrozen (and probably much less) near the surface in the presence of shallow, mature thaw lakes. In addition, the first 150 meters consists of sands and gravels. There are finer grained soils (perhaps clays) below the sands and gravels to the base of permafrost and beyond. Near the base of permafrost, layers of gas hydrates have been identified by Collett (1983).

Some of the electrical properties of ice or ice-rich sands and gravels, frozen clays and methane hydrates are similar. Ice cores from permafrost and natural clay samples have been investigated by Olhoeft (1975) who finds the samples have similar resistivities and dielectric constants as a function of frequency. Lawson et al. (1984) have investigated a natural methane hydrate and obtained a resistivity versus frequency curve which only differs slightly from that of clay or ice. The shape of the dispersion curve of the dielectric constant with frequency is also very much

alike for the materials, although the methane hydrate shows a significant difference in magnitude. The resistivity versus frequency curve shows a decrease of not more than a factor of 2 from essentially DC to about 10 Hz, then a further decrease of about one order of magnitude to 10^4 Hz and then a steep linear variation on a log-log plot. These results suggest the real resistivity versus frequency curve follows a Debye-type relaxation for natural ice, clay, and methane hydrate. The real part of the complex resistivity is

$$\rho_r = \frac{\sigma_r}{\sigma_r^2 + \sigma_i^2}, \tag{5.6}$$

where subscript r stands for the real part and i stands for the imaginary part. From Olhoeft (1975) $\sigma_r = \sigma_0 + \omega\epsilon_i$ and $\sigma_i = \omega\epsilon_r$. With the complex permittivity ϵ expressed in terms of a single Debye relaxation, one finds that as $\omega \rightarrow 0$, $\rho_r \rightarrow \rho_0$ where $\rho_0 = 1/\sigma_0$ the zero frequency or DC resistivity. As $\omega \rightarrow \infty$, $\rho_r \rightarrow 0$.

On the other hand, with the conductivity expressed as in Equation 5.6, one finds that as $\omega \rightarrow 0$, $\rho_r \rightarrow \rho_0$ and that as $\omega \rightarrow \infty$, then $\rho_r \rightarrow (1 - m)\rho_0$. Thus, unless m is nearly equal to one, the Pelton expression (Equation 5.5) can only be made to fit the observed resistivity versus frequency curve over a very limited region, while the real resistivity with a Debye dispersion in the permittivity can be better fitted to the observed dispersion in the resistivity of ice, clay, and perhaps gas hydrates. Also, smaller values of c, the frequency parameter, would tend to make ρ_r slowly fall with frequency while a longer time constant, τ, would shift the beginning of the region of appreciable fall off to earlier times. Thus the opposite extreme in the modelling was chosen, that is, $c = 1$ and a relatively short time constant $\tau = 6.9 \times 10^{-4}$ s.

Thus, larger m and c values and shorter relaxation times τ are more appropriate in modelling the observed signal at the Kuparuk site when using the Pelton

expression, than those normally obtained in standard IP surveys for minerals (e.g. Lee, 1981; Raiche, 1983). In Figure 5.3, m=0.5, c=1, and $\tau = 6.9 \times 10^{-4}$s and studies of the parameters such as that of Figure 5.8 suggest that the modelling could be "fine-tuned" further with a longer τ, larger m, and slightly decreased resistivity. However, the resulting model will not differ qualitatively from that of Figure 5.3.

In conclusion, it is inferred from the modelling that a possible source of the anomalous TEM signal is an IP mechanism associated with ice, clay, and/or gas hydrates. However, massive ground ice and ice-rich soils occur at many other TEM sites on the North Slope region, where the TEM signal could be modelled with simple resistivity (see Appendix A), suggesting that it is not merely the presence of near-surface ice that causes the anomalous signal. In fact, the only known unusual aspect of the earth at the site with double sign reversals in the data is the occurrence of gas hydrates. As an example, the lithology at the Deadhorse site is similar to that of the Kuparuk site but the TEM data taken at Deadhorse does not change sign.

It is interesting to speculate that the anomalous TEM signature presented here may be related to the presence of gas hydrates; however, much additional work must be done to discover the true cause of the anomaly. These data will be discussed further in the last chapter.

CHAPTER 6. SUMMARY, CONCLUSIONS AND RECOMMENDATIONS

6.1 SUMMARY AND CONCLUSIONS

TEM soundings were made at more than 40 sites in Alaska to investigate the application of this method to the study of permafrost in a variety of terrains. Information from drilling, well logs, and seismic studies was used in the development of layered earth models to simulate the TEM sounding data. Layered earth model interpretations that best fit the data were obtained for these sites using a combination of computerized forward and inverse modeling. The theory of the method and the resolution of best fit models were also discussed. This thesis emphasized the interpretations for sites of particular scientific and geotechnical interest. The maximum error in the apparent resistivities due to possible systematic and random errors in the values of the measured transmitter current or turnoff time was estimated to be ±7%. The turnoff time error is not to be confused with the ramp time effect, which can be corrected for.

The major conclusions of this thesis are:

(1) Anomalous TEM Data — Transient electromagnetic data exhibiting anomalous double sign reversals can be modeled as induced polarization effects indicating that they arise from an electrical relaxation phenomenon. The lithology at the Kuparuk site with TEM double sign reversals is similar to many other sites on the Alaskan North Slope which do not give sign changes; the difference between the Kuparuk site and other sites is the occurrence of large amounts of gas hydrates at the Kuparuk site.

(2) Ramp Turnoff Corrections — The most precise interpretation of TEM data requires that the data be corrected for the effects of a finite ramp turnoff time of the transmitter current.

(3) Resolution Estimates — For a given model, the resolution of the ice-bearing permafrost thickness with the TEM method is estimated to be within ±10% of the actual thickness providing sufficient lithologic control exists nearby.

(4) Subsea Permafrost — The TEM measurements seem to show that permafrost near Prudhoe Bay thins with increasing distance offshore, and the TEM and other data suggest the subsea permafrost is multilayered beyond approximately 5 km offshore. The TEM method does not appear capable of resolving the depth to the base of a multilayered ice-bearing region without a reasonably good input model based on well-logs. The TEM method does appear to resolve the depth to the ice-bearing permafrost table.

(5) Operational Details — Experience gained in the course of this research shows that the TEM method is most suited for permafrost investigations when lithologic controls from nearby wells which penetrate the base of permafrost are available. Also the present work shows that the resolution of a deep and more resistive layer in a generally conductive environment will require improvements in equipment and signal processing over the EM-37 used for this research.

(1) Anomalous TEM Data

Any set of TEM data which displays sign changes with signal strengths well above the noise level can be considered anomalous in the sense that this behavior cannot be explained in terms of a purely-resistive layered-earth model. Three TEM sounding sites exhibited sign reversals. The Kuparuk site was of particular interest because a double sign reversal was obtained there. This is the first reported field observation of such a TEM signal, although others have reported the occurrence of single sign reversals in TEM data (e.g. Spies, 1980).

From a modeling study using complex conductivity, it is concluded that the anomalous double sign reversal may arise from an IP effect (electrical relaxation phenomenon). The modeling also shows that sign changes may be produced in the TEM soundings over a range of model parameters. Specifically, the IP effect, modeled with a Cole-Cole conductivity (Lee, 1981), can produce the double sign reversals. The choice of parameter values, namely $c = 1$ and $\tau = 6.9 \times 10^{-4}$ s are not characteristic of mineral deposits such as sulfides. According to Pelton et al. (1978) and Lee (1981), mineral deposits tend to have smaller values for c and longer τ. The choice of $c = 1$ is also supported by the recent modeling of Smith and West (1988).

The anomalous TEM signature may be related to deposits of methane and other gas hydrates known to exist in the vicinity of the Kuparuk sounding. On the other hand, the electrical characteristics of some frozen clays and ice as a function of frequency are similar to those of methane hydrates. Olhoeft (1975) shows that the high frequency portion of the frequency versus resistivity curves for ice and frozen clay are well modeled with short relaxation time constants (τ) and higher values for **c**, while Lawson et al. (1984) show that the frequency dispersion of a methane hydrate is similar to that of ice. Ground ice and ice-rich soils can probably be rejected as the source of the signal since these are common at other sites on the North Slope where the anomaly was not observed. Frozen clays also exist at other sounding sites where sign reversals were not observed and therefore it is unlikely that they are the source of the anomalous TEM signal.

Other possible sources of the anomalous signal include mineralization and three-dimensional resistivity inhomogeneities. These appear less plausible because investigation of well logs from the area show the subsurface materials can be taken to be reasonably well-layered to the depth sounded. Also, Smith and West (1988) argue that the earth must be polarizable for sign changes to occur. It may be possible to lend support to or eliminate the IP effect as the source mechanism by taking a number of additional soundings in the area, using different transmitter loop sizes, and also measuring the other components of the magnetic field.

At the time of this writing, there is a lack of equipment and sufficient funds to undertake the field research that would be required to fully investigate this problem. However, it is clear that additional work should be done to determine whether or not the hypothesis that IP effects are the cause of the anomalous double sign reversal observed at the Kuparuk site is true and whether these can be related to the presence of gas hydrates.

(2) Ramp Turnoff Corrections

A ramp turnoff time correction for raw TEM data is necessary for inverse modeling results to produce the greatest accuracy. The ramp time correction is more important in the initial time gates and is more important when the TEM sounding is taken over higher resistivity ground. The ramp correction procedures developed for this thesis represent early attempts to solve this problem by directly correcting the data for the ramp turnoff time. Three separate procedures were used for ramp turnoff time effects. In relatively resistive ground as on land sites, the data were corrected using the same ratios at each time gate as obtained with the calculation of a late-time homogenous half-space reponse with and without ramp times. In more conductive environments such as the offshore sites, a more complicated expression was used to predict the correction factors. Finally, in modeling the anomalous data which displayed time reversals, a convolution routine was used to predict the effects of a ramp turnoff time on TEM responses to a layered earth having complex resistivity.

However, a more accurate procedure should incorporate the ramp correction into the inverse modeling program so that uncorrected TEM data could be used in inverse modeling. A newer version of the forward modeling program TCILOOP (Anderson, 1981) called FWDTCI which incorporates the ramp correction via direct integration of Equation 2.39 has been recently released (Fitterman and Anderson, 1987). The ramp correction has not yet been installed in a newer version of program NLSTCI (Anderson, 1982).

(3) Resolution Estimates

As suggested by previous studies (Sinha and Stephens, 1983; Ehrenbard et al., 1983), vertical sounding using the TEM method can be productive in discerning the occurrence and depth of permafrost. In particular, the parameter study in

this thesis suggests that under favorable circumstances the thickness of ice-bearing permafrost may be resolved to within 10% of the actual thickness. This estimate is compared to the 5% reported by Sinha and Stephens (1983) who used a curve matching procedure for interpreting TEM data. It is possible, however, that if the inverse modeling procedure had been used by them a localized solution with a better fit could have been obtained.

On the other hand, it is also possible that an inverse model may not correlate well with a thermal log due to nonuniqueness or other problems. In this case, the inverse model may fit the data better than the curve matching model and yet have a thickness which differs more from the thermal log thickness than the curve matching result. Although the nonuniqueness problem has been briefly discussed in this thesis, its effect on the resolution of layer thicknesses by the TEM method has not been determined. The validity of the above conclusion concerning the resolution of permafrost thicknesses is based on having some foreknowledge of the lithology in order to set realistic bounds on the inverse modeling parameters.

(4) Subsea Permafrost

Subsea permafrost farther offshore from the Prudhoe Bay region tends to be warm and is multilayered according to well logs from small offshore islands and other more shallow drill data. These are not the most favorable circumstances for predicting the base of permafrost using an electromagnetic method but nevertheless attempts were made to model the data obtained offshore with 3 to 6 layers. It was thought that there was sufficient background information from well logs and other data to provide good input models for the inverse process. However, the resulting 3 and 6 layer inverse models which disagreed considerably from each other from 7-11 km offshore clearly demonstrated this was not the case. Reindeer Island, for which

there was DIL information on the layering, resulted in a depth to the base of ice-bearing permafrost in good agreement with Osterkamp et al. (1985). Despite the disagreement between the 3 and 6 layer models, some general trends are present in the inverse models and agree in this sense with the more directly known conditions discussed below.

The 3 layer subsea permafrost profile from this study shows that the ice-bearing permafrost tends to decrease in thickness with distance offshore. In addition, the unfrozen layer beneath the seabed tends to be thicker where the water depth is greater. Both these observations from the inverse models support the hypothesis that seawater has inundated the Prudhoe Bay area in recent geological time. Since the mean annual temperature of the sea is greater than the mean annual surface air temperature, the subsea permafrost tends to degrade both from its top and bottom after the land surface has been inundated by the sea.

The models presented in Chapter 4 agree grossly with the available seismic and borehole data on the variation and thickness of the thawed layer above the ice-bearing subsea permafrost. However, it must be borne in mind that the TEM system energizes a volume of earth whereas boreholes sample the materials below a single point on the surface. If there are many layers or isolated plates of ice-bearing material within the conductive, generally unfrozen subsea materials, there will be differences in the interpreted thickness of the unfrozen materials between the TEM technique and the other geophysical methods. No further conclusions can be drawn about the accuracy of the layered models for deeper materials until further exploration provides more direct information on the lithology of the ice-bearing permafrost between 7 and 11 km offshore.

From about 7 to 11 km offshore, the TEM 3 and 6 layer interpretations are divergent. There is already sufficient evidence (DIL records from Reindeer Island

shown in Figure 3.13 and Gull Island (not presented in this thesis but presented in Osterkamp and Payne, 1981) in Prudhoe Bay) to show that the three layer model will be too simplistic for all but the sites very near land. In addition, since the TEM subsea permafrost data are better fit with 6 layers than with the 3 layer models beyond about 5 km, the results support the existence of a fairly complex subsea permafrost structure further offshore, a conclusion which is also supported by the Reindeer Island and Gull Island DIL records.

The predicted bases of subsea permafrost from the 6 layer models at the 5, 7, 9 and 11 km sites appear to be too deep relative to what is known from the well logs taken from Reindeer Island at 13 kilometers. Note, however that the tighter controls on the input model for Reindeer Island led to an inverse model which agreed fairly well with the well logs at that site. The source of the discrepancy is unknown but may be due to the relatively high conductivity of the seawater/saline seabed sediments and the fairly loose bounds for thickness and resistivity parameters used in the modeling. The existence of alternating higher and lower conductivity layers apparently caused the 3 layer model to converge to a solution predicting a shallow permafrost base. Additional in situ data should provide better control of the initial model and hence smaller parameter bounds in the 6 layer inverse modeling process.

Both the 3 layer and 6 layer model results predict a very different profile from that presented in the work of Ehrenbard et al. (1983) for offshore sites. The differences between the depth profile for the subsea permafrost table of Ehrenbard et al. (1983) and the present investigation suggest that their results were from an area with a very different history of inundation. However, some differences may be the result of the exclusive use of 3 layer models in the analysis of Ehrenbard et al. (1983) even in areas farther offshore where the subsea permafrost is known to be

more complex and the permafrost resistivities are considerably lower than the 200 Ω−m values given by them.

(5) Operational Details

Experience with the TEM method has given the following insight into the operational details of the method. First, at sites where the near surface layers tend to be fairly conductive such as offshore at Prudhoe Bay, the determination of deep, relatively resistive structures with the TEM method requires much better signal to noise ratios in the later gates than were obtainable for this study. Better signal to noise ratios may be obtained using higher transmitter currents and better signal processing techniques such as intelligent stacking.

Second, the use of TEM soundings on a reasonably closely-spaced grid or along a line, as in the study of subsea permafrost, will be more productive than soundings from individual, widely separated sites as given in Appendix A. Soundings along the line should extend from sites where subsurface lithology is known to adjacent sites that lack ground truth. This provides a base for modeling purposes to infer changes in, say, the permafrost thickness at the adjacent sites. In light of the need for additional soundings at the Kuparuk site with double sign reversals, it would appear that, at every site, additional soundings should be taken. The additional soundings to the side of the central sounding would be useful to establish the existence of a reasonably layered earth and hence that, in fact, modeling in terms of horizontal layers is appropriate.

Third, the transmitter loop size should be chosen to have a side dimension comparable to the expected depth of the resistivity contrast of interest. For example, a transmitter loop size of 100 m on a side should be used when investigating a

site where the expected permafrost base has a depth comparable to 100 m. However, if possible, other transmitter loop sizes should also be used to obtain a more complete suite of data.

Fourth, uncorrected resistivity profiles from the DIL were used to infer a first guess of the permafrost layering. This estimate is forward modeled for the TEM method and compared with the actual TEM data. There are established procedures for correcting the DIL resistivity, but the available correction curves are not applicable to the large diameter boreholes and associated thawed zones around holes in permafrost. The procedures are also inapplicable in cases where high resistivity is encountered. It was apparent that the TEM resistivity data and the inferred resistivity from the DIL did not agree closely, in many cases differing by a factor of ten or more; however, the DIL records were found to be of value in giving estimates of the depths of resistivity boundaries. This reduced the uncertainties in the choice of the thickness parameters.

Finally, the present study shows that the TEM method has certain limitations but may be used to good advantage in the exploratory studies of permafrost thickness. This is because the thickness of permafrost and its resistivity can be grossly estimated from knowledge of the mean annual surface temperature, local aspect angle, vegetative cover, surface displays of material types, and winter snow cover. This information may allow one to make a reasonable first guess for the inverse modeling process.

6.2 RECOMMENDATIONS

Recommendations for further study are:

(1). It is recommended that more extensive field work be performed with the TEM system at the Kuparuk site to determine whether the IP effect is the source of the anomalous TEM sounding there and also to determine whether the IP effect is associated with gas hydrate deposits.

(2). The apparent success of the IP effect to simulate the TEM data with sign reversals suggests that the data from other sites on the North Slope may contain other and possibly more subtle IP effects. These effects may alter the shape of the transient decay even though the data may not change sign. Future work is recommended at sites such as Deadhorse to eliminate or confirm this possibility.

(3). More information should be gathered at many of the land sites discussed in Appendix A in order to delineate the permafrost with greater confidence. Deeper boreholes extending through the permafrost layer would give more definitive estimates of the base of permafrost and more information on material types. Additional TEM soundings should be taken near these sites to establish that a layered earth is a reasonable model. In general, the TEM method should only be used in those areas where ground truth is available, when accurate inverse models are required.

(4). Subsea permafrost should be investigated with TEM equipment having improved signal to noise ratios in the later gates to resolve the thickness of a deep ice-bearing layer. For future subsea permafrost investigations, a new borehole should be drilled about 9 km offshore along the West Dock - Reindeer Island line to resolve some of the remaining questions regarding the subsea permafrost layering. The thickness of the thawed layer could be better discerned, in general, using

transmitter loops smaller than the 250 m used in this study. For example, a 50 m transmitter loop for the 0.75 and 1 km sites and a 100 m loop for 7, 9 and 11 km sites should provide data that will better resolve the depth to ice-bearing permafrost. The combined use of several smaller loop sizes, say 50, 100, and 150 m transmitter loops, should provide better resolution of the thawed layer.

(5). The problem of nonuniqueness in the geoelectric models for the TEM data must be investigated in greater detail. One approach to this would be to investigate the parameter solution space. A forward modeled set of data could be used as the data for which the various parameter investigations could be compared to provide the rms error. The nonuniqueness could then be graphically investigated by plotting the rms error on the vertical axis using two parameters as variables for the horizontal axes. This three-dimensional plot would produce a surface similar to the plots in Chapter 5. The model from which the data came would appear as a hole in the surface. Nonuniqueness is displayed whenever other holes appear or when a trough or a combination of holes and troughs appear in the graphical representation of the solution space.

While the TEM method, even in its present state of development, can be used to delineate permafrost in a variety of environments under favorable circumstances, it has certain limitations. The method cannot be used to resolve a large number of layers due to the nonuniqueness which arises from the large number of parameters which can be varied. The method is limited in usefulness without lithological information (at least from a nearby site), and is limited by the system noise in the investigation of deeper structures. In addition, a thin (relative to the transmitter loop size) layer over a more conductive layer with a thickness comparable to the

transmitter loop size will not be well resolved by the TEM system. Finally, because the TEM method is relatively new, software for inverting data, when 2 or 3-dimensional structures are suspected, is not available.

The TEM system provides an efficient method of delineating permafrost when the limitations of the technique are not exceeded. It can be a very important tool to be used in concert with other information for the exploration of permafrost. The true utility of this technology is yet to be reached as more effective means of interpretation are only now being developed.

REFERENCES CITED

Akimov, A.T., Melnikov, V.P. and Frolov, A.D., (1979). Geophysical Methods of Study of Permafrost in USSR, U.S. Army Cold Regions Research and Engineering Laboratory Draft Translation DT-707.

Alluad, L.A., (1977). *Schlumberger: The History of a Technique*, John Wiley and Sons Inc.

Anderson, D.M., Tice, A.R. and McKim, H.L., (1973). The Unfrozen Water and the Apparent Specific Heat Capacity of Frozen Soils, Proceedings of the Second International Conference on Permafrost, North American Contribution; held 13-28 July at Yakutsk, USSR, pages 289-294.

Anderson, W.L., (1974). Electromagnetic Fields About a Finite Electric Wire Source (Program EMFIN), U.S. Department of Commerce National Technical Information Service Catalog # PB/238 199. See also: Program EMFIN4 Documentation Supplement, dated 20 June 1977.

Anderson, W.L., (1981). Calculation of Transient Soundings for a Central Induction Loop System (Program TCILOOP), U.S. Geological Survey Open-File Report 81-1309.

Anderson, W.L., (1982). Nonlinear Least-Squares Inversion of Transient Soundings for a Central Induction Loop System (Program NLSTCI), U.S. Geological Survey Open-File Report 82-1129.

Anderson, W.L. and Newman, G.A., (1985). An Album of Three-dimensional Transient Electromagnetic Responses for the Central-Induction Loop Configuration, U.S. Geological Survey Open-File Report 85-745.

Archie, G.E., (1942). The Electrical Resistivity Log as an Aid in Determining Some Reservoir Characteristics, Transactions of the American Institute of Mechanical Engineers, **146**, 54-62.

Bhattacharyya, B.K., (1957). Propagation of Electromagnetic Waves in a Medium of Finite Conductivity, Geophysics, **22**, 75-88.

Bhattacharyya, B.K., (1957). Propagation of an Electric Pulse Through a Homogeneous and Isotropic Medium, Geophysics, **22**, 905-921.

Bhattacharyya, B.K., (1959). Electromagnetic Fields of a Transient Magnetic Dipole on the Earth's Surface, Geophysics, **24**, 89-108.

Bhattacharyya, B.K., (1963). Electromagnetic Fields of a Vertical Magnetic Dipole Placed above the Earth's Surface, Geophysics, **28**, 408-425.

Bhattacharyya, B.K., (1964). Electromagnetic Fields of a Small Loop Antenna on the Surface of a Polarizable Medium, Geophysics, **29**, 814-831.

Born, M. and Wolf, E., (1975). *Principles of Optics*, Fifth Edition, Pergamon Press.

Brown, R.J.E., (1960). The Distribution of Permafrost and its Relation to Air Temperature in Canada and the U.S.S.R., Arctic, **13**, 163-177.

Brown, R.J.E. and Kupsch, W.O., (1974). Permafrost Terminology, Canadian National Research Council Associate Committee Geotechnical Research, Technical Memo 111.

Cagniard, L., (1953). Basic Theory of the Magneto-telluric Method of Geophysical Prospecting, Geophysics, **18**, 605-635.

Carslaw, H.S. and Jaeger, J.C., (1959). *Conduction of Heat in Solids*, Second Edition, Oxford University Press.

Cole, K.S. and Cole, R.H., (1941). Dispersion and Absorption in Dielectrics, Journal of Chemical Physics, **9**, 341-351.

Collett, T.S., (1983). Detection and Evaluation of Natural Gas Hydrates from Well Logs, Prudhoe Bay, Alaska, M.Sc. Thesis, University of Alaska at Fairbanks.

Corwin, R.F., (1983). Marine Permafrost Detection Using Galvanic Resistivity Methods, Proceedings 1983 Offshore Technology Conference, Volume 1, Paper OTC 4480, 329-336.

Corwin, R.F., (1985). Electrical Resistivity Techniques for Offshore Arctic Geotechnical Engineering Applications, Civil Engineering in the Arctic Offshore, Proceedings of the Conference, Arctic 1985, American Society of Civil Engineers, 137-143.

Daniels, J.F., G.V. Keller, and J.J. Jacobson, (1976). Computer-assisted Interpretation of Electromagnetic Soundings Over a Permafrost Section, Geophysics, **41**, 752- 765.

Debye, P., (1929). *Polar Molecules*, Chemical Catalog Company Inc. The book was republished in 1945 by Dover, New York.

Doherty, B.T. and Kester, D.R., (1974). Freezing Point of Seawater, Journal of Marine Research, **32**, 285-300.

Dostovalov, B.N., (1947). Elektricheski Karacteristiki Meizlyk Porod, Akad. Nauk SSSR, Trudy Inst. Merzlotovedeniia im. V.A, Obrucheva, **5**, 18-35.

Ehrenbard, R.L., Hoekstra, P. and Rozenberg, G., (1983). Transient Electromagnetic Soundings for Permafrost Mapping, Proceedings of the Fourth International Conference on Permafrost held at Fairbanks, Alaska, 17-22 July, National Academy Press, 272-277.

Ferrians, O.J., (1965). Permafrost Map of Alaska: U.S. Geological Survey Miscellaneous Geologic Investigations Map I-445, scale 1:2,500,000.

Ferrians, O.J. and Hobson, G.D., (1973). Mapping and Predicting Permafrost in North America: A Review, 1963-1973, North American Contribution to the Second International Conference on Permafrost held in Yakutsk, USSR on 13-28 July, National Academy of Sciences, 479-498.

Fitterman, D.V. and Anderson, W.L., (1987). Effect of Transmitter Turn-Off Time on Transient Soundings, Geoexploration, **24**, 131-146.

Gubatyenko, V.P. and Tikshayev, V.V., (1979). On the Variation of the Sign of the Electromotive Force of Induction in the Transient Electromagnetic Field Method, Izvestiva, Earth Physics, **15**, 217-219.

Hill, N.E., Vaughn, W.E., Price, A.H. and Davies, M., (1969). *Dielectric Properties and Molecular Behavior*, Von Nostrand Reinhold Company, London.

Heiland, C.A., (1940). *Geophysical Exploration*, First Edition, Prentice Hall, New York.

Hoekstra, P. and McNeill, D., (1973). Electromagnetic Probing of Permafrost, North American Contribution to the Second International Conference on Permafrost, held in Yakutsk, USSR on 13-28 July, National Academy of Sciences, 517-526.

Holt, C.A., (1963) *Introduction to Electromagnetic Fields and Waves*, John Wiley and Sons, Inc., New York.

Hopkins, D.M., (1967). Quaternary Marine Transgressions in Alaska, in *The Bering Land Bridge*, edited by D.M. Hopkins, Stanford University Press, 47-90.

Hume, J.D. and Schalk, M., (1967). Shoreline Processes Near Barrow, Alaska: A Comparison of the Normal and Catastrophic, Arctic, **20**, 9, 86-103.

Hume, J.D., Schalk, M., and Hume, P.W., (1972). Short Term Climate Changes and Coastal Erosion, Barrow, Alaska, Arctic, **25**, 272-278.

Jackson, J.D., (1975). *Classical Electrodynamics*, Second Edition, John Wiley and Sons, Inc.

Joesting, H.R., (1941). Magnetometer and Direct-Current Resistivity Studies in Alaska, American Institute of Mining and Metallurgical Engineers, Technical Publication 1284.

Johnston, G.H., (1981). *Permafrost Engineering Design and Construction*, John Wiley and Sons, Inc.

Kaufman, A.A. and Keller, G.V., (1983). *Frequency and Transient Soundings*, Elsevier Science Publishing Company.

Kawasaki, K., Osterkamp, T.E., and Gosink, J.P., (1982). A Preliminary Evaluation of Numerical Models Suitable for Thermal Analysis of Roadways and Airstrips, State of Alaska Department of Transportation and Public Facilities Report #Ak-RD-82-22.

Keller, G.V. and Frischknecht, F.C., (1966). *Electrical Methods in Geophysical Prospecting*, Pergamon Press.

Kittel, C., (1976). *Introduction to Solid State Physics*, Fifth Edition, John Wiley and Sons, Inc.

Kreyszig, E., (1983). *Advanced Engineering Mathematics*, Fifth Edition, John Wiley and Sons, Inc.

Lachenbruch, A.H., Sass, J.H., Marshall, B.V. and Moses, T.H. Jr., (1982). Permafrost Heat Flow and the Geothermal Regime at Prudhoe Bay, Alaska, Journal of Geophysical Research, **87**, B11, 9301-9316.

Lawson, W.F., Reddy, S.M., Gregoire, C.E., and Vassallo, K.L., (1984). Acoustic and Electrical Property Measurements in the DSDP Methane Hydrate Core: paper presented at the American Institute of Chemical Engineers, National Meeting, March, 1984, Atlanta, Georgia.

Lee, T., (1981). Transient Electromagnetic Response of a Polarizable Ground, Geophysics, **46**, 1037-1041.

Legget, R.F., (1963). Permafrost in North America, Proceedings of the First International Conference on Permafrost, 11-15 November 1963 at LaFayette, Indiana, National Academy of Sciences, 2-6.

Lloyd, T., (1962). The Influence of Permafrost on Northern Development, in Proceedings of the First Canadian Conference on Permafrost, 17 and 18 April 1962 at Ottawa, Canadian Research Council Technical Memorandum 76, 1-12

Lunardini, V.J., (1981). *Heat Transfer in Cold Climates*, First Edition, Van Nostrand Reinhold Company.

Mathews, J. and Walker, R.L., (1970). *Mathematical Methods of Physics*, Second Edition, W. A. Benjamin, Inc., Menlo Park, California.

Maxwell, J.C., (1873). *A Treatise on Electricity and Magnetism*, Dover Publications, New York, Third edition in 2 volumes published in 1954.

McGillem, C.D. and Cooper, G.R., (1974). *Continuous and Discrete Signal and System Analysis*, Holt, Rinehart and Winston, Inc.

McNeill, J.D., (1980). EM-37 Ground Transient Electromagnetic System: Calculating Depth of Exploration, Geonics Limited Technical Note TN-10.

McNeill, J.D., (1982). EM-37 Ground Transient Electromagnetic System: Design Features. Geonics Limited.

Middendorff, A.T.V., (1853). Zusatz: 312-16 in Ditmar, C. v., 1853, Über die Eismulden im ostlichen Sibirien (Nakipni der Sibirischen Russen), Akademie Imperiale des Sciences de St. Petersbourg, Bulletin (Classe Phys.-Math) II(19-20), 306-316.

Morrison, H.F., Phillips, R.J. and O'Brien, D.P., (1969). Quantitative Interpretation of Transient Electromagnetic Fields Over a Layered Half Space, Geophysical Prospecting, **17**, 82-101.

Muller, S.W., (1945). Permafrost or Permanently Frozen Ground and Related Engineering Problems, U.S. Engineers Office, Strategic Engineering Study Special Report 62, 136p., reprinted in 1947, Ann Arbor, Michigan, J.W. Edwards, Inc.

Nabighian, M.N., (1979). Quasi-Static Transient Response of a Conducting Half-Space — An Approximate Representation, Geophysics, **44**, 1700-1705.

Newman, G.A., Hohmann, G.W. and Anderson, W.L., (1986). Transient Electromagnetic Response of a Three-dimensional Body in a Layered Earth, Geophysics, **51**, 1608-1627.

Olhoeft, G.R., (1975). The Electrical Properties of Permafrost, Ph.D. Thesis, University of Toronto, Toronto, Canada.

Osterkamp, T.E. and Harrison, W.D., (1977). Sub-Sea Permafrost Regime at Prudhoe Bay, Alaska, U.S.A., Journal of Glaciology, **19**, 627-637.

Osterkamp, T.E. and Payne, M.W., (1981). Estimates of Permafrost Thickness from Well Logs in Northern Alaska, Cold Regions Science and Technology, **5**, 13-27.

Osterkamp, T.E. and Harrison, W.D., (1982). Temperature Measurements in Subsea Permafrost off the Coast of Alaska, Proceedings of the Fourth Canadian Permafrost Conference, 238-248.

Osterkamp, T.E. and Harrison, W.D., (1985). Subsea Permafrost: Probing Thermal Regime and Data Analysis 1975-1981, University of Alaska Geophysical Institute Report UAG R-301.

Osterkamp, T.E., Petersen, J.K. and Collett, T.S., (1985). Permafrost Thickness in the Oliktok Point, Prudhoe Bay, and Mikkelsen Bay Areas of Alaska, Cold Regions Science and Technology, **11**, 99-105.

Pandit, B.I. and King, M.S., (1979). A Study of the Effects of Porewater Salinity on some Physical Properties of Sedimentary Rocks at Permafrost Temperatures, Canadian Journal of Earth Sciences, **16**, 1566-1580.

Paris, D.T. and Hurd, F.K., (1969). *Basic Electromagnetic Theory, McGraw-Hill*, Inc., New York.

Pelton, W.H., Ward, S.H., Hallof, P.G., Sill, W.R. and Nelson, P.H., (1978). Mineral Discrimination and Removal of Inductive Coupling with Multifrequency IP, Geophysics, **43**, 588-609.

Péwé, T.L., (1948). Permafrost Investigations, Fairbanks Area, Alaska: U.S. Geological Survey Permafrost Program Report, U.S. Army Engineering Intelligence Division, Office of Chief Engineer.

Péwé, T.L., (1982). *Geologic Hazards of the Fairbanks Area, Alaska, Special Report 15*, Alaska Division of Geological and Geophysical Surveys.

Rabinovich, B.I. and Stepanova, R.G., (1972). Album of Three-layer Curves for Transient Sounding in the Near Zone (type Q), IGSG SO AN SSSR and SNIIGTIMSA, Issue 5, Novosibirsk.

Rabinovich, B.I., (1978). Comparative Evaluation of Sounding by Transient Fields in the Far and Near Zones, Geol. Geofiz., **11**, 148-152.

Raiche, A.P., (1983). Negative Transient Voltage and Magnetic Field Responses for a Half-space with a Cole-Cole Impedance, Geophysics, **48**, 790-791.

Raiche, A.P. and Gallagher, R.G., (1985). Apparent Resistivity and Diffusion Velocity, Geophysics **50** , 10, 1628-1633.

Raiche, A.P., (1987). Transient Electromagnetic Field Computations for Polygonal Loops on Layered Earths, Geophysics, **52** , **6**, 785-793.

Reimann-Weber, (1912). *Die Partiellen Differentialgleichungen, Physik*, Fifth Edition, **2**, 121.

Rogers, J.C. and Morack, J.L., (1980). Geophysical Evidence of Shallow Nearshore Permafrost, Prudhoe Bay, Alaska, Journal of Geophysical Research, **85**, 4845-4853.

Ryu, J., Morrison, H.F. and Ward, S.H., (1970). Electromagnetic Fields About a Loop Source of Current, Geophysics, **35**, 862-986.

Scott, W.J., Sellmann, P.V., and Hunter, J.A., (1978). Geophysics in the Study of Permafrost, Proceedings of the Third International Conference on Permafrost Volume 1, held in Edmonton, Canada, July 10-13, published by the National Research Council of Canada, 93-115.

Scott, W.J. and Brown, R.J.E., (1980). Proceedings of a Symposium on Permafrost Geophysics (5), held 13 and 14 November 1978, Calgary, National Research Council of Canada Technical Memorandum 128.

Sellmann, P.V. and Chamberlain, E.J., (1980). Permafrost Beneath the Beaufort Sea: Near Prudhoe Bay, Alaska, Journal of Energy Resources Technology, **102**, 35-48.

Sen, P.N., Scala, C. and Cohen, M.H., (1981). A Self Similar Model for Sedimentary Rocks with Application to the Dielectric Constant of Fused Glass Beads, Geophysics, **46**, 5, 781-795.

Sinha, A.K. and Stephens, L.E., (1983). Deep Electromagnetic Soundings Over the Permafrost Terrain in the MacKenzie Delta N.W.T., Canada, Proceedings of the Fourth International Conference on Permafrost, held in Fairbanks, Alaska, July 17-22, 1166-1171.

Smith, R.S. and West, G.F., (1988). Inductive Interaction Between Polarizable Conductors: An Explanation of a Negative Coincident-loop Transient Electromagnetic Response, Geophysics, **53**, 5, 677-690.

Specht, R.N., Brown, A.E., Selman, C.H. and Carlisle, J.H., (1986). Geophysical Case History, Prudhoe Bay Field, Geophysics, **51**, 5, 1039-1049.

Spies, B.R., (1980). A Field Occurrence of Sign Reversals with the Transient Electromagnetic Method, Geophysical Prospecting, **28**, 620-632.

Stefan, J., (1891). Über die Theorie des Eisbildung, insbesonder, über die, Eisbildung um Polarmere, Ann. Phys. U Chem., Neue Folge, Bd. 42, Ht. 2, 269-286.

Stratton, J.A., (1941). *Electromagnetic Theory*, McGraw-Hill, Inc., New York.

Tabarovskiy, L.A., (1979). Album of Theoretical Curves for Depth Sounding with Transient Fields in a Stratified Medium, Akad. Nauk, Sib. Otdel., Inst. Geol. Geofiz., Novosibirsk, pp. 5-72.

Tamura, S.T., (1905). Mathematical Theory of Ice Formation, Monthly Weather Review of Weather Bureau, **33**, 55-59.

Telford, W.M., Geldart, L.P., Sheriff, R.E. and Keys, D.A., (1976). *Applied Geophysics*, Cambridge University Press.

Tice, A.R., Burrous, C.M. and Anderson, D.M., (1978). Determination of Unfrozen Water Content by Pulsed Nuclear Magnetic Resonance, Proceedings of the Third International Conference on Permafrost, Edmonton, Alberta, Canada, 150-155.

Tsytovich, N.A., (1963). Permafrost Problems, Proceedings of the First International Conference on Permafrost, page 7.

Vigdorchik, M.E., (1980). *Arctic Pleistocene History and the Development of Submarine Permafrost*, Westview Press Inc., Boulder, Colorado.

Wait, J.R., (1951). The Magnetic Dipole over the Horizontally Stratified Earth, Canadian Journal of Physics, **29**, 577-592.

Wait, J.R., (1960). Propagation of Electromagnetic Pulses in a Homogeneous Conducting Earth, Applied Scientific Research, Section B, **9**, 213-253.

Wait, J.R., (1962). *Electromagnetic Waves in Stratified Media*, The MacMillan Company, New York.

Wait, J.R., (1982). *Geo-Electromagnetism*, Academic Press, New York City.

Washburn, A.L., (1980). *Geocryology*, John Wiley and Sons Inc.

Wenner, F., (1912). The Four-terminal conductor and the Thomson Bridge, Bulletin of the United States Bureau of Standards, **8**, 559-610.

APPENDIX A. A TEM SOUNDING TRANSECT OF ALASKA

A.1 INTRODUCTION

The purpose of this appendix is to report the interpretations of transient electromagnetic (TEM) soundings at sites, along a north-south transect of Alaska, displayed as triangles in Figure 1.1. Most of the soundings reported in this appendix were taken during August and September of 1983. One site, the Kuparuk site labeled NWEILEEN in Figure 1.1, was sounded in 1983 and 1984 and is reported in Chapter 5 in the discussion of possible induced polarization effects.

The soundings were taken with coplanar coaxial transmitter and receiver coils to measure the vertical magnetic field. The coaxial loops consist of a large, square transmitter loop and a small radius, multi-turn receiver coil located at the center of the large loop. The EM-37 TEM system, made by Geonics Inc. of Canada, was used for all soundings.

Whenever possible, each site has been interpreted in terms of a one-dimensional model of resistivity varying in discrete, horizontal layers, each with uniform, simple resistivity and uniform thickness. Each site was chosen such that it was far from thermally-disturbing sources such as roads, rivers, recent burns, etc. and also was on fairly flat, uniformly-vegetated land with reasonably simple lithology as far as it could be ascertained from available geologic maps, aerial photography, and visual inspection. Conversely, the sites were chosen for good vehicular access to the sounding sites in order to sound as many sites as possible during a short equipment rental time period.

The soundings were taken as an aid for the determination of the presence and thickness of ice-bearing permafrost at each site. Ground truth from wells or boreholes drilled nearby or from other sources of geological information was used in the interpretations whenever possible. Many of the boreholes, however, were relatively shallow ($\leq$ 100 m), so that the ground truth to more desireable depths is lacking or incomplete.

A.2 DATA SITE LOCATIONS

TEM soundings reported in this appendix were undertaken at Barter Island and 31 additional sites roughly along the Trans-Alaska pipeline from Prudhoe Bay to Glennallen. The site locations are marked in Figure 1.1 with triangles. The sounding sites, their location in standard meridian, township and range, and the length of a side of the square transmitter loops used are given in Table A.1. The data collected at each sounding site are presented in Appendix C. Site titles are recognizable from Table A.1 with the exception of HAJ which is the data set for Sawmill Creek site. Shown in the data are the gain and stack receiver settings and the values displayed for each gate (in millivolts). In all sites, the receiver loop had an effective area of 100 square meters (100 m^2) and a preamplifier gain of 52.1. The data in Appendix C are ordered roughly from the northern sites first to the southern sites last.

TABLE A.1 SOUNDING SITE LOCATIONS

#	site name	location T = township, R = range, Sec. = section	loop size (meters)
1	Barter (Island)	mid S side of SE 1/4 Sec. 17 T8N R33E Umiat Prime Meridian	400
2	Prudhoe Bay (West Dock)	SW corner of NW 1/4 Sec. 23 T12N R14E Umiat Prime Meridian	400
3	Deadhorse (Airport)	mid W side NW 1/4 of SE 1/4 Sec. T9N R14E Umiat Prime Meridian	400
4	Franklin (Bluffs)	center of SW 1/4 of NW 1/4 Sec. 28 T4N R14E Umiat Prime Meridian	400
5	Happy (Valley)	SW corner of NW 1/4 of NE 1/4 Sec. 30 T3S R13E Umiat Prime Meridian	400
6	Galbraith (Lake)	SW corner of NW 1/4 of NW 1/4 Sec. 23 T11S R11E Umiat Prime Meridian	400
7	Chandalar (Camp)	center NW 1/4 of SW 1/4 Sec. 10 T16S R11E Umiat Prime Meridian	200
8	Slate (Creek)	SE corner of NW 1/4 of NW 1/4 Sec. 22 T28N R12W Fairbanks Prime Meridian	100
9	Coldfoot	mid W side of NW 1/4 of SW 1/4 Sec. 15 T28N R12W Fairbanks Prime Meridian	100
10	Bonanza (Creek)	center NE 1/4 of SW 1/4 of NW 1/4 Sec. 19 T21N R14W Fairbanks Prime Meridian	100
11	Oldman (Camp)	center of NE 1/4 of NE 1/4 Sec. 30 T19N R14W Fairbanks Prime Meridian	100 200
12	Finger (Mountain)	mid E side of SW 1/4 of SW 1/4 Sec. 25 T18N R14W Fairbanks Prime Meridian	100
13	D78.1 (Dalton mile)	center SE 1/4 of SE 1/4 Sec. 19 T15N R12W Fairbanks Prime Meridian	100
14	Yukon (River)	center NW 1/4 of NW 1/4 of SE 1/4 Sec. 7 T12N R10W Fairbanks Prime Meridian	100
15	D34.4 (Dalton mile)	mid S side of NW 1/4 of SW 1/4 Sec. 31 T11N R8W Fairbanks Prime Meridian	100
16	Hess (Creek)	mid S side of NW 1/4 Sec. 30 T10N R7W Fairbanks Prime Meridian	100

TABLE A.1 SOUNDING SITE LOCATIONS continued

#	site	location	loop size
17	Livengood	center of SE 1/4 of SW 1/4 of NW 1/4 Sec. 21 T8N R5W Fairbanks Prime Meridian	100
18	E54.7 (Elliott mile)	center of SW 1/4 of SW 1/4 of SE 1/4 Sec. 7 T7N R3W Fairbanks Prime Meridian	100
19	Washington (Creek)	mid W side of SW 1/4 of SE 1/4 Sec. 24 T4N R2W Fairbanks Prime Meridian	100
20	Virgin Spruce 1 (Fairbanks)	mid E side of NE 1/4 Sec. 36 T1N R2W Fairbanks Prime Meridian	100
21	Virgin Spruce 2 (Fairbanks)	mid E side of NE 1/4 of NE 1/4 of SE 1/4 Sec. 36 T1N R2W Fairbanks Prime Meridian	100
22	Farm (Fairbanks)	mid S side of NW 1/4 of SE 1/4 Sec. 1 T1S R2W Fairbanks Prime Meridian	100
23	Peat (Fairbanks)	center of SE 1/4 Sec. 32 T1N R1W Fairbanks Prime Meridian	100
24	Farmers Loop (Fairbanks)	center of NW 1/4 of NW 1/4 Sec. 5 T1S R1W Fairbanks Prime Meridian	100
25	Eielson	center NW 1/4 of SW 1/4 of SW 1/4 Sec. 25 T3S R3E Fairbanks Prime Meridian	100
26	Quartz (Lake)	center NE 1/4 of NE 1/4 Sec. 30 T8S R10E Fairbanks Prime Meridian	100
27	Sawmill (Creek)	mid W side NW 1/4 of SW 1/4 Sec. 9 T12S R13E Fairbanks Prime Meridian	100
28	Greely	center NW 1/4 Sec. 13 T13S R10E Fairbanks Prime Meridian	100
29	Fielding (Lake)	center NE 1/4 of NW 1/4 of NW 1/4 Sec. 10 T20S R11E Fairbanks Prime Meridian	100
30	Summit (Lake)	center SE 1/4 of SW 1/4 Sec. 7 T20S R12E Fairbanks Prime Meridian	100
31	Sourdough	mid E side NW 1/4 of SE 1/4 Sec. 29 T10N R1W Copper Prime Meridian	100
32	Glennallen	center SE 1/4 of SW 1/4 of SE 1/4 Sec. 31 T5N R1W Copper Prime Meridian	100

A.3 EXPERIMENTAL PROCEDURE

At each sounding site, the transmitter of the Geonics EM-37 was carried 10 to 50 meters from the vehicular access point. The transmitter generator and transmitter electronics are located at one corner of the transmitter loop. The square transmitter loops used had side dimensions ranging from 400 meters at Prudhoe Bay to 100 m at Glennallen in an attempt to resolve the thicker permafrost at northern sites and the thinner permafrost expected at more southern sites. The bearing of line one is recorded as the angle, measured at the transmitter corner, clockwise from magnetic north to line one (β in Figure 1.5). The bearing of line number one will be given in the following site-by-site description. Line two runs from the transmitter 90° counter-clockwise from line one. Line three runs from the end of the 100 to 400 meter length of line one. Each side of the transmitter loop is formed by unreeling the insulated copper conductor from a backpackable reel with a mass of up to 30 kilograms for the 400 meter length. The most efficient way for a two-person crew to lay out the larger 400 meter-sided loops is for one member to unreel one spool along an appropriate magnetic heading (line one) starting at the transmitter corner while the second member runs line two. They then return for a second 400 meter spool and, taking new bearings, complete the square ensuring the conductors are connected at the corners. The crew returns to the transmitter to test transmitter loop continuity and operate the generator and transmitter.

The receiver and transmitter electronics are phase-locked and the receiver console is then carried to the center of the transmitter loop and connected to the receiver loop. The soundings can be taken using a transmitter pulse repetition frequency of 30, 3, and 0.3 Hz; for all the sites reported in this appendix, a pulse

repetition frequency of 30 Hz was used. Transient returns were digitized and stacked 2^8 or 2^{10} times for each of 20 time gates for each sounding. The time gates are spaced evenly in log time (McNeill, 1982). The digitized results from the EM-37 are manually recorded and the receiver polarity is then reversed for a second sounding with all other receiver settings (gain, stack, etc.) remaining the same. The reversal of receiver polarity helps to reduce noise. The second sounding completes a single set of sounding data. Three to four data sets are taken for each site at various stacking and gain settings.

Data are reduced to signal strength at the receiver coil by removing the receiver gain 2^n, the preamplifier gain and the effective area of the receiver loop from the recorded data. All soundings taken for a particular site and date are averaged and a measure of the repeatability of the data is determined by taking the sample standard deviation of the data sets for each time gate. The averaged data are then corrected for the finite ramp turnoff of the transmitter current waveform and reduced to apparent resistivity using the late time resistivity approximation given in equivalent forms by Kaufman and Keller (1983), Wait (1982), Anderson (1981) and others; see Chapter 2 for a more thorough discussion of TEM theory. The correction algorithms were written by the candidate and the results were compared with the results of Geo-Physi-Con (private communication) for validation. For all these sounding sites, the late stage approximation is valid for all but a few of the first time gates, a feature in marked contrast to the data of the subsea soundings to be reported in Chapter 4. It should be apparent that those data points with very large estimated error should be treated with a great deal of caution and have been removed from the data of some of the sites shown in the following figures. The apparent resistivity data for each sounding site is used by the inversion program NLSTCI (Anderson, 1982) to provide the layered geoelectric model of best

fit using a nonlinear least squares algorithm developed by Dennis et al. (1979). The geoelectric models are given as insets, whenever possible, on Figures A.1 to A.32 with the associated TEM apparent resistivity versus square root of time curve (solid line). The actual data points are marked with the symbol "+". Each model is given in terms of layer thickness and resistivity. The models were computed using bounds on the allowed resistivities and thicknesses and sometimes incorporated a weighting scheme. In the weighting scheme, the more reliable time gates, based on estimates of error from sample standard deviations, were given more weight in the computer inversion process.

A.4 INTERPRETATION

The presence of ice-bearing permafrost in an otherwise unfrozen stratum is associated with an increase in resistivity barring lithologic changes. The increase of resistivity, that occurs when a material containing water freezes, was investigated as early as 1833 when Faraday conducted some experiments on this effect. More recently, this effect has been illustrated by the work of Hoekstra and McNeill (1975) and Pandit and King (1982). For a given material type, it is reasonable to assume that there will be at least a modest increase in resistivity when the temperature is low enough that ice forms in the pore spaces; this change in resistivity should be discernible with the TEM method. Since the resistivity of differing materials may vary dramatically as displayed in Figure 1.3, lithologic variations with depth may confuse an interpretation based solely upon thermal variations with depth. At many of the sites that were chosen, bedrock is overlain by reasonably thick sediments. However, bedrock can have resistivities similar to frozen sediments and

hence, interpretation of thin overburdens over bedrock in terms of a thermally-controlled model can be in error. In such cases, available ground truth from wells and boreholes plays a crucial role.

Not all sites could be interpreted. Two sites showed anomalous sign changes in the early time gates and could not therefore be modelled in terms of a layered earth of simple resistivity. These sites, # 13 at Dalton Highway Mile 78.1 and # 18 at Elliott Highway Mile 54.7, cannot be reduced to apparent resistivity nor modeled. In their respective sections that follow, these two sites have their averaged field strength plotted versus time and the error bars are produced using $\pm$ one sample standard deviation. Another site, located in the Kuparuk Oil Field, displayed two sign reversals in early time and is reported in Chapter 5.

The interpretation process begins with a comparison of the sounding data to published normalized TEM sounding curves of Rabinovich (1977) and Rabinovich and Stepanova (1972). The curve matching procedure was accomplished by plotting the apparent resistivity (ρ_a) from the data versus the square root of time ($\sqrt{t}$) with the same log-log scaling as the published curves. Often this procedure gives an indication of a reasonable first layer resistivity to be used and a possible first layer thickness. However, curve matching using 2 and 3 layer curves sometimes produce starting models that are far from useful because the normalized time scales are misleading. Therefore, many forward curves were run using the actual field loop sizes to develop more useful curve matching models for the inversion process. Additional information, based on the loggings from drillholes, on material types and thicknesses is incorporated into the modelling process whenever possible. Since the resistivity of a material type varies dramatically due to a variety of parameters which cannot be measured at each site (e.g. porosity, pore water conductivity, and saturation), the information on material type can only give a range of possible

values. For instance, Telford et al. (1972) give a range of resistivities for granite of 3 x 10^3 to 10^6 Ω-m. Additionally, the information on depths from temperature drillholes is limited to fairly shallow (less than 60 meters) depths and therefore not always useful.

Relating the theory of circular transmitter loops of Chapter 2 to the actual square transmitter loops used in this thesis is straightforward. The two loops are essentially equivalent if they produce the same field at the center because the receiver loop used is small. Therefore, the circular loop of radius R is $R = 0.555\ L$, where the length of the side of the square transmitter loop is L.

In the following sections of this appendix, each sounding site is discussed, in order, by the sounding number of Table A.1 in terms of location, site description, and the layered earth model results for permafrost. Since the soundings were taken in August and September, 1983, the site descriptions are representative of summer conditions when the thaw depth is near maximum, but probably not more than 1 to 2 meters.

1. Barter Island

Barter Island, the easternmost site surveyed of all the sounding sites, is located above the Arctic National Wildlife Range (ANWR). ANWR is presently of great interest because of its probable petroleum reserves. Unlike most islands along the northern coast of Alaska which are barrier islands, Barter Island appears to be a remnant of higher ground which has been surrounded by the encroaching sea. Therefore, it should have permafrost since the mean annual surface temperature (MAST) is very cold (about −9.5° C). The island is not a very large one, however,

having somewhat less than ten square miles of surface area. Shallow holes drilled on the island display very salty pore water at greater than 10 meters depth. There is a fresh water lake on the island and much of the first few meters of the logs of a nearby drillhole indicates the occurrence of fresh pore water in the sandy gravels. The drillhole also indicates there is cretaceous clay from 25 to at least 250 feet depth, the limit of the drillhole. The site is located at the northern portion of the island, north of the lake and at the end of a gravel road built for the US Air Force DEW radar site. The magnetic bearing of line one was 180 degrees (directly south). The land is covered with a vegetative mat and small bushes with little surface relief.

The TEM data are fairly complicated and requires many layers to obtain a reasonable fit. The interpretation in terms of a 5 layer model shown in Figure A.1 suggests there are about 144 meters of ice-bearing permafrost at this site. This interpretation is suspect, because permafrost, 350 to 500 meters thick, would be expected from the cold MAST and from the extrapolation of the temperature profile at the drillhole location. It is possible that the deeper sediments, while permafrost by definition of temperature, are not ice-bearing due to the freezing point depressions associated with pressure, salinity and interface curvature.

The interpretation also indicates that very conductive sediments underlie this frozen zone implying the existence of highly saline unfrozen zones. This is consistent with the suggestions of Osterkamp and Payne (1981) on the presence of such zones in the Beaufort Sea.

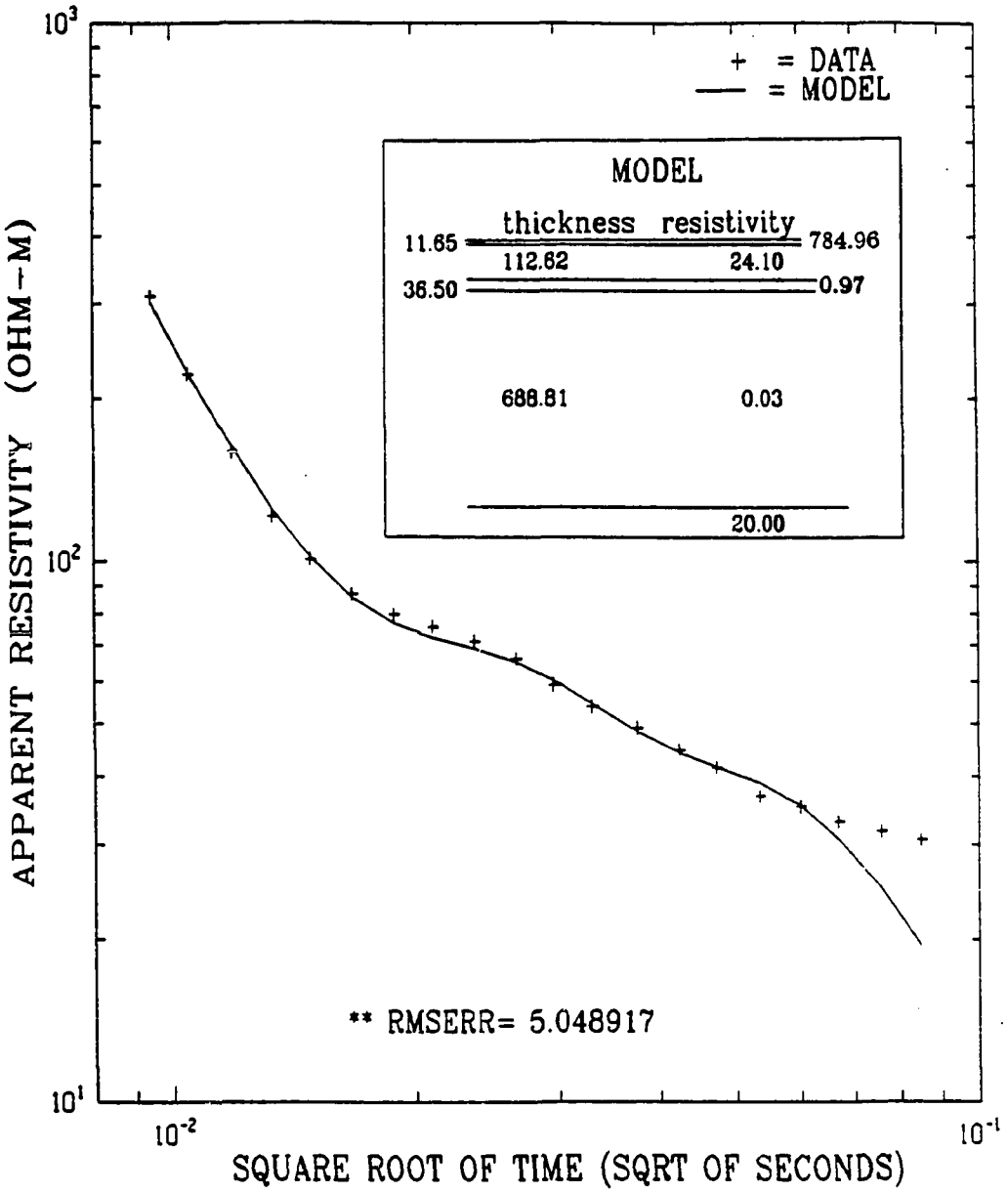

Figure A.1 TEM data and inversion model for the Barter Island site plotted as apparent resistivity versus the square root of time on log-log scales. The inversion geoelectric model is shown in the inset and the root mean square error (RMSERR) of the model to the data is also given.

2. Prudhoe Bay

This TEM site is located approximately 200 meters from the shoreline and 25 meters to the north side of the gravel road to the West Dock causeway at Prudhoe Bay and has a MAST of about $-9.0°$ C. Line one had a magnetic bearing of 260 degrees, running very close to a temperature borehole maintained by Osterkamp (private communication). There are many shallow small lakes, large-scale patterned ground (polygons of about 40 to 60 feet across), and vegetation consisting of grass and a thin vegetative mat at this site. The nearby location of the salty water of Prudhoe Bay would suggest the occurrence of some fairly conductive ground due to sea-level changes, storm surges or other transport process. It is very well known that unconsolidated fluvial deposits of interbedded clays, sands, and gravels exist to depths greater than 1000 meters at this locale.

At this site the depth to the base of permafrost is discernible in the TEM data. The apparent resistivity curve for this site shown in Figure A.2 is fairly simple and easy to interpret and contrasts with the more complex scenario of subsea permafrost extending offshore as reported in Chapter 4. This site fits a simple 3 layer model composed of two distinct layers of higher resistivity material interpreted as ice-bearing permafrost above an unfrozen low resistivity basement. The resistivity values derived from the model compare favorably with the resistivities calculated directly using Archie's law (Equation 1.9), in which 2.5 Ω-m pore water in a 40 percent porosity matrix of saturated sands and gravels with an exponent of 1.5 gives 10 Ω-m bulk resistivity. The resistivity of this material may be 20 to 200 Ω-m upon freezing.

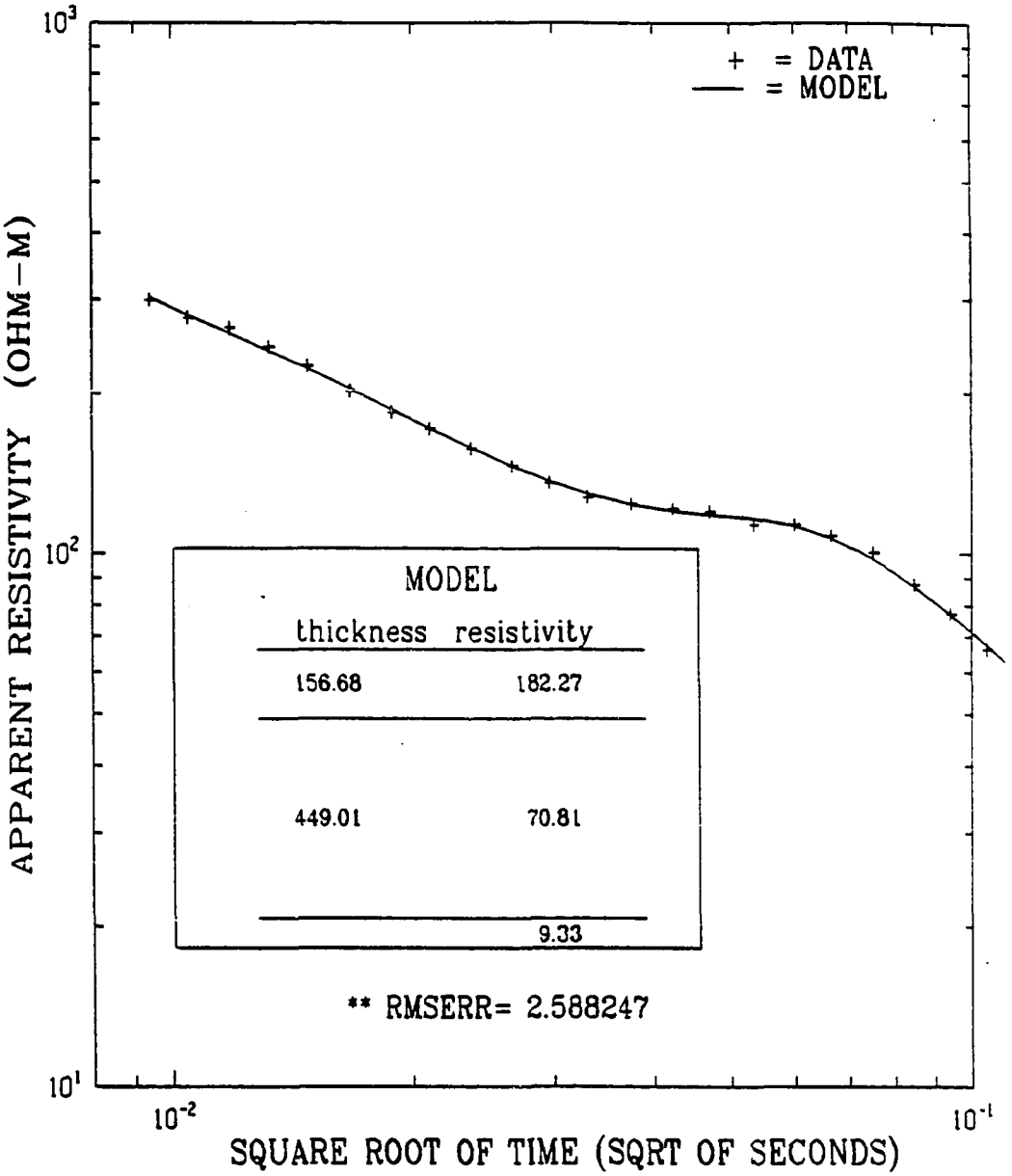

Figure A.2 TEM data and inversion model for the site near the West Dock causeway of Prudhoe Bay. The geoelectric inversion model is given in the inset.

The 606 meter thickness of the permafrost determined by inverting the data compares well to borehole temperature information as reported by Osterkamp and Payne (1981) who give a thickness of 560 meters at ARCO North Prudhoe Bay State #1 well. It is also comparable to the thickness of 565 meters inferred from the Dual Induction Laterlog (DIL) for resistivity at the discovery well Prudhoe Bay State #1 well about 6 kilometers south of West Dock.

3 . Deadhorse

The Deadhorse site lies on the north slope of the Brooks Range near Dalton Highway Mile 411. The site is south of Deadhorse Airport located at Dalton Highway Mile 415. Line one magnetic bearing is 300 degrees and line two passes close to a temperature borehole. The site is covered with a thin vegetative mat, grass and small bushes with some small-scale, patterned ground containing mud boils and ice wedge features with, at the time of the sounding, occasional shallow standing water. Borehole temperature information gives a MAST of about $-8°$ C.

The deposits here are fluvial sands and gravels deposited by the Sagavanirktok River during the Tertiary geological period (see Brown and Kreig, 1983 and Carman and Hardwick, 1982). Again, these deposits are very deep (about 1100 meters) and it is reasonable to expect a strong resistivity change with a thick permafrost zone. The DIL from the ARCO drill site 12-3 indicates about 573 meters for the thickness of permafrost in the area.

Although 2, 3, and 4 layer models were run at this site, the models with greater number of layers were not significantly superior to the 2 layer model. Although no model seems to fit the data very well, the best fit 2 layer inversion model does

appear to give a reasonable estimate of the thickness of permafrost at 616 meters as shown in Figure A.3.

4. Franklin Bluffs

The Franklin Bluffs site is located just west of the bluffs, near Dalton Highway Mile 376 with a line one bearing of 280 degrees and a borehole located at the connection of lines three and four. This site is over the fluvial deposits of the Sagavanirktok River. Due to the general northward thickening of these deposits, the deposits are somewhat thinner (about 700 meters) than at Deadhorse. The vegetative mat at this site is thicker with high grass and more bushes than the sites closer to the coastline, but it is still north of the boreal limit. The ground is uneven and shows strong evidence of patterned ground with mud boils about 60 feet apart and standing water between the ridges of the ice wedge formations.

A distinct resistivity change occurs considerably shallower than the base of the fluvial deposits at this site. This resistivity change has been interpreted as being the base of permafrost. As shown in Figure A.4, the interpreted permafrost thickness is 184 meters consisting of two higher resistivity layers over a low resistivity unfrozen layer. 2 and 3 layer model inversions produced similiar thickness for an upper, more resistive layer, interpreted to be permafrost. The table of permafrost is again near surface and was not discerned with the TEM sounding.

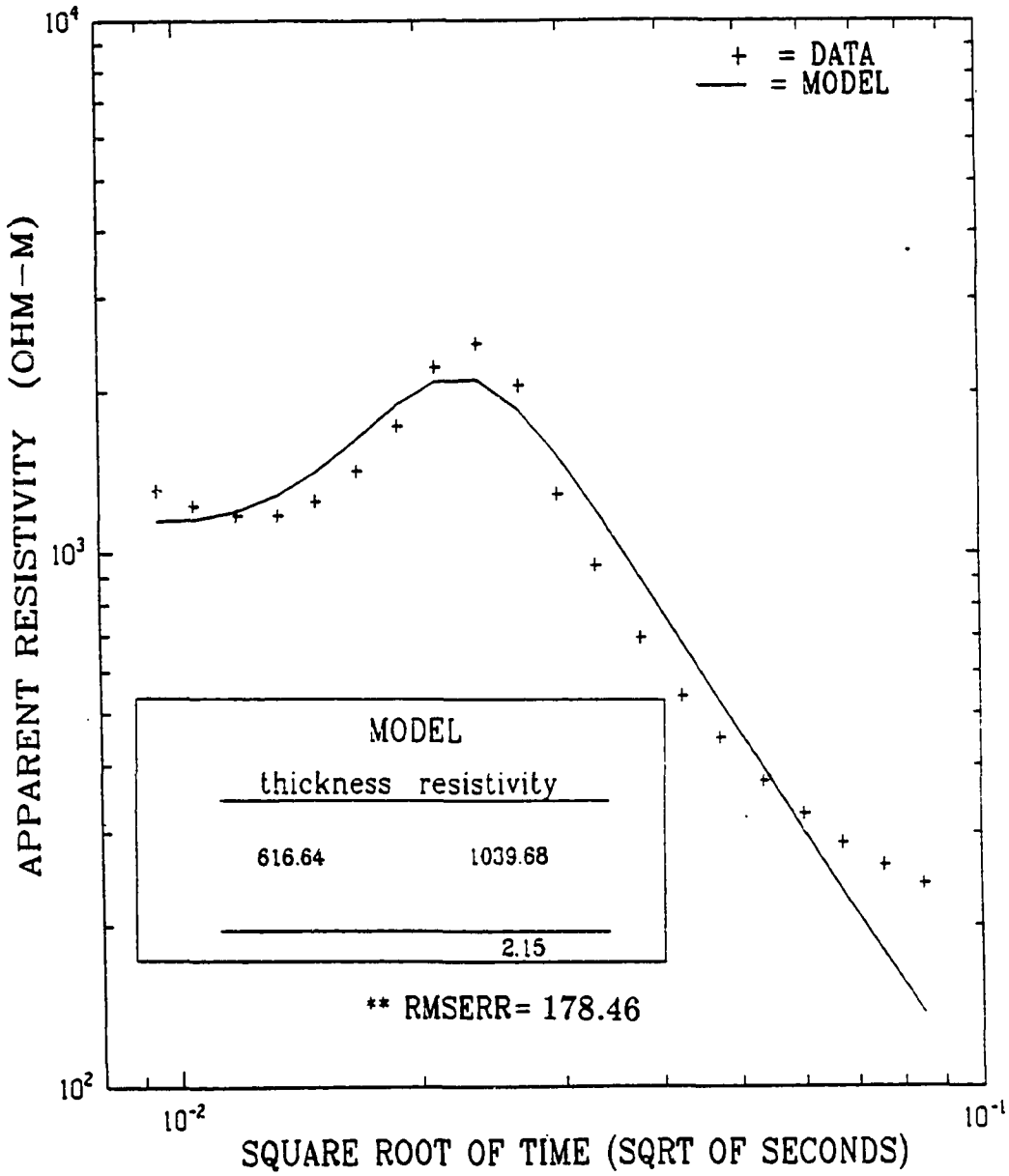

Figure A.3 TEM data and inversion model for the Deadhorse site, located south of the Deadhorse Airport.

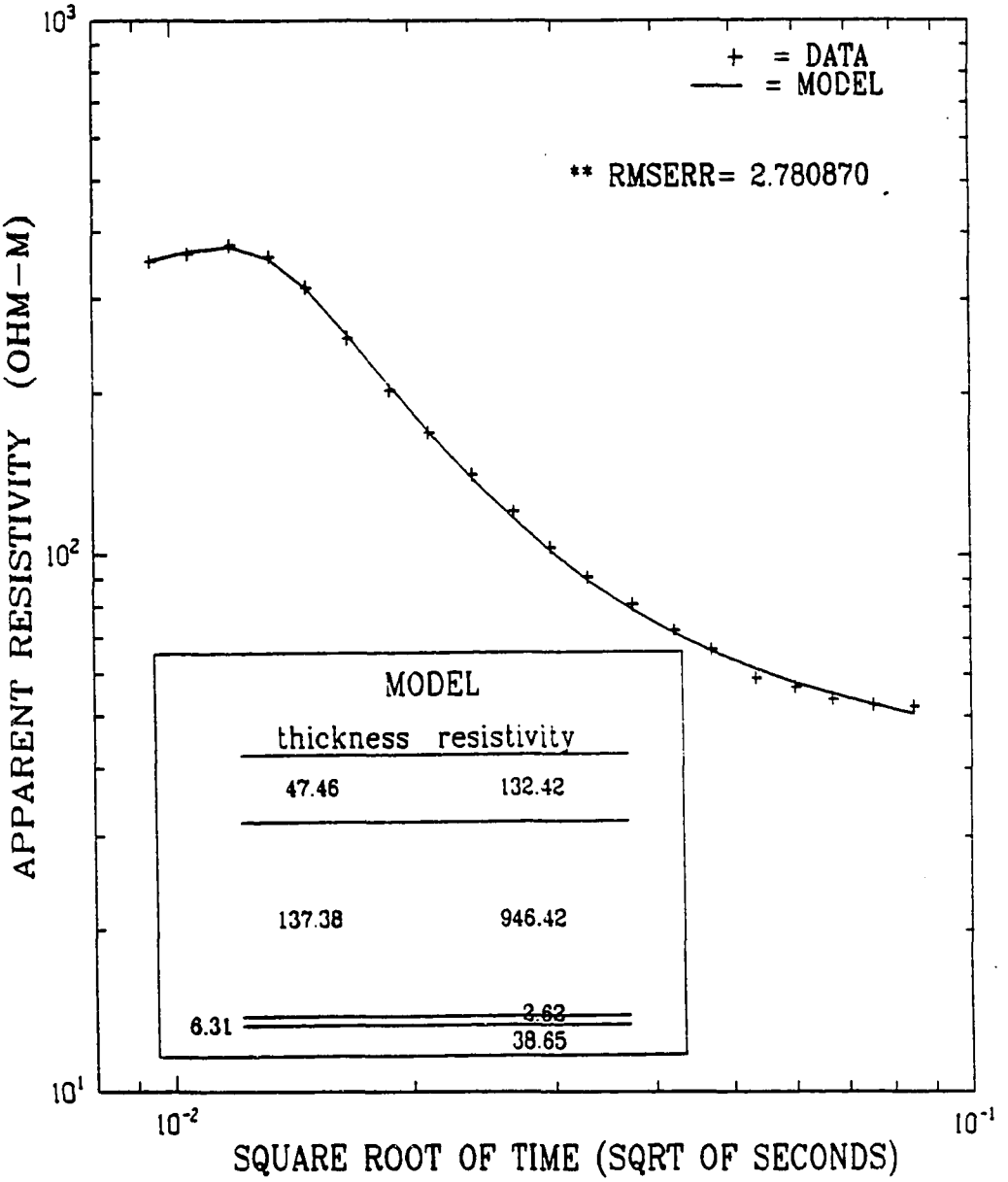

Figure A.4 TEM data and the inversion model match for the Franklin Bluffs site. The site is located south of Franklin Bluffs and just west of the Sagavanirktok River only slightly elevated from the present drainage.

5. Happy Valley

This is an interesting site near Dalton Highway Mile 336.4 with a line one bearing of 330 degrees and line two passing near a borehole. Drilling for the temperature soundings conducted by T.E. Osterkamp (private communication) at this site indicated the presence of very thick, solid ice for some 20 meters. The ground is elevated about 100 feet above the drainage of the Sagavanirktok River and covered with small tussocks and berry bushes.

The TEM soundings invert to a model with a very high resistivity layer, underlain by a somewhat less resistive layer that can also be interpreted to be permafrost lying over a third layer which is the least resistive – interpreted to be unfrozen sediments. As shown in Figure A.5, this interpretation gives a total of about 175 meters of frozen material (solid ice underlain by frozen silt and sands and gravels) over unfrozen sediments. The depth to bedrock cannot be determined with this interpretation. It is worth noting that the inversion model at this site is a particularly good fit to the sounding data.

6. Galbraith Lake

The Galbraith Lake site is located in the Brooks Range near a construction camp for the Alyeska Pipeline. The Galbraith Lake road leading first to the airport and on to the construction camp leaves the highway near Dalton Highway Mile 275. Shortly past the airport entrance, at a junction in the road, a road leads west into the mountains. The site is located about 400 meters along and 15 meters

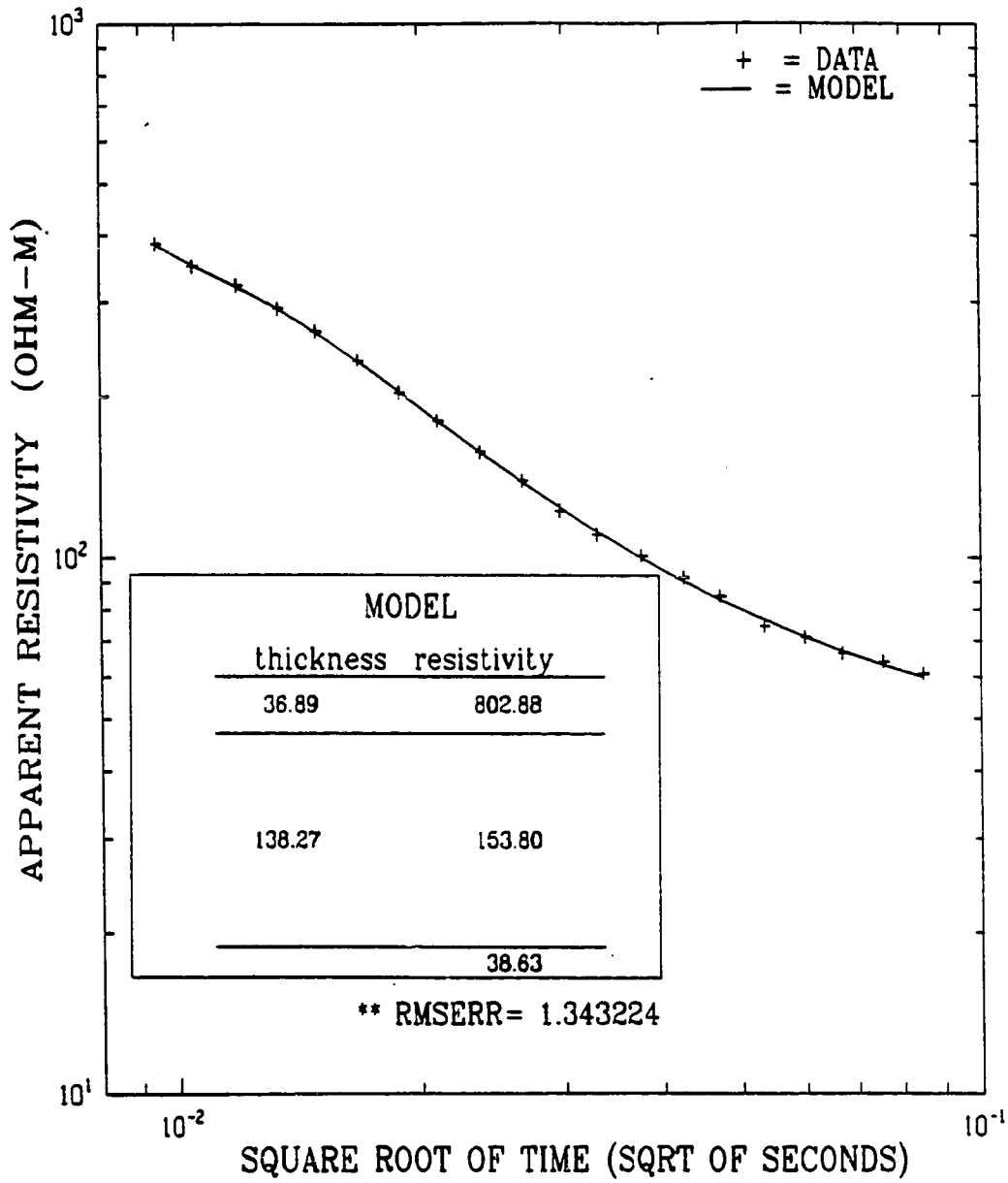

Figure A.5 TEM data and inversion match for the Happy Valley site. Drill-hole information indicates 20 meters of solid ice at this site.

from the road with a line one bearing of 175 degrees. The location of the site in the mountains with fairly steep terrain precluded the selection of a flat site. The terrain displays the surface features common to the ice wedge-associated, polygonal structures found throughout the Arctic (for more information on the features of the northern climes, see Washburn, 1980 and Johnson, 1981). The ground is covered with tussocks and berry bushes. Borehole temperature information indicates a mean annual surface temperature of about $-8°$ C and that the upper 50 meters are relatively dry.

The EM-31 measurements taken at this site display resistivity variations which correlate well with the surface structure. It is evident, however, that the EM-37 cannot detect the presence of the near surface ice wedges; the near surface properties are well hidden in the first few time gates when large transmitter loops ($\geq$ 100 meters on a side) are used. The majority of information will be derived from the material at greater depths (on the order of the transmitter dimensions, see Nabighian, 1979, Anderson, 1981, and Kaufman and Keller, 1983).

The interpretation at this site (see Figure A.6) calls for 229 meters of permafrost. Drillhole information shows that the upper 50 meters of material are very dry and hence should possess relatively high resistivity. On the other hand, the EM-37 inversion model indicates that the upper 42 meters have a relatively lower resistivity than the next 187 meters. It is difficult to make sense of the two apparently opposing pieces of information.

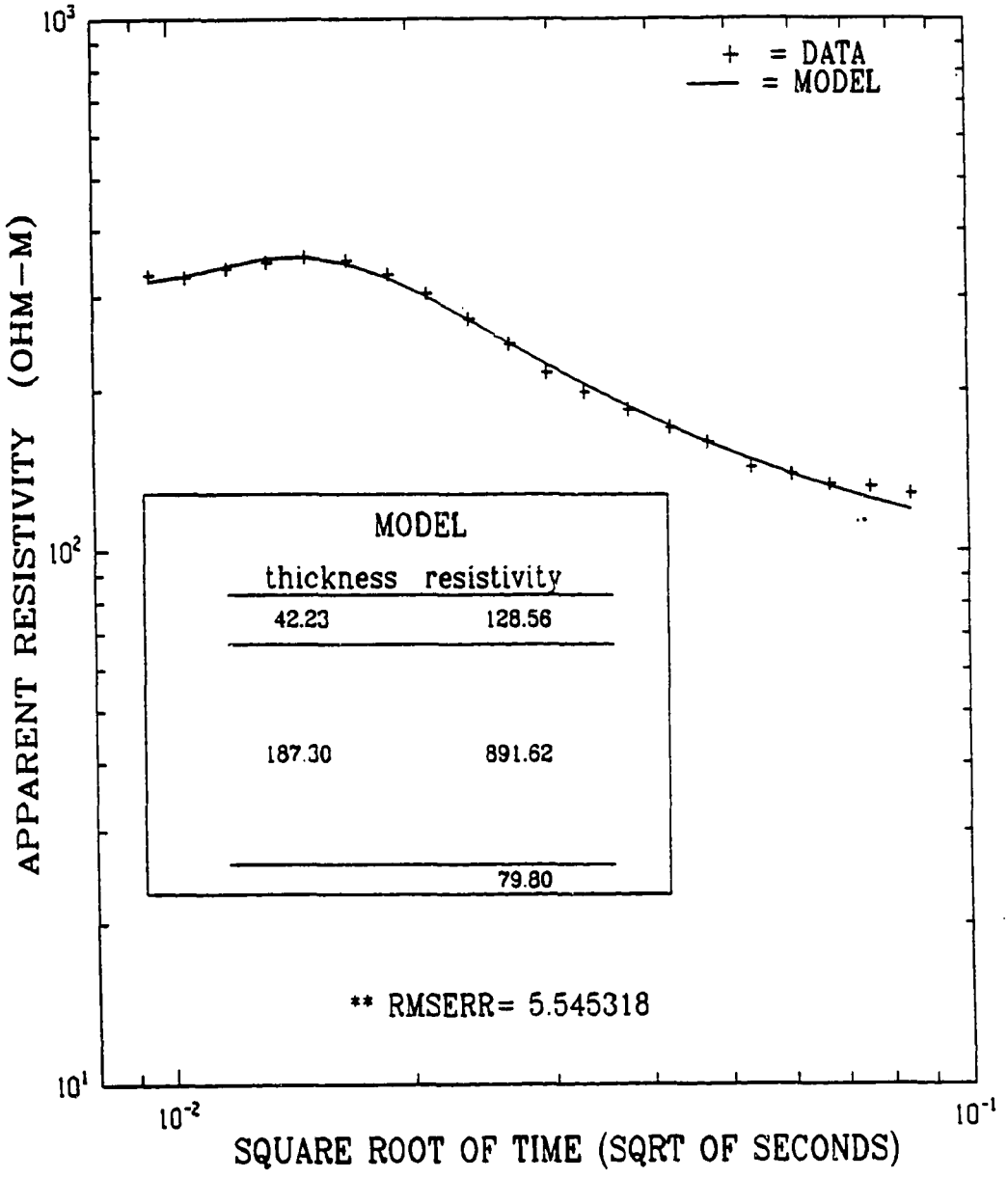

Figure A.6 TEM data and inversion model match for the site near Galbraith Lake, in the northern foothills of the Brooks Range.

7. Chandalar Camp

Chandalar Camp site is located just south of Atigun Pass near the landing strip of the pipeline camp at about Dalton Highway Mile 241.2 with a line one bearing of 155 degrees. The site is located approximately 50 meters to the east of the southern end of the landing strip. The ground is covered with a thick vegetative mat and large berry bushes. The MAST at this site is approximately $-3.5°$ C.

This site is located in the thick muskeg in the valley bottom between two nearby peaks. The past glaciation of the area produced a typical smoothly-rounded, U-shaped valley with a small stream and multiple drainage patterns in the valley bottom. The ground is covered with a thick vegetative mat and occasional large berry bushes.

As may be seen in Figure A.7, the apparent resistivity data for this site show comparatively little change with time. The best fit model predicts a rather thick, 276 meters of permafrost at this site.

8. Slate Creek

The Slate Creek site is about 3 miles to the north and east of Coldfoot Truck Stop. The site is located on the saddle of a small hill in the valley bottom between two much taller peaks (about 1100 meters) in the southern reaches of the Brooks Mountains. Drilling by Osterkamp (private communications) for temperature probing displayed the presence of bedrock at shallow depths. The terrain is covered with a vegetative mat, thick berry bushes and small, scattered black spruce trees.

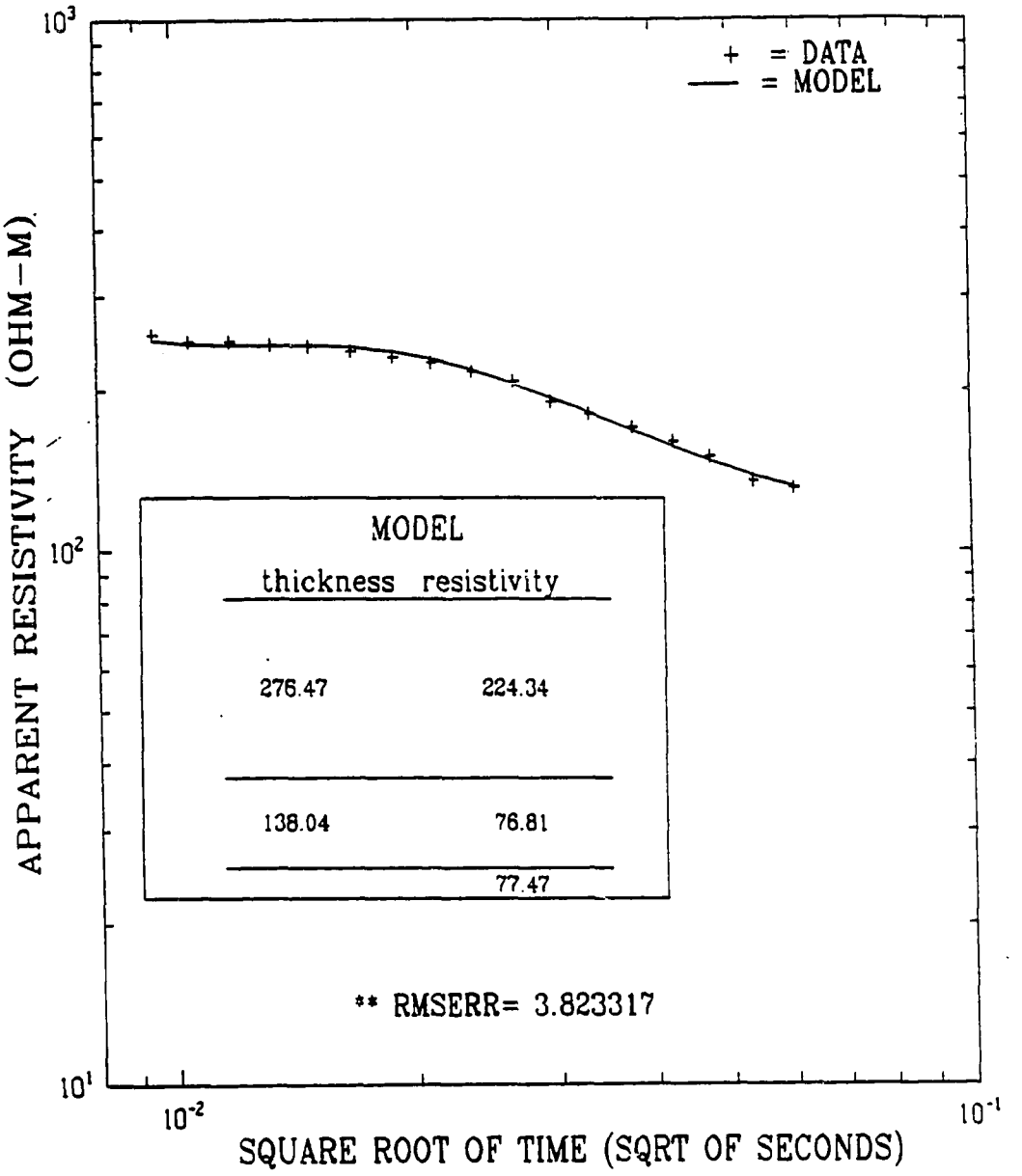

Figure A.7 TEM data and inversion model for the Chandalar site just south of Atigun Pass in the Brooks Range.

As may be seen in Figure A.8, the TEM data clearly exhibits a very resistive basement at a shallow depth. The thickness estimate for the first layer overburden from the inversion data is 9.8 meters. The prediction of a thin layer of weathered material is reasonable, as is the resistivity estimate of $\geq$ 3500 Ω-m for the overlying bedrock. An interesting aspect of this data is the strong upturn in the apparent resistivity with time (indicating high resistivity below). This type of curve demonstrates how quickly the signal strength approaches the noise level in a very resistive ground. This is the reason that only eight data points were retained for the purposes of inversion at this site.

9. Coldfoot

Coldfoot is a site adjacent to the southwestern corner of the Coldfoot Truck Stop cleared area, just north of Dalton Highway Mile 175, with line one bearing 340 degrees. Two shallow water wells (about 12 meters deep) drilled in the area for Dick Mackey, the owner of the truck stop, indicate unfrozen ground and very good water flow. Since the site is located in the floodplain of the Middle Fork of the Koyukuk River just south of its confluence with Slate Creek, the materials are most likely to be sands and gravels down to bedrock. The vegetation consists of a very thick forest cover of various types of trees including willow, birch, and spruce with a medium thickness vegetative mat between trees.

The data and inversion model (Figure A.9) show there are approximately 250 to 300 meters of unfrozen materials above bedrock. The upper 60 meters display

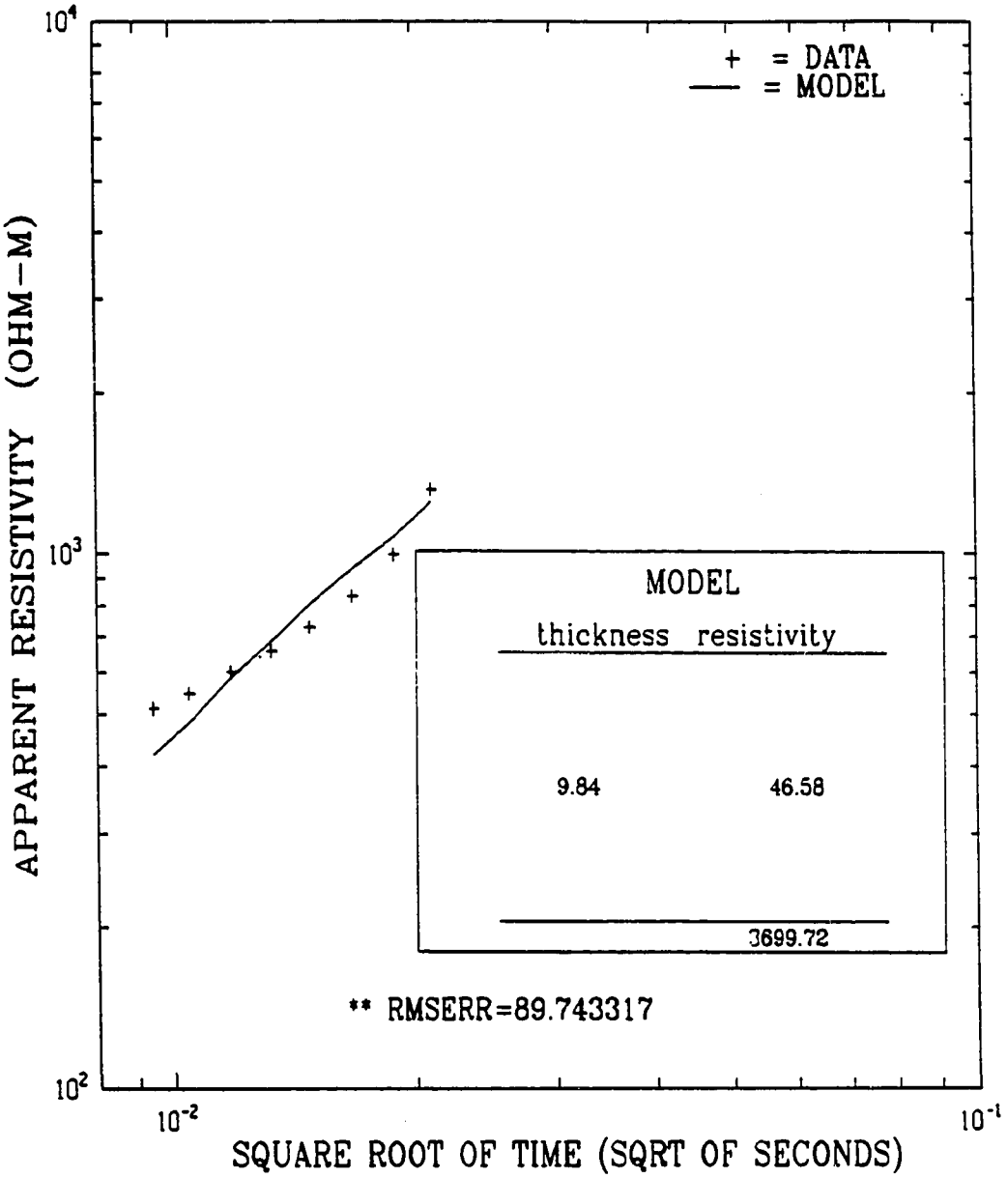

Figure A.8 TEM data and inversion model for the Slate Creek site to the east and north of Coldfoot Truck Stop.

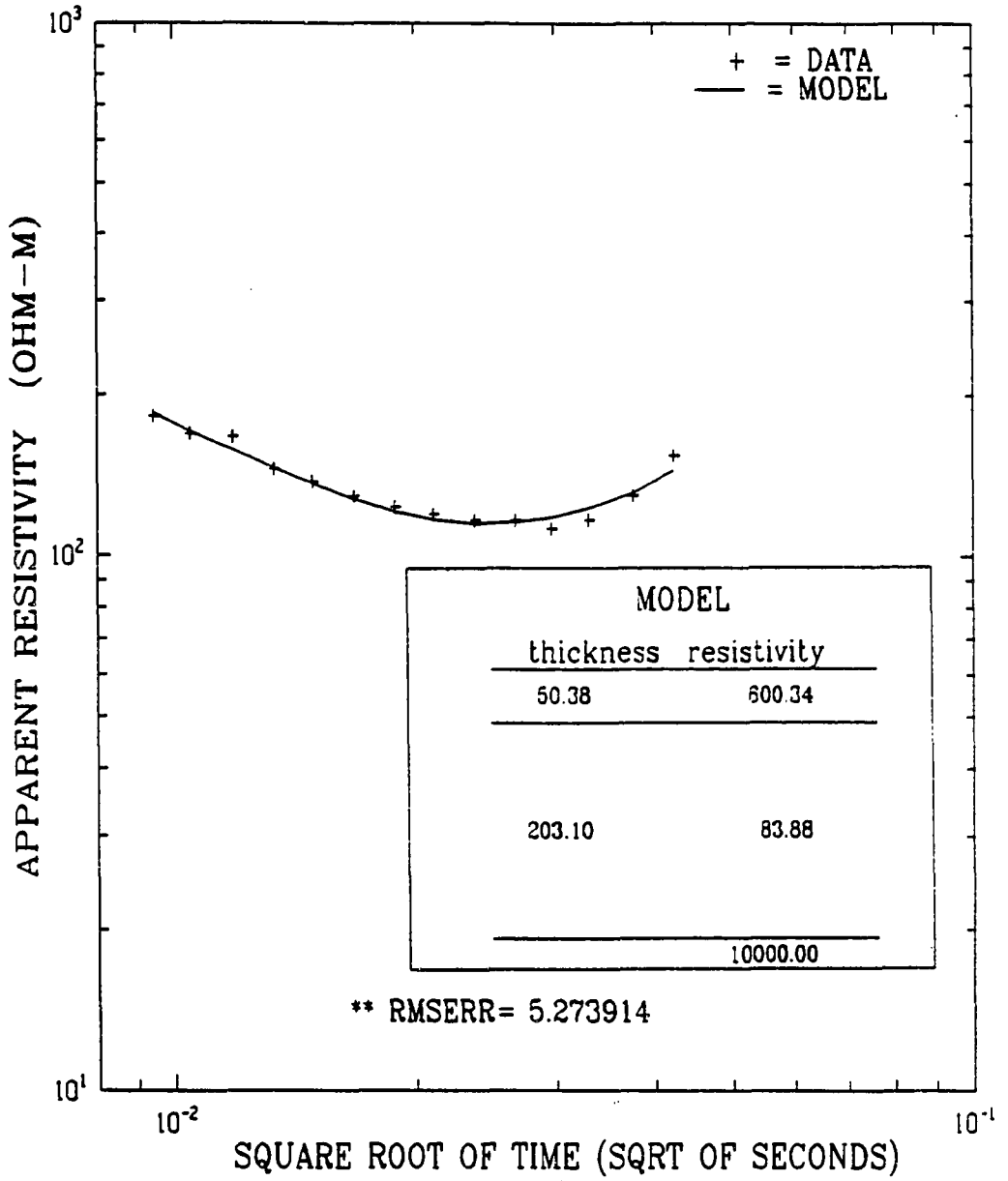

Figure A.9 TEM data and inversion model for the Coldfoot sounding site located at the southern end of the Coldfoot Truck Stop.

resistivities characteristic of fresher pore water whereas the deeper unfrozen materials evidently have greater amounts of impurities in the pore water. The ground water flow must be considerable to keep these materials unfrozen.

10. Bonanza Creek

The Bonanza Creek site is located at Dalton Highway Mile 122.5 with line one bearing 306 degrees. The site is on the western side of the Dalton Highway on the western slope of a hill rising some 1500 feet above the valley of the Bonanza Creek drainage. There are few trees but the site is well covered with a thick vegetative mat and woody berry bushes. There is no other information from drillholes available for this site.

Interpretation of the data (shown in Figure A.10) indicates there are about 104 meters of ice bearing permafrost at this site. The 2 layer model does not indicate the presence of bedrock at this site.

11. Oldman Camp

Oldman Camp is another site near a Trans-Alaska Pipeline construction camp. It is located off a road which leaves the Dalton Highway at mile 105.9 to the east leading to the Oldman airstrip. The TEM site is located about 0.7 mile along this road to the north with a line one bearing of 355 degrees. The borehole at this site is about 800 meters away from the transmitter location at a bearing of 320 degrees. The ground is evenly-sloped with medium-sized tussocks and some standing water

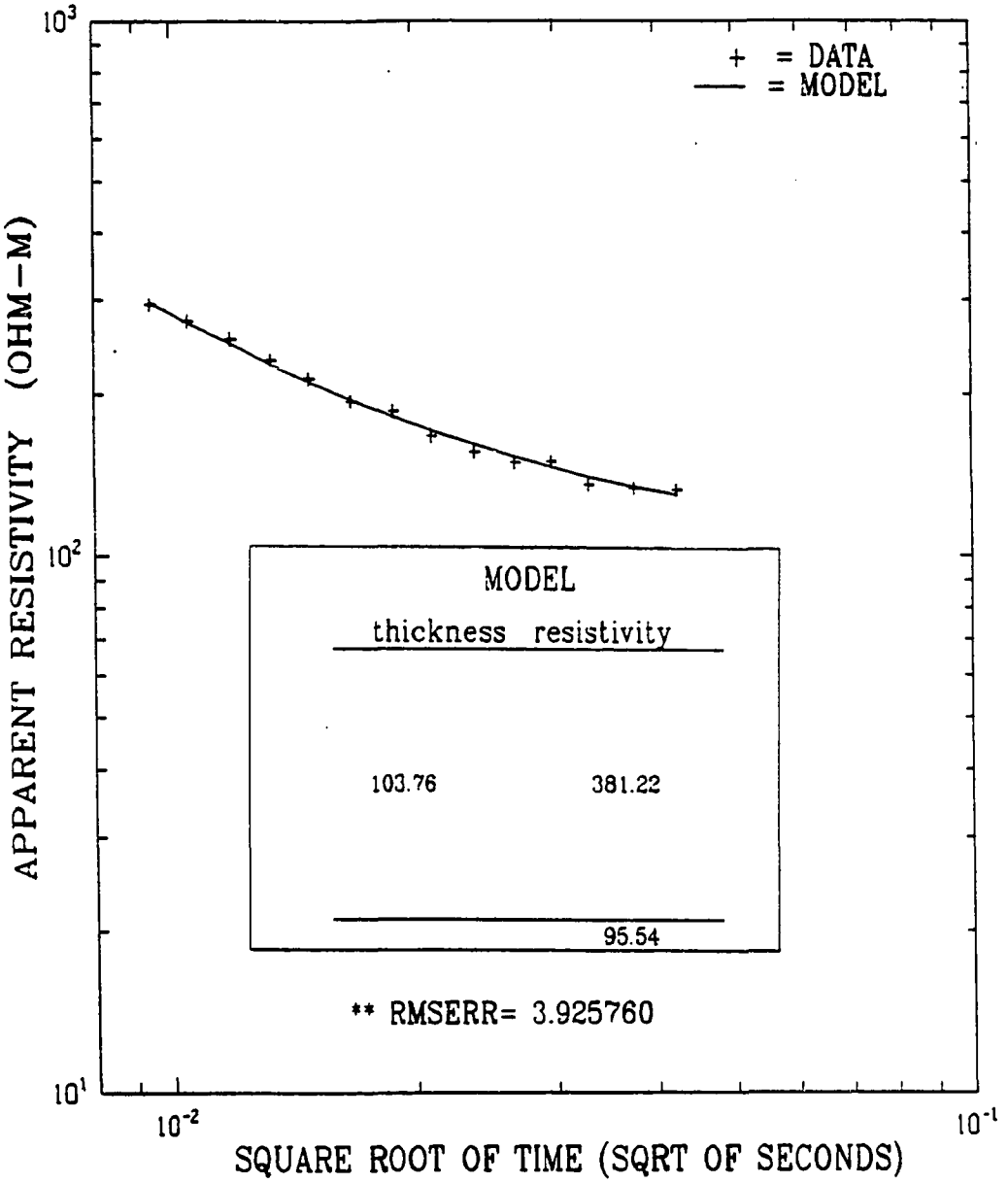

Figure A.10 TEM data and inversion model for the Bonanza Creek sounding site.

in the troughs at the time of the sounding. This site was sounded with both 100 meter and 200 meter square transmitter loops.

The TEM data and inversion model are shown in Figure A.11. The site is interpreted to have 92 meters of permafrost material underlain by 409 meters of unfrozen material on bedrock. This interpretation corresponds well to an extrapolation of temperature borehole information which gives about 90 meters of permafrost at this site.

12. Finger Mountain

The Finger Mountain site is just south of the road at Dalton Highway Mile 97.5, with line one bearing 270 degrees. The site which is fairly flat is covered with a thin vegetative mat and small berry plants and lies on the saddle between two tors near the top of a small hill at about 2200 feet elevation. There are occasional outcropping rocks. It is probable that the site is underlain by granitic bedrock (since the terrain displays granitic tors on the nearby mountain tops as discussed in Brown and Kreig, 1983). However, the interpretation of the TEM profile shown in Figure A.12 would suggest that there are about 151 meters of permafrost material of resistivity 286 Ω-m underlain by unfrozen material at 51 Ω-m.

This site does display the presence of a highly resistive basement in the later gates, but so few of the later gates were well above noise level that it is unclear that the 3 layer model is warranted. This interpretation suggests that the material is extremely weathered to great depths. No borehole information was available at this site.

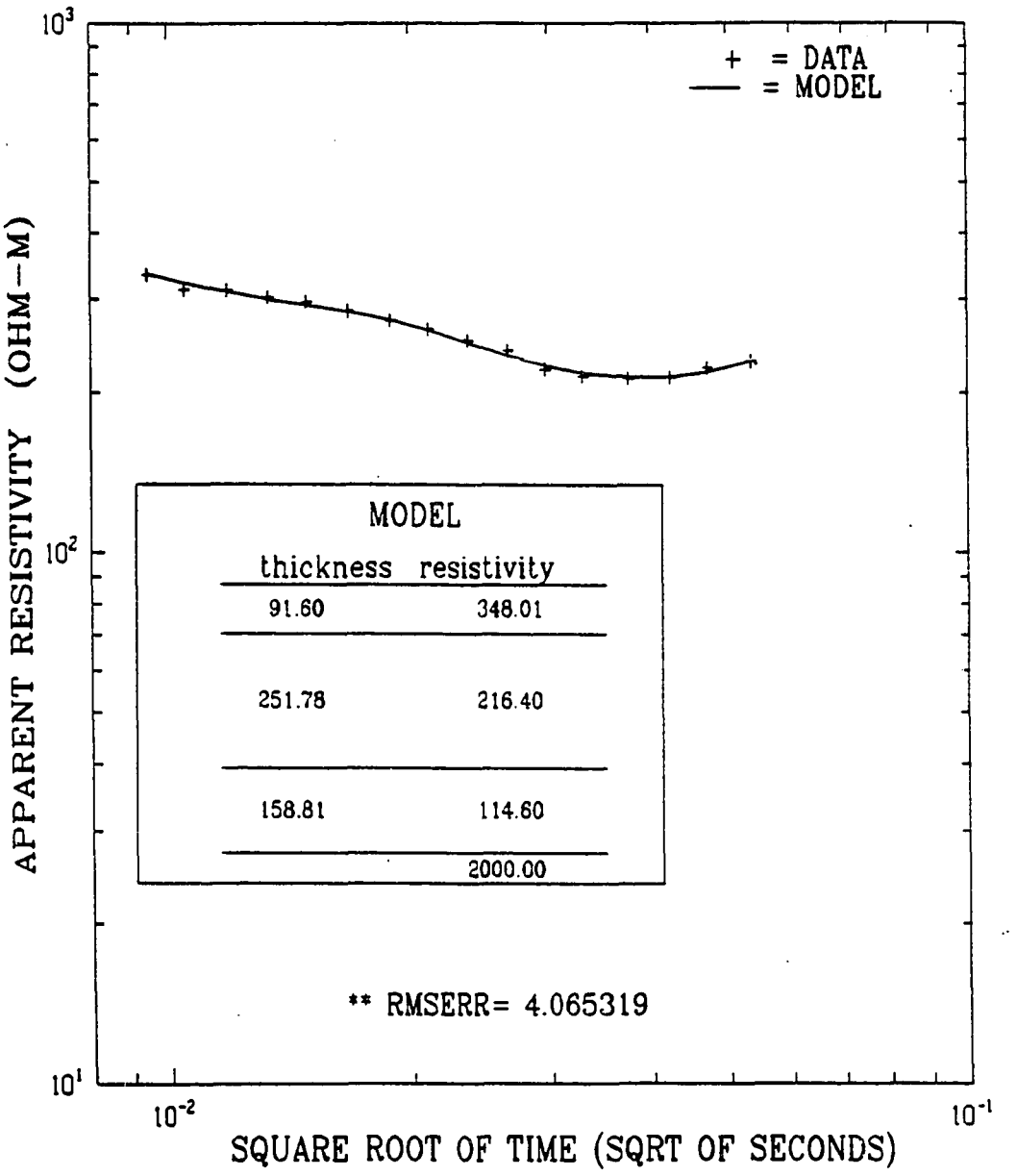

Figure A.11 TEM data and inversion model for the Oldman site, just north of the Oldman Pipeline Construction Camp airstrip.

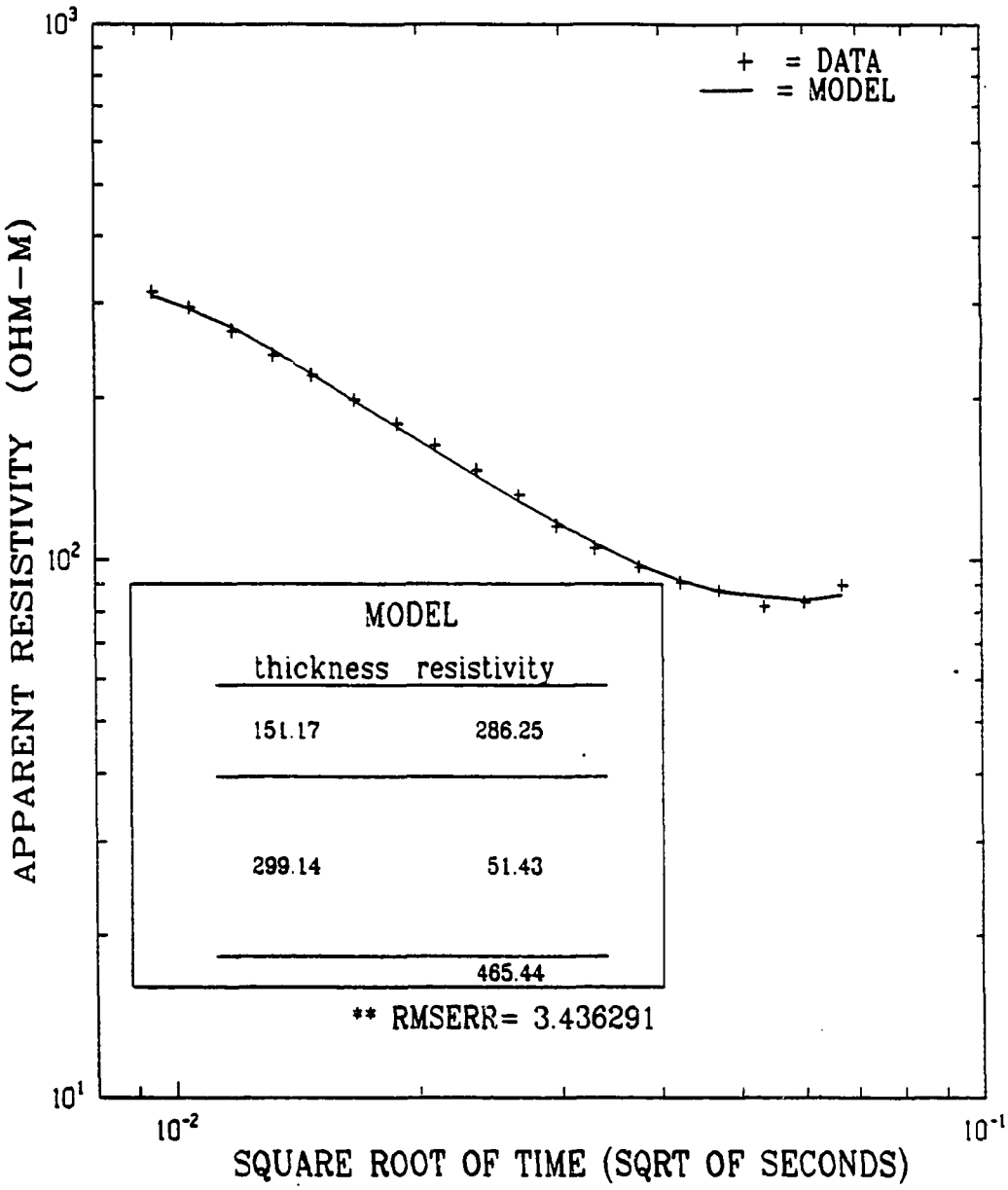

Figure A.12 TEM data and inversion model for the site near Finger Mountain.

13. Site at Dalton Mile 78.1

This site is located at Dalton Highway Mile 78.1, to the north and east of the road (downslope), with line one bearing 90 degrees. The vegetation consists of scattered dense stands of trees with a vegetative mat of medium thickness and little standing water. The roadcuts in the area show tertiary basalt as well as post-Miocene gravel, sands and silts (Brown and Kreig, 1983). The EM-37 data exhibited a sign reversal in early time and thus interpretation in terms of simple conductive horizontal layers was precluded. Further, there was no borehole information at this site to aid in the interpretation of the anomalous signal.

At this site and one other (# 18, Elliott Mile 54.7), the received signal changed sign in early time gates. To show this anomalous signal, the raw field strength at the receiver coil is displayed in Figure A.13 as a function of the square root of time for this site. The computation of sample standard deviation for each gate produced the error bars shown. For comparison, the data from Hess Creek (# 16), which displays the more typical signature which has no early time sign change, is also plotted in Figure A.13. When the signal strength decreases rapidly, the later time gates will often show sign changes since the signal has reached the noise level of the system (about 1 microvolt per meter squared, see McNeill, 1982). A change of sign cannot occur in TEM central induction soundings for the vertical magnetic field over a conductive *layered* earth. Thus the sounding from this site was not interpretable in terms of a layered earth of simple resistivity. It is, however, possible that the change of sign may be due to minerals (recall the evidence of basalt flows in the roadcuts) producing an IP effect (see Chapter 5 for further discussion and references) or to two and three-dimensional resistivity anomalies within the earth.

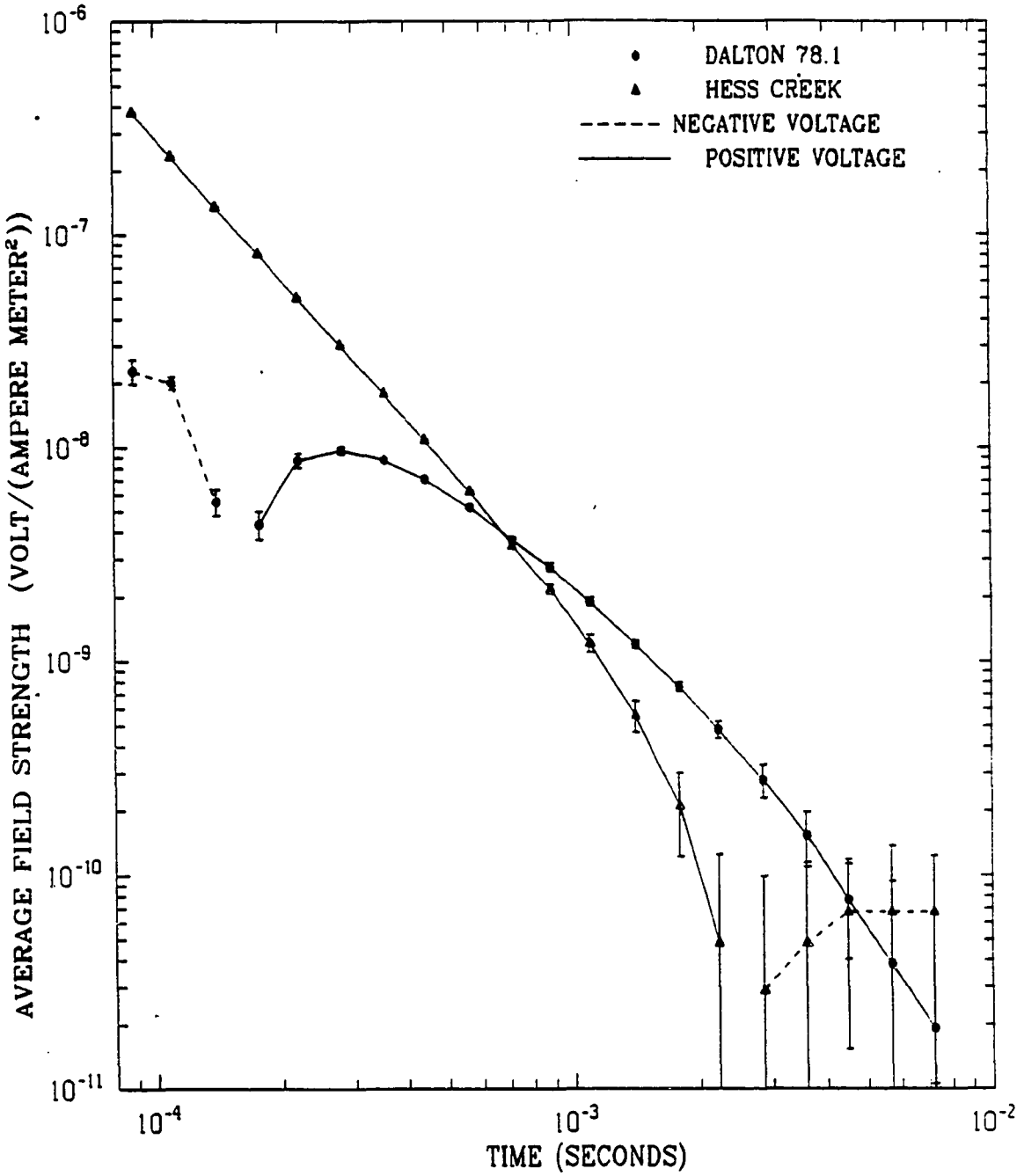

Figure A.13 Averaged raw data for the site at Dalton Highway Mile 78.1 showing an early time sign change and for the Hess Creek site (site # 16).

The only certain thing are that the data is repeatable and not due to equipment malfunction.

14. Yukon River

The Yukon River sounding site is along a small road which heads east from Dalton Highway Mile 55.5. The transmitter was placed about 10 meters north from a gravel pad located about 0.1 mile along this road. Line one has a bearing of 70 degrees across old floodplain deposits of the Yukon River which were covered with very large tussocks with as much as a foot of standing water between tussocks at the time of the sounding.

The interpretation of the data from the site shown in Figure A.14 is contrary to the information derived from the temperature borehole, wherein the thickness of permafrost is extrapolated to be about 70 $\pm$ 2 meters (Osterkamp, personal communications). The TEM interpretation in contrast suggests that 189 meters of frozen material at about 188 Ω-m resistivity lies over unfrozen material 207 meters thick at 92 Ω-m resistivity, which, in turn, overlies bedrock of very high resistivity.

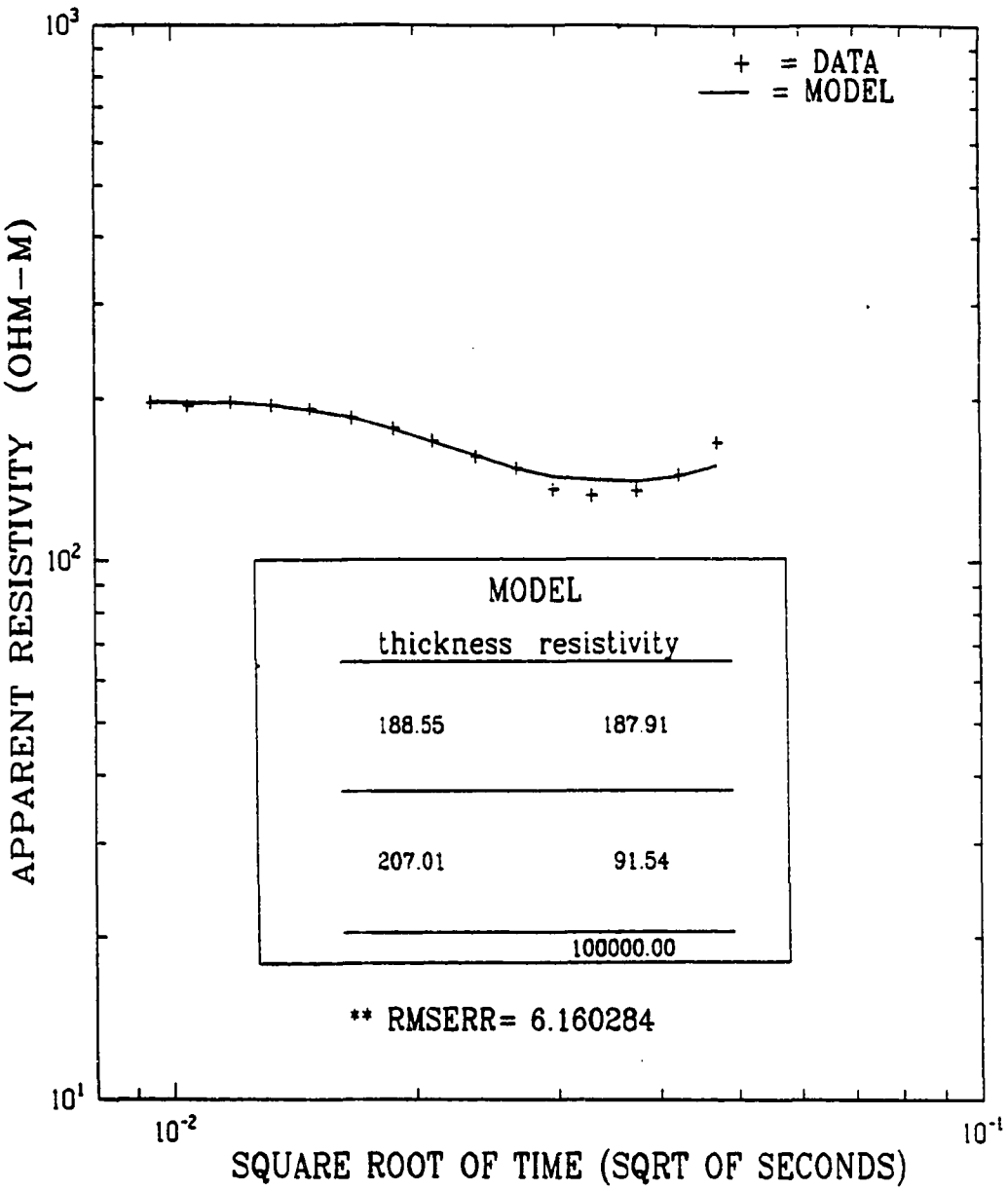

Figure A.14 TEM data and inversion model for the Yukon River site near the Dalton Highway bridge over the Yukon River.

15. Site at Dalton Mile 34.4

This site is located at Dalton Highway Mile 34.4 downslope on the rounded edge of a hill to the south of the highway. Line one has a bearing of 170 degrees. The vegetation is a thick vegetative mat with scattered black spruce. The near surface rocks here are of metamorphic type.

The TEM sounding data and inversion model shown in Figure A.15 suggests there are about 90 to 100 meters of material overlying a highly resistive bedrock. The sounding seems to indicate frozen material, with no evidence of a unfrozen zone, extending to bedrock at this mostly south-facing site. Nearby hills to the south keeps the slope well shaded for much of the year.

16. Hess Creek

Located in the floodplain of Hess Creek, this site is south of the road at Dalton Highway Mile 2A.7 with line one bearing 240 degrees. This is just south of the Hess Creek bridge in a locale of very deep tussocks with as much as six inches of water standing at low points (at the time of the sounding).

The data and inversion model shown in Figure A.16 suggests there are 305 meters of permafrost material at about 200 Ω-m resistivity underlain by 5 meters of unfrozen material at 12 Ω-m resistivity underlain by bedrock of very high resistivity. There is no borehole information at the site but the permafrost thickness seems unduly large for the site location.

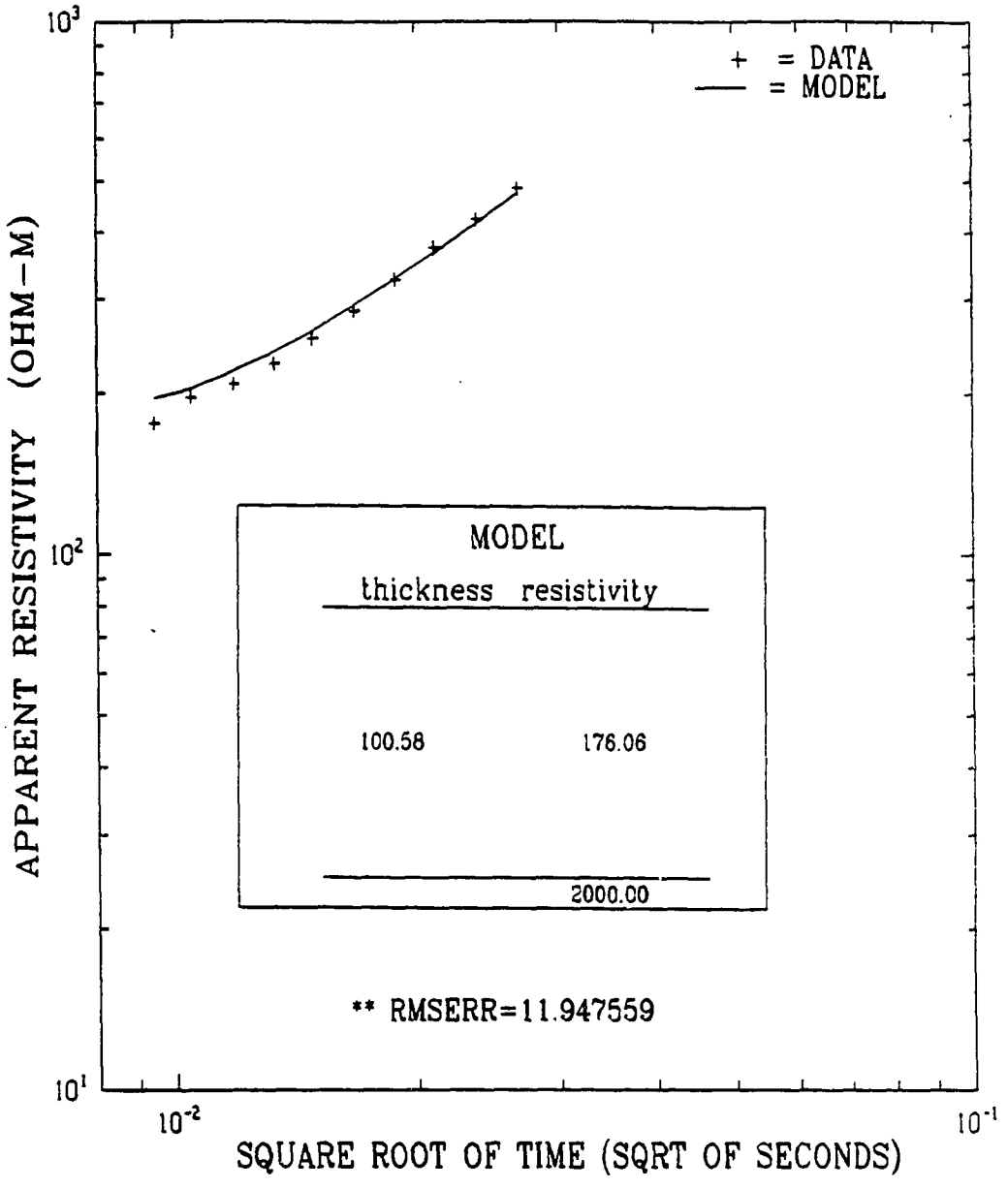

Figure A.15 TEM data and inversion model for the site at Dalton Highway Mile 34.4.

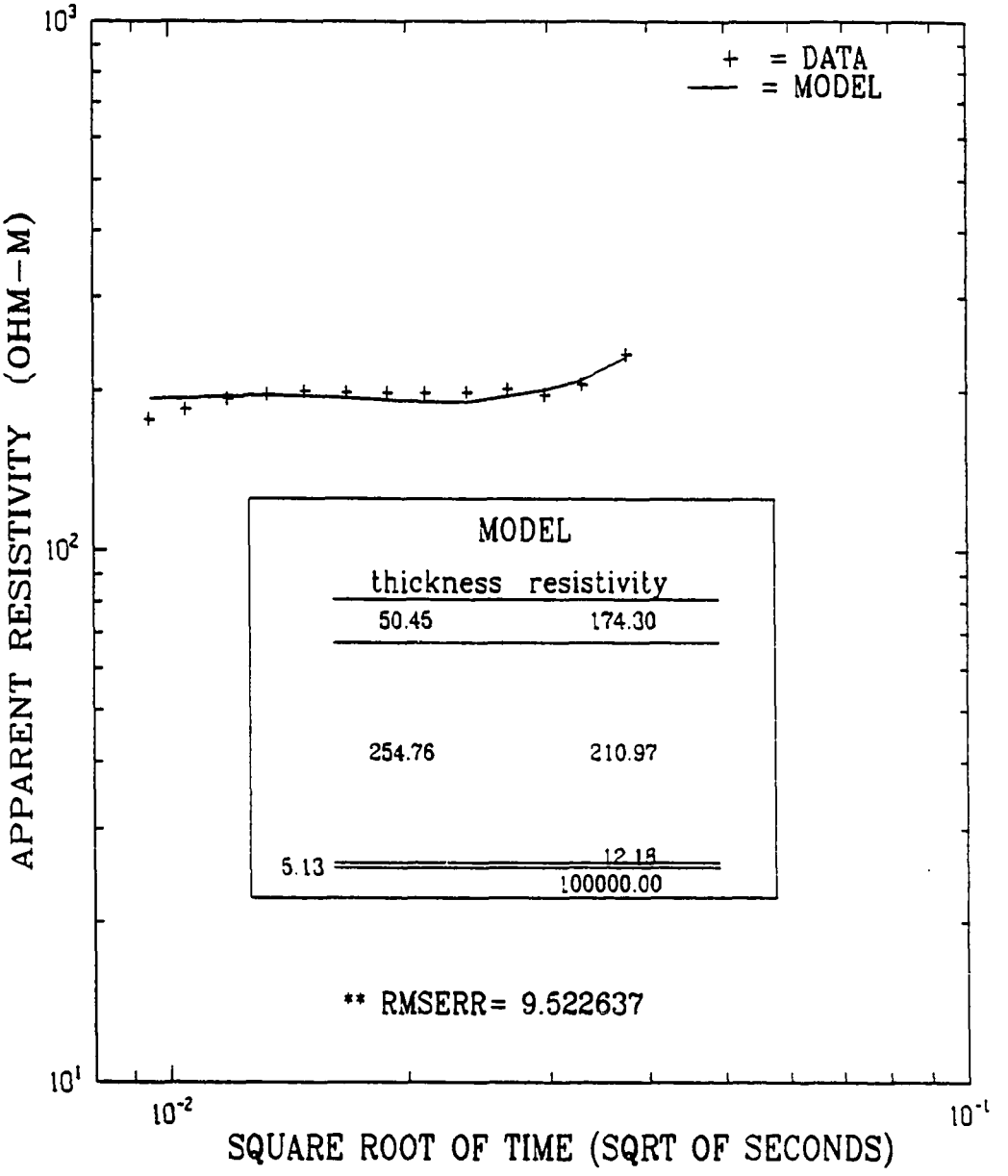

Figure A.16 TEM data and inversion model for the Hess Creek site just south of the Hess Creek bridge.

17. Livengood

This site is located at Elliott Highway Mile 71.1 on the south side of a small roadside turnout with line one bearing 250 degrees. Not far from the Ready Bullion Creek, the lowlands are covered with a thick vegetative mat and small spruce. The deposits here are sands, gravels and silts over metamorphic bedrock (Brown and Kreig, 1983).

The interpretation for the data shown in Figure A.17 calls for four layers: layer one is a permafrost layer 92 meters thick of 530 Ω-m resistivity, layer two is unfrozen at 47 Ω-m resistivity and 117 meters thick, layer three is a very conductive layer of only 2.7 Ω-m resistivity (perhaps a very saline pore water) only 4.6 meters thick, and the fourth layer is bedrock at about ten thousand Ω-m resistivity.

18. Site at Elliott Mile 54.7

This sounding site is east of the road at Elliott Highway Mile 54.7 on the rounded edge of a hill downsloping to the east with line one having a bearing of 120 degrees. The vegetation is a uniformly thick vegetative mat with fairly uniform small (mostly black spruce) trees. There is no borehole information at this site. However, Brown and Kreig (1983) note the presence of large ice-masses and extensive ice-wedges in the permafrost exposed by roadcuts in this area.

This is the second site (the other is D78.1, site # 13) which displayed a single sign change in early time as shown in Figure A.18. This site cannot be interpreted in terms of a layered earth with ordinary resistivity. The sign change was repeatable

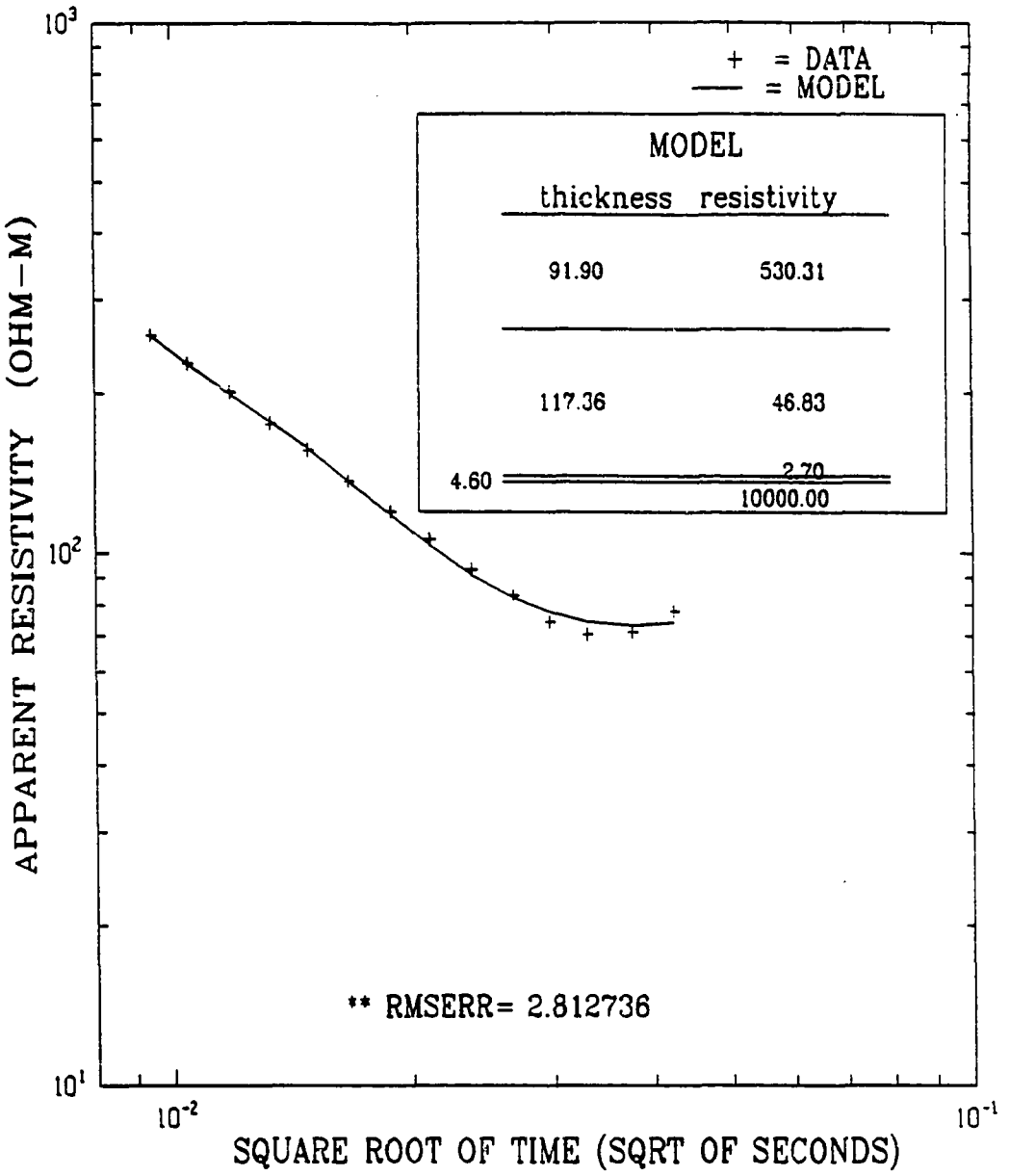

Figure A.17 TEM data and inversion model results for the Livengood site.

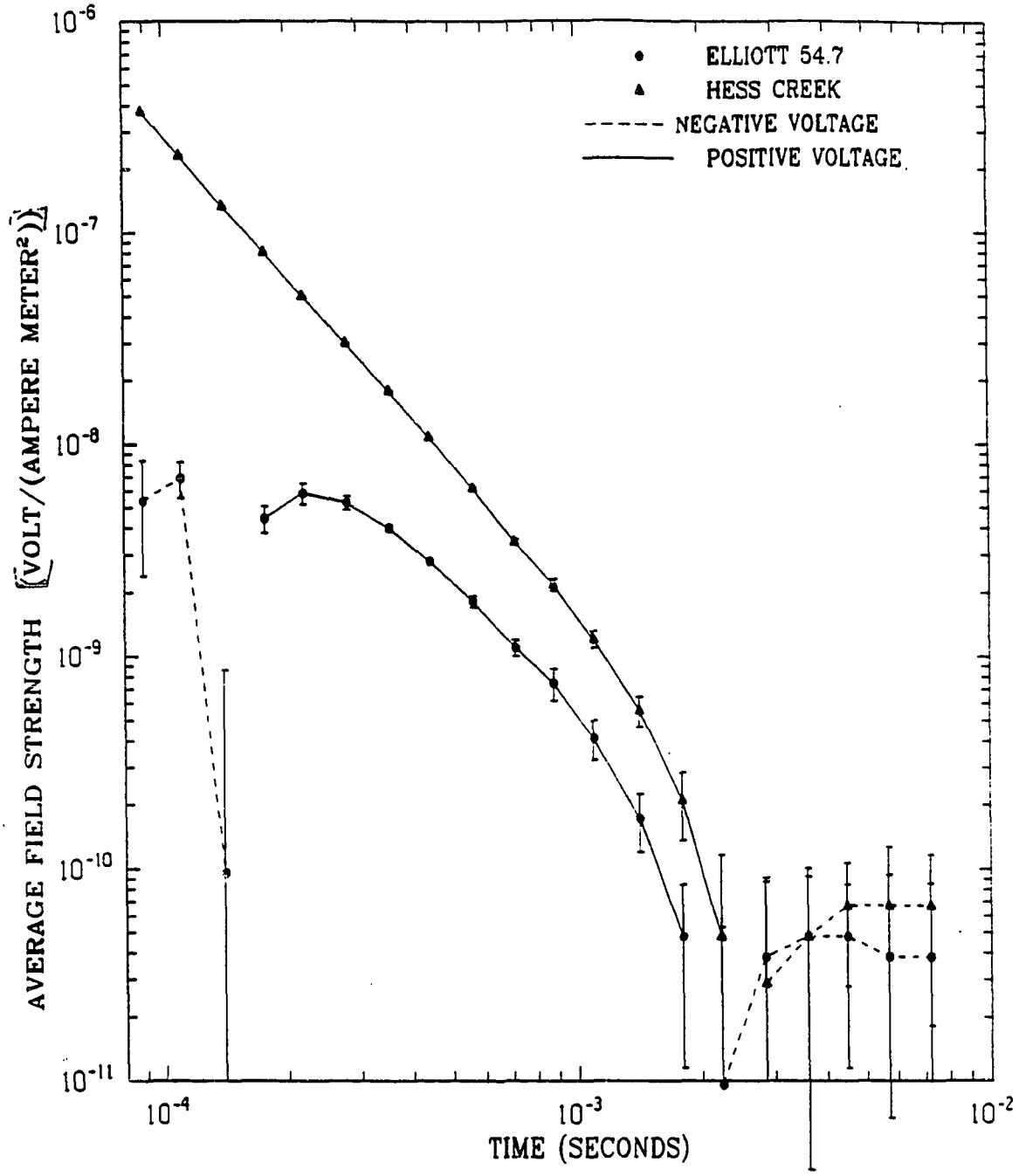

Figure A.18 Averaged raw data for the TEM data for the Elliott Highway Mile 54.7 site showing an early time sign change.

in each of two sounding days taken a few days apart strongly suggesting instrument problems were not the cause of the anomalous signal.

19. Washington Creek

This site is in the floodplain of Washington Creek north of the road at Elliott Highway Mile 19.6 with line one bearing 60 degrees. The bedrock here is the well known Birch Creek schist. A thick vegetative mat and closely-spaced small spruce trees cover the ground.

The geoelectric model for this site (Figure A.19) is difficult to interpret in terms of permafrost. This may be because the zone of permafrost includes a portion of bedrock. A 4 layer model seems to have the best fit: layer one is 50 meters thick at 262 Ω-m resistivity, layer two is 297 meters thick at 415 Ω-m resistivity (perhaps weathered bedrock?), layer three is 9 meters thick at 52 Ω-m, and the basement resistivity is extremely large.

20. Virgin Spruce 1

Located in the Fairbanks area, this site is near a temperature borehole of Osterkamp (personal communications). The site, approximately 1.8 kilometers north of the campus of the University of Alaska, is reached by traveling south along the section line between R2W and R1W at T1N between sections 36 and 31. The transmitter and receiver were located along the brush line of the section line with line one bearing 225 degrees. The land is covered with a vegetative mat,

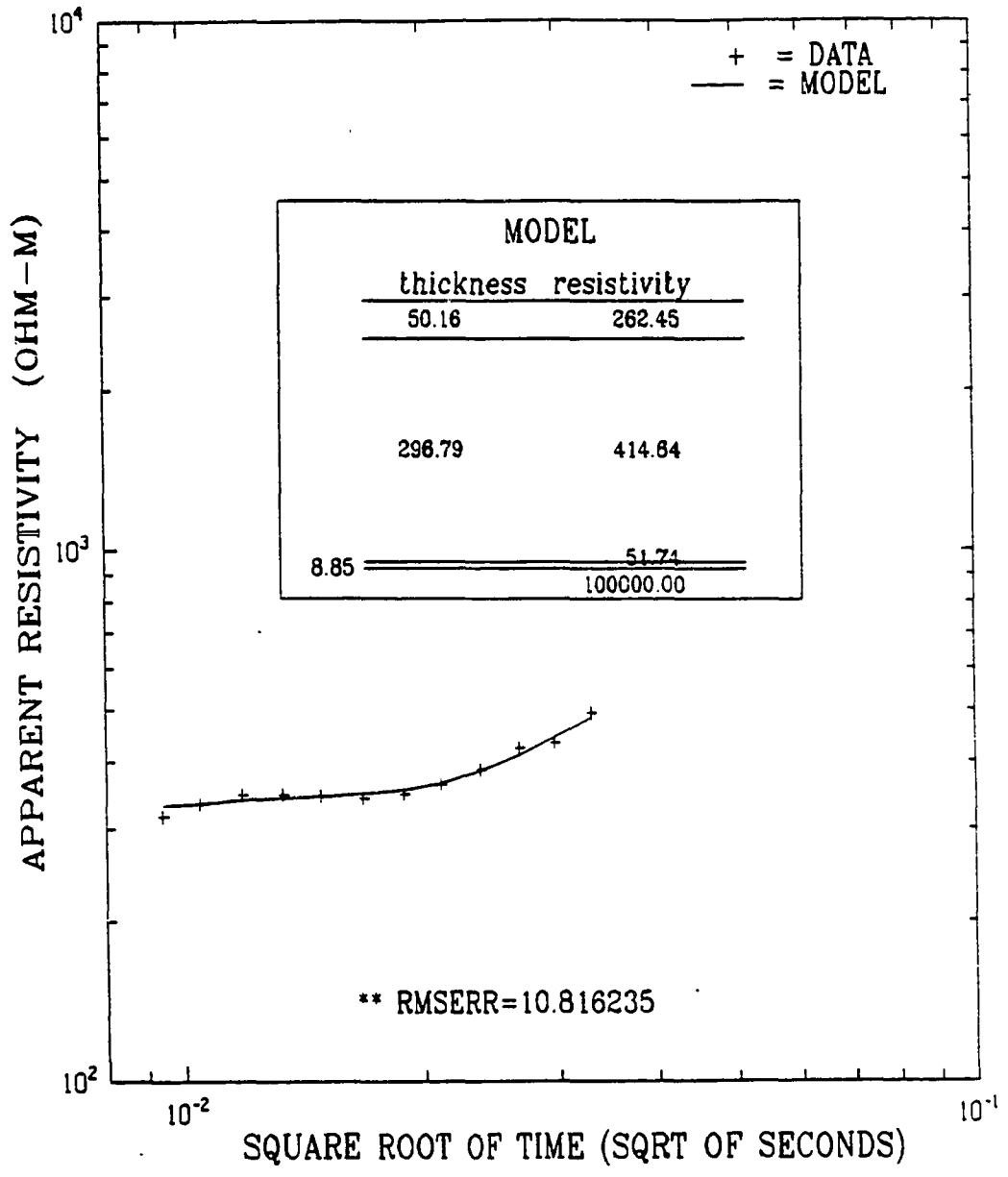

Figure A.19 TEM data and geoelectric model for the Washington Creek site.

various species of evergreen and deciduous trees of varying heights and scattered patches of thick berry bushes. The site area, which slopes slightly to the south, is well drained. The hillsides above Fairbanks are thickly mantled with silts generally overlying sands and gravel deposits. The bedrock in the area consists of schists.

The temperature borehole information suggests perhaps 25 meters of permafrost at this site. The TEM data and simple 2 layer inversion model (not shown) are interpreted to suggest about 75 meters of overburden material on bedrock. In a 3 layer model, the first layer is frozen, the second layer is unfrozen, and the third layer is bedrock. The thickness of a thin layer of frozen material is not resolved in the TEM inversions. The permafrost thickness cannot be estimated from the inversion model of Figure A.20 which displays a typical inversion result.

The model is a good fit to the data but demonstrates the problem with resolving the thin, more resistive permafrost layer. The inversion model is a result of an attempt to fit the data with a 3 layer scenario wherein the thin layer of permafrost overlies unfrozen sediments on bedrock. The first two layers of the inversion model have nearly the same resistivities, indicating a lack of resolution of the thin highly resistive layer. In order to resolve the thin layer, a few more data points on the portion of the curve which decreases with time must be obtained. The data of the next site demonstrates the results when this decreasing portion of the curve is available.

Direct current (DC) resistivity measurements were made earlier at this site by the author. The computer inversion of these unpublished measurements produced a geoelectric model with five layers. This model gives more detailed information on the depth to the permafrost table and base. The model calls for a very thin first layer thickness of 0.24 meters with 36.7 Ω-m resistivity (thawed layer thickness in late September) over a slightly thicker 0.48 meter layer of higher resistivity (5235

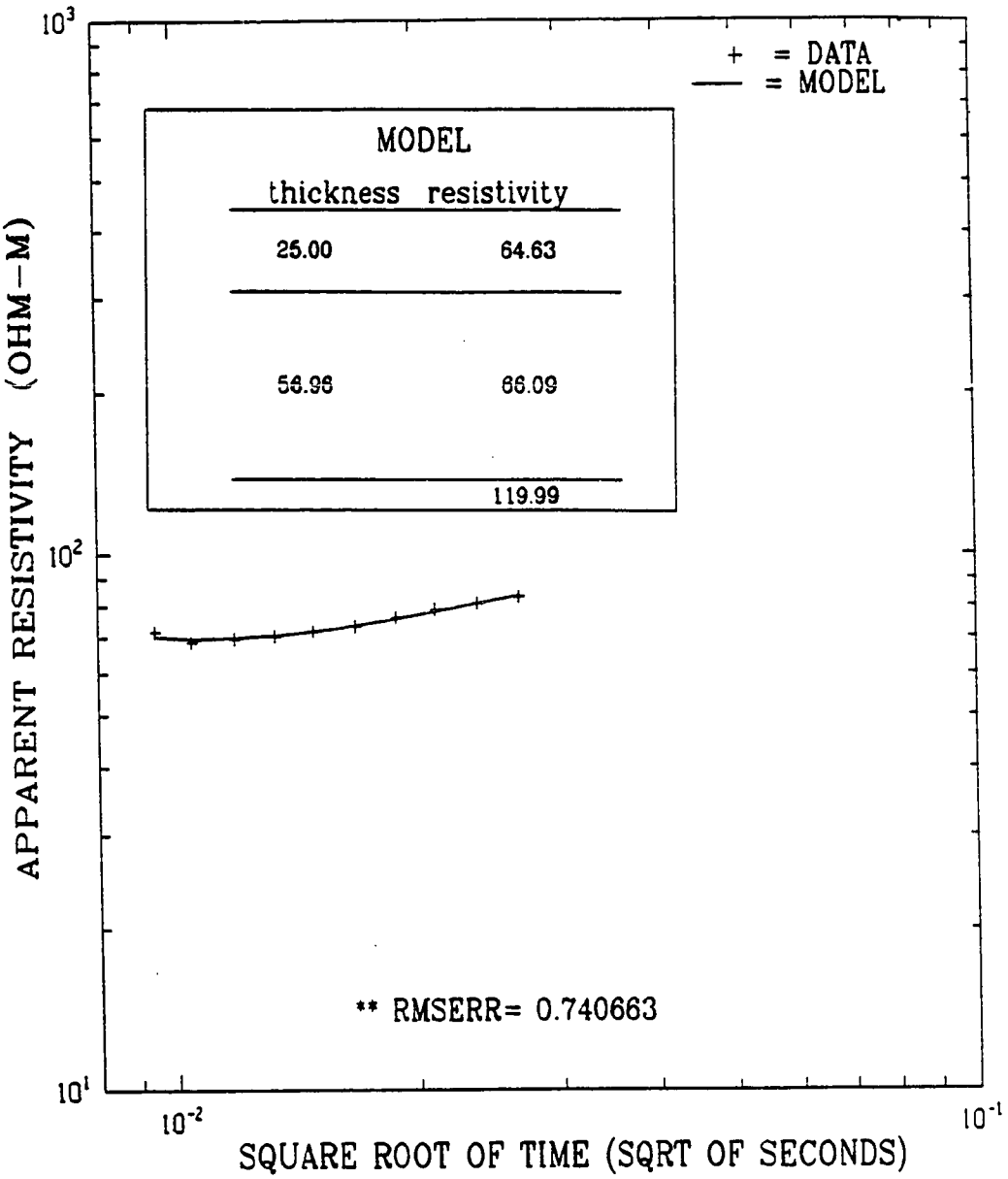

Figure A.20 TEM data and inversion model for Fairbanks area site Virgin Spruce 1 located south of the end of Dalton Trail Road.

Ω-m, ice rich?). These thin layers overlie a third layer, 1.5 meters thick, with 38.4 Ω-m resistivity (perhaps an unfrozen zone) over 22.3 meters of 2324 Ω-m permafrost. The fifth layer, has a resistivity of 37.8 Ω-m. Even though the data were taken with arrays for which the spacing between the outer electrodes varied from 6 feet to 1200 feet, the DC resistivity method did not discern the depth to bedrock. Although the inverted resistivities seem to have too much variation for material changing only in temperature with depth, the fit to the DC resistivity data is good and the depth to the permafrost base is about right from the temperature data.

21. Virgin Spruce 2

This site had line one bearing directly south (180 degrees) along the section line (same section line as Virgin Spruce 1, but approximately 760 feet south) between sections 36 and 31. The borehole is approximately 37 feet directly west of the 1/4 section marker established by the BM General Lands Office in 1910. This is roughly the center of line one for the TEM sounding. The land, covered with a thick vegetative mat, various types of trees dominated by scrub spruce and berry bushes, slopes to the south. The hillsides above Fairbanks such as this one are often mantled with thick, eolian silts overlying bedrock of Birch Creek Schist.

The interpretation of the TEM data shown in Figure A.21 calls for about 81 meters of overburden silt at this site. The thickness of the frozen layer is again not well resolved by the TEM system. Relatively warm permafrost composed of silt, rich in clay minerals, may have fairly low resistivities. Thus the model from the inversion may be interpreted to show the existence of 38 meters of permafrost with resistivity 147 Ω-m, overlying a layer of unfrozen silts 43 meters thick with

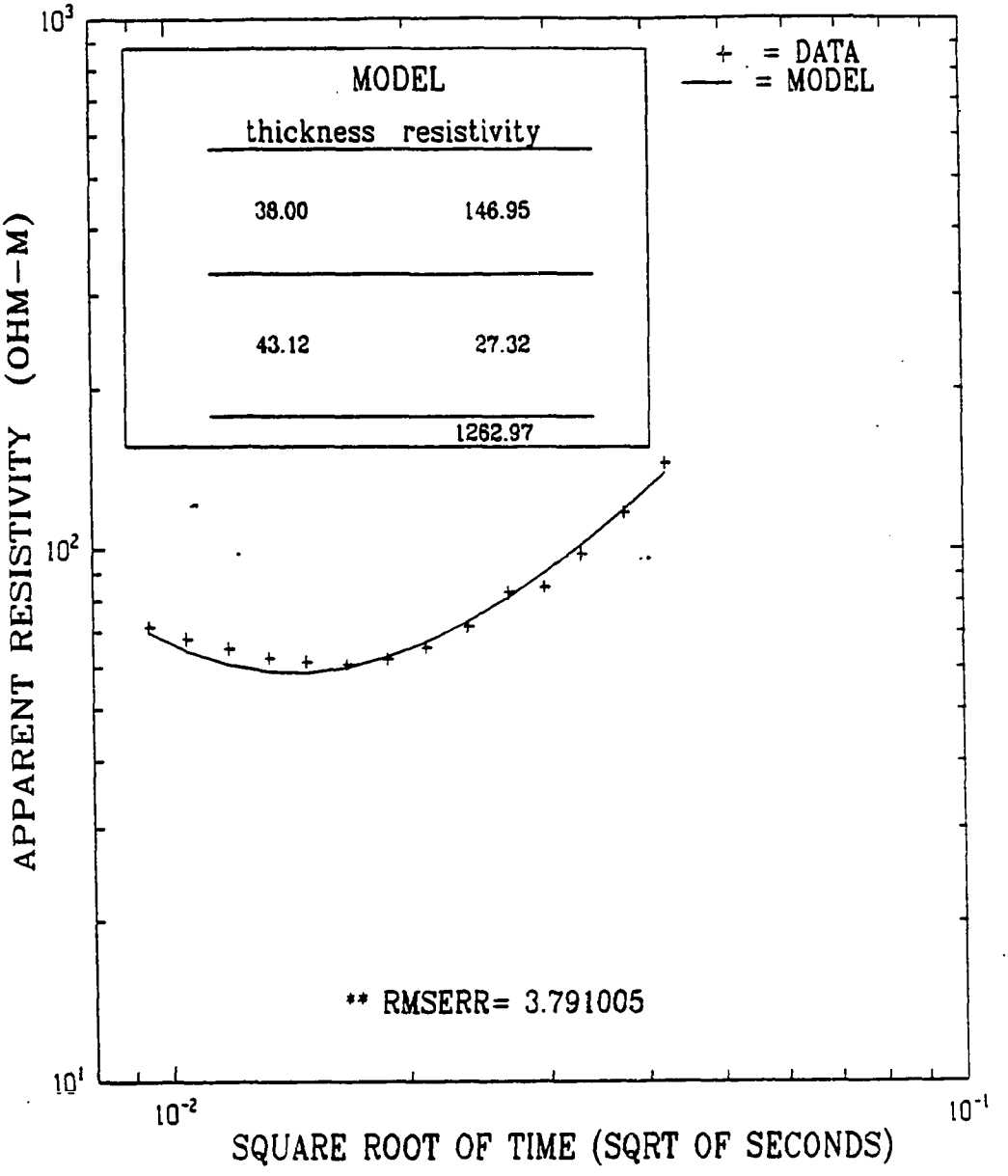

Figure A.21 TEM data and inversion model for the Fairbanks area sounding site Virgin Spruce 2 located south of Dalton Trail Road.

resistivity 27 Ω-m. These layers overlie bedrock with a resistivity of about 1263 Ω-m. This corresponds well with the available temperature extrapolation which is interpreted to show about 38 meters of permafrost occurs at this site.

22. Farm

This Fairbanks area site, located on the University of Alaska, Fairbanks, Agriculture and Forestry Experiment Station (AFES), was the most accessible from the Geophysical Institute and, therefore, served as a test site for the repeatability of the instruments. The site is at the center of a large field which has been under cultivation for many years. The center of line one was 50 feet directly east of the small gray instrumentation shack. The bearing of line one was 160 degrees. Water well drilling logs show that the Tanana River flood plain area, on which this site is located, has a complex structure of interleaved silts, gravels, and sandy layers. However, two drillholes nearby the site show more or less a continuous overburden of silt to a depth between 8 to 30 meters lying over bedrock. These also show that the thawed zone has reached a depth of about 10 meters.

The interpretation of this data shown in Figure A.22 for this site is very difficult since the TEM signature was not well matched by any of the many runs made for inversion geoelectric models. Although more complicated scenarios were attempted, the simple 2 layer model fits the data as well as any model attempted. Unfortunately, the 2 layer inversion has 107 meters of material over bedrock. This model does not give the thickness of permafrost.

The DC resistivity inversion of data taken by the author at this site shows only that very resistive ground begins at approximately 8 meters depth. There is

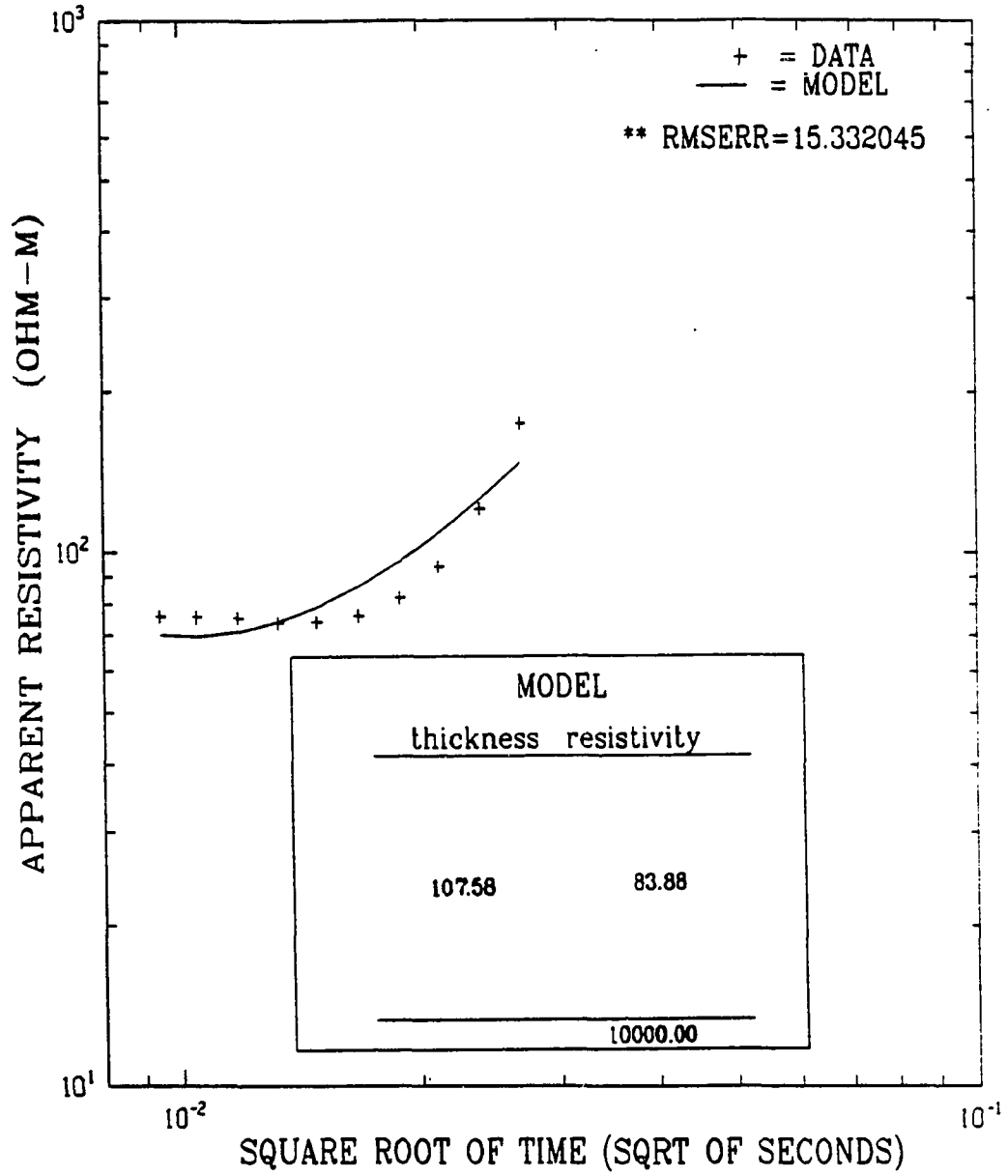

Figure A.22 TEM sounding data and inversion model for the Fairbanks area sounding Farm site located in the University of Alaska agricultural field.

no curve break corresponding to unfrozen ground below the permafrost and above the bedrock. This suite of data strongly argues that permafrost extends into the bedrock.

23. Peat

The Fairbanks area Peat site is located on University of Alaska land between College Road and Farmers Loop Road, east of the University and west of the Tanana Valley Fairgrounds. During the time of the TEM sounding, the site was inaccessible to vehicular traffic and the heavy equipment had to be transported by hand over tussock-covered terrain. The site is in an area of thick peat bogs with the wet ground supporting only a few small, scattered trees and willows.

The data shown in Figure A.23 is interpreted in terms of three layers with a 38 m thick first layer with a resistivity of 554 Ω-m which overlies a layer 141 meters thick having a 55 Ω-m resistivity. The third layer is bedrock. The first layer with the relatively high 554 Ω-m resistivity may be considered frozen ice-rich peat possibly interspersed with sands and gravels. The second layer appears to be unfrozen.

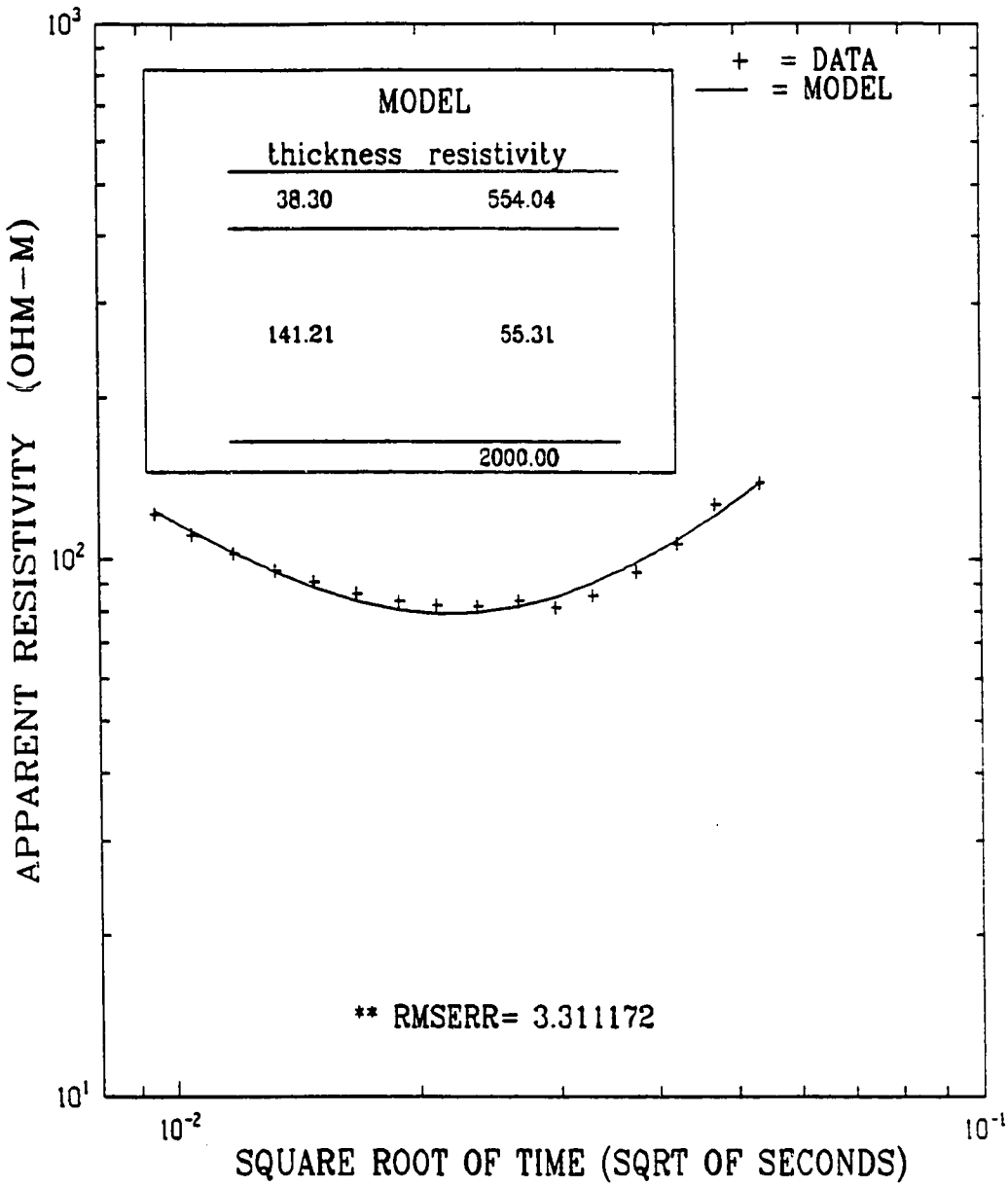

Figure A.23 TEM sounding data and inversion model for the Fairbanks area Peat site.

24. Farmers Loop

This Fairbanks area sounding site is located east of Farmers Loop Road with line one bearing 105 degrees; the site is 0.2 mile north of the main entrance to the University of Alaska and is about 0.6 mile south and west of the previous peat site. A section line served as an access trail. The land is flat, tussocky, with few trees, but many willows.

A geoelectric model with four layers gives an excellent fit to the data of Figure A.24. Layer one is 35 meters thick of 251 Ω-m resistivity, layer two is 285 Ω-m with a thickness of 116 meters, layer three is 90 meters thick of 19 Ω-m, and layer four is a low resistivity basement of 4 Ω-m. The nearby temperature borehole suggests there are about 66 meters of permafrost at this site, which differs considerably from the 151 meter thick layer interpreted from the TEM model.

25. Eielson

This site is located east of the Richardson Highway at Mile Post 337 with line one bearing 100 degrees. The area is covered with brush and small trees and may have been cleared around 30 years ago. The area is on the floodplain of the Tanana River with the many former drainage channels and varied topography typical of such large rivers in central Alaska. (See Péwé and Reger (1983) for information on the Richardson and Glenn Highway geology and landscape features.) The data for this site is shown in Figure A.25. The inversion model is interpreted to indicate the existence of 43 meters of permafrost at this site.

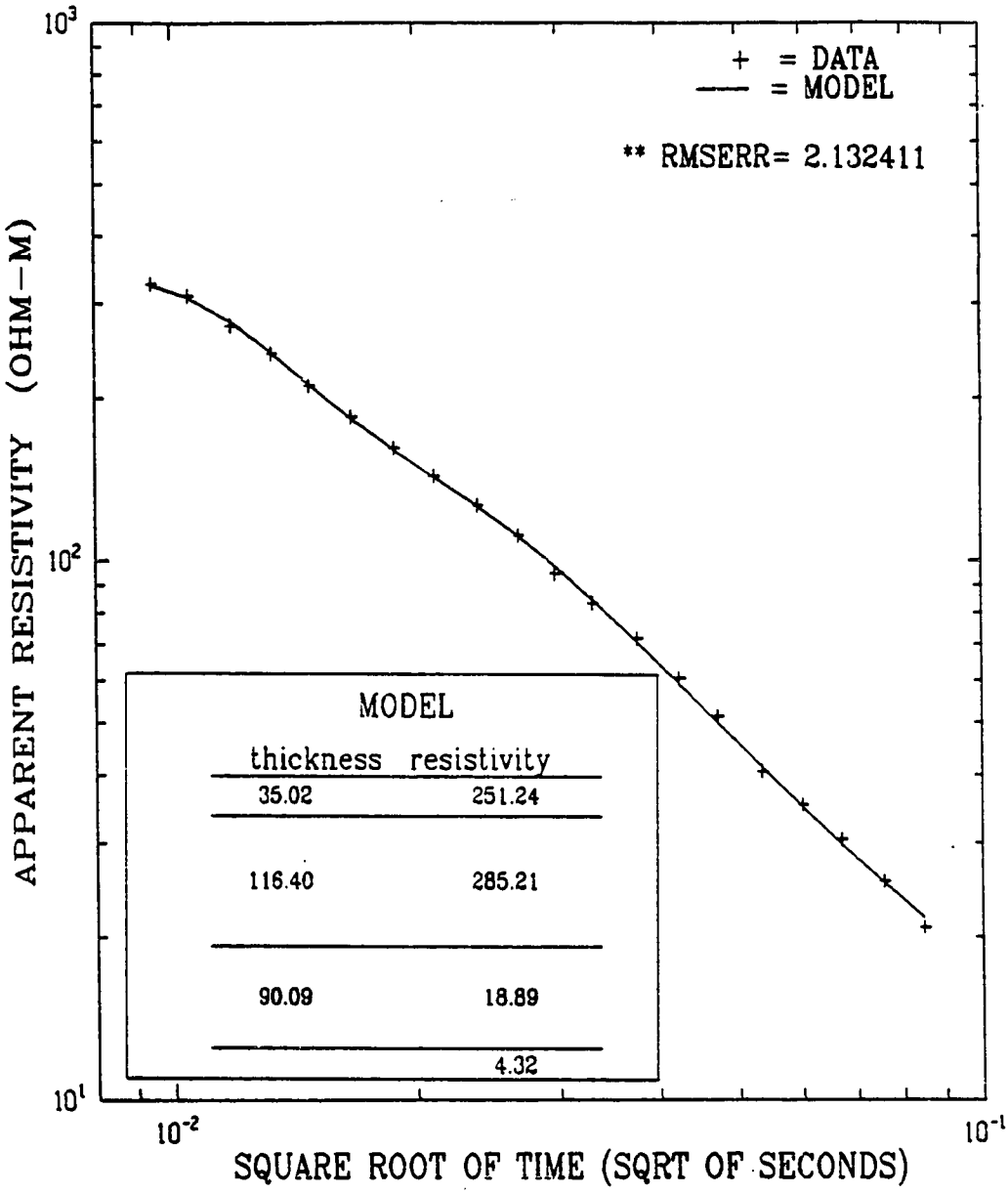

Figure A.24 TEM sounding data and inversion model for the Fairbanks area Farmers Loop site.

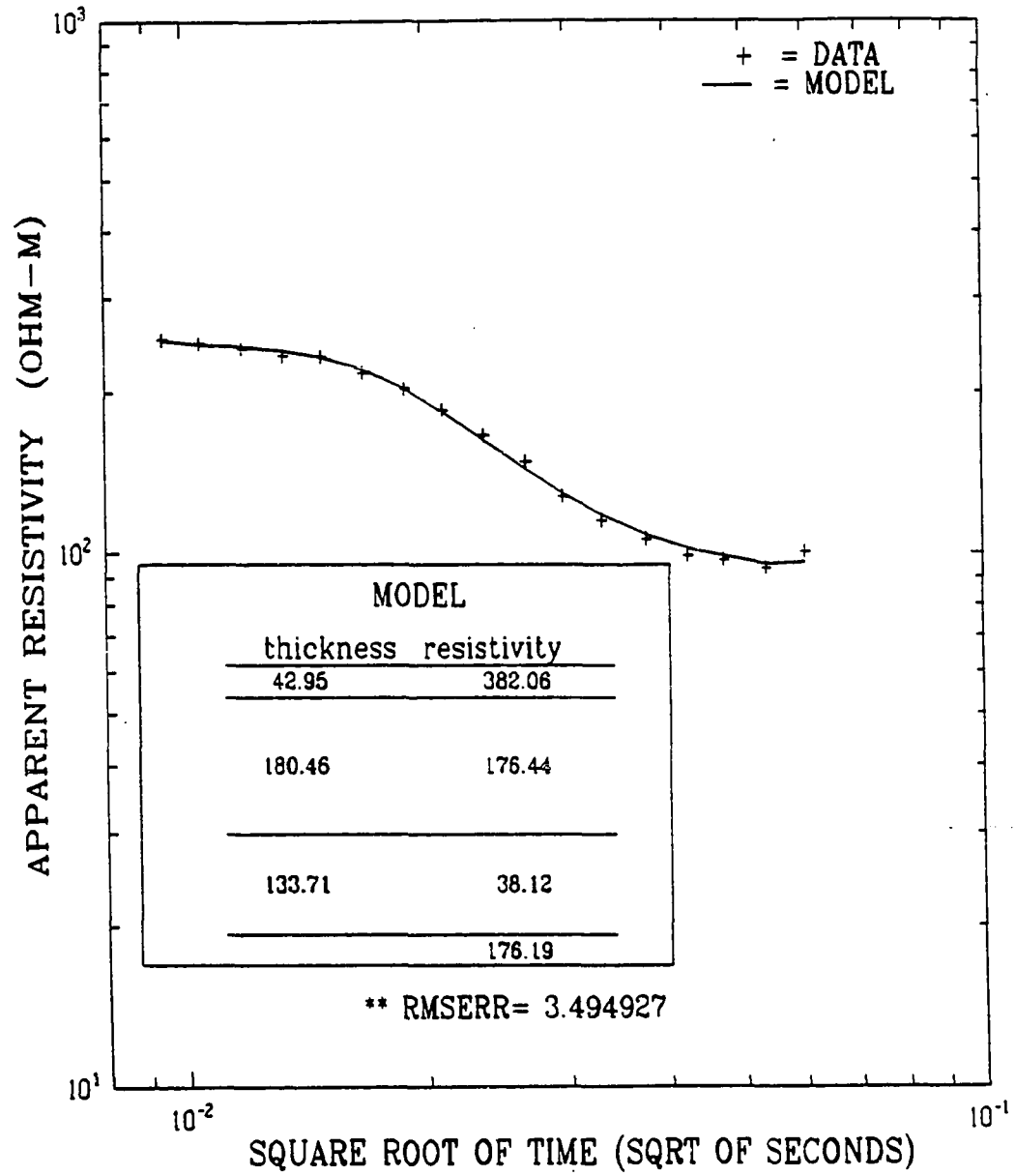

Figure A.25 TEM sounding data and inversion model for the Eielson site just south of the Eielson Air Force Base runway.

26. Quartz Lake

This site is located at Quartz Lake at the end of a maintained gravel road leading five miles north and east from the Richardson Highway Mile 278.9. The TEM sounding was taken with the transmitter at the eastern extreme of some campsites on a loop of the access road with line one bearing 110 degrees. The land was very wet with small streams of water running around tussocks and scattered stands of fairly large trees. The data for this site is shown in Figure A.26.

Because there is a relatively shallow, high resistivity bedrock and a relatively large transmitter loop (compared to the thickness of the overburden) was used, the actual thickness of the permafrost layer could not be accurately interpreted from the inversion modeling. This data did not show sufficient curvature to warrant the application of a 3 layer model. It is believed a decrease in the sounding loop size may be needed for the determination of permafrost. The 2 layer model does not explicitly predict the occurrence of permafrost at this site. The 2 layer interpretation calls for a first layer 81 meters thick with a 213 Ω-m resistivity overlying a basement having 1035 Ω-m resistivity.

27. Sawmill Creek

This site is near Sawmill Creek and is somewhat to the east of the Trans Alaska Pipeline. The site is accessible from the Alaska Highway east of Delta Junction, Alaska. There is a dirt road leading south from about Mile 1402 of the Alaska Highway. There is a wide point in the road that may be used as a turn around a little

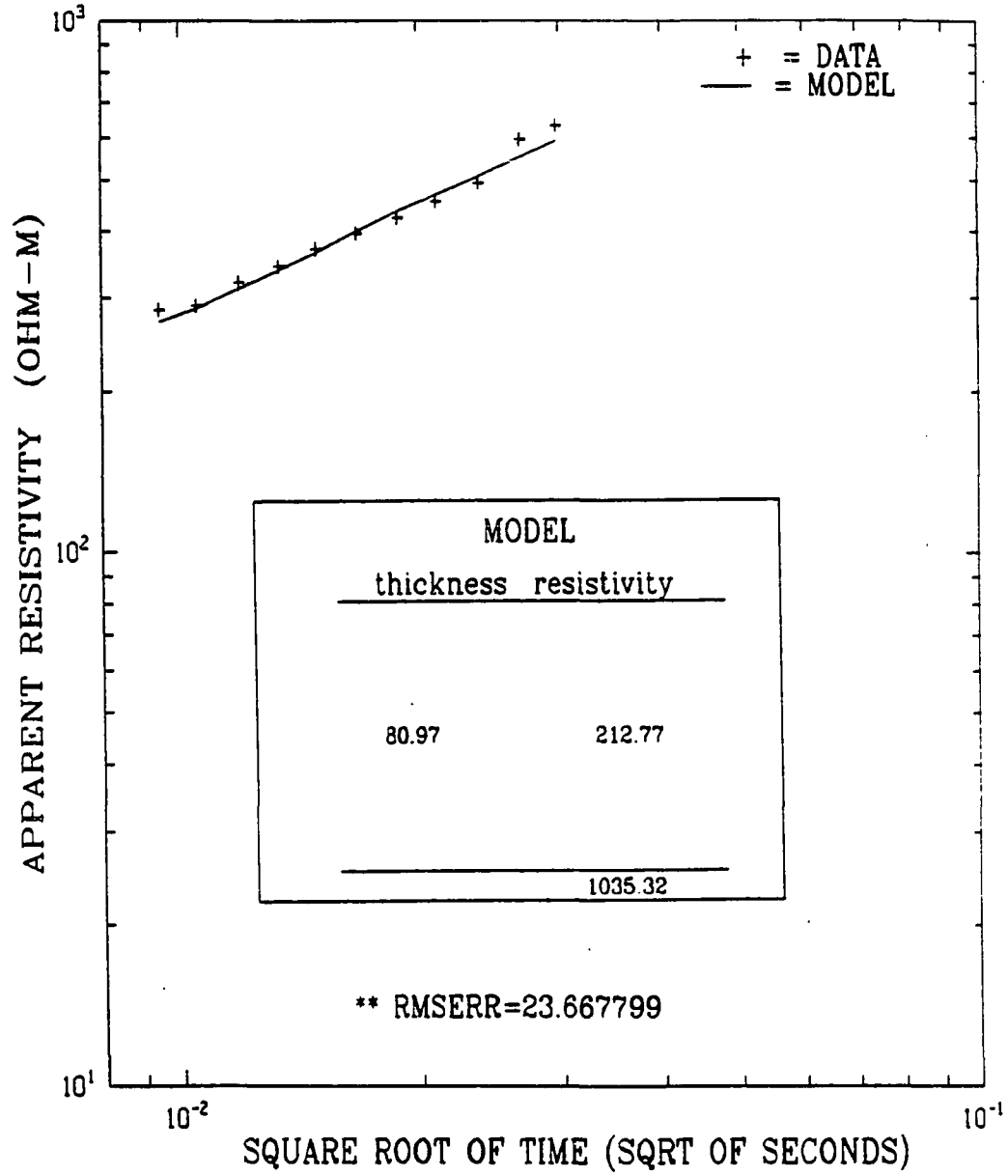

Figure A.26 TEM sounding data and inversion model for the Quartz Lake site.

less than a mile from the main highway. The TEM sounding was taken to the east of this widening in the road with line one bearing 170 degrees. Numerous medium-sized trees of all types with a fairly thick vegetative mat covered the flat landscape. The deposits here consist of fluvially-reworked glacial debris from outwash deposits of old moraines and the more recent moraines deposited by glaciers of the Alaska Range a few miles to the south of the site.

The 2 layer interpretation of the data shown in Figure A.27 calls for very resistive 201 meter thick permafrost having a resistivity of 1712 Ω-m over less resistive material with a resistivity of 335 Ω-m.

28. Greely

This site is located off a dirt road which leads east toward an abandoned radar site from Richardson Highway Mile 248.5, north of Donnelly Dome. The TEM sounding was taken near a point 0.55 miles from the Richardson on the south side of the road with line one bearing 230 degrees. The vegetation here is a thin vegetative mat with berry bushes. The underlying deposits are of glacial origin, probably from the Donnelly Glaciation period.

The data shown in Figure A.28 is interpreted to show the existence of two layers: layer one is 100 meters thick with 110 Ω-m resistivity and layer two has a resistivity of 651 Ω-m. Clearly the TEM data at this site indicates there is no permafrost. Additional support for this interpretation is based on the temperature data from a nearby borehole which gives a MAST of +1.5°.

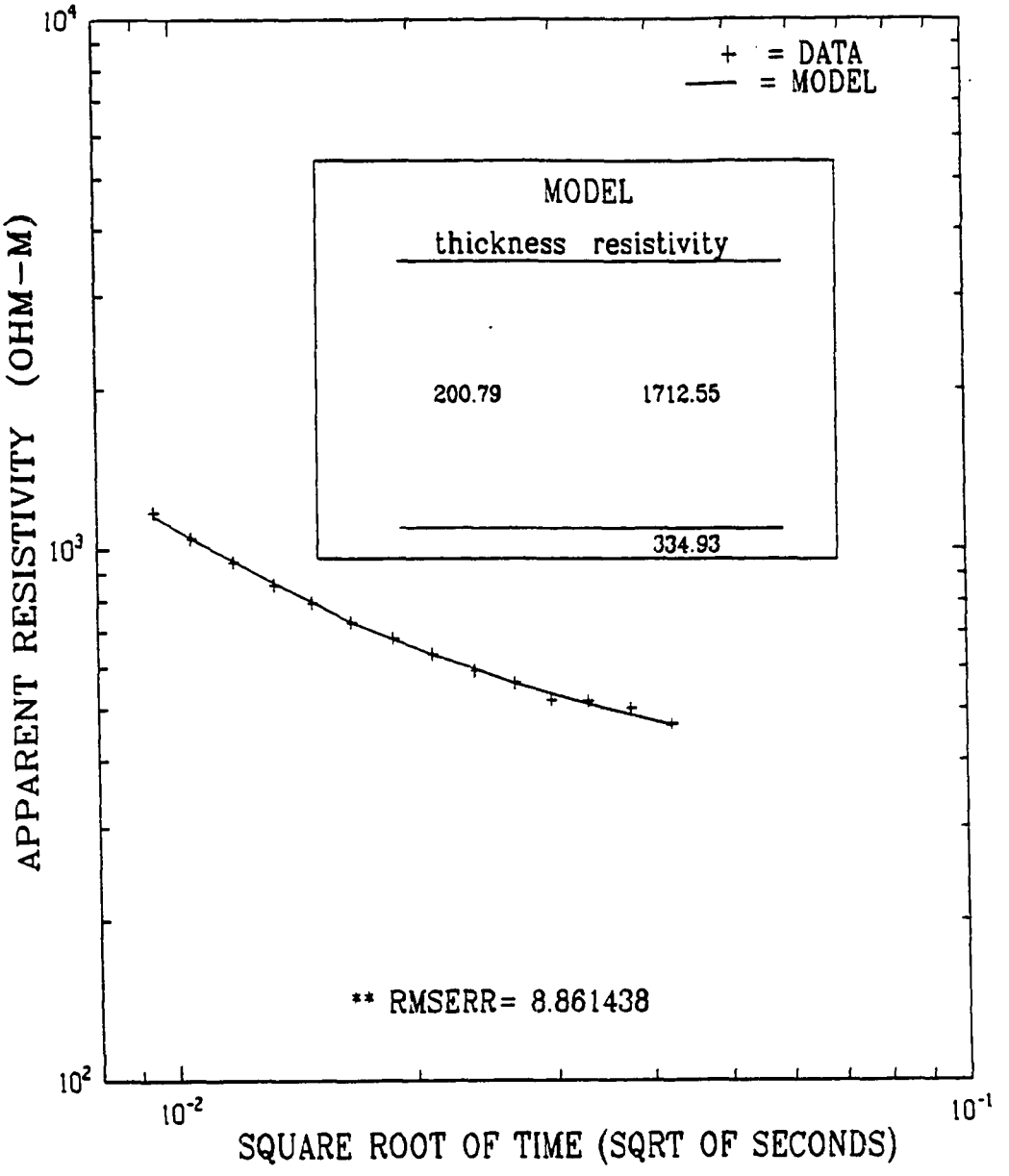

Figure A.27 TEM sounding data and inversion model for the Sawmill Creek site.

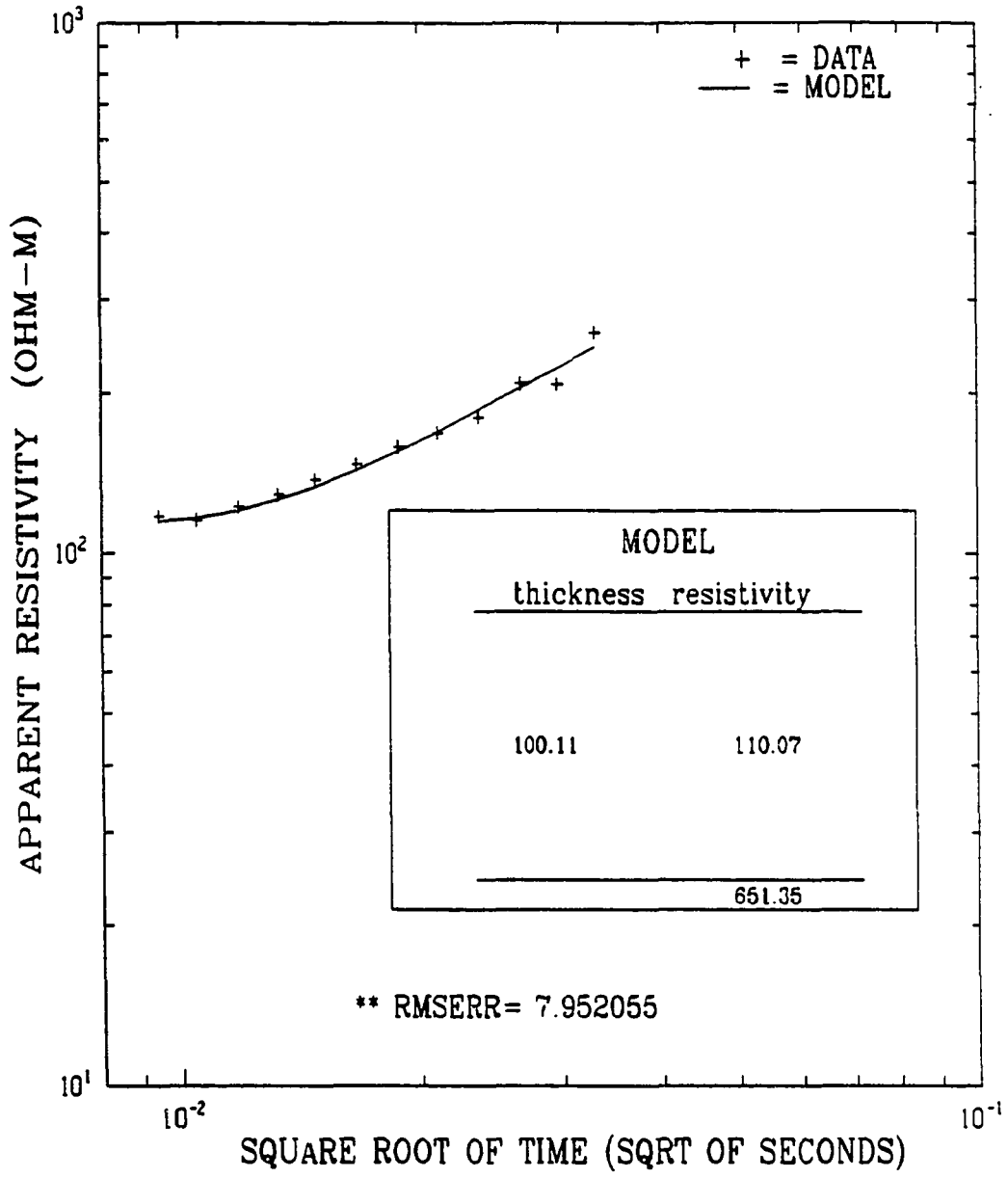

Figure A.28 TEM sounding data and inversion model for the Greely site north of Donnelly Dome.

29. Fielding Lake

The Fielding Lake site is located about 0.6 mile along the access road leading southwest off Mile 200.5 of Richardson Highway. The sounding site is west of the road with line one bearing 349 degrees. The site is on the lowlands of the confluence of Phelan Creek and the outflow creek of Fielding Lake. The ground is covered with medium tussocks and sparse scrub spruce.

The sounding data are shown in Figure A.29. A 3 layer model for this site gives a first layer thickness of 146 meters of 146 Ω-m material. The second layer is 242 meters thick with a resistivity of 36 Ω-m and overlies 1018 Ω-m bedrock. The interpretation of the first layer as permafrost is doubtful but possible. The upper layers may contain permafrost that is not well delineated by the 100 meter sounding loop.

30. Summit Lake

This site is located on the glacial outwash of the Gulkana Glacier and is reached by a dirt road leading north to a pipeline construction camp from Mile 197.7 of the Richardson Highway. The site is on the east side of the road about one mile from the main highway with line one bearing 155 degrees. The vegetation is a thin, patchy vegetative mat with scattered berry bushes; much of the area is not covered with vegetation with exposed patches showing gravel and sand.

The data for this site, shown in Figure A.30, is interpreted to suggest there are about 242 meters of material over bedrock. The uppermost 112 meters of the

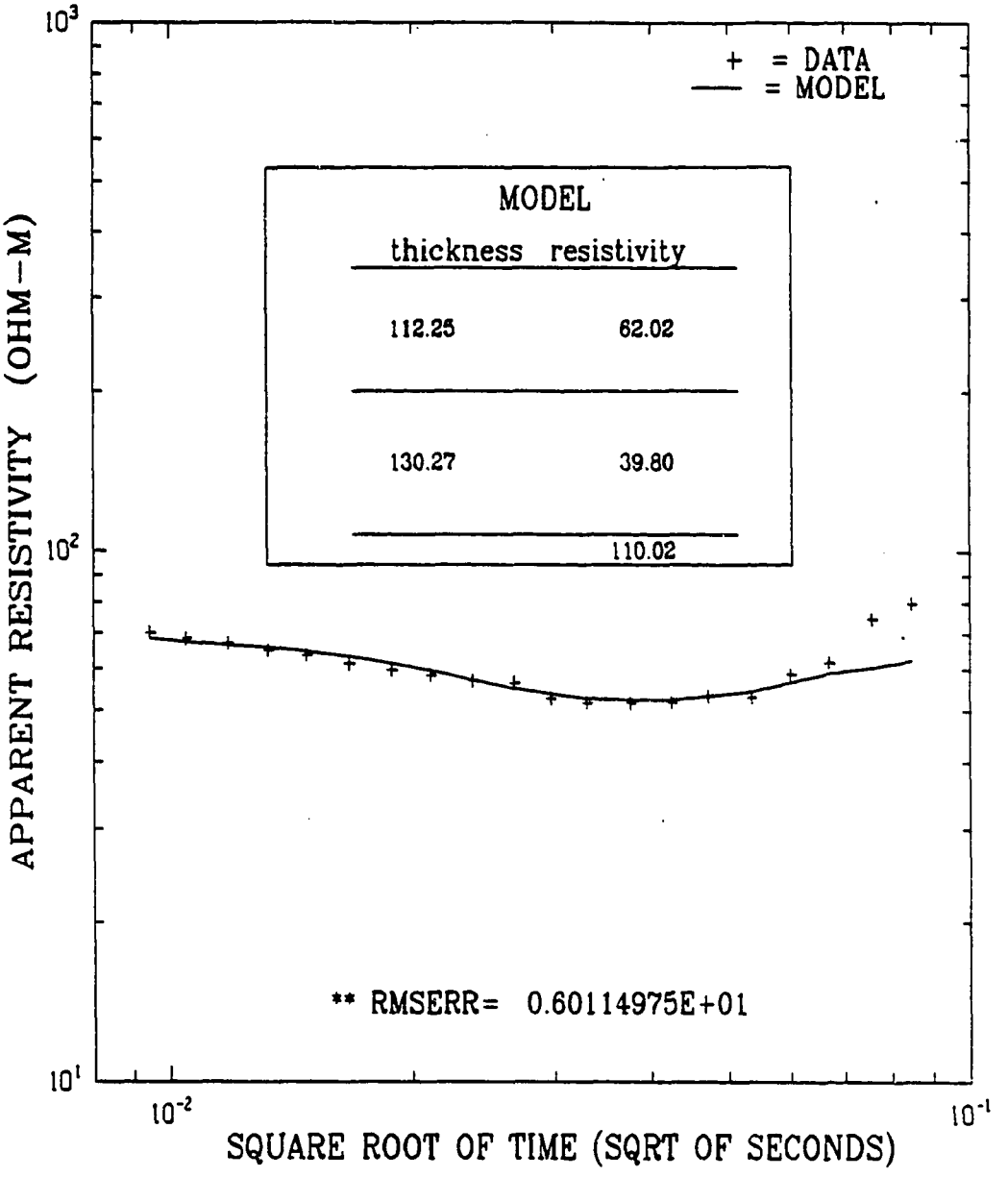

Figure A.29 TEM sounding data and inversion model for the Fielding Lake site.

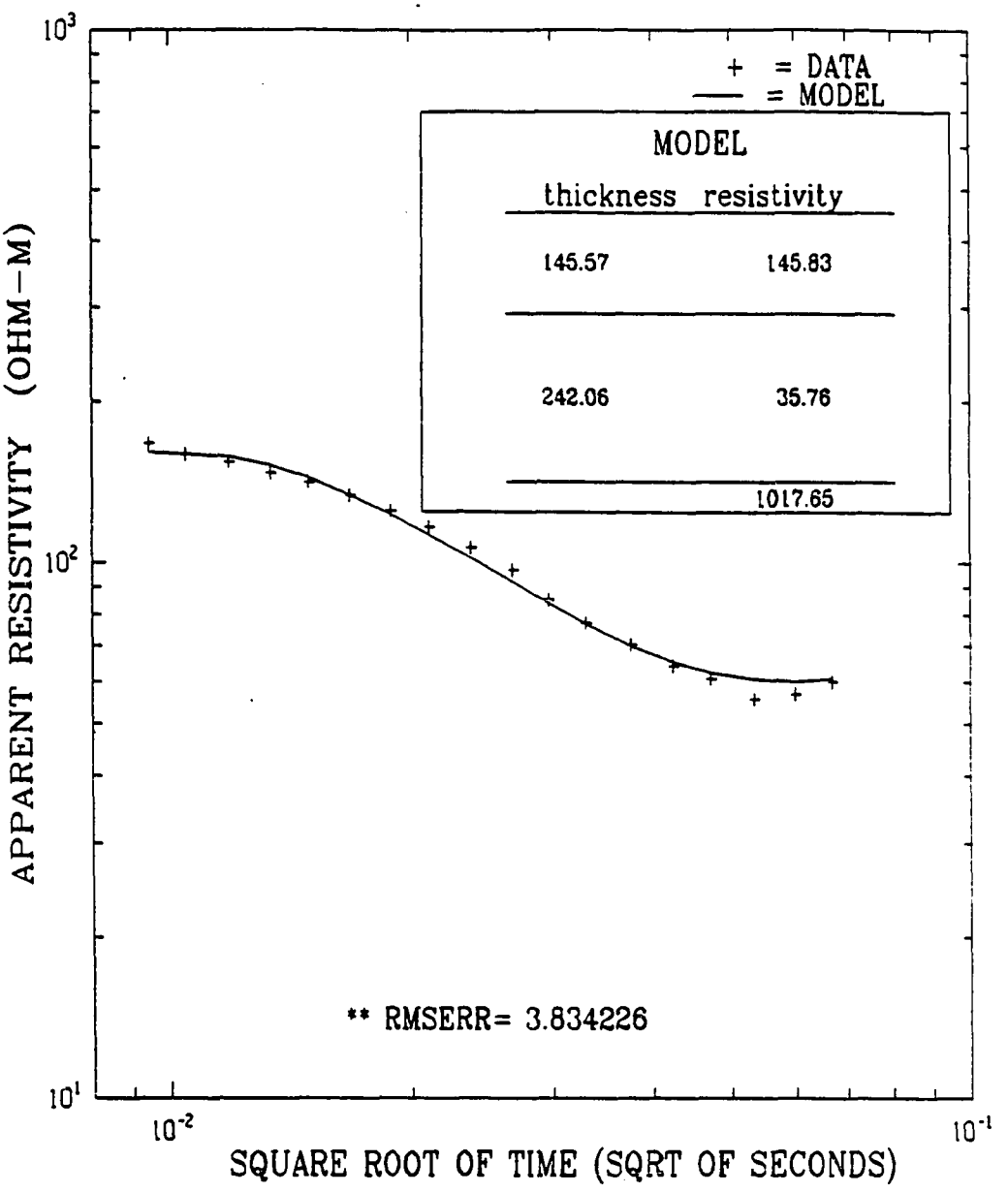

Figure A.30 TEM sounding data and inversion model for the Summit Lake site.

material over bedrock is more resistive than the lower 130 meters; however, the interpretation of the uppermost layer as permafrost is doubtful.

31. Sourdough

The Sourdough site is located about 6 miles north of Sourdough Lodge at a turnout at Richardson Highway Mile 154.5 near Geodetic Survey Marker L8 1923. Unfortunately, the bearing of line one was inadvertently not recorded, but is estimated to be 108 degrees. The terrain was covered with a vegetative mat and uniform small trees of varying types. The overburden here appears to have been deposited in a large ancient glacial lake (for borehole information nearby, see Yehle et al., 1985). This site is near Sourdough Creek which is a tributary of Gulkana River.

The modeling of the data shown in Figure A.31 calls for a first layer 51 meters thick with 463 Ω-m resistivity (interpreted to be permafrost). The second layer is 198 meters thick with a resistivity of 132 Ω-m and overlies bedrock with a resistivity of nearly 75,000 Ω-m. The nearby temperature borehole indicates a MAST of about $-0.5°$ C. Logs of this drillhole shows permafrost occurs to at least a depth of 60 meters, the limit of the borehole.

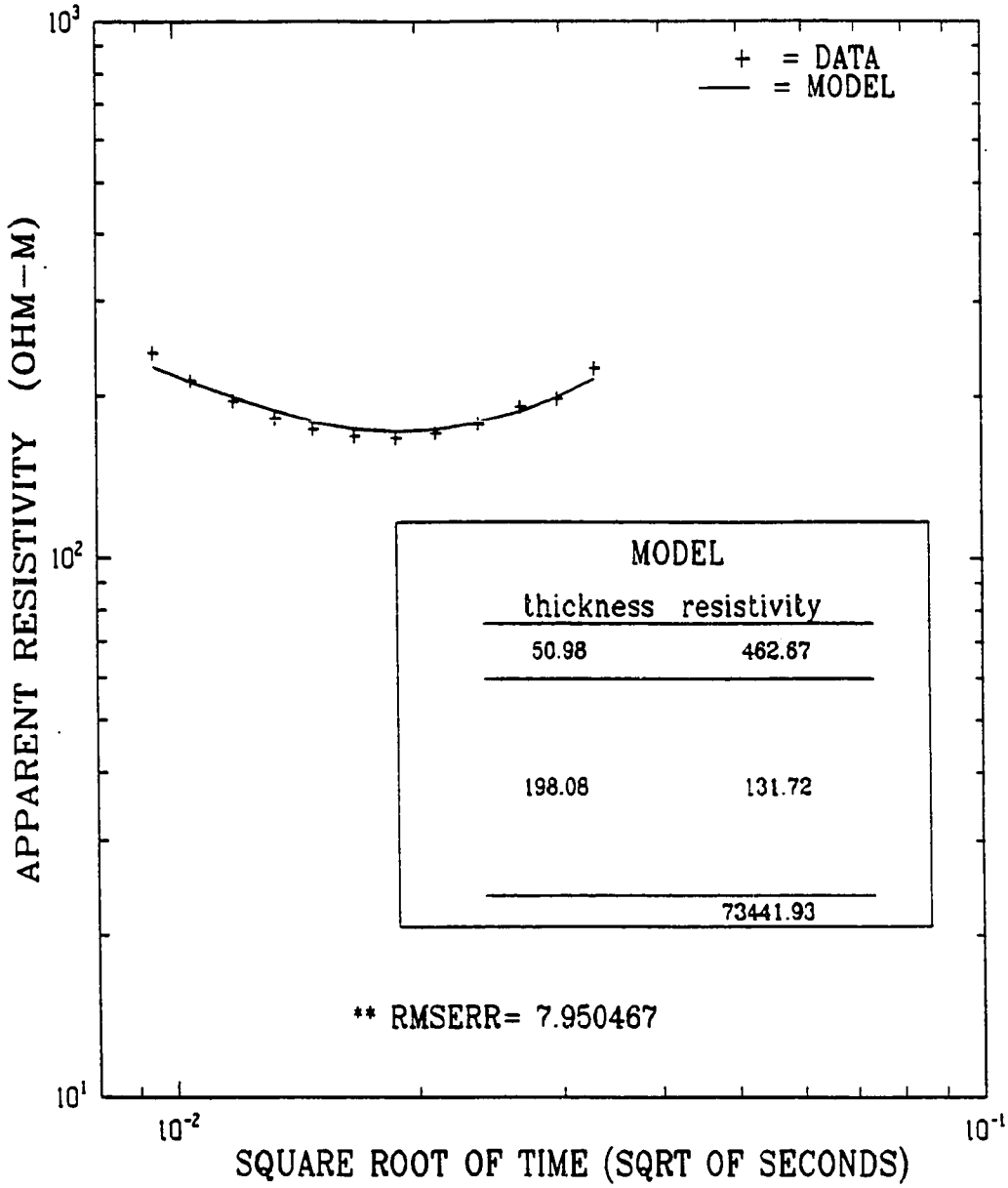

Figure A.31 TEM sounding data and inversion model for the Sourdough site.

32. Glennallen

The southernmost site, near Glennallen, Alaska, is accessed by a dirt road along a section line directed west of Richardson Highway Mile 120.1. The dirt road is just north of the Gulkana airport. The site is on the north side of the dirt road, 0.35 miles from the main highway with line one bearing 18 degrees. The land is flat with tussocks and occasional willows and berry bushes.

The data for this site is shown in Figure A.32. Modeling of the data indicates there are about 31 meters of frozen material (779 Ω-m resistivity) overlying material that decreases in resistivity with depth. There is little evidence of the occurrence bedrock in the sounding. The total depth to a very conductive layer (high salinity for 6 Ω-m) is about 120 meters. Nearby temperature borehole information indicates the existence of an abrupt change in lithology at about 30 meters depth and a permafrost thickness of about 37 meters. The occurrence of high salinity layers in the deposits of the Copper River Basin is thought to be attributable to evaporation and subsequent drying of a large lake that existed during the Pleistocene period (Yehle, Odum, and Reneau, 1985).

SUMMARY

The data from 32 TEM sounding sites located roughly along the Trans Alaska Pipeline from Prudhoe Bay to Glennallen were interpreted, whenever possible, in terms of a geoelectric model of horizontal layers. Each layer has uniform simple resistivity and thickness. The geoelectric model is derived by computer inversion

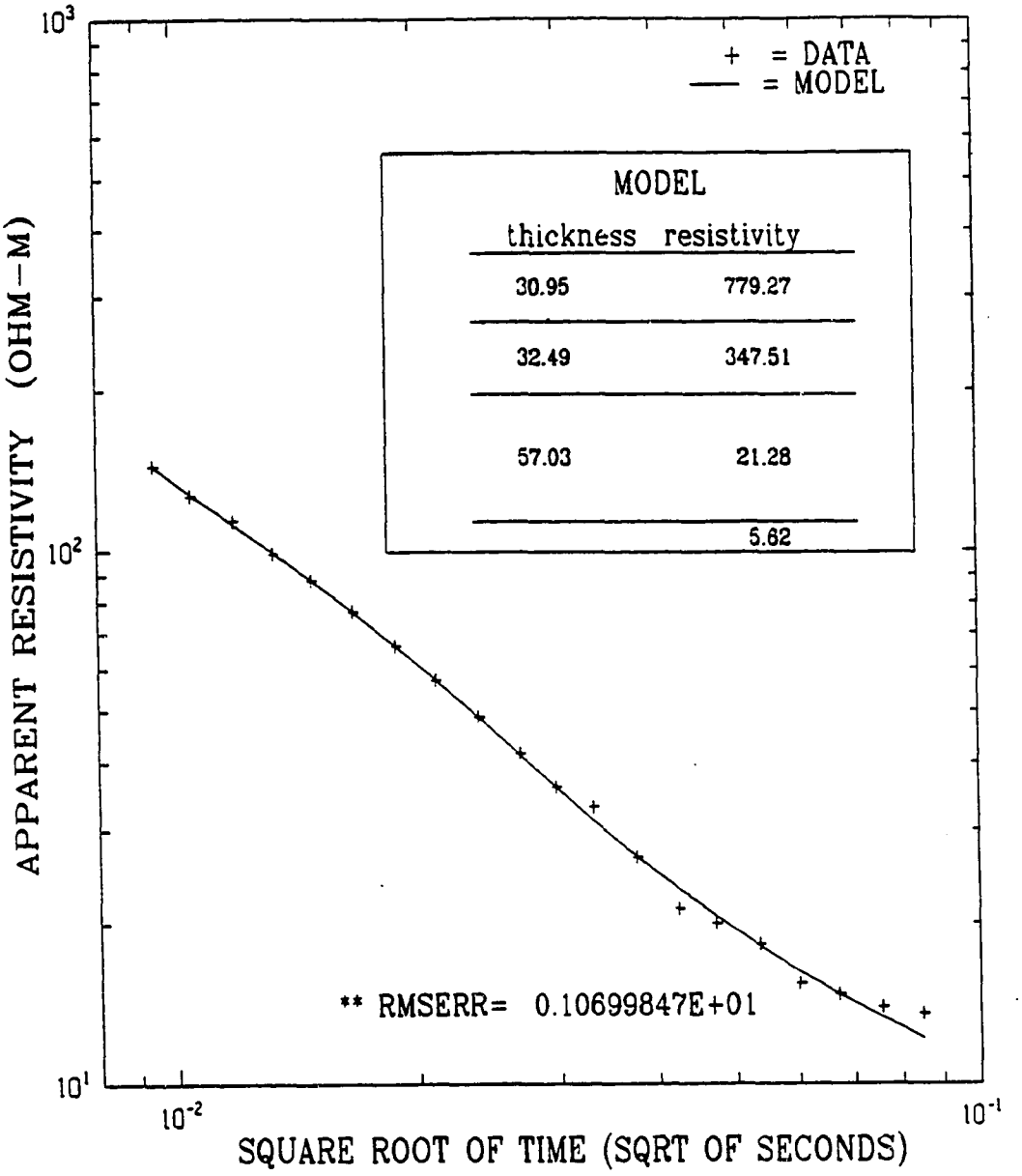

Figure A.32 TEM sounding data and inversion model for the Glennallen site located west of the Gulkana airport.

using a non-linear, least squares algorithm. The geoelectric model with the best fit and most reasonable interpretation is used to infer the thickness of permafrost at each site.

The thickness of permafrost from the TEM sites ranged from 605 meters at Prudhoe Bay near the West Dock to zero at Coldfoot, Alaska. As expected, the TEM data indicates a general trend of permafrost thickness decreasing with decreasing latitude. However, the presence and thickness of permafrost varies tremendously depending upon local conditions as is evidenced by the Coldfoot site which is about one-third of the way along the Prudhoe Bay to Glennallen transect. Since these sites were mostly located at widely-spaced intervals in different drainages and in various terrain conditions, the results cannot be used to extrapolate the extent of permafrost between sites.

Some sites could not be interpreted in terms of a geoelectric model because the sounding data displayed sign reversals in the early time. At a few sites where permafrost is known to exist, the data were inadequate to reveal the presence of thin permafrost. At some sites, a lack of ground truth information inhibited modelling and seemingly unrealistic estimates of permafrost are interpreted from the inversion results. The most effective modeling is that which is based on known lithology. Beyond doubt, however, further modeling with more sophisticated models will lead to improved fits to the data.

APPENDIX B. PROGRAMS

B.1 INTRODUCTION

The purpose of this appendix is to present the various programs written in the pursuit of interpreting TEM soundings and the alterations made in program NLSTCI (Anderson, 1982) primarily for the introduction of a complex conductivity to allow for IP effects.

The following sections give the programs RHOA, RESPONS, and IPVAX and explain the operation of the programs. Program RHOA was written in BASIC programming language for operation on an HP-85 computer. RHOA was written to compute the apparent resistivity and repeatability statistics for TEM sounding data, calculate the corrections to be applied to the sounding data for turnoff time, and plot the results. Program RESPONS was written in FORTRAN programming language for operations on a VAX-785 computer. RESPONS was written to compute the step response for a set of data with a known driving function. Program IPVAX was originally FWDTCI written by Anderson as a latest version of program TCILOOP (see Anderson, 1981 for more details on the program operation) in FORTRAN language for VAX-780 series computers. The program IPVAX introduces complex conductivity to Anderson's FWDTCI to allow for induced polarization effects in the forward modeling of TEM soundings.

B.2 PROGRAM RHOA

Program RHOA expects data stored on tape cassettes to be compatible to the format used by Geonics. This format expects each data set to have a header line containing information on the date, site location, turnoff time, frequency of operation, current, receiver polarity, and the data type. Between the header line and various queries for information from the operator, the program has sufficient information to compute an apparent resistivity for the voltages measured at each gate. The format of the tape storage is such that the measured voltages follow the header line. RHOA interacts with the operator and asks for the name of the data set and what type of correction is desired.

The correction for ramp time turnoff assumes a decay of the voltage received of $t^{-5/2}$ as in Equation (2.36), this correction procedure which is used for most of the TEM sites is explained in Section 2.4. Those sites whose data were not mostly in late stage had to be corrected using the full field expression given by Equation (2.34) using an estimate of the resistivity of the half-space from the values of early stage resistivity from the data in the first 4 or 5 gates. This process is also described in Section 2.4. The program calculates the early time resistivity according to Equation (2.37). The sites reported in Chapter 4 were corrected using the full field expression.

In addition, the program will store the calculated results on magnetic tape and plot the data on an HP-7040 plotter, if desired. The calculation of the full field expression (Equation (2.34)) requires the evaluation of the probability integral $\Theta(u)$ and it takes several minutes to compute the corrected apparent resistivity.

On the following pages are a print out of the program RHOA.

```
10 ! ***** PROGRAM "RHOA"  *****
15 PRINT @ PRINT
20 PRINT "DATE IS 14 MAY 1985"
30 M2=1 @ M3=0 @ P=0 @ M5=0
40 DIM V(24),R1(20),T(20),G2$[50
],G1$[50],W(20),G3$[50],R2(20),R
3(20),T3(20),W1(20),C(20),D(20)
50 DIM D1(20),R(20),T1(20),T2(20
),W2(20),V5(20),V6(20),V7(20),S9
(20),E(20),E1(20),U(20),K(20)
55 DIM M(20),S(20),W3(20),R4(20)
,S6(20)
60 MAT W1=ZER@ MAT V5=ZER@ MAT V
6=ZER@ MAT V7=ZER@ MAT S9=ZER@ M
AT K=CON
70 MAT READ D1 ! DISTORTION FACT
ORS FOR TURN ON AND EARLIER PULS
ES
80 DATA 1,1,1,1,1,1,1,1,1,.9975,
.998,.996,.994,.991,.985,.977,.9
62,.944,.918,.881,.832
90 MAT READ T ! GATE TIMES IN
SECONDS FOR 0.3 HZ
100 DATA 1,.00885,.011,.014,.017
7,.022,.028,.0355,.0443,.0564,.0
716
110 DATA .0885,.11,.14,.178,.22,
.285,.355,.445,.564,.716
120 MAT READ C ! CORRECTION FOR
0.3 HZ RECEIVER LOOP ONLY
130 DATA 1,1,1,1,.994,.985,.97,.
955,.94,.92,.9,.88,.855,.836,.81
5,.79,.77,.75,.73,.71,.695
140 R8=0 @ R6=0
150 R9$="N" @ GOTO 170
160 DISP "DO YOU ONLY WISH TO PL
OT FILES? Y=YES" @ INPUT R9$@ IF
 R9$="Y" THEN R8=1 @ GOTO 1240
170 PRINT "PROGRAM 'RHOA' " @ PR
INT
180 DISP "THIS PROGRAM COMPUTES
APPARENT RESISTIVITY "
190 ! L1=2 @ R5=1 @ GOTO 220
200 DISP "WHAT TYPE OF CORRECTIO
N DO YOU WISH?:   0=NONE
                  1=RAMP ONLY "
210 DISP "        2=RAMP AND PUL
SE TURN ON(AND EARLIER PULSES)
 USE 0 FOR EARLY " @ INPUT R5
250 R4=2.5 @ L1=2
260 R4=2.5 @ IF L1\#1 THEN PRINT
"COMPUTED FOR ";R4;"  DECAY"
290 IF R5=0 THEN PRINT "NO CORRE
CTIONS" @ MAT D1=CON@ MAT D=CON@
GOTO 320
300 IF R5=1 THEN PRINT "CORRECTE
D FOR RAMP ONLY" @ MAT D1=CON@ G
OTO 320
310 IF R5=2 THEN PRINT "CORRECTE
D FOR RAMP AND EARLY PULSES" @ G
OTO 320
320 DISP "WHAT IS TRANSMITTER CU
RRENT IN AMPS? DEFAULT IS [20]"
@ ON ERROR GOTO 340 @ INPUT I0
330 OFF ERROR @ GOTO 360
340 OFF ERROR @ I0=20
350 PRINT "CURRENT IS ";I0;" AMP
ERES"
360 DISP "WHAT IS LENGTH OF TRAN
SMITTER LOOP SIDE IN METERS? [10
0]" @ ON ERROR GOTO 380 @ INPUT
L
370 OFF ERROR @ GOTO 390
380 OFF ERROR @ L=100
390 R=L/SQR(PI) @ M=I0*L**2
400 PRINT "FOR RADIUS ";R;" Mete
rs" @ PRINT "   AND TX MOMENT OF
 ";M;" AMP-m"
410 ! THE TRANSMITTER MOMENT IS
 M;  R=RADIUS
420 DISP "WHAT FILENAME FOR THE
DATA SET?" @ INPUT F$@ PRINT "DA
TA FROM ";F$
430 ! DISP "WHAT IS RAMP TIME IN
 SECONDS?" @ INPUT T0
440 DISP "NOW INSERT TAPE CONTAI
NING THE DATA AND PRESS CONT" @
PAUSE
450 IF R8\#0 THEN 490
460 DISP "FROM HOW MANY RECORDS?
" @ INPUT D3@ PRINT D3;"  RECORD
S"
470 D4=1 @ ! DISP "STARTING FROM
 RECORD \#?" @ INPUT D4
480 DISP "BEGINNING AT RECORD ";
D4
490 ASSIGN\# 2 TO F$
500 FOR J=D4 TO D3+D4-1
510 READ\# 2,J;G1$,V()@ DISP "F
ROM ";F$;" RECORD";J @ DISP G1$
520 N=VAL(G1$[29,29]) @ IF J=D4
THEN N1=N
530 T0=V(21)*.001
540 M1=M^(2/3) @ G=2^N
550 FOR I=1 TO 20
560 V(I)=V(I)/G ! ALLOWS AVERAGI
NG DATA SETS WITH DIFFERENT GAIN
 SETTINGS, ( VOLT AT RX LOOP )
570 V5(I)=V(I)^2 @ V6(I)=V6(I)+V
5(I)
580 W1(I)=W1(I)+V(I) @ V7(I)=W1(
I)^2
```

Figure B.1 Lines 10 through 580 of program RHOA used in ramp turnoff time correction.

```
590 S9(I)=SQR((V6(I)-V7(I)/D3)/(
D3-1))
600 NEXT I
610 NEXT J
630 PRINT "V(I) IS VOLTAGE INDUC
ED IN RECEIVER COIL AND S9(I) IS
 THE STANDARD DEVIATION "
640 PRINT "I  V(I)     S9(I)  "
650 FOR I=1 TO 20
655 W1(I)=W1(I)/D3 ! AVERAGE IND
UCED VOLTAGE AT RX COIL
660 PRINT USING "DD,DDDD.DD,DDD.
DDDD" ; I,W1(I),S9(I)
670 NEXT I
680 C1=.019 @ A3=100
690 IF G1$[27,27]="V" THEN A3=10
00 @ C1=.088
700 PRINT "RX LOOP AREA IS ";A3
@ PRINT "K FOR LOOP IS ";C1
710 IF M3>0 THEN GOTO 780
720 IF G1$[27,27]="H" THEN F=.01

730 IF G1$[27,27]="L" THEN F=.1
740 IF G1$[27,27]="V" THEN F=1
750 FOR I=1 TO 20
760 T2(I)=T(I)*F @ NEXT I
770 IF R6=1 THEN 1360
780 M1=M^(2/3) @ G=2^(2*N/3)
790 DISP "PLEASE WAIT"
800 T1=0
810 IF F\#1 THEN MAT C=CON ! CORR
ECTION FOR 0.3 Hz  ONLY
820 PRINT "RAMP TIME IN SECONDS
IS ";T0
830 O7=0 @ O8=0
832 O4=1 ! ! CORRECT FOR RAMP HHS
835 IF O4=1 THEN GOSUB 2020
840 FOR I=1 TO 20
850 IF R5=0 THEN 880
860 D(I)=(1/T0)*(1/(1-R4))*((T2(
I)+T0)^(1-R4)*T2(I)^R4-T2(I))
865 ! RAMP TIME CORRECTION
FACTORS FOR T^2.5 DECAY
880 T2(I)=T2(I)-T1 @ T3(I)=INT(1
0000*SQR(T2(I)))/10000 ! T3 ARRA
Y IS TIME FOR SQR(T) PLOTS
890 W2(I)=W1(I)*K(I)/(C(I)*D1(I)
) ! W2 IS CORRECTED INDUCED VOLT
AGE (MILLIVOLTS) FOR RHOHHS
895 W3(I)=W1(I)/(D(I)*C(I)*D1(I)
) ! W3 IS CORRECTED INDUCED VOLT
AGE (MILLIVOLTS) FOR DECAY
900 ! K(I) ARE CORRECTIONS FOR H
ALF SPACE, D(I) CORRECTIONS FOR
DECAY, D1(I) FOR 0.3 HZ COIL.
910 R3(I)=C1*M1/(ABS(W2(I))^(2/3
)*(T2(I)*1000)^(5/3)) ! THIS IS
LATE STAGE RHOA FOR HHS
915 R4(I)=C1*M1/(ABS(W3(I))^(2/3
)*(T2(I)*1000)^(5/3)) ! THIS IS
LATE STAGE RHOA FOR -5/2 DECAY
917 S6(I)=R3(I)*2*S9(I)/(3*W1(I)
)
920 T6=SQR(2*PI*10^7*T2(I)*R3(I)
)/R ! THIS IS PARAMETER USED TO
DETERMINE EARLY-LATE STAGE
930 IF O7=1 THEN 950
940 IF T6<2 THEN PRINT "EARLY ST
AGE PRIOR TO GATE ";I @ O7=1
950 IF O8=1 THEN 970
960 IF T6>10 THEN PRINT "LATE ST
AGE FROM GATE ";I @ O8=1
970 R2(I)=INT(ABS(W1(I))*PI*R^5/
(3*M*5210))/1000 ! R2 IS EARLY T
IME RHOA
980 W1(I)=INT(100*W1(I))/100
990 NEXT I
1000 PRINT "GATE  RHO   RHO
 RHO      "
1005 PRINT "      EARLY  HHS
DECAY  HHS"
1010 FOR I=1 TO 20
1020 PRINT USING "DD,DDDD.DD,DDD
DD.DD,DDDDD.DD,DDD.DD" ; I,R2(I)
,R3(I),R4(I),S6(I)
1030 NEXT I
1040 DISP "END OF COMPUTATION  D
O YOU WISH TO STORE REDUCED DATA
 IN A DATA FILE?"
1050 DISP "Y=YES" @ INPUT B$
1060 IF B$="Y" THEN 1070 ELSE 12
10
1070 !
1080 DISP "UNDER WHAT NAME AND R
ECORD : FILENAME,RECORD?" @ INPU
T H$,D2
1090 R2=1 @ GOTO 1110 @ ! DISP "
HAS THE FILE BEEN CREATED ALREAD
Y? Y=YES" @ INPUT R9$
1100 IF R9$="Y" THEN R2=1
1110 PRINT "DATA STORED UNDER FI
LE NAME  ";H$;" RECORD ";D2
1120 DISP "NOW INSERT TAPE TO CO
NTAIN DATA AND PRESS CONT" @ PAU
SE
1130 IF R2=1 THEN 1150 ! FLAG TH
AT FILE HAS ALREADY BEEN CREATED

1140 CREATE H$,8,256
1150 IF R5=1 THEN G1$[1,4]=" R
"
1160 IF R5=2 THEN G1$[1,4]=" RT
"
1170 IF R5=0 THEN G1$[1,4]=" *
"
1180 G1$[30,30]="r" @ ASSIGN\# 4
TO H$ @ R7=1
```

Figure B.1 (Continued) Lines 590 through 1180 of program RHOA used in ramp turnoff time correction.

```
1190 PRINT\# 4,D2 ; G1$,R3()
1200 !
1210 !
1220 IF R7=1 THEN ASSIGN# 4 TO *
1230 DISP "DO YOU WISH TO PLOT A
NY FILES?  Y=YES" @ INPUT R7$@ I
F R7$\#"Y" THEN 2000
1240 IF M5=1 THEN D1=D1+1 @ GOTO
 1270
1250 DISP "WHAT FILENAME,RECORD
DO YOU WISH TO PLOT" @ INPUT F$,
D1@ M5=1
1260 DISP "INSURE THAT TAPE CONT
AINING ";F$;" IS IN PLACE AND PR
ESS CONT" @ PAUSE
1270 ASSIGN\# 2 TO F$
1280 READ\# 2,D1 ; G1$,V()@ DISP
"FROM ";F$;" RECORD ";D1 @ DISP
G1$,"THIS IS THE HEADER"
1290 IF G1$[27,27]="H" THEN F=.0
1
1300 IF G1$[27,27]="L" THEN F=.1

1310 IF G1$[27,27]="V" THEN F=1
1320 FOR I=1 TO 20
1330 T2(I)=T(I)*F @ NEXT I
1340 R6=1 @ R8=2
1350 IF P>0 THEN 1780
1360 DISP "THIS PROGRAM PLOTS EM
37 APPARENT RESISTIVITY FILES"
1370 DISP "WHAT SCALES DO YOU WI
SH? A=1 TO 100 ; B=10 TO 1000 ;
C=100 TO 10000" @ INPUT Z$
1380 PLOTTER IS 705 @ P=0
1390 LIMIT 0,160,0,190
1400 LOCATE 20,96,20,95
1410 B1=.009 @ B2=1
1420 IF Z$="A" THEN A1=1 @ A2=10
0
1430 IF Z$="B" THEN A1=10 @ A2=1
000
1440 IF Z$="C" THEN A1=100 @ A2=
10000
1450 SCALE LOG(B1),LOG(B2),LOG(A
1),LOG(A2)
1460 IF P>0 THEN 1780
1470 FOR Y=A1 TO A2/10 STEP A1
1480 XAXIS LOG(Y)
1490 IF RMD(Y,A1)\#0 THEN 1520
1500 MOVE LOG(B1),LOG(Y) @ LORG
8
1510 LABEL USING "DDDDD,AA" ; Y,
"--"
1520 NEXT Y
1530 FOR Y=2*A2/10 TO A2 STEP A2
/10
1540 XAXIS LOG(Y)
1550 MOVE LOG(B1),LOG(Y) @ LORG
8
1560 LABEL USING "DDDDD,AA" ; Y,
"--"
1570 NEXT Y
1580 MOVE LOG(B1*11),LOG(A1*.55)
 @ LORG 6 @ LDIR 0
1590 LABEL "SQUARE ROOT OF TIME"

1600 MOVE LOG(B1*.4),LOG(A1*10)
@ LORG 5 @ LDIR 0,1
1610 LABEL "APPARENT RESISTIVITY
 (OHM-METERS)"
1620 FOR X=B1 TO .01 STEP .001
1630 YAXIS LOG(X)
1640 MOVE LOG(X),LOG(A1*.85) @ L
ORG 5 @ LDIR 0,1
1650 CSIZE 2
1660 LABEL X
1670 NEXT X
1680 FOR X=.02 TO .1 STEP .01
1690 YAXIS LOG(X)
1700 MOVE LOG(X),LOG(A1*.85) @ L
ORG 5 @ LDIR 0,1
1710 LABEL X
1720 NEXT X
1730 FOR X=.2 TO 1 STEP .1
1740 YAXIS LOG(X)
1750 MOVE LOG(X),LOG(A1*.9) @ LO
RG 5 @ LDIR 0,1 @ LABEL X @ NEXT
 X
1760 MOVE LOG(B1*2),LOG(A2*1.5)
1770 CSIZE 10 @ LDIR 0 @ LABEL "
FILES:"
1780 ! PEN 1
1790 DISP "PLACE DESIRED COLOR I
N RIGHT PEN HOLDER AND PRESS CON
T" @ PAUSE
1800 PEN 2
1810 FOR I=1 TO 20
1820 T3(I)=SQR(T2(I))
1830 PLOT LOG(T3(I)),LOG(ABS(V(I
))
1840 NEXT I
1850 ON P+1 GOTO 1860,1870,1880,
1890,1900,1910,1920,1930,1940
1860 MOVE LOG(.05),LOG(A2*1.8) @
 GOTO 1950
1870 MOVE LOG(.1),LOG(A2*1.8) @
GOTO 1950
1880 MOVE LOG(.3),LOG(A2*1.8) @
GOTO 1950
1890 MOVE LOG(.04),LOG(A2*1.2) @
 GOTO 1950
1900 MOVE LOG(.09),LOG(A2*1.2) @
 GOTO 1950
1910 MOVE LOG(.2),LOG(A2*1.2) @
GOTO 1950
1920 MOVE LOG(.5),LOG(A2*1.2) @
GOTO 1950
1930 MOVE LOG(.04),LOG(A2*2.2) @
 GOTO 1950
```

Figure B.1 (Continued) Lines 1190 through 1930 of program RHOA used in ramp turnoff time correction.

```
1940 MOVE LOG(.2),LOG(A2*2.2) @
GOTO 1950
1950 CSIZE 3 @ LABEL F$,D1;","
1960 PENUP
1970 DISP "DONE,  DO YOU WISH TO
 PLOT ANOTHER ON THIS GRAPH?  Y=
YES" @ INPUT W$
1980 IF W$\#"Y" THEN 2000
1990 R6=0 @ R8=2 @ P=P+1 @ PEN 1
 @ GOTO 1240
2000 MOVE LOG(.005),LOG(5) @ DIS
P "END"
2010 END
2020 !
2030 F3=1
2040 DISP "THIS PROGRAM COMPUTES
 THE CORRECTION FACTORS FOR A HO
MOGENEOUS HALF SPACE"
2050 DISP "HOW MANY DIVISIONS IN
 TO DO YOU WISH?  DEFAULT IS 10"
 @ ON ERROR GOTO 2070 @ INPUT N
2060 OFF ERROR @ GOTO 2080
2070 OFF ERROR @ N=10
2080 ! THE PROGRAM COMPUTES THE
INTEGRAL VIA APPROX WITH A SUM O
F SMALL RECTANGLES
2090 PRINT "FOR ";N;"  DIVISIONS
"
2100 ! DIM T(20),S(20),T1(20),M(
20),E(20),E1(20),K(20),R(20),G$[
50],R1(20)
2110 DISP "WHAT IS RESISTIVITY O
F GROUND?"
2120 DISP " DEFAULT IS 18.9 Ohm-
meters OR LAST " @ ON ERROR GOTO
 2140 @ INPUT R1
2130 OFF ERROR @ GOTO 2150
2140 OFF ERROR @ IF F3=0 THEN 21
50 ELSE R1=18.9
2150 PRINT "FOR EARTH OF ";R1;"
ohm-meters"
2160 ! THIS PROGRAM ASSUMES RECE
IVER LOOP MOMENT IS 5210
2170 M2=5210
2180 A=3*I0*M2*R1/R^3 @ PRINT "A
 IS";A
2190 B=R*SQR(2*PI/(R1*10000000))
 @ PRINT "B IS ";B
2200 DISP "PROGRAM IS RUNNING!!!
"
2210 W=SQR(PI) @ Z=SQR(2) @ F6=1
 @ F7=1
2230 !     COMPUTE S(I)
2235 !  STEP RESPONSE FOR HHS
2270 FOR I=1 TO 20
2280 T=T2(I) @ U(I)=B/SQR(T) @ U
=U(I) @ ! U IS VARIABLE IN ERROR
 FUNCTION (ERF)
2290 IF F6=0 THEN 2310
2300 IF 2*PI/U>2 THEN PRINT "***
 EARLY STAGE AT GATE";I;"  ***"
@ F6=0
2310 IF F7=0 THEN 2330
2320 IF 2*PI/U>10 THEN PRINT "**
* LATE STAGE AT GATE ";I;"  ***"
 @ F7=0
2330 F1=EXP(-(U^2/2)) @ ! F1 IS
MULTIPLIER FOR ERF
2340 E1(I)=SQR(2)*F1*(U+U^3/3)/W

2350 IF U/Z<=3 THEN 2370
2360 IF U/Z>3 THEN 2440
2370 Q0=0 @ F9=1 @ Q=U
2380 FOR K=1 TO INF
2390 F9=F9*K
2400 Q0=(-1)^K*U^(2*K+1)/((2*K+1
)*F9*2^K) ! NEXT TERM IN SERIES
FOR ERF
2410 Q=Q+Q0
2420 IF ABS(Q0)<.0000001 THEN 25
10
2430 NEXT K
2440 Q0=0 @ F9=1 @ Q=1/U
2450 FOR K=1 TO INF
2460 F9=F9*(2*(K-1)+1)
2470 Q0=(-1)^K*F9/U^(2*K+1) ! NE
XT TERM IN SERIES FOR ERF(U) WIT
H U>3
2480 Q=Q+Q0
2490 IF ABS(Q0)<=.0001 THEN 2520

2500 NEXT K
2510 E(I)=Z*Q/W @ GOTO 2530 ! TH
IS IS ERF(U) FOR U<3
2520 E(I)=1-Z*F1*Q/W @ ! THIS IS
 ERF(U) FOR U>3
2530 S(I)=A*(E(I)-E1(I)) @ ! DIS
P E(I),U ! S IS TOTAL FIELD AT G
ATE
2540 NEXT I
2550 ! NOW COMPUTE THE INTEGRAL
FOR M(I) WHERE M(I)=(1/T0)*INTEG
RAL FROM GATE TIME TO GATE TIME
2560 ! PLUS T0 OF:S(t)dt APPROX
THE INTEGRAL WITH N DIVISIONS US
ING S EVALUATED AT MIDPOINT
2580 !    FINDING  M(I)
2600 PRINT "COMPUTED CORRECTIONS
 ARE:       GATE  U(I)  S(I)  M(
I)  K(I)"
2610 FOR I=1 TO 20
2620 M(I)=0
2630 FOR J=1 TO N
2640 T=T2(I)+T0*(J-.5)/N @ U=B/S
QR(T) @ !
2650 F1=EXP(-(U^2/2)) @ F2=SQR(F
1)
```

Figure B.1 (Continued) Lines 1940 through 2650 of program RHOA used in ramp turnoff time correction.

```
2660 Z=SQR(2)
2670 Q1=Z*F1*(U+U^3/3)/W
2680 IF U/Z<=3 THEN 2700
2690 IF U/Z>3 THEN 2780
2700 Q0=0 @ F9=1 @ Q=U
2710 FOR K=1 TO INF
2720 F9=F9*K
2730 Q0=(-1)^K*U^(2*K+1)/((2*K+1
)*F9*2^K) ! NEXT TERM IN SERIES
FOR ERF
2740 Q=Q+Q0
2750 IF ABS(Q0)<.0000001 THEN 28
60
2760 !
2770 NEXT K
2780 Q0=0 @ F9=1 @ Q=1/U
2790 FOR K=1 TO INF
2800 F9=F9*(2*(K-1)+1)
2810 Q0=(-1)^K*F9/U^(2*K+1) ! NE
XT TERM IN SERIES FOR ERF(U) WIT
H U>3
2820 Q=Q+Q0
2830 IF ABS(Q0)<=.0001 THEN 2850

2840 NEXT K
2850 Q=1-Z*F1*Q/W @ GOTO 2870 @
! FOR U>3
2860 Q=Z*Q/W ! FOR U<3
2870 S=A*(Q-Q1) @ ! DISP Q,U ! V
ALUE AT MIDPOINT
2880 M(I)=M(I)+S/N ! THIS IS APP
ROX FOR INTEGRAL
2890 K(I)=S(I)/M(I)
2900 NEXT J
2910 PRINT I;INT(1000*U(I))/1000
;INT(1000*S(I))/1000;INT(1000*M(
I))/1000;INT(1000*K(I))/1000
2920 NEXT I
2930 ! ********      **********
2940 !    FACTORS K(I)
2950 RETURN
```

Figure B.1 (Continued) Lines 2660 through 2950 of program RHOA used in ramp turnoff time correction.

B.3 PROGRAM RESPONS

This program computes the step response from a set of data with a known driving function. This program is applicable for sets of data which are ill behaved e.g. data with sign changes. This type of data cannot be corrected by the program RHOA since the data does not decay as $t^{-5/2}$ nor can the full field expression be used.

RESPONS fits the data with a cubic spline and produces a new data set which is equally spaced in time and has more points per decade in time. This makes the the convolution process more straightforward. The new data set are deconvolved using the known drive function to find the impulse response function. The impulse response function is then convolved with a step function to produce the desired step response.

The following pages give a print out of program RESPONS.

```
C WRITTEN BY GERALD WALKER, THIS PROGRAM COMPUTES THE STEP RESPONSE
C FOR A SET OF DATA WITH A KNOWN DRIVING FUNCTION
PARAMETER MLM=891, MDIM=20, NR=100
DIMENSION X(MDIM), Y(MDIM), R(MLM+NR), H(MLM), DER(2), XX(MLM), YY(MLM),
@ S(MDIM), A(MDIM), B(MDIM), C(MDIM), P(MDIM), H1(MLM+NR), RS(MLM+NR),
@ ERR(MLM), RS2(MLM+NR), R2(MLM+NR), UNIT(MLM+NR), STEPR1(MLM+NR),
@ STEPR2(MLM+NR), YY1(MLM)
DATA DER/0., 0./
M1=MLM+2*NR
M=MDIM
NR1=76
NR2=32
C READ INPUT DATA
DO 11 I=1, M
READ(14, *)X(I), Y(I)
11 CONTINUE
C
C FIT INPUT DATA Y(I) WITH CUBIC SPLINE
CALL SPLIN1(M, 0.0, X, Y, A, B, C, 0, DER, P, S)
C
C NOW FIND VALUES FOR DATA AT EQUAL TIME INCREMENTS YY(I) AT XX(I)
CALL SPOINTM(M, X, Y, A, B, C, XX, YY, MLM)
DO 70 I=1, 20
70 WRITE(6, *)XX(I), YY(I)
C
C DEFINE THE STEP FUNCTION UNIT(I)
DO 60 I=1, MLM+NR
60 UNIT(I)=1.
C
C DEFINE THE DRIVE FUNCTION R1
RNR=1.*NR1
WRITE(6, *)
DO 20 I=1, NR1
R(I)=I/RNR
20 CONTINUE
DO 21 I=NR1, MLM+NR1
21 R(I)=1.
C
C DECONVOLVE THE DRIVE FROM THE DATA YY TO FIND THE IMPULSE RESPONSE H(I)
CALL DECONVO(MLM, YY, R, NR1, H)
C
C CONVOLVE THE DRIVE WITH THE IMPULSE RESPONSE AS A CHECK
CALL CONVOLV(MLM, YY, H, R, NR1, RS, H1)
C
C FIND THE ERROR BETWEEN THE DATA YY(I) AND THE RESPONSE RS(I)
DO 23 I=1, MLM
ERR(I)=YY(I)-RS(I)
23 CONTINUE
C
C CONVOLVE THE DRIVE WITH THE STEP FUNCTION TO GET STEP RESPONSE
CALL CONVOLV(MLM, YY, H, UNIT, NR1, STEPR1, H1)
C
C DEFINE SECOND DRIVE FUNCTION R2(I)
```

Figure B.2 Program RESPONS used to find the step response for ill behaved TEM data using a convolution-deconvolution process.

```
      RNR2=NR2*1.
      DO 40 I=1, NR2
   40 R2(I)=1/RNR2
      DO 41 I=NR2, MLM+NR2
   41 R2(I)=1.
      C
      C READ THE SECOND DATA SET
      DO 50 I=1, M
      READ(11, *)X(I), Y(I)
      WRITE(6, *)X(I), Y(I)
   50 CONTINUE
      C
      C FIT INPUT DATA Y(I) WITH CUBIC SPLINE
      CALL SPLIN1(M, 0.0, X, Y, A, B, C, 0, DER, P, S)
      C
      C NOW FIND VALUES FOR DATA AT EQUAL TIME INCREMENTS YY(I) AT XX(I)
      CALL SPOINTM(M, X, Y, A, B, C, XX, YY1, MLM)
      C
      C DECONVOLVE THE DRIVE FROM THE DATA YY TO FIND THE IMPULSE RESPONSE H(I)
      CALL DECONVO(MLM, YY1, R2, NR2, H)
      C
      C CONVOLVE THE SECOND IMPULSE FUNCTION WITH STEP
      CALL CONVOLV(MLM, YY1, H, UNIT, NR2, STEPR2, H1)
      C
      WRITE(6, *)'I DATA1 DATA2 ERROR1 STEPR2
     2 STEP RESPONSE 1'
      DO 42 I=1, 40
   42 WRITE(6, 43)I, YY(I), YY1(I), ERR(I), STEPR2(I), STEPR1(I)
   43 FORMAT(2X, I4, 5(2X, E10.4))
      END
      C
      C
      SUBROUTINE CONVOLV(MLM, YY, H, R, NR, RS, H1)
      C CONVOLUTION ROUTINE CONVOLVES INPUT FUNCTION R WITH IMPULSE RESPONSE
H
      C BY GERALD WALKER
      DIMENSION XX1(1), YY1(1), R(MLM+NR), RS(MLM+NR), H(MLM),
     2 H1(MLM+NR)
      C H1: EXTENDED ARRAY FOR CONVOLUTION EASE
      C
      C INITIALIZE RS
      DO 4 I=1, MLM+NR
    4 RS(I)=0.
      C EXTEND IMPULSE RESPONSE ARRAY WITH ZEROS
      DO 1 I=1, MLM
      H1(I)=H(I)
    1 CONTINUE
      DO 5 I=1, NR
    5 H1(MLM+I)=0.
      C COMPUTE CONVOLUTION PRODUCT RS
      DO 2 I=1, MLM+NR
      DO 3 J=1, I
      RS1=R(J)*H1(I-J+1)
```

Figure B.2 (Continued) Program RESPONS used to find the step response for ill behaved TEM data using a convolution-deconvolution process.

```
3 RS(I)=RS(I)+RS1
2 CONTINUE
RETURN
END
C
C
SUBROUTINE DECONVO(MLM, YY, R, NR, H)
DIMENSION YY(MLM), R(MLM+NR), H(MLM)
REAL SUM
H(1)=YY(1)/R(1)
DO 2 I=2, MLM
SUM=0.0
DO 1 J=1, I-1
1 SUM=SUM+H(J)*R(I-J+1)
2 H(I)=(YY(I)-SUM)/R(1)
C WRITE(6, *)I, H(I)
RETURN
END
C
C
SUBROUTINE SPLIN1(M, H, X, Y, A, B, C, IT, D, P, S)
C-ONE DIMENSIONAL CUBIC SPLINE COEFFICIENT DETERMINATION.
C BY W.L.ANDERSON, U.S. GEOLOGICAL SURVEY, DENVER, COLORADO
C
C PARMS— M= NUMBER OF DATA POINTS .GT. 2
C H= EQUAL INTERVAL OPTION WHEN H.GT.0. (USE DUMMY X HERE),
C UNEQUAL INTERVALS IF H=0. (X REQUIRED STORAGE)
C X= INDEP.VAR WHEN H=0. (DIM .GE. M).
C Y= DEPENDENT VARIABLE (DIM .GE. M).
C A, B, C=COEFF.ARRAYS (EACH DIM .GE. M)
C RESULTS ARE RETURNED IN 1ST(M-1) ELEMENTS OF A, B, &C.
C ALSO USED AS WORK ARRAYS DURING EXECUTION.
C IT= TYPE OF BOUNDARY CONDITION SUPPLIED IN D ARRAY. USE
C IT=1 IF 1ST DERIVATIVES GIVEN AT END POINTS, OR
C IT=0 IF 2ND DERIVATIVES GIVEN AT END POINTS.
C D= BOUNDARY ARRAY (DIM 2) AT POINT 1 AND M RESPECTIVELY.
C P, S= WORK ARRAYS (EACH DIM=M).
C-ERROR RETURN WITH M=-(ABS(M)) IF ANY PARM OUT OF RANGE.
C THE RESULTING CUBIC SPLINE IS OF THE FORM:
C Y=Y(I)+A(I)*(X-X(I))+B(I)*(X-X(I))**2+C(I)*(X-X(I))**3
C FOR I=1, 2, ..., M-1
C
C
REAL*4 X(1), Y(1), A(1), B(1), C(1), D(2), P(1), S(1), MUL
IF(IT.LT.0.OR.IT.GT.1.OR.H.LT.0..OR.M.LT.3) GO TO 999
N=M-1
IF(IT.EQ.0) GO TO 20
C-1ST DERIVATIVE BOUNDARIES GIVEN
NE=N-1
IF(H) 999, 11, 1
C-EQUAL SPACING H .GT. 0. AND IT=1
1 HH=3.0/H
DO 2 I=1, NE
```

Figure B.2 (Continued) Program RESPONS used to find the step response for ill behaved TEM data using a convolution-deconvolution process.

```
      B(I)=4.0
      C(I)=1.0
      A(I)=1.0
    2 P(I)=HH*(Y(I+2)-Y(I))
      P(1)=P(1)-D(1)
      P(NE)=P(NE)-D(2)
C-SOLUTION OF TRIDIAGONAL MATRIX EQ. OF ORDER NE
    3 C(1)=C(1)/B(1)
      P(1)=P(1)/B(1)
      DO 4 I=2, NE
      MUL=1.0/(B(I)-A(I)*C(I-1))
      C(I)=MUL*C(I)
    4 P(I)=MUL*(P(I)-A(I)*P(I-1))
C-OBTAIN SPLINE COEFFICIENTS
      A(NE+IT)=P(NE)
      I=NE-1
    5 A(I+IT)=P(I)-C(I)*A(I+IT+1)
      I=I-1
      IF(I.GE.1) GO TO 5
      IF(IT.EQ.0) GO TO 6
      A(1)=D(1)
      A(M)=D(2)
    6 IF(H.EQ.0.) GO TO 14
      HH=1.0/H
      DO 7 I=1, N
      MUL=HH*(Y(I+1)-Y(I))
      B(I)=HH*(3.0*MUL-(A(I+1)+2.0*A(I)))
    7 C(I)=HH*HH*(-2.0*MUL+A(I+1)+A(I))
      RETURN
C-UNEQUAL SPACING H=0.. AND IT=1
   11 DO 12 I=1, N
   12 S(I+1)=X(I+1)-X(I)
      DO 13 I=1, NE
      B(I)=2.0*(S(I+1)+S(I+2))
      C(I)=S(I+1)
      A(I)=S(I+2)
   13 P(I)=3.0*(S(I+1)**2*(Y(I+2)-Y(I+1))+S(I+2)**2*(Y(I+1)-Y(I)))/
     @ (S(I+1)*S(I+2))
      P(1)=P(1)-S(3)*D(1)
      P(NE)=P(NE)-S(N)*D(2)
      GO TO 3
   14 DO 15 I=1, N
      HH=1.0/S(I+1)
      MUL=(Y(I+1)-Y(I))*HH**2
      B(I)=3.0*MUL-(A(I+1)+2.0*A(I))*HH
   15 C(I)=-2.0*MUL*HH+(A(I+1)+A(I))*HH**2
      RETURN
C-2ND DERIVATIVE BOUNDARIES GIVEN
   20 NE=N+1
      IF(H) 999, 31, 21
C-EQUAL SPACING H .GT. 0 AND IT=0
   21 HH=3.0/H
      DO 22 I=2, N
```

Figure B.2 (Continued) Program RESPONS used to find the step response for ill behaved TEM data using a convolution-deconvolution process.

```
B(I)=4.0
C(I)=1.0
A(I)=1.0
22 P(I)=HH*(Y(I+1)-Y(I-1))
B(1)=2.0
B(NE)=2.0
C(1)=1.0
C(NE)=1.0
A(NE)=1.0
P(1)=HH*(Y(2)-Y(1))-0.5*H*D(1)
P(NE)=HH*(Y(M)-Y(N))+0.5*H*D(2)
GO TO 3
C-UNEQUAL SPACING H=0 AND IT=0
32 S(I+1)=X(I+1)-X(I)
N1=N-1
DO 33 I=1, N1
B(I+1)=2.0*(S(I+1)+S(I+2))
C(I+1)=S(I+1)
A(I+1)=S(I+2)
33 P(I+1)=3.0*(S(I+1)**2*(Y(I+2)-Y(I+1))+S(I+2)**2*(Y(I+1)-Y(I)))/
* (S(I+1)*S(I+2))
B(1)=2.0
B(NE)=2.0
C(1)=1.0
C(NE)=1.0
P(NE)=3.0*(Y(M)-Y(N))/S(M)+0.5*S(M)*D(2)
GO TO 3
999 M=-IABS(M)
RETURN
END
SUBROUTINE SPOINTM(M, XS, YS, AS, BS, CS, XX, YY, MLM)
C-GIVEN CUBIC SPLINE COEFF'S A, B, C, AND M OBS.DATA ARRAYS X, Y
C SPOINTM EVALUATES THE PIECEWISE CUBIC SPLINE ORDINATE YY AT THE
C ABSCISSAS XX, WHERE XX IS IN THE CLOSED INTERVAL (X(1), X(M)).
C
C PARMS M= NUMBER OF POINTS IN SPLINED DATA YS
C YS= SPLINED DATA FROM SPLIN1 (ORIGINAL DATA) SAMPLED AT XS
C XS= TIME POINTS CORRESPONDING TO DATA YS
C AS, BS, CS ARE THE SPLINED COEFFICIENTS FROM SPLIN1
C XX= NEW TIME POINTS EQUALLY SPACED IN TIME, dt=10microseconds
C YY= NEW VALUES OF DATA AT EQUAL TIME SPACING
C MLM= NUMBER OF POINTS IN NEW ARRAYS
C
DIMENSION XS(M), YS(M), AS(M), BS(M), CS(M), XX(MLM), YY(MLM)
L=1
DELTA=80.E-6
DO 1 I=1, MLM
DELTA=DELTA+10.E-6
XX(I)=DELTA
DO 2 K=L, M-1
J=K
IF (XX(I).LE.XS(K+1)) GOTO 3
2 CONTINUE
3 L=K
Z=XX(I)-XS(J)
YY(I)=YS(J)+((CS(J)*Z+BS(J))*Z+AS(J))*Z
1 CONTINUE
RETURN
END
```

Figure B.2 (Continued) Program RESPONS used to find the step response for ill behaved TEM data using a convolution-deconvolution process.

B.4 PROGRAM IPVAX

Alterations made in the program FWDTCI by Anderson (1981) to introduce induced polarization effects resulted in the new program name of IPVAX. On the following pages is a print out of the program IPVAX with the alterations from FWDTCI delineated with at least 4 asterisks (****) on the right hand side of the print out. The primary changes are for the introduction of the Cole-Cole parameters (in the program these are charge, cole, and tau0), the passing of common variables between subroutines expanded to include the new variables, the transformation of the conductivity to a complex parameter, and the actual computation of the complex conductivity using the Cole-Cole model of Chapter 5, Equation (5.5).

```
******   WARNING ******* The following listing is not complete. Many lines  ****
************ from Program FWDTCI.VAX are deleted here to better point out   ****
************ the changes necessary for a complex resistivity.               ****
C PROGRAM NAME IS NOW IP.VAX EDITED BY GERALD WALKER TO PRODUCE AN INDUCED  ****
C POLARIZATION FROM A COMPLEX RESISTIVITY MODELLED WITH A COLE-COLE FORMULA ****
C ALTERATIONS FROM W. ANDERSON'S PROGRAM ARE NOTED WITH THE ASTERICKS: **   ****
C          20 NOVEMBER 1986  UNIVERSITY OF ALASKA GEOPHYSICAL INSTITUTE     ****
C                            FAIRBANKS, ALASKA 99775-0800                   ****
C
C ORIGINALLY: <FWDTCI>: FORWARD TRANSIENT SOUNDINGS FOR
C  A CENTRAL INDUCTION LOOP SYSTEM OF RADIUS A>0.
C
C** VAX-11/780 VERSION:  2/20/86  **
C
C--BY W.L.ANDERSON, U.S. GEOLOGICAL SURVEY, DENVER, COLORADO.
C
C*********************************************************************
C REFERENCES:
C
C   ANDERSON, W.L., 1982, NONLINEAR LEAST-SQUARES INVERSION OF
C     TRANSIENT SOUNDINGS FOR A CENTRAL INDUCTION LOOP SYSTEM:
C     (PROGRAM NLSTCI): USGS OPEN-FILE REPT. 82-1129, 85 P.
C
C   ---------, 1981, CALCULATION OF TRANSIENT SOUNDINGS FOR A
C     CENTRAL INDUCTION LOOP SYSTEM: USGS OPEN-FILE REPT 81-1309.
C
C   ---------, 1982, ADAPTIVE NONLINEAR LEAST-SQUARES SOLUTION FOR
C       CONSTRAINED OR UNCONSTRAINED MINIMIZATION PROBLEMS
C       (SUBPROGRAM NLSOL): USGS OPEN-FILE REPT. 82-68, 65 P.
C
C   ---------, 1984, A GENERAL INTERFACE FOR PRODUCING FORWARD
C       SOLUTION PROGRAMS (SUBPROGRAM FWDSOL): USGS OPEN-FILE REPT.
C       84-348, 43 P.
C
C*********************************************************************
     ******   WARNING *******  Program lines deleted here **********************
      REAL FUNCTION HZLOOP(B2)
C--COSINE-TRANSFORM KERNEL FOR CENTRAL INDUCTION LOOP WITH
C  A>0,R=0, AND Z>=0.0.
C
      DATA PI/3.1415926535897930/                                          ****
      REAL SIG(10),H(10),Z,PI,TAU0(10),CHARGE(10),COLE(10)                 ****
      COMPLEX ZHANKS,ZAC4,K2(10),KS1,ZFLD,COLEC,CSIG(10),CHARGE1,ONE       ****
      COMMON/MODEL/K2,KS1,H,Z,A,R,HMAX,M
      COMMON/COLEP/TAU0,CHARGE,COLE                                        ****
      COMMON/PASS/ZAC4,ANORM,CURI,DC,SIG,B0,BM,SIG1,EPS,ISTEP
      COMMON/SPLN/XS(200),YS(200),AS(200),BS(200),CS(200),NS,ISPLN
      EXTERNAL F3ZH
      DATA ONE/(1.0,0.0)/                                                  ****
      B=SQRT(B2)
      IF(B.LT.B0) GO TO 3
      IF(B.GT.BM) GO TO 4
      IF(ISPLN.EQ.0) GO TO 10
C--ISPLN=1 (NB>0 OPTION)  INTERPOLATE PRE-SPLINED FREQ. FUNCTION
```

Figure B.3 Program IPVAX showing the alterations to the original program by Anderson (1981) marked on the right hand side with asterisks.

```
      CALL SPOINT(NS,XS,YS,AS,BS,CS,B,HZLOOP)
      RETURN
10    F=(B/A)**2/(39.47841762E-7*SIG1)
      KS1=CMPLX(0.0,-7.895683523E-6*F)
      DO 1 I=1,M
      CHARGE1=CMPLX(CHARGE(I),0.0)                                          ******
      COLEC=CMPLX(0.0,2*PI*F*TAU0(I))**COLE(I)                              ******
      CSIG(I)=CMPLX(SIG(I),0.0)*(COLEC+ONE)/(ONE+(ONE-CHARGE1)*COLEC)       ******
1     K2(I)=KS1*CSIG(I)                                                     ******
      ZFLD=ANORM*ZHANKS(1,ANORM,F3ZH,EPS,LL,1) + ZAC4
      ZFLD=CMPLX(CURI,0.0)*ZFLD
      HZLOOP=REAL(ZFLD)/DC
      RETURN
3     HZLOOP=1.0
      RETURN
4     HZLOOP=0.0
      RETURN
      END
 ******   WARNING *******  Program lines deleted here **********************
      SUBROUTINE FCODE(Y,X,B,PRNT,F,IN,IDER)
C--FUNCT. EVAL. FOR 'NLSTCI'
C
C--PARAMETERS--
C       Y=       OBSERVED DEPENDENT VARIABLE ARRAY (DIM. N)
C       X=       OBSERVED INDEPENDENT VARIABLE ARRAY (DIM. N,5)
C       B=       CURRENT PARAMETER ARRAY ESTIMATES (DIM. K)
C       PRNT=    WORK AND PRINT ARRAY (DIM. 5)
C       F=       OUTPUT FUNCTION VALUE EVAL. FOR GIVEN Y,X,B AT OBS. IN
C       IN=      OBSERVATION NO. TO EVAL. F (1<=IN<=N)
C       IDER=    0 IF ANALYTIC DERIVATIVES ARE USED LATER (PCODE CALLED)
C                1 IF ESTIMATED DERIVATIVES USED ONLY (PCODE NOT CALLED)
C [NOTE: CURRENTLY ONLY IDER=1 CAN BE USED; IDER=0 MAY BE ADDED LATER]
C
      REAL*8 X0,X1,TV,FX1,SQPI,XL,XR
      PARAMETER (SQPI=1.772453850905516D0)
      COMPLEX K2(10),KS1,C4,ZA,ZAC4
      REAL Y(1),X(500,5),B(1),PRNT(5),SIG(10),H(10),DER(2),
     1 BSAVE(20),W2(200), APPRES(500),TAR(500,2),
     2 T(500),VSAVE(500)
      EXTERNAL HZLOOP,FCTCI
      COMMON/PASSER/TV,LATE
      COMMON/PASS/ZAC4,ANORM,CURI,DC,SIG,B0,BM,SIG1,EPS,ISTEP
      COMMON/FPASS/AA,TMIN,TMAX,T0,TM,DB,BMTEST, TASY,TOFF,A3,
     * M1,M21,M2,JSPLN,NN,IFIRST,IOPT
      COMMON/SPLN/XS(200),YS(200),AS(200),BS(200),CS(200),NS,ISPLN
      COMMON/MODEL/K2,KS1,H,Z,A,R,HMAX,M
      COMMON/COLEP/TAU0,CHARGE,COLE                                         ******
      DATA DER/2*0.0/,XMU0/1.2566371E-6/
      IF(IN.GT.1.OR.M.EQ.1) GO TO 20
      DO 10 J=2,M
      IF(B(J).EQ.B(J-1)) CALL ERRMSG('SOME SIG(J)=SIG(J-1)',4,6,16)
10    CONTINUE
20    DO 30 J=1,5
30    PRNT(J)=X(IN,J)
```

Figure B.3 (Continued) Program IPVAX showing the alterations to the original program by Anderson (1981) marked on the right hand side with asterisks.

```
      IF(IN.GT.1) GO TO 800
      IF(IDER.EQ.1) GO TO 8001
35    SIG1=B(1)
      RSIG1=1./SIG1
      HMAX=A
      IF(M.EQ.1) GO TO 45
      DO 40 J=1,M1
      H(J)=B(M+J)
40    SIG(J)=B(J)
      CALL MINMAX(H,M1,HMIN,HMAX)
45    SIG(M)=B(M)
      ANORM=A/HMAX
      TCON=6.28318531E-7*SIG1*AA
      IF(JSPLN.EQ.0) GO TO 49
C--GET PRE-SPLINED FREQ FUNCTION (NB>0 OPTION)
      NS=0
      TEM=B0/DB
      ISPLN=0
46    TEM=TEM*DB
      IF(TEM.GE.BMTEST) GO TO 47
      NS=NS+1
      IF(NS.GT.200) CALL ERRMSG('SPLINED NS>200 IN FCODE',3,6,16)
      XS(NS)=TEM
      YS(NS)=HZLOOP(TEM*TEM)
      GO TO 46
47    CALL SPLIN1(NS,0.0,XS,YS,AS,BS,CS,0,DER,T,W2)
      ISPLN=1
49    T0=.5*TMIN/TCON
        TM=TMAX/TCON
C** PRESET FOR POSSIBLE ASYMPTOTIC APPROXIMATION (IF TASY.NE.0.0)
      IF(TASY.NE.0.0) CALL SETASY(B,AA,M)
      NEW=1
      LATE=0
C*****************************************************************
C GET ENTIRE TRANSIENT FOR ALL REAL-TIME IN X(I,1), I=1,NN,
C BEFORE APP.RES. CALC AND POSSIBLE ASYMPTOTIC APPROXIMATIONS.
C*****************************************************************
      DO 70 I=1,NN
      T(I)=X(I,1)/TCON
      IF(TASY.GT.0.0.AND.X(I,1).GE.TASY) GO TO 70
C--GET TRANSIENT IMPULSE RESPONSE VIA LAGGED CONVOLUTION IN TIME.
         TRANS=.63661977*RFLAGS(0,HZLOOP,EPS,T0,TM,T(I),NEW)
         NEW=0
        VSAVE(I)=TRANS                                                    ******
70    CONTINUE
******   WARNING *******  Program lines deleted here **********************
      SUBROUTINE SUBZ(Y,X,B,PRNT,NPRNT,N,TITLE,IOUT)
C-- INITIALIZATION ROUTINE (CALLED ONCE)
C
C  SUBZ IS CALLED BY NLSOL AFTER THE DATA Y(I),X(I,5) ARE READ.
C  SUBZ CHECKS FOR DATA ERRORS, READS ADDITIONAL $INIT
C  PARAMETERS, AND LOADS SOME CONSTANTS IN COMMON STORAGE...
C
C--PARAMETERS--
```

Figure B.3 (Continued) Program IPVAX showing the alterations to the original program by Anderson (1981) marked on the right hand side with asterisks.

```
C       Y,X,B,PRNT SAME AS IN SUBROUTINE FCODE.
C       NPRNT=  CONTROL PARAMETERS TO USE PRNT(NPRNT) ARRAY
C               NPRNT REPRESENTS THE NO. X(I,NPRNT) VALUES
C       N=      NO. OBSERVATIONS GIVEN IN Y(N),X(N,5)
C       TITLE=  ALPHA TITLE ARRAY READ IN BY PGM IMSLMQ.
C       IOUT=   1 IF UNIT 6 AND 16 PRINT FILES USED
C               0 IF ONLY UNIT 6 PRINT FILE USED.
C
      CHARACTER*16 OPT(-1:2)
      COMPLEX K2(10),KS1,C4,ZA,ZAC4
      CHARACTER*80 TITLE
      REAL Y(1),X(500,5),B(1),PRNT(1),SIG(10),H(10),                          *****
     @ TAU0(10),CHARGE(10),COLE(10)                                           *****
      COMMON/PASS/ZAC4,ANORM,CURI,DC,SIG,B0,BM,SIG1,EPS,ISTEP
      COMMON/FPASS/AA,TMIN,TMAX,T0,TM,DB,BMTEST, TASY,TOFF,A3,
     & M1,M21,M2,JSPLN,NN,IFIRST,IOPT
      COMMON/SPLN/FILL(1000),NS,ISPLN
      COMMON/COLEP/TAU0,CHARGE,COLE                                            *****
      COMMON/MODEL/K2,KS1,H,Z,A,R,HMAX,M
      NAMELIST/INIT/MM,A,Z,EPS,B0,BM,NB,ISTEP,IOPT, TASY,TOFF
      DATA ISUBZ/0/,OPT/'Y(I) (VOLTS/AMP)','Y(I)/SIG1',
     1 'APP.RES._1','APP.RES._2'/
      IF(ISUBZ.NE.0) GO TO 10
C--PRESET
      WRITE(6,666)
666   FORMAT('0** FWDTCI IS RUNNING ... PRINT FILE IS FOR016.DAT'/)
******   WARNING *******  Program lines deleted here **********************
      SUBROUTINE FWDSOL(FCODE,SUBZ)
******   WARNING *******  Program lines deleted here **********************
C$$$$$$$$$$$$$$$$$$$$$$$$$$$$$$$$$$$$$$$$
$$$$$$$$$$$$$$$$$$$$$$$$$$$$$$$$
C
      CHARACTER*80 TITLE
      CHARACTER*40 TITLES(4),XT,YT
      CHARACTER*132 LINE
      COMMON/COLEP/TAU0,CHARGE,COLE                                            *****
      DIMENSION B(KDIM),X(NDIM,MDIM),Y(NDIM),W(5),XNX(NDIM),
     1 SIG(10),RHO(10),H(9),TAU0(10),CHARGE(10),COLE(10),                      *****
     2 YFWD(NDIM),XVAR(NDIM)
      EQUIVALENCE (TITLES(1),XT),(TITLES(2),YT)
C**
      NAMELIST/FWD/MM,MODE,SIG,RHO,H,SHIFT,B,
     1 X1,NX,XM,XNX,X2,X3,X4,IPLT,XT,YT,TAU0,CHARGE,COLE                       *****
      NAMELIST/FWD0/MM,MODE,B,
     1 X1,NX,XM,XNX,X2,X3,X4,IPLT,XT,YT
      DATA MODE/1/,IPLT/0/,XT/'X'/,YT/'Y'/,SHIFT/1.0/,
     1 X2/1.0/,X3/1.0/,X4/1.0/
******   WARNING *******  Program lines deleted here **********************

     CALL SUBZ(Y,X,B,W,NPRNT,N,TITLE,1)
 C     ********************************
C
C  WRITE $FWD ON FOR006 AND FOR016
C
```

Figure B.3 (Continued) Program IPVAX showing the alterations to the original program by Anderson (1981) marked on the right hand side with asterisks.

```
C//   WRITE(6,42) TITLE
42    FORMAT(' <FWDSOL>:',5X,A80/2X,'------')                          *******
      WRITE(16,42) TITLE
      OPEN(UNIT=98,STATUS='SCRATCH')
      IF(MODE.NE.0) THEN
        WRITE(98,FWD)
      ELSE
        WRITE(98,FWD0)
      ENDIF
C--REFMT WRITE(98,NAMELIST) TO UNIT=6 AND 16 TO BREAK OUT ARRAY LISTS
      REWIND 98
9910  READ(98,9920,END=9940) LINE
9920  FORMAT(A)
      I=INDEX(LINE,'$')
      IF(I.NE.0) GO TO 9930
      I=INDEX(LINE,'=')
      IF(I.NE.0) GO TO 9930
      LINE(11:)=LINE
      LINE(1:10)=' '
9930  CALL NONBLANK(LINE,I)
      IF(I.EQ.0) I=1
C//   WRITE(6,9920) LINE(1:I)
      WRITE(16,9920) LINE(1:I)
      GO TO 9910
9940  CLOSE(UNIT=98)
C//   WRITE(6,44) TITLE
44    FORMAT('1<FWDSOL>:',5X,A<NB>//3X,'I',4X,'X(I)',12X,'Y(I)'/)
      WRITE(16,44) TITLE
      IF(IPLT.GT.0) OPEN(UNIT=12,STATUS='NEW',CARRIAGECONTROL='LIST')
C
C  NOW GET THE FORWARD SOLUTION VIA FCODE FOR I=1,N
C
      DO I=1,N
          CALL FCODE(Y,X,B,W,F,I,1)
C         ************************
C//       WRITE(6,50) I,X(I,1),F
          WRITE(14,50) I,X(I,1),F                                     *******
50        FORMAT(1X,I3,2E16.8)
          WRITE(16,50) I,X(I,1),F
          YFWD(I)=F
          XVAR(I)=X(I,1)
      ENDDO
      WRITE(14,441) TITLE                                             *******
441   FORMAT(' <IPFWDSOL>:',5X,A<NB>)                                 *******
      IF(IPLT.EQ.0) GO TO 10
C
C  PREPARE FOR012 FOR PLOT12 OUTPUT (IPLT>0)
```

Figure B.3 (Continued) Program IPVAX showing the alterations to the original program by Anderson (1981) marked on the right hand side with asterisks.

APPENDIX C: TRANSIENT SOUNDING DATA

This appendix contains all the sounding data taken during two field seasons for the purpose of permafrost investigation. The following table gives the gate time in seconds for each gate at each transient repetition frequency.

	FREQUENCY		
	H or 30 Hz	L or 3 Hz	V or 0.3 Hz
Gate			
1	.000089	.00089	.0089
2	.000110	.00110	.0110
3	.000140	.00140	.0140
4	.000177	.00177	.0177
5	.000220	.00220	.0220
6	.000280	.00280	.0280
7	.000355	.00355	.0355
8	.000443	.00443	.0443
9	.000564	.00564	.0564
10	.000713	.00713	.0713
11	.000881	.00881	.0881
12	.001096	.01096	.1096
13	.001411	.01411	.1411
14	.001795	.01795	.1795
15	.002224	.02224	.2224
16	.002850	.02850	.2850
17	.003550	.03550	.3550
18	.004490	.04490	.4490
19	.005640	.05640	.5640
20	.007190	.07190	.7190

The sounding data in the subsequent tables are the raw data taken in the field. On the heading line for each data set is the site name, a four digit number for day and month, the year, the transmitter loop size and transmitter frequency, and the transmitter current. For instance:

Site BARTER 0509 1983 400 H 19.1A

means that Barter Island site was sounded on the fifth of September, 1983 with a transmitter loop of 400 meters on a side with a frequency of 30 Hertz and a current of 19.1 amperes. In frequencies, H stands for 30 Hertz, L stands for 3 Hertz, and V stands for 0.3 Hertz.

The next line gives the receiver gain and stack settings for each sounding. This line is labeled n/N where n is the gain setting and N is the stack setting. Note that two adjacent sounding columns have the same n/N settings, but as discussed in the text, the sounding columns differ in receiver polarity. The next line with TO at the beginning gives the turnoff time in milliseconds for each sounding. The line labeled Gate simply gives the primary field strength for each sounding set. All subsequent lines are begun with the gate number. All the recorded numbers are in millivolts as displayed on the receiver console.

APPENDIX C: TRANSIENT SOUNDING DATA CONTINUED

Site	BARTER	0509	1983	400 H	20A			
n/N	3/8	3/8	2/8	2/8	2/10	2/10	3/10	3/10
TO	.300	.300	.300	.300	.300	.300	.300	.300
Gate	597.0	596.0	298.0	298.0	302.0	302.0	608.0	607.0
1	4163.0	4158.0	2040.0	2038.0	2044.0	2036.0	4168.0	4161.0
2	3832.0	3849.0	1879.0	1868.0	1868.0	1863.0	3811.0	3826.0
3	3290.0	3302.0	1604.0	1591.0	1591.0	1586.0	3261.0	3274.0
4	2649.0	2626.0	1281.0	1276.0	1276.0	1284.0	2658.0	2636.0
5	1969.0	1976.0	951.0	944.0	944.0	961.0	1992.0	2000.0
6	1328.0	1327.0	640.0	636.0	644.0	643.0	1338.0	1338.0
7	847.0	848.0	411.0	407.0	405.0	406.0	839.0	841.0
8	536.0	536.0	261.0	259.0	260.0	260.0	536.0	536.0
9	334.0	332.0	162.0	162.0	163.0	161.0	333.0	332.0
10	213.0	210.0	102.0	104.0	106.0	103.0	216.0	213.0
11	151.5	154.4	77.1	73.6	73.9	77.0	151.9	154.9
12	105.0	107.4	53.8	51.0	50.7	53.2	104.2	106.6
13	68.2	70.0	35.1	33.1	33.0	34.8	67.9	69.6
14	44.1	45.7	23.1	21.3	21.5	23.2	44.6	46.1
15	29.4	31.3	16.0	14.0	14.1	16.0	29.7	31.4
16	18.5	20.6	10.8	8.6	8.7	10.8	18.7	20.8
17	11.4	13.4	7.1	5.2	5.1	7.1	11.4	13.3
18	7.1	8.8	4.7	3.1	3.0	4.7	7.1	8.7
19	3.8	5.7	3.2	1.4	1.3	3.3	3.8	5.7
20	1.8	3.8	2.3	0.4	0.4	2.3	1.9	3.7

Site	BARTER	0509	1983	400 L	20A	NWEI2	1984	400 H
n/N	6/12	6/12	5/12	5/12		0507	6/10	6/10
TO	.303	.303	.303	.303		22A	.760	.760
Gate	3241.0	3134.0	1918.0	1977.0			4917.0	5323.0
1	4220.0	6158.0	6160.0	6160.0			27.0	16.0
2	2067.0	6147.0	6177.0	3142.0			-18.0	-14.0
3	1056.0	1948.0	3470.0	7010.0			-53.0	-59.0
4	601.0	902.0	813.0	3978.0			-91.0	-84.0
5	375.0	507.0	371.0	778.0			-114.0	-100.0
6	239.0	297.0	193.0	309.0			-113.0	-116.0
7	143.0	167.0	100.0	138.0			-112.0	-111.0
8	92.0	102.0	57.0	75.0			-94.0	-98.0
9	55.0	64.0	35.0	40.0			-74.0	-75.0
10	33.0	41.0	22.0	21.0			-51.0	-48.0
11	27.0	25.3	12.3	17.6			-32.7	-32.0
12	17.6	16.8	8.1	10.9			-13.8	-13.5
13	11.1	10.3	4.7	6.7			0.0	0.0
14	7.2	6.4	2.8	4.3			7.8	7.4
15	4.8	4.2	1.7	2.9			11.5	11.0
16	3.5	2.3	0.5	2.4			12.3	12.6
17	2.2	1.4	0.2	1.6			12.5	12.7
18	1.6	0.8	0.0	1.3			11.5	11.4
19	1.1	0.3	-0.1	1.0			9.9	9.7
20	0.8	0.1	-0.2	0.8			710.3	590.2

APPENDIX C: TRANSIENT SOUNDING DATA CONTINUED

Site	BARTER	0509	1983	400 H	20A			
n/N	3/8	3/8	2/8	2/8	2/10	2/10		
TO	.298	.298	.298	.298	.298	.298		
Gate	602.0	600.0	300.0	300.0	304.0	303.0		
1	4183.0	4168.0	2050.0	2039.0	2050.0	2047.0		
2	3876.0	3841.0	1883.0	1879.0	1878.0	1869.0		
3	3333.0	3302.0	1607.0	1606.0	1601.0	1591.0		
4	2653.0	2661.0	1291.0	1282.0	1296.0	1294.0		
5	2000.0	1979.0	956.0	953.0	972.0	966.0		
6	1345.0	1333.0	644.0	641.0	651.0	648.0		
7	858.0	850.0	411.0	411.0	411.0	407.0		
8	541.0	538.0	262.0	260.0	262.0	261.0		
9	334.0	334.0	164.0	161.0	162.0	163.0		
10	211.0	213.0	105.0	102.0	104.0	106.0		
11	155.1	151.3	73.9	76.6	77.4	73.8		
12	107.7	105.0	51.3	53.3	53.3	50.7		
13	69.9	68.2	33.3	34.7	34.9	33.0		
14	45.6	44.1	21.5	22.7	23.2	21.5		
15	31.1	29.5	14.2	15.7	16.0	14.1		
16	20.5	18.5	8.7	10.6	10.8	8.6		
17	13.2	11.5	5.3	6.9	7.0	5.1		
18	8.6	7.2	3.2	4.6	4.7	3.0		
19	5.5	3.9	1.5	3.1	3.2	1.3		
20	3.6	2.0	0.5	2.2	2.2	0.4		
Site	NWEI1	2808	1983	400 H	20A			
n/N	5/8	5/8	4/8	4/8	5/10	5/10	4/10	4/10
TO	.319	.319	.319	.319	.319	.319	.319	.319
Gate	2488.0	2500.0	1255.0	1255.0	2553.0	2555.0	1280.0	1273.0
1	2177.0	2190.0	1072.0	1106.0	2305.0	2311.0	1102.0	1101.0
2	1412.0	1419.0	697.0	712.0	1466.0	1473.0	710.0	706.0
3	771.0	775.0	382.0	385.0	793.0	800.0	387.0	381.0
4	386.0	387.0	191.0	193.0	403.0	405.0	196.0	193.0
5	157.0	157.0	77.0	77.0	164.0	167.0	80.0	78.0
6	10.0	10.0	4.0	3.0	12.0	13.0	5.0	3.0
7	-60.0	-60.0	-29.0	-31.0	-61.0	-59.0	-29.0	-31.0
8	-80.0	-80.0	-39.0	-40.0	-81.0	-81.0	-40.0	-40.0
9	-70.0	-71.0	-35.0	-34.0	-70.0	-71.0	-35.0	-34.0
10	-46.0	-47.0	-23.0	-22.0	-46.0	-48.0	-24.0	-22.0
11	-26.2	-26.4	-12.4	-14.8	-28.7	-26.9	-12.6	-14.9
12	-8.9	-9.0	-3.9	-5.7	-10.4	-9.1	-3.9	-5.7
13	2.7	2.6	1.6	0.5	2.0	2.6	1.6	0.5
14	7.9	7.8	4.2	3.2	7.4	7.9	4.3	3.2
15	9.7	9.6	5.1	3.9	9.0	9.7	5.2	4.0
16	9.9	9.7	5.3	3.7	8.8	9.8	5.3	3.8
17	8.9	8.8	4.7	3.4	7.9	8.8	4.7	3.4
18	7.5	7.4	4.0	2.9	6.8	7.4	4.0	2.9
19	6.1	6.0	3.4	2.0	5.1	6.0	3.4	2.0
20	4.8	4.6	2.7	1.3	3.7	4.6	2.7	1.3

APPENDIX C: TRANSIENT SOUNDING DATA CONTINUED

Site	WEST1	2309	1983	400 H	12.5A			
n/N	4/8	4/8	5/8	5/8	5/10	5/10	4/10	4/10
TO	.230	.230	.230	.230	.230	.230	.230	.230
Gate	796.0	795.0	1598.0	1602.0	1623.0	1621.0	809.0	802.0
1	1506.0	1506.0	3109.0	3129.0	3116.0	3097.0	1472.0	1460.0
2	1169.0	1176.0	2400.0	2398.0	2381.0	2384.0	1153.0	1138.0
3	818.0	826.0	1680.0	1675.0	1660.0	1664.0	811.0	797.0
4	602.0	606.0	1229.0	1229.0	1235.0	1234.0	604.0	597.0
5	451.0	456.0	922.0	918.0	932.0	934.0	459.0	452.0
6	335.0	336.0	680.0	680.0	688.0	685.0	337.0	334.0
7	241.0	243.0	491.0	489.0	487.0	487.0	240.0	236.0
8	170.0	170.0	345.0	345.0	346.0	345.0	170.0	168.0
9	116.0	116.0	235.0	235.0	236.0	235.0	116.0	115.0
10	77.0	76.0	155.0	157.0	159.0	157.0	77.0	78.0
11	54.1	56.5	112.4	110.7	111.2	112.4	56.4	53.7
12	35.7	37.7	74.7	73.3	72.9	73.8	37.2	35.0
13	21.2	22.6	44.6	43.7	43.6	44.1	22.3	20.9
14	12.1	13.5	26.1	25.4	25.7	26.2	13.4	12.1
15	6.9	8.4	16.0	15.0	15.1	16.0	8.4	7.0
16	3.5	5.2	9.5	8.2	8.3	9.3	5.1	3.5
17	1.7	3.2	5.5	4.5	4.4	5.3	3.1	1.7
18	0.8	2.1	3.4	2.5	2.5	3.2	2.0	0.8
19	0.0	1.6	2.3	1.2	1.2	2.1	1.5	0.1
20	-0.1	1.3	1.6	0.5	0.5	1.4	1.2	0.0

Site	WEST2	2309	1983	400 L	20A
n/N	8/8	8/8	8/8		
TO	.325	.325	.325		
Gate	5071.0	5051.0	5049.0	0.0	
1	1231.0	1201.0	1232.0	0.0	
2	857.0	826.0	860.0	0.0	
3	524.0	500.0	533.0	0.0	
4	331.0	288.0	321.0	0.0	
5	208.0	181.0	216.0	0.0	
6	140.0	109.0	145.0	0.0	
7	91.0	59.0	97.0	0.0	
8	66.0	35.0	73.0	0.0	
9	54.0	16.0	56.0	0.0	
10	44.0	6.0	45.0	0.0	
11	48.6	-18.9	20.7	0.0	
12	28.8	-9.7	30.8	0.0	
13	24.5	-10.8	30.4	0.0	
14	23.9	-15.5	25.4	0.0	
15	18.0	-13.6	27.2	0.0	
16	46.0	-40.5	1.6	0.0	
17	34.3	-34.7	7.5	0.0	
18	21.6	-28.9	14.1	0.0	
19	13.9	-24.8	12.9	0.0	
20	7.3	-21.7	11.2	0.0	

APPENDIX C: TRANSIENT SOUNDING DATA CONTINUED

Site	DEAD1	2208	1983	400 H	20.1A			
n/N	5/8	5/8	4/8	4/8	6/8	6/8	5/10	5/10
TO	.318	.318	.318	.318	.318	.318	.318	.318
Gate	2553.0	2534.0	1276.0	1268.0	5062.0	4981.0	2589.0	2568.0
1	1747.0	1742.0	865.0	855.0	3489.0	3483.0	1733.0	1716.0
2	1345.0	1335.0	655.0	652.0	2724.0	2703.0	1326.0	1317.0
3	937.0	927.0	455.0	457.0	1889.0	1873.0	917.0	916.0
4	612.0	609.0	299.0	298.0	1234.0	1230.0	611.0	606.0
5	379.0	375.0	184.0	185.0	766.0	760.0	380.0	379.0
6	205.0	203.0	100.0	99.0	414.0	412.0	205.0	204.0
7	99.0	96.0	46.0	48.0	199.0	196.0	96.0	97.0
8	42.0	41.0	20.0	20.0	85.0	85.0	41.0	41.0
9	14.0	14.0	6.0	6.0	29.0	29.0	14.0	14.0
10	4.0	5.0	2.0	1.0	9.0	11.0	5.0	3.0
11	4.7	2.7	0.7	2.9	8.4	7.0	2.9	4.7
12	4.7	3.1	1.0	2.9	8.5	7.6	3.2	4.6
13	4.6	3.6	1.4	2.6	8.7	8.3	3.7	4.5
14	4.1	3.3	1.2	2.4	7.7	7.5	3.4	4.1
15	3.6	2.6	0.8	2.2	6.6	6.2	2.7	3.6
16	3.0	1.7	0.4	1.9	5.3	4.5	1.8	3.0
17	2.2	1.1	0.1	1.5	3.9	3.3	1.2	2.2
18	1.6	0.7	0.0	1.1	2.8	2.4	0.8	1.6
19	1.4	0.2	-0.1	1.1	2.0	1.4	0.3	1.3
20	1.0	0.0	-0.3	0.9	1.4	0.9	0.0	1.0

Site	DEAD2	2209	1983	400 H	20A			
n/N	5/8	5/8	6/8	6/8	5/10	5/10	6/10	6/10
TO	.315	.315	.315	.315	.315	.315	.315	.315
Gate	2538.0	2522.0	5025.0	4978.0	2581.0	2563.0	5088.0	5008.0
1	1786.0	1770.0	3577.0	3582.0	1789.0	1770.0	3587.0	3591.0
2	1432.0	1431.0	2901.0	2892.0	1433.0	1427.0	2905.0	2889.0
3	976.0	979.0	1980.0	1970.0	972.0	973.0	1974.0	1961.0
4	641.0	640.0	1295.0	1293.0	647.0	645.0	1308.0	1305.0
5	393.0	396.0	802.0	796.0	401.0	403.0	817.0	811.0
6	214.0	212.0	431.0	432.0	217.0	215.0	438.0	438.0
7	100.0	102.0	207.0	205.0	100.0	102.0	207.0	205.0
8	43.0	44.0	89.0	88.0	43.0	44.0	89.0	89.0
9	14.0	15.0	30.0	30.0	14.0	15.0	30.0	31.0
10	5.0	4.0	9.0	11.0	5.0	4.0	9.0	11.0
11	2.9	4.6	8.2	7.0	3.0	4.5	8.4	7.1
12	3.1	4.7	8.5	7.4	3.2	4.6	8.5	7.5
13	3.6	4.5	8.5	8.1	3.7	4.5	8.7	8.2
14	3.3	4.1	7.7	7.4	3.4	4.1	7.9	7.5
15	2.5	3.6	6.6	5.9	2.6	3.6	6.7	6.1
16	1.7	2.9	5.1	4.4	1.8	2.9	5.3	4.6
17	1.1	2.2	3.8	3.2	1.2	2.2	3.8	3.3
18	0.7	1.6	2.6	2.2	0.8	1.5	2.7	2.3
19	0.2	1.3	1.9	1.3	0.2	1.2	2.0	1.4
20	0.0	1.0	1.3	0.7	0.0	0.9	1.4	0.8

APPENDIX C: TRANSIENT SOUNDING DATA CONTINUED

Site	DEAD5	0705	1984	400 H	23A
n/N	6/10	6/10	6/10	6/10	
TO	.350	.350	.350	.350	
Gate	4898.0	5322.0	4900.0	5322.0	
1	7000.0	7000.0	7000.0	7000.0	
2	7000.0	7000.0	7000.0	7000.0	
3	7000.0	7000.0	7000.0	7000.0	
4	7000.0	7000.0	7000.0	7000.0	
5	7000.0	6027.0	7000.0	7000.0	
6	5209.0	5129.0	4871.0	5029.0	
7	1523.0	1490.0	1478.0	1480.0	
8	558.0	548.0	543.0	545.0	
9	170.0	166.0	166.0	166.0	
10	37.0	41.0	36.0	40.0	
11	13.6	13.3	13.4	13.3	
12	8.1	8.1	8.0	8.1	
13	9.1	9.0	9.0	9.1	
14	9.5	8.3	9.4	8.3	
15	8.2	7.1	8.1	7.2	
16	5.3	6.3	5.3	6.3	
17	3.8	5.0	3.8	5.0	
18	3.2	3.0	3.2	3.1	
19	2.2	2.0	2.2	2.0	
20	-0.2	1.9	0.9	1.8	

Site	FRANKLIN		2109	1983	400 H	20A		
n/N	4/8	4/8	3/8	3/8	5/8	5/8	4/10	4/10
TO	.315	.315	.315	.315	.315	.315	.315	.315
Gate	1244.0	1237.0	621.0	619.0	2491.0	2479.0	1266.0	1259.0
1	1491.0	1471.0	700.0	700.0	3025.0	3005.0	1467.0	1472.0
2	986.0	982.0	473.0	467.0	2000.0	1999.0	975.0	971.0
3	616.0	618.0	303.0	295.0	1247.0	1250.0	614.0	606.0
4	439.0	440.0	218.0	214.0	885.0	885.0	443.0	440.0
5	360.0	364.0	182.0	177.0	725.0	729.0	371.0	365.0
6	323.0	321.0	160.0	160.0	647.0	645.0	326.0	325.0
7	286.0	287.0	143.0	141.0	575.0	575.0	287.0	283.0
8	243.0	242.0	121.0	120.0	488.0	487.0	244.0	242.0
9	195.0	194.0	97.0	96.0	391.0	391.0	196.0	194.0
10	149.0	148.0	74.0	74.0	300.0	298.0	151.0	151.0
11	118.5	119.7	60.5	58.3	238.3	239.2	120.9	118.6
12	88.9	90.2	45.7	43.6	179.0	180.0	90.0	88.0
13	61.4	62.4	31.6	30.1	123.9	124.4	62.4	61.0
14	41.5	42.4	21.6	20.2	84.0	84.5	43.1	41.9
15	28.4	29.6	15.2	13.7	57.9	58.7	30.0	28.7
16	18.3	19.6	10.2	8.6	37.6	38.6	19.9	18.4
17	11.3	12.6	6.6	5.1	23.7	24.5	12.6	11.3
18	7.0	8.0	4.3	3.0	14.8	15.5	8.1	7.0
19	3.7	5.0	2.9	1.3	8.4	9.4	5.1	3.7
20	1.9	3.1	1.8	0.4	4.7	5.7	3.2	1.9

APPENDIX C: TRANSIENT SOUNDING DATA CONTINUED

Site	HAPPY	2009	1983	400 H	20A	
n/N	5/8	5/8	4/8	4/8	5/10	5/10
TO	.315	.315	.315	.315	.315	.315
Gate	2552.0	2532.0	1269.0	1266.0	2569.0	2561.0
1	2606.0	2594.0	1262.0	1263.0	2562.0	2550.0
2	2108.0	2085.0	1021.0	1027.0	2064.0	2043.0
3	1585.0	1566.0	768.0	777.0	1553.0	1535.0
4	1219.0	1209.0	595.0	599.0	1213.0	1204.0
5	954.0	943.0	465.0	470.0	959.0	949.0
6	739.0	735.0	364.0	364.0	740.0	737.0
7	578.0	573.0	283.0	285.0	570.0	565.0
8	447.0	443.0	219.0	220.0	444.0	441.0
9	334.0	332.0	164.0	165.0	332.0	330.0
10	242.0	242.0	120.0	119.0	244.0	244.0
11	187.7	185.4	91.5	93.5	187.4	185.1
12	136.0	134.0	66.0	67.9	134.2	132.2
13	90.3	89.1	43.8	45.2	89.5	88.2
14	59.7	58.8	28.8	30.0	60.1	59.1
15	41.3	40.2	19.5	20.9	41.4	40.2
16	27.3	26.1	12.5	14.0	27.4	26.2
17	17.7	16.6	7.8	9.2	17.5	16.4
18	11.4	10.6	4.9	6.0	11.3	10.5
19	7.1	6.0	2.5	3.9	7.1	6.0
20	4.5	3.4	1.3	2.6	4.4	3.4

Site	GALBRAITH		1909	1983	400 H	20A
n/N	5/8	5/8	4/8	4/8	4/10	4/10
TO	.315	.315	.315	.315	.315	.315
Gate	2472.0	2464.0	1242.0	1234.0	1252.0	1254.0
1	3319.0	3273.0	1617.0	1610.0	1608.0	1611.0
2	2345.0	2305.0	1141.0	1142.0	1134.0	1129.0
3	1476.0	1451.0	718.0	722.0	717.0	710.0
4	934.0	924.0	458.0	458.0	461.0	459.0
5	608.0	600.0	298.0	300.0	304.0	301.0
6	399.0	395.0	197.0	196.0	199.0	198.0
7	279.0	275.0	136.0	138.0	138.0	135.0
8	203.0	201.0	100.0	100.0	101.0	100.0
9	147.0	146.0	73.0	72.0	73.0	72.0
10	103.0	105.0	53.0	50.0	51.0	53.0
11	80.1	77.9	38.4	40.4	40.6	38.3
12	56.8	55.0	27.1	28.6	28.6	26.6
13	36.8	35.8	17.6	18.6	18.7	17.3
14	23.9	23.1	11.2	12.1	12.4	11.1
15	16.3	15.3	7.3	8.4	8.5	7.1
16	10.7	9.4	4.3	5.7	5.8	4.2
17	6.9	5.8	2.5	3.7	3.8	2.3
18	4.4	3.6	1.4	2.4	2.5	1.3
19	2.9	1.7	0.5	1.7	1.8	0.3
20	1.9	0.8	0.0	1.2	1.3	0.0

APPENDIX C: TRANSIENT SOUNDING DATA CONTINUED

Site	CHANDALAR		1809	1983	200 H	20A
n/N	5/8	5/8	6/8	6/8	5/10	5/10
TO	.175	.175	.175	.175	.175	.175
Gate	4989.0	5046.0	5045.0	5087.0	5060.0	5043.0
1	1913.0	1911.0	3878.0	3885.0	1927.0	1905.0
2	1359.0	1370.0	2781.0	2772.0	1367.0	1361.0
3	873.0	883.0	1789.0	1781.0	874.0	876.0
4	572.0	577.0	1167.0	1165.0	580.0	580.0
5	376.0	382.0	773.0	768.0	385.0	387.0
6	241.0	243.0	493.0	491.0	246.0	246.0
7	153.0	156.0	315.0	313.0	154.0	155.0
8	99.0	101.0	204.0	203.0	100.0	101.0
9	62.0	63.0	128.0	127.0	63.0	63.0
10	39.0	39.0	79.0	80.0	40.0	39.0
11	26.8	28.5	56.4	55.0	27.1	28.5
12	17.5	18.9	37.2	36.2	17.6	18.7
13	10.8	11.7	22.8	22.4	10.9	11.5
14	6.6	7.0	14.2	13.9	6.8	7.4
15	4.1	5.1	9.5	9.0	4.3	5.0
16	2.3	3.5	6.2	5.3	2.4	3.4
17	1.3	2.3	3.9	3.2	1.3	2.2
18	0.7	1.5	2.4	1.9	0.7	1.4
19	0.0	1.1	1.5	0.7	0.1	1.0
20	0.0	0.7	0.8	0.1	0.0	0.7

Site	SLATE	1808	1983	100 H	20A	
n/N	8/8	8/8	7/8	7/8	7/10	7/10
TO	.095	.095	.095	.095	.095	.095
Gate	5114.0	5143.0	5080.0	5030.0	5045.0	5087.0
1	2245.0	2189.0	1034.0	995.0	946.0	937.0
2	1266.0	1276.0	608.0	602.0	586.0	589.0
3	680.0	691.0	326.0	328.0	319.0	315.0
4	363.0	376.0	175.0	177.0	175.0	172.0
5	194.0	205.0	93.0	97.0	97.0	92.0
6	97.0	100.0	46.0	46.0	45.0	46.0
7	43.0	49.0	20.0	21.0	21.0	19.0
8	16.0	21.0	8.0	8.0	8.0	8.0
9	4.0	5.0	1.0	0.0	1.0	1.0
10	0.0	-1.0	-1.0	0.0	0.0	0.0
11	-7.7	0.6	-2.6	-1.4	-1.3	-2.8
12	-8.1	-0.3	-3.2	-2.0	-1.7	-3.0
13	-7.9	-0.6	-2.8	-2.0	-1.9	-2.9
14	-7.4	-0.7	-2.5	-1.8	-1.8	-2.7
15	-6.3	-0.7	-2.4	-1.7	-1.4	-2.5
16	-5.3	-0.5	-2.1	-1.4	-1.2	-2.1
17	-4.8	-0.3	-1.7	-1.2	-1.0	-1.8
18	-3.7	-0.4	-1.4	-1.0	-0.9	-1.5
19	-4.1	0.6	-1.3	-0.7	-0.5	-1.5
20	-3.4	0.3	-1.1	-0.5	-0.3	-1.2

APPENDIX C: TRANSIENT SOUNDING DATA CONTINUED

Site	COLDFOOT		1809	1983	100 H	20.1A
n/N	6/8	6/8	7/8	7/8	6/10	6/10
TO	.095	.095	.095	.095	.095	.095
Gate	5083.0	5122.0	5097.0	5046.0	5061.0	5100.0
1	2442.0	2443.0	4828.0	4792.0	2426.0	2419.0
2	1798.0	1786.0	3550.0	3560.0	1792.0	1778.0
3	1247.0	1237.0	2469.0	2478.0	1245.0	1231.0
4	866.0	860.0	1714.0	1702.0	874.0	866.0
5	596.0	588.0	1175.0	1182.0	607.0	597.0
6	386.0	384.0	768.0	767.0	391.0	389.0
7	247.0	244.0	489.0	491.0	247.0	243.0
8	156.0	154.0	310.0	311.0	157.0	155.0
9	93.0	93.0	186.0	185.0	93.0	93.0
10	52.0	53.0	107.0	105.0	53.0	55.0
11	34.7	32.9	66.3	68.4	34.8	33.1
12	19.9	18.2	37.1	39.3	19.6	18.0
13	9.5	8.5	17.6	19.2	9.4	8.5
14	4.3	3.3	7.5	8.9	4.2	3.4
15	2.0	0.8	2.7	4.0	1.9	0.9
16	0.8	-0.3	0.2	1.3	0.6	-0.2
17	0.0	-0.8	-0.6	0.2	0.0	-0.8
18	-0.1	-0.9	-0.7	-0.3	-0.2	-0.9
19	0.0	-1.0	-1.1	-0.2	-0.1	-1.0
20	0.0	-1.0	-0.9	-0.3	-0.1	-1.0

Site	BONANZA		1709	1983	100 H	20A
n/N	7/8	7/8	8/8	8/8	7/10	7/10
TO	.095	.095	.095	.095	.095	.095
Gate	5045.0	5083.0	5061.0	5007.0	5022.0	5063.0
1	2378.0	2378.0	4719.0	4685.0	2338.0	2337.0
2	1722.0	1727.0	3463.0	3487.0	1728.0	1721.0
3	1201.0	1199.0	2413.0	2434.0	1203.0	1193.0
4	848.0	849.0	1704.0	1697.0	860.0	855.0
5	604.0	601.0	1210.0	1225.0	619.0	611.0
6	413.0	413.0	831.0	838.0	421.0	417.0
7	279.0	277.0	560.0	566.0	280.0	176.0
8	186.0	186.0	374.0	379.0	188.0	186.0
9	118.0	118.0	238.0	240.0	119.0	118.0
10	71.0	72.0	146.0	146.0	73.0	74.0
11	19.2	47.7	94.3	101.9	49.9	48.0
12	30.9	29.5	57.9	64.5	30.7	29.4
13	17.5	16.6	32.1	38.2	17.5	16.5
14	9.8	9.2	17.6	22.5	10.1	9.4
15	5.9	5.2	9.7	14.3	6.1	5.3
16	3.4	2.6	5.0	8.4	3.4	2.7
17	1.7	1.2	2.0	5.1	1.7	1.2
18	0.5	0.4	0.7	2.9	0.6	0.5
19	0.1	-0.2	-1.0	2.4	0.3	-0.1
20	0.0	-0.4	-1.1	1.4	0.0	-0.3

APPENDIX C: TRANSIENT SOUNDING DATA CONTINUED

Site	OLDMAN 1709		1983	200 H	20.1A	
n/N	6/8	6/8	5/8	5/8	6/10	6/10
TO	.175	.175	.175	.175	.175	.175
Gate	5077.0	5022.0	5025.0	5046.0	5060.0	5018.0
1	2628.0	2591.0	1273.0	1273.0	2597.0	2572.0
2	1948.0	1947.0	960.0	953.0	1945.0	1942.0
3	1267.0	1269.0	627.0	618.0	1260.0	1262.0
4	852.0	850.0	420.0	416.0	857.0	855.0
5	570.0	572.0	283.0	278.0	579.0	581.0
6	375.0	375.0	186.0	183.0	379.0	379.0
7	245.0	245.0	122.0	119.0	243.0	244.0
8	162.0	162.0	80.0	79.0	162.0	162.0
9	103.0	103.0	51.0	50.0	103.0	103.0
10	65.0	63.0	31.0	32.0	66.0	64.0
11	44.0	45.0	22.8	21.5	44.4	45.2
12	27.9	28.5	14.6	13.6	27.8	28.4
13	15.9	16.3	8.4	7.8	16.0	16.3
14	8.9	9.2	4.8	4.3	9.0	9.2
15	4.8	5.2	2.9	2.3	5.0	5.4
16	2.2	2.9	1.8	0.9	2.3	3.0
17	0.9	1.4	1.0	0.3	1.0	1.4
18	0.2	0.6	0.6	0.0	0.3	0.6
19	-0.2	0.3	0.5	-0.2	-0.1	0.4
20	-0.3	0.1	0.4	-0.2	-0.2	0.1

Site	OLDMAN 1709		1983	100 H	20A	
n/N	7/8	7/8	8/8	8/8	7/10	7/10
TO	.095	.095	.095	.095	.095	.095
Gate	5093.0	5023.0	5031.0	5073.0	5060.0	5020.0
1	2206.0	2134.0	4239.0	4167.0	2074.0	2066.0
2	1466.0	1446.0	2939.0	2909.0	1440.0	1451.0
3	915.0	908.0	1843.0	1825.0	898.0	907.0
4	588.0	584.0	1179.0	1171.0	586.0	591.0
5	379.0	378.0	770.0	756.0	381.0	386.0
6	238.0	127.0	481.0	476.0	239.0	240.0
7	149.0	149.0	303.0	298.0	147.0	148.0
8	95.0	94.0	193.0	191.0	95.0	95.0
9	58.0	57.0	118.0	118.0	59.0	58.0
10	35.0	34.0	71.0	72.0	36.0	35.0
11	22.9	24.3	51.3	44.2	23.6	24.2
12	13.6	14.8	32.3	26.1	13.8	14.7
13	7.0	7.9	18.6	12.6	7.3	7.8
14	3.2	3.9	10.3	5.5	3.6	4.0
15	-1.1	2.0	6.0	1.6	1.4	1.9
16	0.0	0.8	3.3	-0.3	0.1	0.7
17	-0.6	0.0	1.7	-1.5	-0.3	0.0
18	-0.7	-0.2	0.8	-1.6	-0.5	-0.2
19	-1.2	0.0	1.1	-2.6	-0.8	-0.1
20	-1.1	-0.1	0.6	-2.2	-0.8	-0.2

APPENDIX C: TRANSIENT SOUNDING DATA CONTINUED

Site	FINGER	1609	1983	100 H	19.8A	
n/N	7/8	7/8	6/8	6/8	7/10	7/10
TO	.095	.095	.095	.095	.095	.095
Gate	5065.0	5008.0	5021.0	5066.0	5050.0	5010.0
1	2125.0	2088.0	1056.0	1062.0	2089.0	2063.0
2	1531.0	1531.0	774.0	771.0	1524.0	1524.0
3	1102.0	1104.0	557.0	552.0	1092.0	1095.0
4	797.0	795.0	401.0	400.0	803.0	801.0
5	569.0	572.0	288.0	284.0	577.0	580.0
6	398.0	398.0	200.0	198.0	401.0	401.0
7	274.0	276.0	139.0	137.0	273.0	274.0
8	192.0	191.0	96.0	95.0	192.0	191.0
9	129.0	129.0	65.0	64.0	129.0	129.0
10	87.0	86.0	42.0	43.0	89.0	87.0
11	62.9	64.2	32.6	31.2	63.4	64.8
12	43.6	44.3	22.4	21.4	43.1	43.8
13	27.4	27.9	14.0	13.4	27.4	27.8
14	16.7	17.3	8.5	8.2	17.2	17.6
15	10.4	10.9	5.5	5.0	10.6	11.1
16	6.0	6.7	3.4	2.6	6.1	6.7
17	3.3	3.6	2.0	1.2	4.1	3.8
18	1.8	1.9	1.1	0.5	2.0	2.0
19	0.5	1.2	0.6	0.0	0.9	1.1
20	0.0	0.6	0.3	-0.1	0.2	0.5

Site	D78.1	3009	1983	100 H	20A	
n/N	8/8	8/8	7/8	7/8	7/10	7/10
TO	.096	.096	.096	.096	.096	.096
Gate	5055.0	5102.0	5079.0	5030.0	5047.0	5089.0
1	-630.0	-615.0	-293.0	-305.0	-306.0	-295.0
2	-552.0	-553.0	-262.0	-264.0	-264.0	-258.0
3	-158.0	-161.0	-74.0	-69.0	-70.0	-73.0
4	117.0	110.0	58.0	59.0	60.0	58.0
5	237.0	227.0	114.0	117.0	119.0	115.0
6	261.0	258.0	129.0	128.0	130.0	129.0
7	238.0	233.0	116.0	116.0	117.0	114.0
8	192.0	189.0	94.0	94.0	94.0	94.0
9	141.0	142.0	71.0	68.0	69.0	70.0
10	99.0	99.0	50.0	47.0	48.0	50.0
11	78.2	69.0	35.9	36.9	37.5	35.6
12	55.3	46.9	24.7	25.8	25.8	24.1
13	36.2	28.8	15.7	16.2	16.2	15.3
14	24.2	17.0	9.8	10.2	10.5	9.6
15	16.1	10.0	6.0	6.7	6.7	5.9
16	10.4	5.1	3.2	4.0	4.1	3.2
17	7.0	1.8	1.7	2.2	2.3	1.5
18	4.6	0.5	0.9	1.1	1.1	0.7
19	4.2	-1.2	0.0	0.8	0.7	0.0
20	3.1	-1.3	-0.1	0.4	0.3	-0.2

APPENDIX C: TRANSIENT SOUNDING DATA CONTINUED

Site	D78.10	3009	1983	100 H	20A
n/N	7/8	7/8			
TO	.096	.096			
Gate	5065.0	5100.0			
1	-281.0	-287.0			
2	-244.0	-244.0			
3	-58.0	-63.0			
4	69.0	65.0			
5	123.0	120.0			
6	134.0	131.0			
7	120.0	117.0			
8	96.0	95.0			
9	70.0	72.0			
10	49.0	50.0			
11	37.9	35.4			
12	26.4	24.2			
13	16.7	15.2			
14	10.5	9.4			
15	6.9	5.7			
16	4.3	3.0			
17	2.5	1.4			
18	1.3	0.6			
19	0.9	0.0			
20	0.5	-0.1			

Site	YUKON	1609	1983	100 H	20A	
n/N	6/8	6/8	7/8	7/8	7/10	7/10
TO	.095	.095	.095	.095	.095	.095
Gate	5081.0	5013.0	5018.0	5062.0	5043.0	5005.0
1	2182.0	2161.0	4298.0	4300.0	4323.0	4278.0
2	1450.0	1456.0	2908.0	2888.0	2890.0	2889.0
3	879.0	884.0	1764.0	1751.0	1747.0	1747.0
4	552.0	555.0	1105.0	1100.0	1113.0	1109.0
5	353.0	360.0	716.0	707.0	721.0	726.0
6	225.0	224.0	448.0	448.0	454.0	452.0
7	142.0	143.0	286.0	285.0	285.0	284.0
8	93.0	93.0	187.0	186.0	188.0	187.0
9	59.0	59.0	118.0	118.0	119.0	118.0
10	36.0	36.0	73.0	73.0	75.0	74.0
11	24.9	25.4	50.7	50.2	50.6	50.8
12	15.1	15.9	31.8	31.1	31.0	31.6
13	8.0	8.6	17.4	16.7	16.8	17.3
14	3.8	4.3	8.9	8.4	8.6	9.0
15	1.5	2.3	4.6	4.0	4.0	4.5
16	0.1	0.9	1.8	1.4	1.4	1.9
17	-0.3	0.2	0.5	0.5	0.0	0.0
18	-0.6	0.0	-0.1	-0.4	-0.3	-0.1
19	-0.9	0.0	-0.2	-0.8	-0.8	-0.2
20	-0.8	-0.1	-0.3	-0.8	-0.8	-0.3

APPENDIX C: TRANSIENT SOUNDING DATA CONTINUED

Site	D34.4	3009	1983	100 H	20A	
n/N	6/8	6/8	7/8	7/8	7/10	7/10
TO	.095	.095	.095	.095	.095	.095
Gate	5110.0	5039.0	5045.0	5095.0	5077.0	5036.0
1	2580.0	2553.0	5081.0	5084.0	5098.0	5059.0
2	1508.0	1507.0	2009.0	3002.0	3003.0	3000.0
3	808.0	811.0	1617.0	1614.0	1609.0	1608.0
4	436.0	437.0	873.0	872.0	881.0	880.0
5	233.0	236.0	471.0	468.0	477.0	479.0
6	115.0	117.0	234.0	233.0	236.0	237.0
7	55.0	57.0	114.0	112.0	112.0	113.0
8	27.0	27.0	56.0	56.0	57.0	56.0
9	13.0	12.0	26.0	28.0	28.0	26.0
10	6.0	5.0	12.0	14.0	14.0	12.0
11	3.1	4.7	8.9	7.3	7.4	9.1
12	1.5	2.6	5.2	3.8	3.9	5.3
13	0.6	1.2	2.7	1.9	2.0	2.7
14	0.0	0.5	1.3	0.5	0.8	1.5
15	-0.3	0.2	0.5	0.6	0.0	0.0
16	-0.7	0.2	0.2	-0.4	-0.2	0.3
17	-0.7	-0.5	-0.4	0.0	0.0	0.0
18	-0.7	-0.6	-0.5	-0.1	0.0	0.0
19	-0.9	-0.8	-0.7	0.0	0.0	0.0
20	-0.9	-0.8	-0.7	0.0	0.0	0.0

Site	HESS	2909	1983	100 H	20A	
n/N	6/8	6/8	7/8	7/8	6/10	6/10
TO	.096	.096	.096	.096	.096	.096
Gate	5051.0	5091.0	5071.0	5018.0	5033.0	5074.0
1	2545.0	2543.0	4991.0	5012.0	2519.0	2512.0
2	1554.0	1550.0	3066.0	3109.0	1558.0	1552.0
3	901.0	895.0	1779.0	1802.0	903.0	895.0
4	541.0	539.0	1073.0	1082.0	548.0	546.0
5	335.0	332.0	663.0	671.0	343.0	339.0
6	201.0	198.0	396.0	402.0	205.0	201.0
7	120.0	118.0	237.0	240.0	120.0	118.0
8	72.0	72.0	144.0	145.0	73.0	72.0
9	40.0	41.0	84.0	83.0	41.0	42.0
10	22.0	23.0	47.0	46.0	23.0	24.0
11	15.2	13.6	27.9	30.4	15.5	13.7
12	8.5	7.4	15.6	17.1	8.6	7.4
13	3.9	3.3	7.2	8.2	4.0	3.3
14	1.5	1.1	2.9	3.5	1.6	1.2
15	0.5	0.0	0.6	1.3	0.6	0.0
16	0.0	-0.6	-0.4	0.2	0.1	-0.6
17	-0.1	-0.7	-0.8	-0.2	-0.1	-0.7
18	-0.3	-0.8	-0.8	-0.6	-0.2	-0.7
19	-0.2	-0.9	-1.1	-0.3	-0.1	-0.9
20	-0.2	-0.8	-1.0	-0.4	-0.1	-0.8

APPENDIX C: TRANSIENT SOUNDING DATA CONTINUED

Site	LIVENGOOD		1608	1983	100 H	20A
n/N	7/8	7/8	6/8	6/8	6/10	6/10
TO	.095	.095	.095	.095	.095	.095
Gate	5065.0	5106.0	5081.0	5031.0	5047.0	5086.0
1	2899.0	2891.0	1467.0	1440.0	1439.0	1443.0
2	2282.0	2275.0	1152.0	1146.0	1140.0	1132.0
3	1711.0	1703.0	859.0	859.0	853.0	843.0
4	1289.0	1286.0	648.0	648.0	652.0	645.0
5	973.0	964.0	485.0	487.0	495.0	487.0
6	705.0	703.0	355.0	352.0	357.0	355.0
7	512.0	508.0	256.0	256.0	255.0	252.0
8	370.0	368.0	185.0	185.0	185.0	184.0
9	258.0	258.0	130.0	129.0	129.0	128.0
10	173.0	174.0	88.0	86.0	88.0	88.0
11	126.2	123.8	62.2	63.1	63.5	61.8
12	82.2	80.1	40.1	41.1	40.8	39.4
13	45.5	44.0	21.9	22.5	22.4	21.6
14	22.4	21.5	10.5	11.0	11.2	10.5
15	10.3	9.1	4.2	5.0	4.0	4.2
16	3.3	2.3	0.7	1.6	1.5	0.6
17	0.1	-0.4	-0.5	-0.6	0.0	0.0
18	-0.7	-1.2	-0.9	-0.3	-0.3	-0.9
19	-0.5	-1.4	-1.1	-0.2	-0.2	-1.1
20	-0.3	-1.2	-1.0	-0.1	-0.1	-1.0

Site	E54.7	0209	1983	100 H	20A			
n/N	8/8	8/8	7/8	7/8	7/10	7/10	8/10	8/10
TO	.083	.083	.083	.083	.083	.083	.083	.083
Gate	5051.0	5080.0	5068.0	5028.0	5035.0	5074.0	5028.0	5057.0
1	-146.0	-167.0	-65.0	-69.0	-73.0	-69.0	392.0	397.0
2	-197.0	-198.0	-87.0	-90.0	-91.0	-87.0	272.0	280.0
3	-3.0	-10.0	0.1	-1.0	-0.0	-0.0	202.0	187.0
4	121.0	114.0	59.0	60.0	61.0	60.0	134.0	125.0
5	162.0	153.0	77.0	79.0	80.0	78.0	87.0	88.0
6	147.0	138.0	68.0	72.0	73.0	69.0	60.0	54.0
7	112.0	106.0	52.0	55.0	54.0	52.0	33.0	35.0
8	78.0	74.0	37.0	37.0	37.0	37.0	21.0	16.0
9	49.0	50.0	25.0	23.0	23.0	25.0	9.0	13.0
10	29.0	31.0	16.0	13.0	13.0	16.0	5.0	4.0
11	24.8	15.6	8.6	11.0	11.2	8.7	8.2	-1.8
12	15.2	7.8	4.5	6.3	6.3	4.5	6.0	-1.9
13	8.4	1.5	1.7	2.8	2.8	1.8	3.2	-2.2
14	4.7	-1.1	0.0	0.9	0.9	0.4	2.6	-2.9
15	2.5	-2.8	-0.5	0.3	0.1	-0.6	2.0	-2.4
16	1.3	-3.0	-1.1	-1.0	1.4	-2.1	0.0	0.0
17	0.9	-3.0	-1.1	-0.2	-0.3	-0.9	1.4	-1.9
18	0.5	-2.5	-0.9	-0.4	-0.5	-0.9	0.9	-1.4
19	1.4	-3.1	-1.0	-0.1	-0.2	-0.9	1.5	-2.0
20	1.0	-2.6	-0.9	-0.1	-0.2	-0.8	1.1	-1.5

APPENDIX C: TRANSIENT SOUNDING DATA CONTINUED

Site	E54.70	3008	1983	100 H	20A	
n/N	8/8	8/8	7/8	7/8	7/10	7/10
TO	.095	.095	.095	.095	.095	.095
Gate	5045.0	5086.0	5072.0	5022.0	5038.0	5081.0
1	31.0	34.0	17.0	18.0	17.0	19.0
2	87.0	87.0	44.0	42.0	43.0	45.0
3	124.0	120.0	58.0	62.0	62.0	58.0
4	128.0	122.0	60.0	62.0	63.0	61.0
5	117.0	111.0	54.0	56.0	57.0	55.0
6	95.0	91.0	44.0	46.0	47.0	45.0
7	73.0	70.0	34.0	35.0	35.0	34.0
8	53.0	51.0	25.0	25.0	25.0	25.0
9	34.0	36.0	17.0	15.0	15.0	17.0
10	21.0	24.0	11.0	8.0	8.0	12.0
11	19.5	11.1	6.3	8.0	8.3	6.3
12	12.5	5.5	3.3	4.8	4.8	3.3
13	7.3	1.0	1.0	2.2	2.1	1.2
14	4.1	-0.9	0.0	0.7	0.7	0.0
15	2.4	-2.2	-0.7	-0.6	0.0	0.0
16	1.5	-2.3	-1.1	-1.0	0.0	0.0
17	1.1	-2.5	-1.1	-0.3	-0.2	-1.1
18	0.5	-2.2	-1.1	-0.4	-0.4	-0.9
19	1.2	-2.8	-1.2	0.0	-0.1	-1.1
20	0.8	-2.3	-1.1	-0.2	-0.1	-1.0

Site	E54.71	3008	1983	100 H	20A
n/N	7/8	7/8	8/8	8/8	
TO	.095	.095	.095	.095	
Gate	5095.0	5031.0	5034.0	5075.0	
1	-128.0	-146.0	-343.0	-353.0	
2	-122.0	-126.0	-265.0	-266.0	
3	-19.0	-16.0	-44.0	-43.0	
4	47.0	46.0	92.0	88.0	
5	67.0	68.0	139.0	134.0	
6	62.0	64.0	130.0	126.0	
7	49.0	50.0	103.0	98.0	
8	35.0	35.0	73.0	72.0	
9	24.0	22.0	46.0	48.0	
10	15.0	12.0	29.0	31.0	
11	8.6	10.9	23.5	16.4	
12	4.8	6.3	15.0	8.6	
13	2.1	3.0	8.5	2.8	
14	0.4	1.2	4.5	0.0	
15	-0.2	0.4	2.8	-1.5	
16	-0.8	0.0	1.2	-2.2	
17	-0.9	0.0	0.9	-2.2	
18	-0.8	-0.2	0.2	-2.0	
19	-1.1	-0.1	0.9	-2.5	
20	-1.0	-0.2	0.5	-2.0	

APPENDIX C: TRANSIENT SOUNDING DATA CONTINUED

Site	WASH1	2009	1983	100 H	19.9A			
n/N	7/8	7/8	8/8	8/8	8/10	8/10	7/10	7/10
TO	.092	.092	.092	.092	.092	.092	.092	.092
Gate	5058.0	5096.0	5077.0	5025.0	5038.0	5081.0	5069.0	5028.0
1	1669.0	1668.0	3345.0	3309.0	3321.0	3332.0	1648.0	1630.0
2	1040.0	1032.0	2084.0	2076.0	2080.0	2076.0	1026.0	1023.0
3	627.0	616.0	1248.0	1252.0	1250.0	1241.0	613.0	617.0
4	391.0	386.0	780.0	788.0	797.0	787.0	390.0	392.0
5	253.0	246.0	497.0	508.0	518.0	507.0	251.0	255.0
6	152.0	148.0	301.0	307.0	311.0	305.0	151.0	153.0
7	88.0	85.0	171.0	178.0	178.0	172.0	85.0	87.0
8	49.0	48.0	97.0	100.0	101.0	96.0	48.0	48.0
9	23.0	25.0	50.0	50.0	50.0	50.0	25.0	23.0
10	10.0	11.0	23.0	23.0	24.0	24.0	11.0	10.0
11	6.8	4.5	7.9	17.0	16.9	8.1	4.8	6.8
12	3.0	1.0	0.5	8.7	8.7	0.7	1.2	2.8
13	0.3	-0.7	-3.4	3.8	3.8	-3.1	-0.6	0.3
14	-0.5	-1.4	-4.6	1.2	1.3	-4.5	-1.4	-0.5
15	-0.8	-1.9	-5.0	0.2	0.2	-4.9	-1.7	-0.9
16	-0.9	-1.9	-4.6	-0.2	-0.3	-4.5	-1.9	-0.9
17	-0.9	-1.7	-4.2	-0.3	-0.2	-4.1	-1.6	-1.0
18	-1.0	-1.4	-3.5	-0.5	-0.5	-3.3	-1.3	-0.9
19	-0.6	-1.4	-3.8	0.1	0.3	-3.6	-1.4	-0.6
20	-0.4	-1.2	-2.9	0.0	0.3	-2.8	-1.1	-0.4

Site	WASH2	0209	1983	100 H	20A			
n/N	7/8	7/8	8/8	8/8	8/10	8/10	7/10	7/10
TO	.096	.096	.096	.096	.096	.096	.096	.096
Gate	5054.0	5085.0	5067.0	5016.0	5030.0	5073.0	5072.0	5024.0
1	2165.0	2135.0	4270.0	4184.0	4174.0	4216.0	2065.0	2031.0
2	1276.0	1267.0	2586.0	2573.0	2577.0	2585.0	1274.0	1267.0
3	747.0	740.0	1508.0	1506.0	1503.0	1500.0	740.0	741.0
4	460.0	455.0	926.0	928.0	940.0	933.0	462.0	461.0
5	293.0	287.0	586.0	591.0	604.0	595.0	294.0	297.0
6	177.0	173.0	354.0	358.0	363.0	357.0	176.0	178.0
7	103.0	100.0	205.0	209.0	209.0	204.0	100.0	102.0
8	57.0	57.0	117.0	120.0	120.0	117.0	58.0	58.0
9	29.0	31.0	62.0	61.0	62.0	62.0	31.0	29.0
10	13.0	16.0	32.0	30.0	31.0	32.0	16.0	14.0
11	9.5	7.5	14.3	21.8	22.2	14.2	7.8	9.7
12	4.8	3.3	5.5	13.0	12.7	5.6	3.5	4.8
13	2.0	0.9	0.7	7.0	6.7	0.8	1.0	2.0
14	0.5	-0.1	-1.4	4.0	3.8	-1.4	0.0	0.5
15	0.0	-0.5	-2.4	2.4	2.3	-2.3	-0.5	0.0
16	-0.1	-1.0	-2.2	1.5	1.2	-2.5	-0.9	-0.1
17	-0.3	-0.9	-2.3	1.1	0.8	-2.5	-0.9	-0.3
18	-0.4	-0.8	-1.9	0.6	0.3	-2.2	-0.9	-0.5
19	-0.2	-1.0	-2.5	1.4	1.1	-2.8	-1.0	-0.2
20	-0.3	-0.9	-1.9	1.0	0.7	-2.2	-0.9	-0.2

APPENDIX C: TRANSIENT SOUNDING DATA CONTINUED

Site	VIRG1	0509	1983	100 H	20A	
n/N	4/8	4/8	3/8	3/8	3/10	3/10
TO	.095	.095	.095	.095	.095	.095
Gate	4610.0	4594.0	2303.0	2304.0	2342.0	2336.0
1	1704.0	2712.0	1287.0	1283.0	1295.0	1298.0
2	1770.0	1769.0	850.0	848.0	850.0	851.0
3	1071.0	1068.0	516.0	519.0	518.0	516.0
4	645.0	650.0	317.0	313.0	317.0	321.0
5	394.0	394.0	193.0	192.0	196.0	197.0
6	229.0	224.0	109.0	113.0	115.0	110.0
7	129.0	126.0	62.0	63.0	63.0	62.0
8	74.0	73.0	36.0	36.0	36.0	36.0
9	41.0	40.0	19.0	20.0	20.0	20.0
10	22.0	23.0	11.0	10.0	10.0	12.0
11	16.1	13.4	6.1	8.4	8.6	6.2
12	9.3	8.2	4.0	4.5	4.8	4.0
13	5.2	4.2	1.9	2.5	2.7	2.0
14	2.9	2.1	0.9	1.2	1.4	1.0
15	1.8	0.9	0.3	0.7	0.8	0.3
16	1.5	0.0	-0.2	0.6	0.7	-0.2
17	0.9	-0.1	-0.2	0.3	0.4	-0.2
18	0.7	-0.2	-0.2	0.1	0.2	-0.3
19	0.9	-0.4	-0.5	0.3	0.3	-0.5
20	0.8	-0.3	-0.4	0.2	0.2	-0.4

Site	VIRG2	0508	1983	100 H	20A	
n/N	4/8	4/8	3/8	3/8	3/10	3/10
TO	.095	.095	.095	.095	.095	.095
Gate	4389.0	4404.0	2206.0	2202.0	2237.0	2235.0
1	2537.0	2529.0	1212.0	1218.0	1224.0	1213.0
2	1791.0	1792.0	866.0	866.0	866.0	862.0
3	1176.0	1179.0	574.0	571.0	570.0	570.0
4	770.0	767.0	374.0	376.0	380.0	377.0
5	496.0	497.0	244.0	242.0	247.0	248.0
6	299.0	301.0	149.0	146.0	148.0	150.0
7	172.0	174.0	86.0	83.0	83.0	85.0
8	96.0	97.0	48.0	47.0	47.0	48.0
9	48.0	50.0	24.0	23.0	24.0	24.0
10	23.0	23.0	10.0	11.0	12.0	10.0
11	11.9	13.9	7.5	5.3	5.5	7.4
12	5.7	6.8	3.7	2.4	2.6	3.6
13	2.3	3.1	1.8	0.8	0.9	1.7
14	0.8	1.4	0.9	0.1	0.3	0.8
15	0.1	0.9	0.7	0.6	0.0	0.0
16	-0.2	0.7	0.7	-0.4	-0.3	0.6
17	-0.3	0.5	0.5	-0.3	-0.3	0.4
18	-0.3	0.3	0.4	-0.3	-0.2	0.3
19	-0.5	0.5	0.6	-0.5	-0.4	0.5
20	-0.5	0.4	0.5	-0.4	-0.3	0.4

APPENDIX C: TRANSIENT SOUNDING DATA CONTINUED

Site	FARM1	0408	1983	100 H	20A	
n/N	4/10	4/10	3/10	3/10	3/8	3/8
TO	.095	.095	.095	.095	.095	.095
Gate	4324.0	4306.0	2173.0	2163.0	2136.0	2136.0
1	2324.0	2326.0	1109.0	1110.0	1109.0	1109.0
2	1526.0	1522.0	736.0	735.0	739.0	739.0
3	947.0	943.0	462.0	458.0	461.0	461.0
4	602.0	602.0	294.0	294.0	293.0	293.0
5	380.0	378.0	187.0	185.0	183.0	183.0
6	219.0	216.0	108.0	105.0	104.0	104.0
7	115.0	113.0	57.0	54.0	55.0	55.0
8	57.0	57.0	28.0	27.0	27.0	27.0
9	23.0	22.0	11.0	10.0	11.0	11.0
10	7.0	8.0	2.0	4.0	4.0	4.0
11	4.6	2.4	2.9	0.6	0.8	0.8
12	2.7	1.2	1.7	0.3	0.4	0.4
13	2.1	1.0	1.4	0.3	0.4	0.4
14	1.7	0.9	1.1	0.3	0.3	0.3
15	1.4	0.6	1.0	0.1	0.1	0.1
16	1.4	0.0	1.1	-0.1	-0.1	-0.1
17	1.1	0.0	0.9	-0.2	-0.2	-0.2
18	0.8	0.0	0.7	-0.2	-0.3	-0.3
19	0.9	-0.3	0.8	-0.4	-0.6	-0.6
20	0.6	-0.5	0.6	-0.4	-0.6	-0.6

Site	FARM2	0209	1983	100 H	20A	
n/N	4/8	4/8	5/8	5/8	5/10	5/10
TO	.096	.096	.096	.096	.096	.096
Gate	4221.0	4224.0	5062.0	5100.0	5087.0	5045.0
1	1784.0	1776.0	3649.0	3606.0	3627.0	3620.0
2	1222.0	1222.0	2499.0	2460.0	2460.0	2467.0
3	776.0	779.0	1587.0	1559.0	1555.0	1564.0
4	495.0	495.0	1006.0	989.0	1000.0	1005.0
5	309.0	311.0	630.0	615.0	627.0	635.0
6	176.0	178.0	360.0	349.0	353.0	362.0
7	93.0	95.0	190.0	183.0	182.0	189.0
8	46.0	46.0	93.0	90.0	90.0	94.0
9	19.0	18.0	37.0	37.0	36.0	37.0
10	7.0	5.0	12.0	14.0	14.0	12.0
11	1.9	4.1	7.3	4.8	4.4	7.9
12	0.8	2.3	4.3	2.8	2.2	4.5
13	0.6	1.6	3.4	2.1	1.9	3.3
14	0.4	1.3	2.8	1.3	1.9	2.4
15	0.0	1.1	2.3	0.3	1.6	1.8
16	-0.4	1.1	1.7	0.1	0.9	1.6
17	-0.6	0.7	0.9	0.3	0.3	1.4
18	-0.4	0.4	0.5	0.0	0.1	1.2
19	-0.7	0.7	0.8	1.3	0.0	0.0
20	-0.5	0.7	0.9	-0.1	-0.4	1.5

APPENDIX C: TRANSIENT SOUNDING DATA CONTINUED

Site	FARM3	0209	1983	100 H	20A	
n/N	4/8	4/8	3/8	3/8	4/10	4/10
TO	.083	.083	.083	.083	.083	.083
Gate	4195.0	4218.0	2136.0	2125.0	4249.0	4257.0
1	3090.0	3109.0	1480.0	1472.0	3076.0	3080.0
2	1927.0	1944.0	941.0	928.0	1909.0	1922.0
3	1133.0	1138.0	559.0	547.0	1117.0	1130.0
4	680.0	679.0	332.0	330.0	678.0	683.0
5	402.0	403.0	195.0	196.0	405.0	407.0
6	215.0	214.0	102.0	106.0	216.0	214.0
7	104.0	103.0	48.0	52.0	103.0	101.0
8	47.0	44.0	20.0	24.0	47.0	45.0
9	17.0	14.0	6.0	9.0	17.0	14.0
10	6.0	3.0	0.0	3.0	6.0	3.0
11	2.1	3.5	2.2	0.5	1.4	3.4
12	1.5	2.8	1.9	0.1	0.7	2.5
13	1.5	2.3	1.6	0.1	0.7	2.1
14	1.3	2.0	1.3	0.0	0.6	1.8
15	0.9	1.8	1.1	0.0	0.3	1.5
16	0.5	1.6	1.0	-0.3	0.0	1.3
17	0.4	1.3	0.8	-0.4	0.0	0.9
18	0.0	1.3	0.5	-0.4	-0.1	0.5
19	-0.5	1.1	0.5	-0.7	-0.3	0.6
20	-0.7	0.8	0.4	-0.8	-0.3	0.4

Site	FARM4	3108	1983	100 H	20A			
n/N	4/8	4/8	5/8	5/8	5/10	5/10	4/10	4/10
TO	.095	.095	.095	.095	.095	.095	.095	.095
Gate	4166.0	4170.0	5066.0	5096.0	5078.0	5037.0	4266.0	4247.0
1	2637.0	2623.0	5408.0	5464.0	5514.0	5489.0	2662.0	2667.0
2	1700.0	1698.0	3485.0	3488.0	3503.0	3507.0	1711.0	1706.0
3	1028.0	1031.0	2108.0	2090.0	2103.0	2107.0	1036.0	1028.0
4	628.0	631.0	1283.0	1271.0	1302.0	1293.0	643.0	639.0
5	375.0	382.0	783.0	762.0	792.0	792.0	393.0	386.0
6	201.0	210.0	431.0	418.0	434.0	432.0	217.0	208.0
7	97.0	106.0	216.0	210.0	215.0	213.0	108.0	101.0
8	43.0	49.0	99.0	99.0	102.0	99.0	50.0	47.0
9	15.0	17.0	36.0	38.0	39.0	36.0	18.0	17.0
10	6.0	4.0	9.0	13.0	14.0	10.0	5.0	6.0
11	1.6	3.7	6.5	4.1	5.2	7.1	4.4	2.1
12	1.3	2.4	4.0	2.6	3.3	5.0	3.1	1.6
13	1.3	1.8	3.2	2.7	3.1	4.5	2.7	1.6
14	1.2	1.5	2.3	2.7	2.7	4.1	2.4	1.4
15	0.8	1.1	1.9	1.7	1.9	3.7	2.2	0.9
16	0.3	1.0	2.2	0.8	1.1	3.5	2.2	0.4
17	0.1	0.7	1.8	0.5	0.6	3.3	1.9	0.3
18	0.0	0.5	1.0	0.3	0.1	2.2	1.3	0.0
19	-0.3	0.6	1.5	1.9	1.3	-0.5	0.0	0.0
20	-0.6	0.8	2.1	-0.2	-0.3	0.5	0.5	-0.6

APPENDIX C: TRANSIENT SOUNDING DATA CONTINUED

Site	PEAT	0509	1983	100 H	19.5A			
n/N	4/8	4/8	5/8	5/8	5/10	5/10		
TO	.098	.098	.098	.098	.098	.098		
Gate	3996.0	3968.0	5040.0	4980.0	4995.0	5029.0		
1	1046.0	1043.0	2135.0	2126.0	2133.0	2123.0		
2	798.0	795.0	1620.0	1619.0	1615.0	1602.0		
3	561.0	556.0	1133.0	1135.0	1130.0	1118.0		
4	384.0	386.0	783.0	777.0	784.0	783.0		
5	262.0	261.0	530.0	530.0	539.0	535.0		
6	171.0	165.0	338.0	341.0	346.0	340.0		
7	106.0	104.0	212.0	213.0	212.0	209.0		
8	66.0	65.0	132.0	132.0	132.0	131.0		
9	38.0	37.0	77.0	77.0	77.0	76.0		
10	20.0	21.0	43.0	42.0	43.0	43.0		
11	14.3	12.3	25.9	27.3	27.6	25.6		
12	7.8	7.0	14.6	14.8	14.8	14.0		
13	3.9	3.3	7.0	7.1	7.2	6.6		
14	2.0	1.5	3.2	3.1	3.4	2.9		
15	1.1	0.6	1.4	1.5	1.7	1.1		
16	1.0	0.0	0.2	0.9	1.1	0.0		
17	0.6	-0.1	0.0	0.3	0.5	-0.2		
18	0.4	-0.2	-0.2	0.1	0.2	-0.4		
19	0.5	-0.5	-0.5	0.1	0.2	-0.6		
20	0.3	-0.4	-0.5	-0.5	0.0	0.0		
Site	FLS1	3109	1983	100 H	20A			
n/N	7/8	7/8	6/8	6/8	6/10	6/10	7/10	7/10
TO	.110	.110	.110	.110	.110	.110	.110	.110
Gate	5065.0	5100.0	5077.0	5027.0	5042.0	5044.0	5042.0	5040.0
1	1840.0	1842.0	924.0	909.0	918.0	922.0	1852.0	1859.0
2	1325.0	1313.0	661.0	658.0	660.0	662.0	1325.0	1330.0
3	1005.0	995.0	500.0	503.0	502.0	503.0	1003.0	1006.0
4	743.0	736.0	370.0	371.0	377.0	378.0	755.0	759.0
5	581.0	571.0	286.0	289.0	296.0	296.0	593.0	595.0
6	425.0	420.0	211.0	212.0	216.0	216.0	434.0	436.0
7	311.0	307.0	155.0	156.0	156.0	156.0	314.0	315.0
8	226.0	224.0	113.0	112.0	114.0	114.0	230.0	231.0
9	158.0	159.0	80.0	78.0	79.0	79.0	160.0	162.0
10	110.0	111.0	55.0	53.0	56.0	55.0	113.0	114.0
11	86.2	82.4	41.9	42.5	43.2	43.3	87.7	89.0
12	61.2	60.2	29.8	30.6	31.1	31.1	64.2	64.3
13	44.1	41.7	21.0	21.3	21.6	21.8	45.5	45.3
14	31.3	29.9	15.1	15.2	15.6	15.8	33.9	32.5
15	24.2	22.2	11.2	11.8	12.1	12.1	25.9	24.5
16	18.8	16.6	8.1	8.9	9.0	9.4	19.6	18.1
17	13.5	12.1	5.5	6.6	6.4	6.9	14.5	13.1
18	9.7	8.8	3.7	4.8	4.5	4.9	10.7	9.2
19	6.8	5.7	2.2	3.5	3.2	3.4	8.6	8.2
20	4.8	3.3	1.2	2.3	2.0	2.2	7.4	9.2

APPENDIX C: TRANSIENT SOUNDING DATA CONTINUED

Site	FLS2	0209	1983	100 H	20A	
n/N	7/8	7/8	6/8	6/8	7/10	7/10
TO	.100	.100	.100	.100	.100	.100
Gate	5077.0	5105.0	5086.0	5038.0	5052.0	5094.0
1	1943.0	1936.0	977.0	969.0	1943.0	1938.0
2	1379.0	1371.0	693.0	690.0	1373.0	1366.0
3	1041.0	1032.0	520.0	521.0	1036.0	1025.0
4	770.0	763.0	385.0	383.0	773.0	767.0
5	597.0	591.0	298.0	297.0	606.0	599.0
6	440.0	433.0	217.0	220.0	444.0	436.0
7	322.0	318.0	159.0	161.0	319.0	314.0
8	233.0	230.0	116.0	115.0	234.0	230.0
9	162.0	164.0	82.0	80.0	162.0	162.0
10	112.0	115.0	58.0	55.0	114.0	115.0
11	93.4	83.2	42.0	43.9	88.6	82.6
12	69.1	59.5	20.4	32.4	64.1	59.0
13	50.6	39.8	21.3	22.5	44.6	40.8
14	37.6	25.7	14.9	16.6	32.8	29.4
15	29.9	18.1	10.7	13.1	25.0	22.2
16	22.9	13.0	7.2	10.3	18.8	16.1
17	16.8	8.7	5.0	7.7	14.0	11.7
18	11.0	6.0	3.1	5.6	10.5	9.0
19	7.0	4.2	1.8	3.7	8.9	5.4
20	4.0	3.4	1.1	2.3	6.8	1.9

Site	EIELSON	1209	1983	100 H	20.2A			
n/N	7/8	7/8	6/8	6/8	6/10	6/10	7/8	7/8
TO	.098	.098	.098	.098	.098	.098	.098	.098
Gate	5042.0	5081.0	5060.0	5012.0	5027.0	5062.0	5054.0	5007.0
1	2965.0	2962.0	1488.0	1469.0	1482.0	1493.0	2945.0	2901.0
2	2000.0	1993.0	1003.0	1001.0	1008.0	1006.0	2005.0	1984.0
3	1259.0	1251.0	629.0	632.0	634.0	728.0	1259.0	1250.0
4	806.0	803.0	405.0	403.0	411.0	509.0	808.0	801.0
5	530.0	523.0	264.0	266.0	273.0	267.0	527.0	526.0
6	359.0	345.0	176.0	174.0	179.0	176.0	349.0	346.0
7	233.0	227.0	117.0	116.0	118.0	114.0	231.0	231.0
8	161.0	157.0	82.0	80.0	82.0	80.0	161.0	161.0
9	109.0	105.0	56.0	54.0	56.0	54.0	109.0	109.0
10	74.0	71.0	39.0	36.0	38.0	37.0	75.0	73.0
11	56.6	51.2	29.5	28.3	29.6	27.3	55.8	56.2
12	39.8	33.5	21.0	20.2	20.7	18.4	38.9	39.9
13	25.5	19.6	13.7	12.7	13.3	11.4	25.1	25.4
14	16.2	10.4	8.7	8.2	8.3	6.9	15.8	15.9
15	10.9	4.8	5.4	5.4	5.2	3.5	10.6	9.8
16	7.6	1.6	2.8	3.4	2.9	1.2	7.0	5.2
17	6.1	0.2	1.1	2.2	1.2	0.0	5.4	1.3
18	5.5	-0.1	0.1	1.2	0.1	-0.5	4.2	-1.6
19	3.8	-0.2	-0.7	0.6	-0.1	-0.9	2.1	-3.5
20	1.2	0.0	-1.4	0.0	-0.3	-0.7	0.8	-2.5

APPENDIX C: TRANSIENT SOUNDING DATA CONTINUED

Site	QUARTZ	1109	1983	100 H	20.4A	
n/N	7/8	7/8	6/8	6/8	7/10	7/10
TO	.092	.092	.092	.092	.092	.092
Gate	5028.0	5072.0	5050.0	5002.0	5017.0	5058.0
1	2612.0	2579.0	1288.0	1273.0	2566.0	2574.0
2	1649.0	1645.0	826.0	825.0	1646.0	1636.0
3	887.0	880.0	440.0	444.0	881.0	872.0
4	486.0	486.0	244.0	243.0	490.0	489.0
5	276.0	272.0	136.0	138.0	280.0	276.0
6	149.0	146.0	72.0	74.0	151.0	147.0
7	81.0	78.0	38.0	40.0	80.0	77.0
8	44.0	43.0	20.0	21.0	44.0	43.0
9	22.0	22.0	10.0	11.0	22.0	22.0
10	10.0	10.0	4.0	4.0	10.0	10.0
11	6.4	4.2	1.6	3.3	6.3	4.3
12	2.6	1.2	0.1	1.1	2.4	1.0
13	0.2	-0.6	-0.5	0.0	0.2	-0.4
14	-0.4	-1.1	-0.8	-0.4	-0.6	-1.2
15	-0.8	-1.3	-1.0	-0.5	-0.8	-1.4
16	-0.8	-1.6	-1.2	-0.3	-0.8	-1.5
17	-0.8	-1.3	-1.0	-0.4	-0.9	-1.4
18	-0.8	-1.1	-0.8	-0.5	-0.8	-1.1
19	-0.6	-1.2	-0.9	-0.2	-0.5	-1.2
20	-0.4	-1.0	-0.8	-0.2	-0.4	-0.9

Site	SAWMILL		0809	1983	100 H	19.1A
n/N	9/8	9/8	9/10	9/10	8/10	8/10
TO	.094	.094	.094	.094	.094	.094
Gate	5046.0	4996.0	5007.0	5043.0	5035.0	4999.0
1	1137.0	1137.0	1143.0	1148.0	572.0	561.0
2	888.0	893.0	893.0	887.0	443.0	440.0
3	639.0	649.0	648.0	638.0	317.0	319.0
4	449.0	469.0	473.0	454.0	230.0	231.0
5	311.0	334.0	342.0	317.0	162.0	166.0
6	212.0	226.0	228.0	215.0	109.0	111.0
7	137.0	153.0	152.0	138.0	70.0	73.0
8	90.0	103.0	104.0	92.0	47.0	49.0
9	59.0	65.0	65.0	60.0	30.0	31.0
10	36.0	40.0	42.0	36.0	19.0	19.0
11	12.5	39.3	39.7	13.1	10.4	15.1
12	2.9	28.8	28.0	3.8	5.3	9.6
13	3.5	20.1	19.6	-3.0	1.8	5.4
14	6.4	14.0	13.5	-6.1	-0.1	3.0
15	-8.4	10.0	9.8	-7.7	-1.0	1.6
16	-7.6	6.6	6.6	-7.1	-1.6	0.5
17	-8.0	5.2	5.4	-7.3	-1.7	0.1
18	-7.0	3.9	3.9	-6.5	-1.6	-0.1
19	-8.5	5.8	5.9	-8.1	-1.9	0.2
20	-6.9	4.6	4.8	-6.6	-1.5	0.0

APPENDIX C: TRANSIENT SOUNDING DATA CONTINUED

Site	GREELY	0809	1983	100 H	19.7A	
n/N	5/8	5/8	4/8	4/8	5/10	5/10
TO	.094	.094	.094	.094	.094	.094
Gate	5056.0	4998.0	4243.0	4217.0	5062.0	5009.0
1	1530.0	2500.0	1222.0	1222.0	2519.0	2502.0
2	1576.0	1571.0	768.0	767.0	1580.0	1577.0
3	897.0	896.0	441.0	436.0	892.0	893.0
4	511.0	507.0	249.0	250.0	516.0	512.0
5	291.0	291.0	144.0	142.0	296.0	297.0
6	155.0	158.0	79.0	75.0	157.0	160.0
7	82.0	84.0	42.0	39.0	82.0	84.0
8	45.0	46.0	23.0	22.0	46.0	46.0
9	24.0	24.0	12.0	11.0	24.0	24.0
10	12.0	10.0	4.0	6.0	12.0	11.0
11	5.6	7.6	4.2	2.3	5.7	7.6
12	2.2	3.2	1.9	1.0	2.4	3.2
13	0.4	1.1	0.7	0.1	0.6	1.1
14	-0.1	0.2	0.2	0.2	0.0	0.0
15	-0.4	0.1	0.2	-0.1	-0.2	0.1
16	-0.9	0.2	0.3	-0.5	-0.7	0.1
17	-0.8	0.0	0.1	-0.4	-0.7	0.0
18	-0.8	0.0	0.1	-0.4	-0.6	0.0
19	-1.0	0.1	0.3	-0.5	-0.8	0.0
20	-0.9	0.0	0.2	-0.5	-0.7	0.0

Site	FIELD	0908	1983	100 H	20A	
n/N	6/8	6/8	5/8	5/8	5/10	5/10
TO	.095	.095	.095	.095	.095	.095
Gate	5050.0	5083.0	5060.0	5019.0	5036.0	5078.0
1	2819.0	2779.0	1373.0	1354.0	1360.0	1369.0
2	1970.0	1954.0	970.0	969.0	971.0	969.0
3	1285.0	1274.0	630.0	634.0	633.0	626.0
4	850.0	844.0	417.0	417.0	422.0	420.0
5	571.0	563.0	277.0	281.0	286.0	281.0
6	368.0	366.0	181.0	181.0	184.0	182.0
7	243.0	239.0	117.0	120.0	120.0	116.0
8	162.0	160.0	79.0	80.0	81.0	79.0
9	107.0	105.0	52.0	53.0	53.0	51.0
10	70.0	70.0	34.0	34.0	35.0	35.0
11	52.0	50.6	24.7	26.1	26.3	24.7
12	36.2	34.8	16.9	18.3	18.1	16.7
13	23.3	22.4	10.8	11.8	11.7	10.7
14	14.9	14.2	6.8	7.6	7.6	6.8
15	9.9	9.1	4.2	5.1	5.1	4.2
16	6.2	5.3	2.2	3.4	3.4	2.2
17	3.6	2.9	1.1	2.1	2.0	1.1
18	2.1	1.4	0.4	1.3	1.2	0.4
19	1.2	0.3	0.0	0.9	0.8	0.0
20	0.6	0.0	-0.3	0.6	0.5	-0.3

APPENDIX C: TRANSIENT SOUNDING DATA CONTINUED

Site	SUMMIT	0909	1983	100 H	19.8A	
n/N	4/8	4/8	3/8	3/8	4/10	4/10
TO	.095	.095	.095	.095	.095	.095
Gate	4336.0	4336.0	2176.0	2170.0	4376.0	4372.0
1	2557.0	2543.0	1213.0	1219.0	2556.0	2531.0
2	1749.0	1745.0	840.0	840.0	1735.0	1726.0
3	1112.0	1113.0	541.0	537.0	1101.0	1099.0
4	718.0	714.0	348.0	349.0	720.0	714.0
5	465.0	465.0	228.0	226.0	470.0	470.0
6	290.0	291.0	144.0	142.0	293.0	293.0
7	180.0	182.0	90.0	87.0	178.0	180.0
8	112.0	113.0	56.0	55.0	112.0	113.0
9	67.0	67.0	33.0	33.0	67.0	67.0
10	40.0	38.0	18.0	20.0	40.0	38.0
11	24.8	27.0	14.0	11.8	25.0	27.1
12	15.1	16.6	8.7	7.1	15.0	16.4
13	8.3	9.3	5.0	3.9	8.4	9.3
14	4.4	5.3	2.9	2.0	4.6	5.4
15	2.3	3.3	1.9	0.9	2.4	3.3
16	0.7	2.1	1.5	0.1	0.8	2.2
17	0.0	1.2	1.0	0.0	0.1	1.2
18	0.0	0.7	0.6	-0.1	0.0	0.7
19	-0.4	0.6	0.7	-0.4	-0.4	0.6
20	-0.5	0.5	0.6	-0.4	-0.4	0.5

Site	SOURDOUGH		1008	1983	100 H	19.2A
n/N	7/8	7/8	6/8	6/8	6/10	6/10
TO	.092	.092	.092	.092	.092	.092
Gate	5029.0	5069.0	5045.0	4997.0	5012.0	5052.0
1	3080.0	3141.0	1596.0	1567.0	1556.0	1564.0
2	2482.0	2472.0	1246.0	1236.0	1224.0	1213.0
3	1746.0	1738.0	873.0	872.0	860.0	848.0
4	1195.0	1198.0	601.0	598.0	599.0	593.0
5	809.0	799.0	400.0	404.0	408.0	398.0
6	501.0	502.0	252.0	249.0	250.0	250.0
7	301.0	299.0	150.0	150.0	148.0	146.0
8	177.0	176.0	88.0	88.0	87.0	86.0
9	96.0	96.0	47.0	48.0	47.0	46.0
10	49.0	49.0	24.0	24.0	24.0	24.0
11	28.2	27.8	13.8	13.9	13.9	13.6
12	14.5	13.3	6.3	7.1	7.0	6.3
13	5.8	4.8	2.2	2.8	2.7	2.1
14	1.9	1.1	0.3	0.8	0.8	0.3
15	0.3	-0.3	-0.3	0.1	0.1	-0.3
16	-0.1	-0.7	-0.6	0.0	-0.1	-0.7
17	-0.5	-0.9	-0.7	-0.2	-0.3	-0.7
18	-0.6	-0.9	-0.7	-0.2	-0.3	-0.7
19	-0.4	-1.1	-0.8	0.0	-0.1	-0.8
20	-0.3	-0.9	-0.7	-0.1	-0.1	-0.7

APPENDIX C: TRANSIENT SOUNDING DATA CONTINUED

Site	GLEN1	1008	1983	100 H	20A	
n/N	5/8	5/8	4/8	4/8	5/10	5/10
TO	.092	.092	.092	.092	.092	.092
Gate	5049.0	4997.0	4324.0	4310.0	5060.0	4999.0
1	1719.0	1722.0	845.0	848.0	1819.0	1812.0
2	1395.0	1398.0	695.0	697.0	1401.0	1396.0
3	1011.0	1018.0	505.0	502.0	1015.0	1016.0
4	775.0	776.0	383.0	384.0	788.0	785.0
5	576.0	582.0	289.0	284.0	592.0	594.0
6	418.0	424.0	211.0	206.0	428.0	430.0
7	309.0	315.0	157.0	152.0	312.0	315.0
8	233.0	237.0	118.0	115.0	237.0	239.0
9	169.0	172.0	86.0	84.0	172.0	173.0
10	121.0	123.0	61.0	61.0	127.0	126.0
11	87.6	95.6	48.3	43.3	92.8	98.3
12	56.4	65.7	32.2	29.6	62.5	66.7
13	41.1	51.1	25.4	23.9	48.6	51.4
14	31.1	40.2	19.5	18.1	38.8	40.8
15	21.2	27.6	13.0	10.1	25.8	27.2
16	11.8	16.6	8.3	6.5	14.9	16.8
17	8.1	12.7	6.6	4.5	11.3	13.0
18	4.1	7.4	4.9	3.5	5.8	7.3
19	2.1	4.4	4.0	1.1	3.2	5.2
20	1.3	3.0	2.7	0.8	-0.2	3.3

Site	GLEN2	1008	1983	100 H	19.8A
n/N	6/8	6/8	5/8	5/8	
TO	.092	.092	.092	.092	
Gate	5016.0	5055.0	5045.0	4991.0	
1	3680.0	3674.0	1810.0	1686.0	
2	2835.0	2808.0	1391.0	1327.0	
3	2061.0	2051.0	1009.0	969.0	
4	1560.0	1570.0	773.0	741.0	
5	1186.0	1170.0	574.0	556.0	
6	863.0	852.0	418.0	404.0	
7	644.0	630.0	310.0	301.0	
8	485.0	473.0	233.0	226.0	
9	351.0	344.0	170.0	164.0	
10	253.0	251.0	123.0	120.0	
11	194.1	188.6	91.6	93.9	
12	131.7	127.9	61.5	63.3	
13	102.0	100.6	47.5	49.4	
14	79.3	75.5	37.6	37.6	
15	53.2	36.9	24.8	28.2	
16	32.6	19.1	14.6	16.3	
17	25.8	14.6	11.8	12.6	
18	18.9	4.3	5.6	7.0	
19	24.4	-0.1	2.6	5.0	
20	12.7	1.6	1.1	2.6	

APPENDIX C: TRANSIENT SOUNDING DATA CONTINUED

Site	-2a	0705	1984	400 H	400 L	22.5A		
n/N	6/10	6/10	6/10	6/10	6/10	6/10	6/10	6/10
TO	.750	.750	.750	.750	.325	.325	.740	.740
Gate	5000.0	5000.0	5352.0	4963.0	5359.0	4963.0	4964.0	5351.0
1	871.0	870.0	864.0	868.0	5953.0	7009.0	103.0	78.0
2	778.0	772.0	772.0	771.0	5969.0	7019.0	74.0	46.0
3	668.0	673.0	663.0	672.0	5940.0	7015.0	52.0	23.0
4	575.0	572.0	571.0	571.0	5948.0	7005.0	41.0	14.0
5	485.0	476.0	482.0	475.0	5923.0	7019.0	30.0	7.0
6	384.0	383.0	371.0	382.0	5926.0	7085.0	25.0	4.0
7	304.0	304.0	303.0	303.0	2495.0	2562.0	9.0	4.0
8	228.0	230.0	227.0	230.0	1252.0	1274.0	8.0	2.0
9	165.0	167.0	164.0	167.0	679.0	689.0	6.0	1.0
10	111.0	112.0	111.0	112.0	376.0	380.0	3.0	1.0
11	82.7	80.5	82.1	80.2	242.0	234.9	2.4	3.1
12	48.3	48.3	48.0	48.2	128.9	129.8	2.8	2.0
13	27.1	27.2	26.9	27.2	63.1	63.5	2.6	1.3
14	14.6	15.0	14.5	15.0	29.2	29.7	1.9	1.2
15	8.3	9.1	8.2	9.0	14.2	15.1	1.8	0.5
16	4.9	5.2	4.8	5.1	7.1	7.3	1.1	0.7
17	3.1	3.6	3.1	3.5	4.0	4.4	0.9	0.5
18	2.1	2.5	2.1	2.4	2.6	2.8	1.0	0.2
19	1.3	1.8	1.3	1.8	1.5	1.9	0.5	0.4
20	578.8	707.9	578.9	707.9	0.0	0.9	0.0	0.8

Site	WestDock	0705	1984	400 H	23A			
n/N	3/8	3/8	3/8	3/8	6/10	6/10	6/10	6/10
TO	.400	.400	.400	.400	.400	.400	.800	.800
Gate	5000.0	5000.0	5000.0	5000.0	5000.0	5000.0	5000.0	5000.0
1	4304.0	4353.0	4287.0	4358.0	5000.0	5000.0	1236.0	1210.0
2	4234.0	4282.0	4217.0	4287.0	5000.0	5000.0	1125.0	1100.0
3	4120.0	4161.0	4102.0	4166.0	5000.0	5000.0	999.0	972.0
4	3925.0	3916.0	3860.0	3904.0	5000.0	5000.0	881.0	848.0
5	1553.0	1515.0	1480.0	1490.0	5000.0	5000.0	746.0	724.0
6	535.0	528.0	523.0	525.0	4308.0	4330.0	598.0	586.0
7	279.0	279.0	275.0	278.0	2270.0	2272.0	478.0	472.0
8	176.0	173.0	171.0	175.0	1394.0	1396.0	371.0	364.0
9	109.0	106.0	105.0	109.0	877.0	878.0	280.0	275.0
10	66.0	63.0	62.0	66.0	524.0	525.0	198.0	194.0
11	43.6	46.3	45.9	43.5	356.4	342.3	146.1	150.7
12	26.0	25.5	25.2	26.1	205.4	205.2	97.4	96.8
13	14.3	13.7	13.5	14.3	113.2	113.3	60.5	60.0
14	8.1	6.9	6.7	8.1	60.6	61.1	36.5	35.8
15	4.9	3.2	3.1	4.9	33.6	34.7	23.0	21.8
16	2.2	1.8	1.7	2.2	17.3	17.9	13.2	12.5
17	1.2	0.7	0.6	1.3	9.4	10.1	8.2	7.5
18	0.8	0.1	0.0	0.8	5.4	6.0	5.2	4.7
19	0.6	0.0	0.0	0.6	2.9	3.7	3.5	2.7
20	0.0	0.4	0.4	0.1	3.0	2.5	706.8	574.2

APPENDIX C: TRANSIENT SOUNDING DATA CONTINUED

Sites	.75a	0706	1984	250 H	17A	West Dock0705	400 L	26A
n/N	2/8	2/8	2/8	2/8		6/10	6/10	
TO	.300	.300	.300	.300		.670	.670	
Gate	5000.0	5000.0	5000.0	5000.0		5000.0	5000.0	
1	1848.0	1812.0	1834.0	1808.0		211.0	179.0	
2	1877.0	1856.0	1865.0	1851.0		150.0	117.0	
3	1871.0	1845.0	1860.0	1839.0		101.0	68.0	
4	1879.0	1867.0	1868.0	1861.0		74.0	42.0	
5	1854.0	1852.0	1846.0	1845.0		49.0	24.0	
6	1763.0	1748.0	1756.0	1740.0		28.0	14.0	
7	1589.0	1580.0	1584.0	1573.0		15.0	9.0	
8	1373.0	1362.0	1367.0	1356.0		12.0	4.0	
9	1092.0	1085.0	1088.0	1079.0		8.0	3.0	
10	805.0	802.0	802.0	798.0		5.0	2.0	
11	591.1	576.9	589.0	576.9		3.7	3.9	
12	395.4	393.7	394.1	391.7		3.5	2.2	
13	233.9	233.1	233.2	231 8		2.9	1.5	
14	133.4	132.3	133.0	131.5		2.2	1.1	
15	75.6	74.2	75.5	73.7		2.0	0.6	
16	37.3	37.0	37.2	36.8		1.5	0.5	
17	18.0	17.7	18.0	17.5		1.2	0.3	
18	8.4	7.9	8.4	7.8		1.2	0.0	
19	3.6	3.0	3.6	2.9		0.8	0.1	
20	1.0	1.5	1.0	1.4		0.1	0.5	

Site	.75b	0605	1984	250 L	20A	
n/N	5/10	5/10	5/10	5/10	5/10	5/10
TO	.310	.310	.310	.310	.310	.310
Gate	5000.0	5000.0	5000.0	5000.0	5000.0	5000.0
1	4758.0	4821.0	4747.0	4826.0	4773.0	4795.0
2	3204.0	3235.0	3196.0	3238.0	3193.0	3217.0
3	1911.0	1915.0	1904.0	1917.0	1902.0	1905.0
4	1104.0	1093.0	1097.0	1094.0	1096.0	1088.0
5	619.0	612.0	615.0	613.0	614.0	609.0
6	309.0	308.0	305.0	309.0	305.0	307.0
7	151.0	148.0	149.0	148.0	148.0	147.0
8	68.0	68.0	65.0	68.0	65.0	68.0
9	28.0	28.0	26.0	28.0	26.0	28.0
10	11.0	9.0	9.0	9.0	9.0	9.0
11	6.2	3.3	5.5	3.7	5.2	3.5
12	2.1	1.9	1.6	2.1	1.4	2.2
13	0.6	1.0	0.3	1.2	0.2	1.3
14	0.2	0.4	0.1	0.6	0.0	0.7
15	0.0	0.4	0.0	0.7	0.0	0.8
16	0.0	0.1	0.0	0.5	0.0	0.6
17	0.0	0.0	0.0	0.5	0.0	0.5
18	-0.2	0.0	-0.1	0.7	-0.3	0.7
19	-0.1	-0.2	0.0	0.4	-0.1	0.5
20	0.0	-0.7	0.1	0.0	0.0	0.0

APPENDIX C: TRANSIENT SOUNDING DATA CONTINUED

Site	1a	0505	500 H	23A	1d	500 L	23A	
n/N	2/10	2/10	2/10	2/10	6/10	6/10	7/10	7/10
TO	.680	.680	.680	.680	.720	.720	.720	.720
Gate	5000.0	5000.0	5000.0	5000.0	6000.0	6000.0	6000.0	6000.0
1	218.0	212.0	212.0	215.0	5074.0	4936.0	5865.0	5865.0
2	221.0	219.0	219.0	218.0	4860.0	4717.0	5878.0	5878.0
3	224.0	219.0	220.0	220.0	4334.0	4218.0	5852.0	5852.0
4	232.0	225.0	225.0	228.0	3629.0	3553.0	5863.0	5863.0
5	239.0	237.0	232.0	236.0	2815.0	2761.0	5625.0	5597.0
6	249.0	244.0	245.0	245.0	1964.0	1930.0	3926.0	3910.0
7	261.0	255.0	255.0	257.0	1312.0	1290.0	2620.0	2618.0
8	275.0	268.0	269.0	271.0	801.0	785.0	1598.0	1599.0
9	287.0	280.0	280.0	281.0	457.0	446.0	911.0	911.0
10	299.0	292.0	292.0	294.0	239.0	232.0	475.0	475.0
11	299.2	306.5	306.5	295.2	130.3	131.6	253.9	261.0
12	285.8	281.5	281.4	282.0	65.9	62.9	130.2	129.4
13	256.9	252.9	252.8	253.3	29.2	26.2	56.7	55.3
14	215.1	211.0	210.9	212.1	13.0	10.6	24.6	22.8
15	168.3	164.6	164.5	165.8	6.8	4.5	12.3	10.3
16	116.1	114.1	114.1	114.3	3.8	1.8	5.8	5.2
17	76.3	74.7	74.8	75.1	2.7	0.8	3.6	3.1
18	46.7	45.3	45.4	45.9	2.3	0.3	2.9	1.6
19	25.9	24.6	24.7	25.4	1.7	0.2	1.9	1.1
20	16.8	16.6	16.7	16.4	0.9	0.6	0.6	1.0

Sites	1b	0605	250 H	17A	5a	0505	500 L	22A
n/N	2/8	2/8	2/8	2/8	6/10	6/10	6/10	6/10
TO	.290	.290	.290	.290	.700	.700	.700	.700
Gate	5000.0	5000.0	5000.0	5000.0	5000.0	5000.0	5000.0	5000.0
1	1378.0	1392.0	1370.0	1395.0	1860.0	1825.0	1828.0	1851.0
2	1387.0	1394.0	1379.0	1397.0	1877.0	1844.0	1848.0	1867.0
3	1353.0	1366.0	1345.0	1370.0	1873.0	1846.0	1849.0	1864.0
4	1356.0	1358.0	1347.0	1361.0	1845.0	1830.0	1835.0	1835.0
5	1353.0	1349.0	1345.0	1352.0	1746.0	1733.0	1736.0	1738.0
6	1312.0	1317.0	1303.0	1320.0	1595.0	1579.0	1583.0	1588.0
7	1255.0	1259.0	1247.0	1262.0	1431.0	1421.0	1423.0	1425.0
8	1174.0	1179.0	1166.0	1182.0	1172.0	1163.0	1166.0	1167.0
9	1043.0	1048.0	1036.0	1050.0	926.0	918.0	920.0	922.0
10	872.0	874.0	865.0	875.0	673.0	669.0	671.0	670.0
11	576.0	704.8	576.2	704.8	478.4	485.1	485.8	476.2
12	528.4	529.7	524.8	530 8	334.4	332.1	332.8	333.0
13	349.2	350.0	346.8	350.7	209.5	207.6	208.1	208.7
14	217.1	218.5	215.7	218.9	127.7	126.4	126.8	127.2
15	131.2	132.5	130.3	132.8	79.8	78.3	78.6	79.5
16	70.5	70.7	70.0	70.8	44.8	43.9	44.1	44.7
17	36.8	37.1	36.5	37.1	25.6	24.9	25.1	25.7
18	18.4	19.0	18.3	19.0	14.5	13.6	13.8	14.7
19	8.2	8.9	8.2	8.9	7.3	7.1	7.2	7.7
20	3.9	3.5	3.8	3.4	3.2	4.1	4.0	3.6

APPENDIX C: TRANSIENT SOUNDING DATA CONTINUED

Site	1c	0605	1984	250 L	20A	
n/N	5/10	5/10	5/10	5/10	5/10	5/10
TO	.300	.300	.300	.300	.300	.300
Gate	5000.0	5000.0	5000.0	5000.0	5000.0	5000.0
1	5782.0	5882.0	5789.0	5872.0	5778.0	5879.0
2	4324.0	4400.0	4330.0	4391.0	4322.0	4396.0
3	2877.0	2909.0	2881.0	2903.0	2876.0	2907.0
4	1820.0	1824.0	1823.0	1820.0	1819.0	1822.0
5	1098.0	1101.0	1101.0	1098.0	1099.0	1099.0
6	593.0	599.0	596.0	598.0	594.0	599.0
7	317.0	319.0	318.0	318.0	318.0	319.0
8	158.0	164.0	160.0	164.0	160.0	164.0
9	75.0	79.0	76.0	79.0	76.0	79.0
10	33.0	35.0	34.0	35.0	34.0	35.0
11	17.5	16.8	18.0	16.4	18.0	16.4
12	6.7	8.5	7.0	8.1	6.9	8.1
13	2.0	3.7	1.9	3.5	1.9	3.3
14	0.5	1.7	0.1	1.5	0.2	1.3
15	0.0	1.3	-0.5	1.1	-0.3	0.8
16	0.0	0.7	-0.5	0.6	-0.2	0.2
17	0.0	0.5	-0.7	0.5	-0.3	0.0
18	-0.1	0.6	-0.9	0.7	-0.4	0.0
19	0.0	0.2	-0.7	0.5	-0.1	-0.1
20	0.3	-0.1	-0.2	0.0	0.2	-0.6

Site	3a	0605	500 L	22A	3d	250 H	17A	
n/N	6/10	6/10	6/10	6/10	2/8	2/8	2/8	2/8
TO	.720	.720	.720	.720	.290	.290	.290	.290
Gate	5000.0	5000.0	5000.0	5000.0	5000.0	5000.0	5000.0	5000.0
1	2878.0	2828.0	2864.0	2834.0	1040.0	1034.0	1044.0	1035.0
2	2932.0	2879.0	2917.0	2886.0	1055.0	1054.0	1059.0	1055.0
3	2905.0	2858.0	2889.0	2866.0	1051.0	1043.0	1054.0	1043.0
4	2753.0	2726.0	2736.0	2737.0	1059.0	1058.0	1061.0	1059.0
5	2424.0	2403.0	2410.0	2409.0	1066.0	1069.0	1066.0	1070.0
6	1965.0	1945.0	1953.0	1951.0	1050.0	1045.0	1049.0	1047.0
7	1525.0	1514.0	1516.0	1517.0	1012.0	1008.0	1011.0	1009.0
8	1081.0	1070.0	1074.0	1073.0	959.0	951.0	957.0	953.0
9	736.0	729.0	731.0	731.0	872.0	866.0	871.0	867.0
10	474.0	469.0	470.0	470.0	761.0	756.0	760.0	757.0
11	312.3	319.7	310.1	320.4	653.4	573.2	652.3	573.4
12	203.6	201.1	201.7	201.6	529.5	527.1	528.8	528.0
13	119.6	117.2	118.1	117.4	392.0	390.3	391.5	391.0
14	67.8	65.8	66.5	66.1	275.5	273.3	275.2	273.8
15	39.3	37.0	38.1	37.2	186.4	184.4	186.1	184.7
16	20.0	18.3	19.0	18.4	111.9	111.4	111.8	111.6
17	10.7	8.9	9.6	9.0	65.9	65.3	65.8	65.4
18	6.0	4.0	5.0	4.1	37.6	36.9	37.6	36.9
19	3.3	1.8	2.3	1.9	20.2	19.4	20.2	19.4
20	1.6	1.1	0.7	1.2	10.2	10.5	10.2	10.5

APPENDIX C: TRANSIENT SOUNDING DATA CONTINUED

Site	3b	0505	1984	500 V	22A			
n/N	6/10	6/10	6/10	6/10	7/10	7/10	6/10	6/10
TO	.720	.720	.720	.720	.720	.720	.720	.720
Gate	5000.0	5000.0	5000.0	5000.0	5000.0	5000.0	5000.0	5000.0
1	2175.0	2263.0	2148.0	2216.0	2919.0	2964.0	2251.0	2172.0
2	1651.0	1710.0	1621.0	1681.0	2339.0	2429.0	1701.0	1640.0
3	1054.0	1117.0	1053.0	1069.0	1782.0	1752.0	1079.0	1060.0
4	596.0	632.0	595.0	607.0	1136.0	1117.0	617.0	596.0
5	329.0	353.0	331.0	334.0	678.0	655.0	341.0	330.0
6	161.0	179.0	165.0	164.0	341.0	326.0	171.0	164.0
7	81.0	90.0	82.0	82.0	171.0	161.0	87.0	80.0
8	36.0	47.0	41.0	37.0	83.0	75.0	43.0	39.0
9	16.0	24.0	19.0	16.0	40.0	33.0	21.0	18.0
10	7.0	13.0	10.0	7.0	19.0	11.0	11.0	8.0
11	6.1	7.7	4.4	5.8	0.0	-0.8	9.6	4.2
12	2.6	6.9	3.7	2.7	-18.9	15.1	5.9	3.6
13	1.1	5.2	2.3	1.1	-1.1	-5.6	4.1	2.3
14	0.5	4.2	1.4	0.6	-2.1	-8.2	3.5	1.4
15	0.0	3.8	1.2	0.0	-0.7	-10.8	2.7	1.1
16	0.0	3.0	0.6	0.0	-3.7	-8.9	2.6	0.5
17	-0.4	2.8	0.3	0.0	-11.5	-1.3	2.4	0.3
18	-1.8	2.3	0.3	-0.2	-3.4	-9.7	1.9	0.4
19	-2.1	0.4	-0.4	0.0	-2.4	-12.0	1.7	0.1
20	-1.7	-0.4	-2.6	0.4	-5.2	-11.3	0.6	-0.1

Site	3e	0605	1984	250 L	20A	
n/N	5/10	5/10	5/10	5/10	5/10	5/10
TO	.300	.300	.300	.300	.300	.300
Gate	6000.0	6000.0	6000.0	6000.0	6000.0	6000.0
1	5396.0	5479.0	5382.0	5475.0	5376.0	5463.0
2	4388.0	4460.0	4377.0	4456.0	4371.0	4446.0
3	3272.0	3309.0	3264.0	3307.0	3260.0	3299.0
4	2338.0	2343.0	2333.0	2342.0	2330.0	2336.0
5	1580.0	1585.0	1578.0	1583.0	1576.0	1579.0
6	970.0	974.0	970.0	973.0	969.0	971.0
7	588.0	590.0	588.0	589.0	588.0	588.0
8	337.0	343.0	338.0	342.0	338.0	341.0
9	189.0	194.0	191.0	193.0	190.0	193.0
10	102.0	107.0	105.0	106.0	104.0	106.0
11	64.2	62.8	65.9	62.4	66.0	62.4
12	35.0	37.6	36.8	37.1	36.9	37.1
13	17.3	20.2	19.0	19.7	19.2	19.7
14	7.9	10.7	9.7	10.2	9.8	10.2
15	3.0	6.1	4.8	5.6	5.0	5.7
16	0.4	3.1	2.1	2.5	2.3	2.5
17	-0.7	1.9	0.7	1.1	0.9	1.2
18	-1.5	1.5	0.0	0.6	0.0	0.7
19	-1.6	0.9	-0.1	0.1	0.0	0.2
20	-1.1	0.1	0.0	-0.1	0.1	0.0

APPENDIX C: TRANSIENT SOUNDING DATA CONTINUED

Site	5b	0505	1984	500 V	22A	
n/N	6/10	6/10	6/10	6/10	6/10	6/10
TO	.700	.700	.700	.700	.700	.700
Gate	5000.0	5000.0	5000.0	5000.0	5000.0	5000.0
1	2648.0	2806.0	2700.0	2767.0	2764.0	2716.0
2	2162.0	2354.0	2258.0	2258.0	2256.0	2268.0
3	1690.0	1756.0	1680.0	1764.0	1761.0	1686.0
4	1167.0	1212.0	1161.0	1213.0	1208.0	1161.0
5	719.0	745.0	714.0	753.0	752.0	716.0
6	409.0	418.0	401.0	430.0	429.0	403.0
7	234.0	238.0	231.0	248.0	249.0	232.0
8	131.0	129.0	126.0	140.0	141.0	127.0
9	70.0	65.0	66.0	77.0	79.0	65.0
10	37.0	32.0	33.0	42.0	44.0	32.0
11	18.3	14.5	16.2	19.2	18.3	13.8
12	11.8	6.9	8.5	16.2	15.6	6.8
13	6.0	1.0	1.8	10.5	12.0	0.7
14	3.3	-0.9	-1.1	7.9	9.9	-1.3
15	2.3	-2.3	-2.5	6.6	9.0	-2.7
16	1.5	-2.6	-2.8	5.3	7.4	-3.0
17	1.5	-2.9	-3.1	4.8	7.0	-3.3
18	2.9	-2.7	-3.3	4.4	6.4	-3.6
19	3.1	-1.0	-3.0	3.0	4.2	-3.2
20	2.5	0.6	-2.4	-0.1	0.0	-2.5

Site	5c	0605	250 H	17A	5d	250 L	20A	
n/N	2/8	2/8	2/8	2/8	5/10	5/10	5/10	5/10
TO	.285	.285	.285	.285	.300	.300	.300	.300
Gate	5000.0	5000.0	5000.0	5000.0	6000.0	6000.0	6000.0	6000.0
1	593.0	577.0	581.0	577.0	5465.0	5356.0	5455.0	5369.0
2	616.0	602.0	605.0	602.0	4594.0	4495.0	4584.0	4505.0
3	630.0	616.0	620.0	617.0	3522.0	3459.0	3513.0	3466.0
4	662.0	645.0	651.0	646.0	2609.0	2582.0	2600.0	2587.0
5	695.0	685.0	688.0	685.0	1881.0	1862.0	1875.0	1865.0
6	725.0	716.0	719.0	717.0	1274.0	1262.0	1268.0	1264.0
7	755.0	746.0	751.0	747.0	865.0	858.0	862.0	859.0
8	776.0	764.0	771.0	764.0	559.0	550.0	556.0	551.0
9	768.0	758.0	764.0	758.0	350.0	343.0	347.0	344.0
10	719.0	709.0	415.0	710.0	208.0	202.0	205.0	203.0
11	643.4	570.4	640.3	570.6	128.2	131.2	126.2	131.1
12	537.3	532.4	534.9	532.7	78.7	75.7	76.2	75.6
13	409.7	405.9	407.9	406.1	43.9	41.2	42.0	40.9
14	299.5	295.7	298.2	295.9	25.0	22.5	23.1	22.3
15	214.9	211.6	214.0	211.8	15.4	12.8	13.6	12.6
16	141.6	140.4	141.0	140.5	8.8	6.8	7.1	6.7
17	93.3	92.2	92.9	92.2	5.6	3.6	3.9	3.6
18	59.2	58.0	59.0	58.1	4.0	1.6	2.4	1.7
19	35.0	33.9	34.9	33.9	2.8	0.7	1.1	1.1
20	19.3	19.4	19.2	19.4	1.3	0.5	0.2	1.1

APPENDIX C: TRANSIENT SOUNDING DATA CONTINUED

Site	7a	0505	500 L	22A	9a	0505	500 L	22A
n/N	6/10	6/10	6/10	6/10	6/10	6/10	6/10	6/10
TO	.680	.680	.680	.680	.680	.680	.680	.680
Gate	5000.0	5000.0	5000.0	5000.0	5000.0	5000.0	5000.0	5000.0
1	1701.0	1670.0	1697.0	1664.0	1611.0	1581.0	1610.0	1576.0
2	1757.0	1730.0	1753.0	1724.0	1686.0	1661.0	1685.0	1654.0
3	1814.0	1791.0	1809.0	1785.0	1772.0	1748.0	1769.0	1742.0
4	1851.0	1840.0	1814.0	1834.0	1837.0	1826.0	1833.0	1821.0
5	1810.0	1799.0	1803.0	1793.0	1817.0	1805.0	1812.0	1799.0
6	1707.0	1691.0	1700.0	1685.0	1726.0	1707.0	1721.0	1702.0
7	1565.0	1555.0	1559.0	1549.0	1584.0	1572.0	1580.0	1566.0
8	1295.0	1285.0	1289.0	1281.0	1310.0	1299.0	1306.0	1294.0
9	1020.0	1012.0	1016.0	1009.0	1035.0	1026.0	1032.0	1022.0
10	730.0	727.0	727.0	724.0	746.0	742.0	744.0	740.0
11	506.6	512.4	504.4	510.1	522.2	527.0	520.4	525.4
12	344.7	343.1	343.3	341.4	360.3	358.1	359.0	356.6
13	209.3	208.1	208.5	206.9	220.6	218.7	219.6	218.0
14	125.2	124.4	124.7	123.6	131.1	129.9	130.4	129.3
15	77.9	77.1	77.6	76.4	79.9	78.5	79.3	78.1
16	44.5	44.0	44.3	43.5	43.9	43.0	43.4	42.9
17	26.2	25.8	26.1	25.4	24.9	24.1	24.4	24.1
18	15.4	14.7	15.3	14.3	14.2	13.0	13.7	13.1
19	8.2	7.9	8.1	7.7	7.6	6.7	7.0	6.8
20	3.8	4.4	3.7	4.3	3.8	3.6	3.1	3.9

Site	7b	0505	1984	500 V	22A	
n/N	6/10	6/10	6/10	6/10	6/10	6/10
TO	.680	.680	.680	.680	.680	.680
Gate	5000.0	5000.0	5000.0	5000.0	5000.0	5000.0
1	2697.0	2732.0	2742.0	2731.0	2828.0	2728.0
2	2179.0	2274.0	2209.0	2273.0	2287.0	2271.0
3	1675.0	1667.0	1696.0	1666.0	1762.0	1663.0
4	1130.0	1133.0	1145.0	1132.0	1190.0	1129.0
5	693.0	697.0	704.0	697.0	729.0	694.0
6	399.0	399.0	408.0	399.0	420.0	397.0
7	236.0	238.0	242.0	238.0	247.0	238.0
8	135.0	136.0	140.0	136.0	140.0	135.0
9	75.0	74.0	79.0	74.0	76.0	74.0
10	39.0	40.0	43.0	40.0	39.0	40.0
11	19.1	17.0	22.8	16.2	18.4	15.7
12	13.1	12.6	16.3	12.8	10.5	12.5
13	6.8	5.9	10.5	6.1	4.1	5.8
14	3.7	3.0	7.8	3.2	1.1	3.0
15	2.4	1.2	6.2	1.5	0.5	1.2
16	1.3	0.4	4.8	0.8	0.8	0.4
17	0.8	0.0	4.3	0.4	0.8	0.0
18	0.7	-1.4	4.0	0.1	0.7	-1.6
19	0.1	-3.5	3.3	0.7	0.2	-3.9
20	-1.1	-3.3	2.5	3.6	-0.1	-3.6

APPENDIX C: TRANSIENT SOUNDING DATA CONTINUED

Site	7c	0605	250 H	17A	7d	0605	250 L	20A
n/N	2/8	2/8	2/8	2/8	5/10	5/10	5/10	5/10
TO	.270	.270	.270	.270	.300	.300	.300	.300
1	504.0	506.0	501.0	504.0	5698.0	5768.0	5658.0	5746.0
2	526.0	529.0	524.0	527.0	4964.0	5034.0	4930.0	5015.0
3	542.0	546.0	540.0	544.0	3955.0	3998.0	3928.0	3984.0
4	570.0	577.0	567.0	575.0	3009.0	3020.0	2989.0	3009.0
5	611.0	617.0	608.0	614.0	2173.0	2183.0	2160.0	2175.0
6	651.0	651.0	648.0	648.0	1452.0	1453.0	1444.0	1448.0
7	692.0	695.0	689.0	692.0	960.0	962.0	956.0	959.0
8	727.0	732.0	724.0	729.0	597.0	603.0	594.0	600.0
9	748.0	753.0	744.0	749.0	358.0	364.0	358.0	362.0
10	731.0	736.0	727.0	732.0	202.0	209.0	203.0	208.0
11	565.6	686.0	565.9	682.0	127.8	124.1	128.7	123.6
12	566.0	596.0	567.2	592.7	70.8	73.7	72.2	73.4
13	472.5	473.4	469.8	470.7	36.9	40.5	38.2	40.0
14	352.4	354.4	350.5	352.3	19.4	22.2	20.6	22.2
15	253.4	255.5	252.1	254.0	10.5	13.4	11.7	13.4
16	165.9	166.1	165.1	165.2	5.3	7.2	6.5	7.2
17	105.9	106.6	105.6	106.0	2.3	4.1	3.6	4.2
18	64.6	65.5	64.5	65.2	0.5	2.4	1.7	2.5
19	36.1	37.3	36.2	37.2	0.0	0.9	1.0	1.1
20	19.6	19.8	19.8	19.7	0.0	0.0	0.8	0.0

Site	9b	0505	1984	500 V	22A	
n/N	6/10	6/10	6/10	6/10	6/10	6/10
TO	.680	.680	.680	.680	.680	.680
Gate	5000.0	5000.0	5000.0	5000.0	5000.0	5000.0
1	2878.0	2787.0	2923.0	2874.0	2902.0	2874.0
2	2340.0	2339.0	2458.0	2341.0	2438.0	2340.0
3	1822.0	1727.0	1821.0	1825.0	1799.0	1823.0
4	1240.0	1177.0	1249.0	1245.0	1223.0	1242.0
5	746.0	715.0	763.0	752.0	738.0	747.0
6	414.0	393.0	422.0	418.0	402.0	415.0
7	232.0	223.0	244.0	237.0	225.0	232.0
8	127.0	122.0	136.0	131.0	120.0	127.0
9	67.0	64.0	75.0	72.0	59.0	67.0
10	34.0	33.0	44.0	38.0	28.0	34.0
11	17.9	7.6	15.7	22.2	3.3	17.7
12	9.8	10.6	18.4	13.6	3.8	9.6
13	4.0	2.2	11.1	7.9	-2.4	3.9
14	1.2	-0.5	9.1	5.0	-4.3	1.1
15	0.2	-4.3	7.2	3.7	-5.6	0.0
16	-0.5	-6.5	6.1	2.6	-5.2	-0.7
17	-1.0	-6.9	4.6	2.2	-4.8	-1.2
18	-0.9	-7.2	0.4	2.0	-2.0	-1.3
19	-0.8	-6.7	-0.1	1.3	0.0	-1.5
20	-0.3	-6.2	0.0	0.0	0.1	-1.4

APPENDIX C: TRANSIENT SOUNDING DATA CONTINUED

Site	9c	0505	250 H	14	9d	0505	250 L	20A
n/N	2/8	2/8	2/8	2/8	5/10	5/10	5/10	5/10
TO	.260	.260	.260	.260	.290	.290	.290	.290
Gate	5000.0	5000.0	5000.0	5000.0	5000.0	5000.0	5000.0	5000.0
1	371.0	353.0	367.0	353.0	5193.0	5068.0	5191.0	5072.0
2	379.0	376.0	375.0	375.0	4771.0	4657.0	4768.0	4661.0
3	392.0	381.0	388.0	381.0	3986.0	3905.0	3984.0	3908.0
4	410.0	409.0	406.0	408.0	3124.0	3088.0	3121.0	3090.0
5	436.0	443.0	432.0	442.0	2296.0	2278.0	2295.0	2280.0
6	473.0	465.0	469.0	464.0	1561.0	1543.0	1560.0	1544.0
7	508.0	505.0	505.0	504.0	1040.0	1034.0	1040.0	1035.0
8	550.0	546.0	547.0	544.0	655.0	649.0	654.0	649.0
9	592.0	587.0	589.0	586.0	397.0	393.0	397.0	393.0
10	611.0	609.0	608.0	607.0	227.0	226.0	227.0	226.0
11	597.2	578.9	594.3	578.9	137.9	140.0	137.9	140.2
12	552.7	550.2	550.1	548.8	80.5	79.4	80.5	79.5
13	462.3	460.4	460.2	459.2	42.9	41.6	43.1	41.8
14	359.4	356.9	357.7	356.0	22.8	21.8	22.8	22.0
15	264.5	262.5	263.3	261.9	12.9	11.9	12.9	12.0
16	175.1	174.7	174.3	174.3	6.6	5.8	6.6	5.9
17	113.7	113.4	113.2	113.1	3.6	2.7	3.5	2.9
18	70.6	70.0	70.2	69.9	2.2	1.0	1.9	1.2
19	40.5	39.9	40.3	39.8	1.0	0.3	0.8	0.5
20	21.7	22.2	21.5	22.2	0.1	0.5	0.0	0.7

Site	11a	0505	1984	500 L	22A
n/N	6/10	6/10	6/10	6/10	
TO	.700	.700	.700	.700	
Gate	5000.0	5000.0	5000.0	5000.0	
1	1455.0	1480.0	1452.0	1477.0	
2	1538.0	1557.0	1534.0	1553.0	
3	1640.0	1657.0	1634.0	1653.0	
4	1747.0	1750.0	1739.0	1746.0	
5	1770.0	1772.0	1761.0	1768.0	
6	1723.0	1730.0	1713.0	1727.0	
7	1626.0	1628.0	1617.0	1625.0	
8	1367.0	1370.0	1358.0	1367.0	
9	1091.0	1094.0	1084.0	1091.0	
10	792.0	792.0	787.0	790.0	
11	557.5	552.1	553.9	550.8	
12	379.5	379.4	376.8	378.4	
13	229.2	229.5	227.3	228.8	
14	134.0	134.3	132.7	133.8	
15	79.8	80.1	78.7	79.8	
16	42.8	43.0	41.9	42.7	
17	23.6	23.6	22.7	23.3	
18	12.6	13.0	11.9	12.7	
19	6.5	6.4	5.8	6.2	
20	3.7	2.4	3.2	2.4	

APPENDIX C: TRANSIENT SOUNDING DATA CONTINUED

Site	11b	0505	1984	500 V	22A	
n/N	6/10	6/10	6/10	6/10	6/10	6/10
TO	.700	.700	.700	.700	.700	.700
Gate	5000.0	5000.0	5000.0	5000.0	5000.0	5000.0
1	2805.0	2970.0	2904.0	2951.0	2833.0	2833.0
2	2287.0	2503.0	2367.0	2484.0	2302.0	2388.0
3	1784.0	1849.0	1844.0	1832.0	1788.0	1762.0
4	1214.0	1263.0	1246.0	1248.0	1209.0	1203.0
5	725.0	755.0	740.0	743.0	721.0	714.0
6	397.0	408.0	402.0	399.0	393.0	383.0
7	220.0	231.0	220.0	221.0	217.0	214.0
8	121.0	126.0	118.0	117.0	118.0	115.0
9	66.0	69.0	61.0	59.0	62.0	61.0
10	35.0	39.0	29.0	30.0	31.0	32.0
11	15.4	19.2	10.5	12.7	10.6	16.9
12	11.9	15.7	7.7	6.9	7.4	10.5
13	6.6	9.8	2.9	1.3	2.1	5.1
14	3.8	7.4	1.3	-0.7	-2.0	2.9
15	2.4	5.8	1.8	-2.0	-3.2	1.6
16	1.4	4.8	1.4	-2.7	-3.9	0.7
17	0.8	4.2	0.9	-3.1	-4.5	0.3
18	0.4	2.5	0.8	-3.3	-4.3	0.0
19	-1.6	0.1	0.4	-2.9	-4.5	0.0
20	-4.2	0.5	0.0	-1.9	-4.9	0.0

Site	11c	0505	250 H	24A	11d	250 L	20A	
n/N	2/8	2/8	2/8	2/8	5/10	5/10	5/10	5/10
TO	.700	.700	.700	.700	.275	.275	.275	.275
Gate	5000.0	5000.0	5000.0	5000.0	5000.0	5000.0	5000.0	5000.0
1	701.0	691.0	699.0	685.0	4705.0	4758.0	4799.0	4884.0
2	711.0	714.0	710.0	707.0	4455.0	4568.0	4546.0	4623.0
3	716.0	710.0	715.0	703.0	3863.0	3947.0	3943.0	3996.0
4	732.0	734.0	[illegible]	727.0	3140.0	3172.0	3203.0	3212.0
5	751.0	759.0		751.0	2352.0	2374.0	2401.0	2404.0
6	769.0	764.0		756.0	1605.0	1625.0	1638.0	1646.0
7	775.0	774.0	[illegible]	766.0	1074.0	1083.0	1096.0	1096.0
8	781.0	778.0	779.0	769.0	669.0	676.0	683.0	685.0
9	772.0	768.0	770.0	759.0	402.0	407.0	410.0	412.0
10	736.0	735.0	734.0	726.0	229.0	230.0	233.0	234.0
11	681.0	579.1	680.2	579.2	141.2	138.1	144.0	140.7
12	606.7	581.0	606.1	580.5	79.5	80.4	81.0	81.9
13	499.9	499.8	499.4	493.4	41.2	42.3	42.1	43.4
14	391.9	390.7	391.4	385.7	21.3	22.1	21.7	22.9
15	294.2	293.0	293.7	289.2	11.3	12.1	11.6	12.8
16	199.6	199.8	199.2	197.3	5.2	5.9	5.3	6.6
17	132.6	132.6	132.4	130.9	2.3	2.8	2.4	3.6
18	83.9	83.5	83.7	82.4	0.6	1.5	0.6	2.3
19	49.1	48.5	49.0	47.9	0.0	0.4	0.0	1.3
20	37.8	38.2	37.6	37.9	0.1	-0.2	0.1	0.3

APPENDIX C: TRANSIENT SOUNDING DATA CONTINUED

Site	13a	0605	500 L	22A	13d	1984	250 H	25A
n/N	6/10	6/10	6/10	6/10	2/8	2/8	2/8	2/8
TO	.700	.700	.700	.700	.400	.400	.400	.400
Gate	5000.0	5000.0	5000.0	5000.0	5000.0	5000.0	5000.0	5000.0
1	2488.0	2438.0	2474.0	2429.0	1990.0	2006.0	1978.0	1991.0
2	2420.0	2376.0	2405.0	2367.0	1883.0	1887.0	1872.0	1873.0
3	2311.0	2273.0	2298.0	2265.0	1701.0	1713.0	1691.0	1700.0
4	2165.0	2146.0	2151.0	2138.0	1562.0	1560.0	1554.0	1548.0
5	1928.0	1914.0	1918.0	1907.0	1421.0	1412.0	1414.0	1401.0
6	1627.0	1609.0	1618.0	1603.0	1241.0	1245.0	1235.0	1237.0
7	1332.0	1323.0	1326.0	1318.0	1075.0	1076.0	1071.0	1069.0
8	1000.0	992.0	995.0	987.0	929.0	931.0	926.0	926.0
9	726.0	719.0	722.0	716.0	781.0	784.0	779.0	779.0
10	493.0	491.0	491.0	489.0	643.0	643.0	641.0	639.0
11	337.0	344.5	335.9	343.3	550.2	533.4	548.3	530.5
12	228.6	227.3	228.0	226.5	421.8	422.1	470.5	419.9
13	140.4	139.0	140.2	138.6	310.0	310.2	309.0	308.5
14	84.4	83.4	84.4	83.4	220.6	221.4	219.9	220.3
15	52.0	51.1	52.2	51.3	153.5	154.7	153.1	153.9
16	29.1	28.4	29.4	28.7	97.8	97.8	97.6	97.3
17	16.7	16.1	17.1	16.6	61.3	61.4	61.2	61.2
18	9.7	8.8	10.2	9.4	37.0	37.5	37.0	37.3
19	5.1	4.6	5.5	5.2	20.9	21.5	20.9	21.4
20	2.1	2.8	2.4	3.4	12.0	11.6	12.0	11.5

Site	13b	0605	1984	500 V	22A			
n/N	6/10	6/10	6/10	6/10	6/10	6/10	6/12	6/12
TO	.700	.700	.700	.700	.700	.700	.700	.700
Gate	5000.0	5000.0	5000.0	5000.0	5000.0	5000.0	5000.0	5000.0
1	2282.0	2363.0	2391.0	2303.0	2390.0	2397.0	2349.0	2450.0
2	1787.0	1892.0	1876.0	1836.0	1870.0	1913.0	1853.0	2101.0
3	1281.0	1313.0	1349.0	1270.0	1336.0	1324.0	1305.0	1294.0
4	790.0	826.0	836.0	793.0	822.0	825.0	812.0	812.0
5	477.0	498.0	504.0	479.0	494.0	498.0	493.0	494.0
6	274.0	281.0	292.0	269.0	280.0	277.0	285.0	279.0
7	158.0	167.0	171.0	158.0	160.0	162.0	163.0	162.0
8	92.0	95.0	101.0	90.0	90.0	91.0	96.0	93.0
9	52.0	54.0	58.0	50.0	49.0	50.0	54.0	51.0
10	28.0	31.0	33.0	29.0	24.0	28.0	29.0	30.0
11	14.6	14.8	18.5	16.1	7.8	16.8	12.3	18.8
12	10.9	10.5	14.4	10.2	5.6	9.0	10.4	10.8
13	6.0	5.3	8.8	4.9	1.7	3.9	6.3	5.4
14	3.5	3.1	4.8	2.5	-0.1	2.3	3.7	3.3
15	2.3	1.6	2.1	0.2	0.0	1.6	2.4	1.8
16	1.7	0.8	1.2	-1.6	1.1	0.7	1.3	0.9
17	1.8	0.5	0.8	-2.5	0.9	0.3	0.8	0.5
18	3.5	0.2	0.7	-2.8	0.7	0.0	0.7	0.2
19	3.9	0.1	0.3	-2.5	0.3	0.0	0.2	0.3
20	3.2	0.3	-0.1	-2.0	0.0	0.5	0.1	0.6

APPENDIX C: TRANSIENT SOUNDING DATA CONTINUED

Site	14a	0605	400 L	25A	14c	250 H	1984	17A
n/N	6/10	6/10	6/10	6/10	2/8	2/8	2/8	2/8
TO	.700	.700	.700	.700	.260	.260	.260	.260
Gate	5000.0	5000.0	5000.0	5000.0	5000.0	5000.0	5000.0	5000.0
1	4437.0	4335.0	4438.0	4343.0	411.0	428.0	416.0	429.0
2	4538.0	4438.0	4538.0	4445.0	436.0	442.0	443.0	443.0
3	4474.0	4388.0	4473.0	4395.0	453.0	459.0	453.0	460.0
4	4194.0	4151.0	4191.0	4157.0	489.0	484.0	488.0	485.0
5	3642.0	3612.0	3640.0	3617.0	529.0	519.0	531.0	520.0
6	2920.0	2887.0	2918.0	2891.0	558.0	565.0	564.0	566.0
7	2243.0	2227.0	2242.0	2229.0	618.0	611.0	613.0	613.0
8	1575.0	1563.0	1575.0	1565.0	656.0	660.0	661.0	662.0
9	1062.0	1056.0	1062.0	1057.0	709.0	701.0	703.0	704.0
10	672.0	670.0	671.0	671.0	715.0	709.0	714.0	712.0
11	431.7	440.2	431.6	440.7	578.0	676.9	578.1	679.2
12	276.4	275.5	276.4	275.6	579.9	607.5	580.1	609.7
13	158.8	157.9	158.8	158.0	492.6	488.3	491.8	490.2
14	90.0	89.6	89.9	89.5	364.2	363.4	365.1	364.9
15	52.9	52.5	52.7	52.4	258.2	255.7	256.4	256.7
16	28.3	27.9	28.1	27.8	161.0	159.6	161.0	160.2
17	15.8	15.4	15.5	15.3	98.6	97.4	98.2	97.8
18	9.1	8.4	8.7	8.2	57.7	57.3	57.3	57.8
19	4.9	4.5	4.5	4.3	31.1	31.3	31.0	31.4
20	2.3	2.8	1.7	2.6	16.5	16.0	16.7	16.1

Site	14b	0605	1984	400 V	25A	
n/N	6/10	6/10	6/12	6/12	6/12	6/12
TO	.700	.700	.700	.700	.700	.700
Gate	5000.0	5000.0	5000.0	5000.0	5000.0	5000.0
1	2697.0	2606.0	2642.0	2788.0	2648.0	2793.0
2	2089.0	2072.0	2063.0	2441.0	2067.0	2448.0
3	1488.0	1413.0	1446.0	1440.0	1449.0	1446.0
4	891.0	853.0	870.0	874.0	874.0	878.0
5	512.0	489.0	502.0	505.0	505.0	507.0
6	280.0	260.0	276.0	271.0	278.0	272.0
7	159.0	147.0	151.0	151.0	152.0	152.0
8	92.0	80.0	86.0	83.0	86.0	84.0
9	53.0	43.0	47.0	45.0	47.0	45.0
10	31.0	24.0	25.0	25.0	25.0	25.0
11	15.4	15.5	9.5	16.5	8.7	16.4
12	13.5	8.6	4.9	9.1	-0.9	9.2
13	10.9	4.0	4.5	4.5	3.6	4.4
14	9.1	1.9	2.9	2.7	1.8	2.7
15	8.2	0.8	2.1	1.5	1.0	1.4
16	6.9	0.1	1.3	0.7	0.3	0.6
17	6.3	-0.5	0.8	0.4	0.6	0.3
18	5.6	-0.7	1.1	0.0	0.7	0.0
19	2.4	-0.6	0.6	0.1	0.2	0.1
20	-0.3	0.0	-0.2	0.6	-0.1	0.6

APPENDIX C: TRANSIENT SOUNDING DATA CONTINUED

Site	14d	0605	1984	250 L	19A	
n/N	5/10	5/10	5/10	5/10	5/10	5/10
TO	.290	.290	.290	.290	.290	.290
Gate	6000.0	6000.0	6000.0	6000.0	6000.0	6000.0
1	5548.0	5535.0	5389.0	5638.0	5757.0	5860.0
2	4944.0	4926.0	4799.0	5022.0	5137.0	5226.0
3	3983.0	3952.0	3865.0	4032.0	4141.0	4198.0
4	3017.0	2959.0	2926.0	3020.0	3137.0	3145.0
5	2126.0	2082.0	2063.0	2125.0	2212.0	2213.0
6	1360.0	1338.0	1320.0	1365.0	1415.0	1421.0
7	859.0	842.0	835.0	859.0	894.0	894.0
8	511.0	505.0	498.0	515.0	533.0	535.0
9	296.0	293.0	289.0	300.0	310.0	311.0
10	166.0	163.0	162.0	167.0	174.0	173.0
11	102.2	98.4	100.3	100.8	107.4	104.4
12	57.4	57.8	56.7	59.5	60.9	61.4
13	29.9	31.0	29.8	32.4	32.2	33.0
14	15.6	16.4	15.6	17.5	17.1	17.6
15	8.1	9.3	8.2	10.3	9.1	10.0
16	3.8	4.6	3.7	5.5	4.4	5.0
17	1.6	2.2	1.5	3.2	2.0	2.5
18	0.4	1.2	0.1	2.1	0.5	1.3
19	0.0	0.3	0.0	1.1	0.0	0.3
20	0.3	-0.2	0.0	0.2	0.0	-0.3